

FACILITY FORM 602

N66-20995

(ACCESSION NUMBER)

(THRU)

242

1

(PAGES)

(CODE)

CR 65272

14

(NASA CR OR TMX OR AD NUMBER)

(CATEGORY)

GPO PRICE \$ _____

CFSTI PRICE(S) \$ _____

Hard copy (HC) 6.00

Microfiche (MF) 1.50

653 July 65

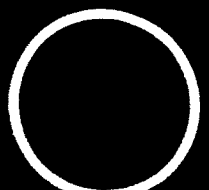
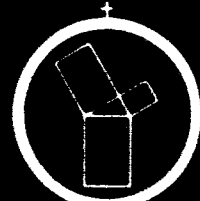
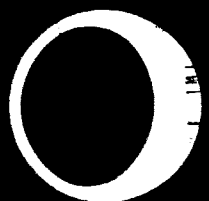
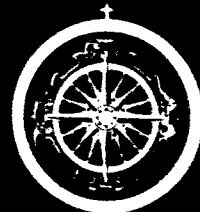
STUDY OF QUANTITATIVE METHODS FOR LEM LANDING SITE SELECTION

CONTRACT NO. NAS 9-3418

FINAL REPORT



TEXAS INSTRUMENTS
INCORPORATED
SCIENCE SERVICES DIVISION



LIBRARY COPY

MAR 22 1966

**MANNED SPACECRAFT CENTER
HOUSTON, TEXAS
STUDY OF QUANTITATIVE METHODS FOR LEM
LANDING-SITE SELECTION**

**FINAL REPORT
CONTRACT NAS 9-3418**

15 March 1966

**Prepared for
NATIONAL AERONAUTICS AND SPACE ADMINISTRATION
Manned Spacecraft Center
Houston 1, Texas**



**TEXAS INSTRUMENTS INCORPORATED
Science Services Division
6000 Lemmon Avenue
Dallas, Texas**

FOREWORD

Contract NAS 9-3418 was awarded to Texas Instruments Incorporated on September 2, 1964. The study was undertaken to define requirements and develop a quantitative methodology for certification of Lunar Excursion Module (LEM) landing areas based on surface geometry measurements and mission requirements. The philosophical approach to this program emphasized mathematical model studies, supplemented by geological field and office investigations, which provide insight into practical difficulties of data acquisition and reliability unattainable by mathematical exercise alone.

In general, the detailed geometry of terrain surfaces at a scale appropriate for landing-site evaluation is too complex to afford analytical description, and tractable mechanistic theories are unavailable for this purpose. The only alternative is statistical treatment. Developed were two parallel approaches involving theory of stochastic processes on one hand and classical distribution theory on the other. Dr. Claude Horton (University of Texas) developed application of the former technique, while Dr. James Dugundji (University of Southern California) is credited with the latter approach. Both are Texas Instruments consultants.

About 25 man-months of professional effort were devoted to this study. Major contributions are credited to the following individuals:

Dr. James Dugundji
Department of Mathematics
University of Southern
California

Map Analysis Techniques,
Protuberance Distribution
Theory

Dr. Richard O. Stone
Department of Geology
University of Southern
California

Map Analysis Techniques,
Field Geological Studies

Dr. Claude W. Horton
Department of Physics
University of Texas

Description of Topographic
Surfaces as Stochastic
Processes

Mrs. Martha Shultz Fowler
Texas Instruments

Topographic Model Analysis
by Stochastic Techniques

Dr. Dmetro Andrychuk
Texas Instruments

Optical Data Processing
Investigations

Ronald E. Becker
Texas Instruments

Program Management,
Photointerpretation, System
Evaluation


Dr. Jack R. Van Lopik
Texas Instruments

Technical Direction,
Review

Mrs. Ruth Wilson performed technical editing of this report.

Mr. Wendell Mendell, NASA-MSD, was technical monitor for the project from its inception until September 1, 1965. He was succeeded by Mr. James Dragg, who served during the remaining period.

TEXAS INSTRUMENTS INCORPORATED

A handwritten signature in cursive script that reads "Jack R. Van Lopik". The signature is written in dark ink and is positioned above the printed name and title.

Jack R. Van Lopik
Manager and Technical Director
Space and Environmental Sciences

ABSTRACT

N66-20995

Mathematical, statistical and optical-Fourier methods were developed for prediction of LEM landing safety against excessive slope and protuberance hazards. Systems utilizing data in elevation matrix, contour map and photographic formats were considered. Detailed treatments based on elevation matrix data offer more promise than those involving contour maps because of physical handling problems and mechanization difficulties associated with the latter. Optical-Fourier techniques appear feasible for rapid comparison of gross regional features, but further development is required to attain operational status.

In order to make certification measurements with 90 percent confidence in required accuracy, it was determined that improvements in the contemplated Orbiter camera system resolution and viewing geometry are required. Alternately, increased reliance must be placed on slope and protuberance measurements derived from Ranger and Surveyor photographs in conjunction with statistical estimates.

Author

TABLE OF CONTENTS

Chapter	Title	Page
	FOREWORD	i
	ABSTRACT	iii/iv
	SYNOPSIS	xiii/xviii
I	INTRODUCTION	I- 1
	A. PURPOSE AND SCOPE	I- 1
	B. SITE CRITERIA AND SYSTEM PARAMETERS	I- 2
	1. Landing-Site Specifications	I- 2
	2. Data Sources	I- 3
	3. System Characteristics	I- 4
	C. STUDY GUIDES AND PREVIOUS WORK	I- 6
	D. ORGANIZATION OF REPORT	I- 7
	E. REFERENCES CITED	I- 8
II	SITE EVALUATION FROM CONTOUR MAPS AND PHOTOGRAPHS	II- 1
	A. GENERAL APPROACH TO PROBLEM	II- 1
	B. STATISTICAL TREATMENT OF SLOPES AND PROTUBERANCES	II- 2
	1. LEM Measurements	II- 2
	2. Slope Conditions and Derivation of Contour Interval	II- 3
	3. Extraction of Non-tipping Landing Probability from a $\kappa = 0.83164$ -meter Contour Map	II- 9
	4. Impalement	II-12
	5. Derivation and Application of "Confidence" in Safe Landing Probability Estimation	II-14
	6. Use of the Above Results to Partition Maps	II-16
	7. The Use of Different Contour Intervals and Probability of Tipping When One Contour Line is Exposed	II-17
	8. Map Inaccuracy	II-20
	C. FIELD EXPERIMENTS AND DATA ANALYSIS	II-21
	1. Topographic Map and Aerial Photograph Requirements	II-21
	2. Field Mapping and Testing	II-23
	3. Area Descriptions and Test Results	II-26
	D. REFERENCES	II-43

TABLE OF CONTENTS (CONTD)

Chapter	Title	Page
III	STATISTICAL PROPERTIES OF TOPOGRAPHIC SURFACES	III- 1
	A. APPROACH TO PROBLEM	III- 1
	B. DEVELOPMENT OF STATISTICAL PROCESS	III- 1
	1. Introductory Comments	III- 1
	2. Assumptions Regarding Frequency Functions of Topography	III- 3
	3. Relation Between True Slope and Apparent Slope	III- 6
	4. Statistical Properties of the Slope Along a Profile	III- 6
	5. Statistical Properties of the True Slope	III- 9
	6. Probability Evaluation	III-11
	7. Effect of Regional Trends	III-12
	C. APPLICATION OF THE METHOD TO THE MT. PISGAH AREAS	III-15
	1. Acquisition of Data	III-15
	2. Calculations	III-16
	D. EXAMINATION OF ASSUMPTIONS	III-20
	1. Gaussian Assumption from Kerrville Data	III-20
	2. Gaussian Assumption from the Mt. Pisgah Data	III-24
	3. Correlation Analysis	III-28
	4. Summary	III-43
	E. REFERENCES	III/45-46
IV	APPLICATION OF OPTICAL DATA PROCESSING TO LEM LANDING SITE SELECTION	IV- 1
	A. GENERAL APPROACH TO PROBLEM	IV- 1
	1. The Role of Optical Computers	IV- 1
	2. The Search for a Comparison Criterion	IV- 2
	B. EXPERIMENTAL STUDIES	IV- 5
	1. The Optical Fourier Transform	IV- 5
	2. The Correlation Step	IV-12
	C. CONCLUSIONS AND RECOMMENDATIONS	IV-24
	1. Summary of Current Findings	IV-24
	2. Other Proposed Approaches	IV-25
	D. REFERENCES	IV-30

TABLE OF CONTENTS (CONTD)

Chapter	Title	Page
V	PHOTOGRAPHIC MEASUREMENTS	V-1
	A. APPROACH TO THE PROBLEM	V-1
	B. IMAGE INTERPRETABILITY	V-2
	C. PHOTOGRAMMETRIC CAPABILITIES	V-5
	D. RELATIONSHIP OF CONTOUR ACCURACY TO CONFIDENCE IN SLOPE PROBABILITY MEASUREMENT	V-8
	E. MICRODENSITOMETRIC ACCURACY	V-11
	F. METHOD FOR DETERMINING SAFE LANDING PROBABILITY (PROTUBERANCES) FROM SURVEYOR SAMPLE AREA AND ORBITER PHOTOGRAPHS	V-17
	G. CONCLUSIONS AND RECOMMENDATIONS	V-23
	H. REFERENCES CITED	V-26
VI	ADDITIONAL READING	VI-1

LIST OF APPENDIXES

A	DERIVATION OF TRUE SLOPES FROM APPARENT SLOPES
B	CALCULATIONS FOR DETERMINING AVERAGE VALUES OF TANGENT θ_1 AND TANGENT ² θ_1
C	TRANSFORMATION OF COORDINATE SYSTEM
D	TREND PLANE REMOVAL
E	PEARSON'S METHOD OF CURVE FITTING (Kendall, 1947; Elderton, 1927)
F	FINITE, EQUISPACED DATA

LIST OF TABLES

Table	Title	Page
II-1	BOULDER MEASUREMENTS (Death Valley, California)	II-40
III-1	TREND PLANE PARAMETERS	III-16
III-2	CALCULATED STATISTICAL PARAMETERS	III-19
III-3	EVALUATION OF EQUATION III-29	III-20
III-4	CALCULATED MOMENTS AND PEARSON κ	III-24
IV-1	LUNAR SURFACES ON WHICH CRATERS HAVE BEEN COUNTED	IV- 7
V-1	CALCULATION OF DENSITY PROFILE OF PHOTO- GRAPHIC IMAGE OF THE STANDARD PROTUBERANCE	V - 17
V-2	CALCULATED DENSITY OBTAINABLE BY SCANNING THE IMAGE OF THE STANDARD 2-M. BASE DIAMETER PROTUBERANCE WITH A DENSITOMETER APERTURE EQUIVALENT TO $\frac{1}{2}$ -M DIAMETER	V - 18

LIST OF ILLUSTRATIONS

Figure	Title	Page
I-1	Geometry of the LEM Landing Gear	I- 4
II-1	Template Conditions for a Map with Contour Interval $\kappa = \frac{R \tan \tau}{2} = 0.4158 \text{ m}$	II-6
II-2	Template Conditions for Map with Contour Interval $\kappa = R \tan \tau = 0.83 \text{ m}$	II-8
II-3	Application of Template Test to Contour Map with $\kappa = R \tan \tau$	II-10
II-4	Stereogram of Neenach Ranch Test Area	II-27/28
II-5	Location Map, Neenach Ranch Test Area, Neenach Quadrangle, 15-Min Series (California)	II-29
II-6	Stereogram of Covina Knolls Test Area	II-31/32
II-7	Location Map, Covina Knolls Test Area, 1:24000 Scale	II-33
II-8	Location Map Pisgah Crater Area	II-35
II-9	Location Map of Death Valley, California	II-39
II-10	Sample Survey Plots	II-41
III-1	Relationship Between True Dip and Apparent Dip	III-4

LIST OF ILLUSTRATIONS (CONTD)

Figure	Title	Page
III-2	The (t_1, t_2) Plane	III-10
III-3	Topographic Cross-Section Parallel to the X-Axis	III-12
III-4	Maximum Dip of Trend	III-17
III-5	Matrix Representation of Elevation Point Data	III-18
III-6	Distribution Function of Elevations	III-23
III-7	Distribution Function of Elevation Differences	III-23
III-8	Frequency Distribution of Elevations for Areas A, B, C, and D	III-25/26
III-9	Probability Scale for Frequency Distribution of Elevations (Areas A, B, C, and D)	III-27
III-10	Frequency Distribution of Elevation Differences (Area D)	III-29
III-11	Frequency Distribution of Elevation Differences (Area B)	III-30
III-12	Frequency Distribution of Elevation Differences (Area A)	III-31
III-13	Frequency Distribution of Elevation Differences (Area C)	III-32
III-14	Frequency Distribution of Elevation Differences (West to East) on Probability Scale	III-33
III-15	Frequency Distribution of Elevation Differences (South to North) on Probability Scale	III-34
III-16	Frequency Distribution of Elevation Differences (South-west to Northeast) on Probability Scale	III-35
III-17	Autocorrelation Functions	III-38
III-18	Averaged Autocorrelation Function for All Areas	III-39
III-19	Autocorrelation Function Based on Multiples of 10.3 Meters Lag and 5.15 Meters Lag (Area D)	III-40
III-20	Power Spectra	III-41
IV- 1	Objective of the Optical Data Process	IV- 3
IV- 2	Search for Criterion	IV- 4
IV- 3	Crater Frequency (Cumulative) as a Function of Crater Diameter. Data and computed curve are shown (after Dodd, Salisbury and Icarus, 1963)	IV- 6

LIST OF ILLUSTRATIONS (CONTD)

Figure	Title	Page
IV- 4	Post-Mare Diameter Distribution of Lunar Craters from Earth-Based and Ranger Photographs (Hartmann)	IV- 8
IV- 5	Constancy of Fourier Transform	IV- 9
IV- 6	Equipment	IV-11
IV- 7	Fourier Transforms Ranger IX	IV-13/IV-14
IV- 8	Behavior of a Correlation Similarity of φ_2^j with φ^2 Is a Measure of Similarity Between $f_2^j(x)$ and $f_1(x)$	IV-16
IV- 9	Correlation Optics	IV-17
IV-10	Equipment Check, Autocorrelation of Two Ronchi Rulings	IV-18
IV-11	Crosscorrelation of Fourier Transforms, Ranger IX	IV-19/IV-20
IV-12	Crosscorrelation of Fourier Transforms Using Pissgah Crater Photographs	IV-22
IV-13	Crosscorrelation of Fourier Transforms, Pissgah Crater with Ranger Close-Range Shots	IV-23
IV-14	Cumulative Area-Slope Characteristic of the Known Area	IV-26
IV-15	Cumulative Area-Slope Characteristic for Searched Area Computed by Equation IV-7	IV-27
IV-16	Cumulative Area-Slope from the Fourier Transform	IV-28
IV-17	Enlargement Step	IV-29
IV-18	Pattern Recognition Step	IV-30
V- 1	Hypothetical Ridge	V- 4
V- 2	Lunar Photometric Function of φ Vs α	V- 4
V- 3	The Uncertainty in Position of Boundary of Tilt Area As a Function of the Standard Deviation σ in Height Accuracy	V- 9
V- 4	Cone Geometry and Condition of Illumination	V-13
V- 5	Characteristic Curve Film SO-243	V-14

LIST OF ILLUSTRATIONS (CONTD)

Figure	Title	Page
V- 6	Aperture Positions for Which Density Was Computed	V- 18
V- 7	Comparison of Microdensitometered Density with True Density	V- 19
V- 8	Geometry for Wide Base Convergent Photography	V- 20
V- 9	Conceptual Camera System	V- 25

SYNOPSIS

In execution of its responsibility for processing lunar topographic data to certify LEM landing sites, NASA-MSC contracted with Texas Instruments to develop methods for analyzing surface geometric data in terms of LEM safe landing criteria. Context of the program objectives emphasized treatment of terrain data as contained in, or extracted from, contour maps and supplemental photographs. Consideration of more than 200 references concerned with schemes for topographic map portrayal and analysis was accomplished as a basis for development of the two formal site evaluation procedures outlined in paragraphs A and B following. Extended discussions of these methods are presented in Chapters II and III; Chapter IV presents results of a feasibility investigation concerning correlation of terrain photographic images by means of their optical Fourier transforms. Chapter V treats a number of operational factors, including the Lunar Orbiter photographic system, which may adversely affect the realization of lunar contour maps showing sufficient detail for reliable certification analysis.

A. CONTOUR MAP SPECIFICATIONS AND GRAPHIC ESTIMATION OF TIPPING PROBABILITY

For available specifications of LEM landing pad configuration and maximum allowable tilt, it is shown (Chapter II) that a contour map having a 0.4158-m contour interval will enable unambiguous determination of probability of a non-tipping landing. Also it is shown that a 0.83164-m contour interval map will enable classification of safe, unsafe, and uncertain areas; the uncertainty can be resolved if one is willing to accept reasonable intuitive arguments, but theoretical proofs of these arguments are presently lacking. Since the 0.83164-m contour interval seems to be a reasonable compromise between theoretical rigor and practical expediency, it is adopted for subsequent discussions.

Map scale is important only insofar as it affects an individual's ability to discriminate individual contour lines from each other and to distinguish secant contour lines (relative to an 8-m scale-diameter template circle drawn on transparent acetate film) from tangent lines. A 1-cm diameter template circle would thus establish the map scale as 1:800. Graphic map testing is accomplished systematically as follows:

1. Parallel lines at spacings equivalent to the template circle diameter are drawn across a map of the test area.
2. The template circle is passed across each zone between two adjacent lines. A short line segment normal to the grid lines is drawn tangent

to the circle's trailing edge when an unsafe condition is encountered; a similar mark tangent to the circle's leading edge is made when the terminal extremity of an unsafe zone is reached.

* Unsafe conditions are considered to prevail whenever:

- Two contour lines at different elevations appear within the template circle which cross a common radius
- More than two contour lines appear within the template circle.

3. An estimate of the probability (P) of making an unsafe "tipping" landing is determined as the ratio of total unsafe area traversed to total area traversed by the template circle.

4. The results determined in (3) can be improved by repeating the testing process in an orthogonal direction, and combining the independent test results as $P = \sqrt{P_x \cdot P_y}$ where subscripts x and y denote the two orthogonal directions.

A non-systematic procedure can be effected by visually identifying zones where contour spacing indicates slopes greater than 12° , and moving the template along contours which define the boundaries of these zones. In this system the upper and lower boundaries of each "unsafe" area are thus established by the locus points on the outermost extremities of the circle diameter crossed by the contours in question, according to the criteria stated in 2. above. Lateral extremities of unsafe areas are defined by circle radii orthogonal to contour lines where the shortest horizontal distance barely exceeds the critical value. When all "unsafe" areas are completely bounded in this manner, the ratio of total unsafe area to total map area is an estimate of the unsafe tipping probability.

It is not feasible to predict protuberances and other bottoming hazards which protrude more than 50 cm from the apparent plane surface defined by the LEM pads with any measure of reliability from an 83-cm contour interval map. A mathematical treatment was developed for computing the bottoming probability associated with discrete objects such as boulders, pinnacles, etc. which would presumably be identified from photographs. This is described in Chapter II, paragraph B (4), and is demonstrated in Chapter II.C.3.a. by a sample computation which utilized field measurements of boulders on an alluvial terrace. Also discussed (Ch II. 7, 8) are probabilities associated with use of a contour interval greater than that specified, and an arbitrary method to account for contour inaccuracies.

B. METHOD FOR ANALYSIS OF TERRAIN FROM A GRID OF ELEVATION DATA

An alternative method was developed which employs spot elevation data in a rectangular grid pattern. This data can be read manually from contour maps (extrapolating elevations between contour lines as necessary) or may be acquired directly from photographs in digital tape format. Several state-of-the-art automatic map compilation systems and scanning photometers have this capability.

The method results in the following simple expression for the probability (P) of encountering slopes greater than some critical value θ_c :

$$P = \exp - \frac{\tan^2 \theta_c}{2\sigma_t^2} \quad (\text{III-26})$$

where σ_t is estimated from a grid of elevation data by the following formula:

$$\hat{\sigma}_t = \frac{\hat{\sigma}}{\Delta x} \sqrt{2(1-\hat{\tau})} \quad (\text{III-20})$$

in which $\hat{\sigma}$ = standard deviation of elevations
 $\hat{\tau}$ = one-lag correlation coefficient
 Δx = sampling interval

Formulae for these parameters are developed in the text.

Key assumptions pertinent to the expression given for P in this development are:

- Elevations are distributed normally within the sample area.
- The surface of interest is isotropic.
- The surface of interest is stationary.

If a regional trend in elevation exists within the area of interest, the surface will not be stationary. The elevation data can be made stationary, however, by fitting a regression surface and extracting the departures from that plane in lieu of raw elevations. A procedure is given in subsection B-7 for handling this condition which employs a chi-squared random variable. If assumptions necessary for P in the form presented must be relaxed (possibly due to strongly non-Gaussian behavior of elevation data), it is still possible to determine P, but a more complex equation will be required. An effort to fit non-Gaussian distributions by other curves, as described in subsection C.2, is typical of the approach one must take in this case. As an alternative to seeking a closed form or numeric approximation to an integral expression, one may plot a cumulative probability density curve of slopes and integrate the function graphically over the range of slopes which do not exceed the critical value.

This method will not, in general, enable prediction of LEM tipping probability with high reliability, because there is no provision for certain arrangements of the LEM pads on that surface. It will, however, serve as a reasonable basis for selection of the best sites or areas within a group, so that more detailed studies can be performed on those areas which offer the best hope of landing success.

These conditions enable one to establish an intuitive basis for comparison of "roughness" between different areas sampled at the same scale and sampling interval. One would want to employ a sampling interval which has some physical relationship to the problem of interest, such as the LEM pad spacing employed in this instance. In general, for a given distribution of elevation points on a surface, there is a tendency for apparent slopes to flatten as the sampling interval is increased.

The foregoing method of analysis was applied to data extracted from four 25-cm contour maps of lava flow and Playa lake features near Mt. Pisgah, California. Data treatment and results are discussed in Ch III. C

C. RECAPITULATION OF CONTRACT TASK EFFORT

Paragraphs A and B above have outlined salient features of two explicit methods for topographic analysis of LEM landing sites. The program task objectives as incorporated in these methods or other program effort were achieved as follows:

Task 1: Determine the most suitable map scale and contour interval for LEM landing site analysis.

Response: For method A above, map scale is not critical but should be great enough to facilitate manual scanning by a circle template at least 1 cm in diameter. This implies at least a 1:800 map scale. Contour interval is more critical; to extract an unambiguous determination of non-tipping landing probability the contour interval should be $\kappa = \frac{R \tan \tau}{2}$,

where R = radius of circle through landing pads

τ = critical slope

Certain assumptions permit relaxation of this specification to $\kappa = R \tan \tau$. Contour intervals greater than this may yield useful information about relative terrain roughness, but do not afford adequate sensitivity to possible LEM landing gear orientation.

Maps at various scales and surface configurations were analyzed to demonstrate the methods. Results are discussed in Chapters II and III.

Aerial photographs were collected and analyzed by conventional photointerpretive techniques to evaluate their use for prediction of bottoming hazards. The photographic coverage gathered for contour-mapped study areas did not yield reliable estimates of bottoming hazards as small as 50 cm. It is apparent that spot elevation measurement of such obstacles by means of projection stereometric mapping systems would be feasible if the photos themselves were amenable to contouring at 50 cm. Shadow measurement as described by other investigators is a more promising technique for evaluation of protuberances.

Task 2: Sampling techniques will be investigated for use in analyzing prospective LEM landing sites.....

Response: Fulfillment of this task is implicit in the two methods presented. Method A employs a circular sampling template equivalent to the scale diameter of the LEM landing pad arrangement, which is swept across the entire test area. Method B is predicated on use of a sampling grid dimension equivalent to the spacing of opposing LEM pads.

Task 3: Criteria will be established for description and classification of possible LEM landing sites.

Response: Method A yields a direct determination of tipping probability, which suffices to describe the site. Method B yields a probability P for the occurrence of slopes less than or equal to some critical values. It also enables a subjective estimation of relative roughness between different areas through comparison of second-order cumulative probability density curves. At both volcanic flow sites, inordinately complex surfaces existed which gave a general impression of roughness far greater than any photographic image or parametric equation could convey. Difficulties in negotiating this terrain on foot confirmed an initial impression that such areas would be totally unsuitable for landing any sort of airborne vehicle.

Task 4: Selected Terrestrial terrains will be checked.....

Response: It is almost impossible to comprehend the complexity of volcanic flow surfaces or to appreciate limitations of contour map representations of such surfaces without first-hand field investigation of such features.

Visits to the Pispah flow near Amboy , California, and the Bonita Flow near Flagstaff, Arizona, were made by program personnel for this purpose. Other program participants performed field mapping investigations as described in Chapter II.C.

Task 5: A technique will be established for comparing the suitability of terrains for a) landing site areas, and b) touchdown areas.

Response: The techniques presented are sufficiently general so that they serve for either purpose. However, the NASA specification that a landing site must incorporate an 0.8 km CEP serves to remove any distinction between landing sites and touchdown areas, insofar as detailed certification of topograph surface is concerned.

CHAPTER I

INTRODUCTION

A. PURPOSE AND SCOPE

Classical methods for characterizing terrain surfaces consist of conventional contour mapping — a smoothing process — and descriptive physiographic systems based on genetic origin of surface features. While both methods may prove useful for mapping gross features of the lunar surface and may enable qualitative predictions concerning surface geometry and functional character at any site, neither system affords sufficient objectivity or analytical precision to permit valid statistical ranking or comparison of detailed surface microstructure directly at a scale appropriate to certification studies for the Lunar Excursion Module. Consequently, this study has sought to establish a methodology for comparative evaluation of terrain in terms of specific LEM landing-site requirements.

A system for performing this task must be guided by a number of limiting assumptions regarding

- LEM stability criteria
- Character of available input data
- Assumed confidence requirements

These are discussed in the next section.

Since appropriate lunar topographic measurements for a program of this type have not yet been achieved, this study utilized maps, photographs and field observations of terrestrial surfaces as experimental data. While it is not possible to state that any known terrestrial area constitutes a valid lunar analog, it is reasonable to hypothesize that mathematical treatments which suffice to characterize the distributions of slopes, depressions and protuberances of earth terrains will serve as well on lunar surfaces. It also was hoped that a sufficiently objective and utilitarian approach could be developed to suffice as a general quantitative system for expressing, classifying and mapping micro relief units. Obviously, such a system should involve a minimum number of measurements and the fewest parameters possible to specify the properties of interest adequately.

The objectives of any mapping process are generalization and display. Terrain data in most elemental form consist of measured elevations and positional coordinates from an assumed origin. It is conventional to visualize and express such 3-dimensional surfaces in terms of contours and, indeed, the vertical measurement accuracy of photogrammetric plotting systems is customarily expressed in terms of the empirical C factor which relates the flight attitude to a contour interval for which at least 90 percent of all plotted

and interpolated elevations are accurate within one-half the contour interval. Thus, in conventional usage, the contour interval is significant as a statistical parameter as well as a pictorial artifice. This circumstance, as well as the fact that virtually all sufficiently detailed terrain measurements for micro-terrain studies existed in contour format, dictated that the program tasks be expressed in contour-mapping terminology.

There is insufficient information available at this time to estimate either the precision or accuracy of elevation measurements which are extracted from monoscopic lunar photographs by photometric techniques currently undergoing development for this purpose. However it seems that some assumptions must ultimately be made in order to attach measures of confidence to the results. A detailed study of this problem, involving establishment of an appropriate datum, adjustment of photographic models to that datum, and analysis of errors from each element of the photographic system and cartographic process, entails an effort far beyond the scope of this program and possibly beyond present state-of-the art. However, a simplified analysis of the Lunar Orbiter camera system and related effects was undertaken, as reported in Chapter V, to ascertain whether map requirements for landing site analysis are consistent with the quality of data which that system will provide.

B. SITE CRITERIA AND SYSTEM PARAMETERS

1. Landing-Site Specifications

Requirements for a verified safe LEM landing site are essentially as discussed in "Requirements for Data in Support of Project APOLLO" dated November 18, 1963:

- A landing site must be large enough to include a circle 1600 m in diameter
- Within the landing site, the probability of randomly encountering an effective slope greater than 12° (over the 8-m dia. of the LEM landing gear) shall be less than 5 percent
- Within the landing site, the probability of randomly encountering an effective protuberance greater than 50 cm within the effective bottoming area shall be less than 5 percent. The bottoming area is considered to be that within the 8-m diameter circle passing through centers of the four landing pads — a quite conservative assumption.

It is further noted that the second and third specifications must be certified with 90 percent confidence.

Geometry of the LEM landing gear is illustrated in Figure I-1.

2. Data Sources

The task of site selection and verification is shared by three unmanned programs — Ranger, Surveyor and Lunar Orbiter.

The Ranger series already has provided regional television coverage and needed information concerning detailed appearance of selected areas and, through its calibrated camera systems, has provided improved estimates of surface luminances. It also has confirmed the existence of protuberances large enough to pose bottoming hazards.

The Surveyor series, in turn, will soft-land at predetermined points and enable television viewing of local terrain in the immediate vicinity. This hopefully will yield more detailed coverage and viewing perspective not afforded by the Ranger photographs. The Surveyor series also will provide the first — and possibly only — estimates of sinkage and bearing strength available prior to an APOLLO manned landing.

Lunar Orbiter missions will yield photographic coverage on a "production" basis for detailed examination of large areas to be selected within a region of interest bounded by lunar coordinates $\pm 10^\circ$ latitude and $\pm 45^\circ$ longitude. The Orbiter photographic missions share many elements in common with terrestrial hyperaltitude photographic reconnaissance and mapping activities including viewing geometry, camera systems and applicable cartographic techniques. On the other hand, constraints imposed by adoption of proven flight system components and the realities of lunar orbital mechanics create unprecedented demands on photointerpretation and measurement technology.

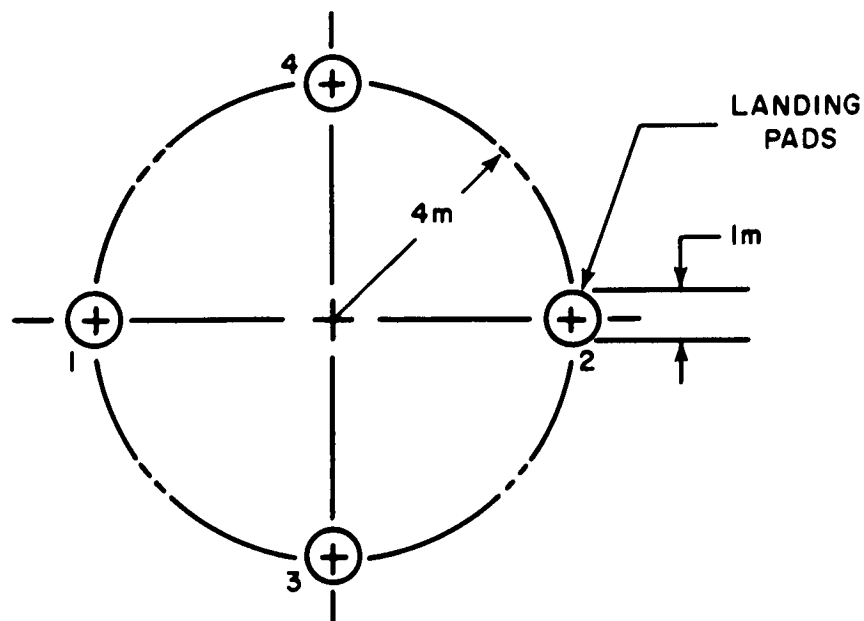


Figure I-1. Geometry of the LEM Landing Gear

3. System Characteristics

The principal features of the Orbiter dual-framing camera system and photo missions, described by Kosofsky and Broome (1965) and elsewhere, are summarized briefly here to facilitate discussion in later chapters:

Lunar Orbiter Mission Coverage

Flight altitude: 46 km
 Camera axis: vertical
 Total coverage: 40,000 km²

Medium Resolution System

Scale: 1:600,000
Total coverage: 40,000 km²
Frame format: 33 km x 36 km
End/up: 50 percent (4-frame stereo sequence)
87 percent (14-frame high-resolution sequence)

High-Resolution System

Scale: 1:75,000
Total coverage: 8000 km²
Frame format: 4.1 km x 16.4 km
End/up: none (4-frame stereo sequence)
5 percent (14-frame high-resolution sequence)

Medium-Resolution Camera

Xenotar 80-mm (3-in.)
F-No.: 2.8 stopped down to 5.6
Resolution: 76 line-pairs/mm (cascaded through scanning,
transmission and ground
reconstruction)

High-Resolution Camera

Pacific Optical Company
Focal length: 24 in. (0.61 m)
F-No.: 5.6
Exposure speed : 1/25 sec
Resolution: 76 line-pairs/mm (cascaded through scanning,
transmission and ground
reconstruction)

Film

Kodak SO-243
Bimat strip developer process (SO-111)

Image-Motion Compensation

Not to exceed allowable error of 1 percent of
distance across target area during exposure

C. STUDY GUIDES AND PREVIOUS WORK

It is axiomatic that lunar areas having slopes greater than 12° on a gross scale (on the order of a kilometer) will not qualify as LEM landing sites despite any amount of refinement in measuring techniques, resolution or statistical treatment. Techniques for slope-mapping of gross features have been demonstrated by several investigators; in this regard, the photometric mapping methods developed by the U.S. Geological Survey group at Flagstaff, Arizona, utilizing the known variation of the photometric function with slope are well known. Despite acknowledged inaccuracies of this method which result from variations in albedo and other sources, it is adequate to eliminate a large percentage of unsuitable areas from consideration as landing sites. In this respect, the medium resolution (1:75,000-scale) coverage stereoscopic photography to be obtained from the Lunar Orbiter system will be redundant or will supplant photometry by enabling preparation of contour maps through conventional stereophotogrammetric methods. Since gross areas with slopes greater than 12° can thus be eliminated from consideration, it is apparent that the major task of interest will be detection and measurement of microrelief features on gross slopes from 0° to 12° .

Previous efforts to describe and classify terrain geometry are of interest mainly insofar as they offer information about the statistical behavior of microrelief features. Carr and Van Lopik (1962) surveyed the literature of terrain quantification and identified more than 200 references dealing with surface geometry; 69 discrete surface geometry measurements and properties were evaluated according to potential military usefulness. A companion report (Carr, Becker and Van Lopik, 1963) examined 14 methods for obtaining field microrelief measurements and concluded that none were entirely adequate to meet military requirements of a generalized nature.

Various techniques based on generalized harmonic analysis deserve special comment because they afford sound, technically correct, potentially useful methods for studying microrelief. Basic problems in applying autocorrelation and energy density spectra to the study of terrain profiles, including considerations involved in taking data, are examined by Carr and Van Lopik (1962) and several reference papers are reviewed.

Stone and Dugundji (1963) undertook the quantitative expression of known profiles by examination of the harmonic properties of 22 micro-terrains as reflected by computed Fourier series coefficients. Profile results were generalized to two dimensions through use of radial profiles spaced at 15° intervals. Harmonic amplitudes were employed in computing four roughness factors which, taken as a vector quality, serve to define roughness. The analyzed terrain profiles also were ranked visually according to roughness; a high degree of statistical correlation with rankings based on computed roughness vectors was demonstrated.

A recent application of spectral density techniques for analysis of terrain profiles was reported by Van Deusen and Hoppe (1965). This report is unique in that it reviews and compares results of profile analyses by Fourier series, Fourier integral and power spectral density techniques. A discussion of the amplitude probability distribution includes two natural terrain profile plots (from work by Kozin, Cole and Bogdanoff, 1963) which show departures from Gaussian distributions in the extreme ranges but close Gaussian behavior within the 10 to 90 percentile range. The extent to which Gaussian behavior of terrain properties such as amplitude, elevation and slope predominates is a very important factor in selecting methods for processing LEM site certification data, as will be evident from discussions in later sections.

Harmonic analysis evidently affords a valuable approach for ground mobility studies and offers some promise as a general classification system for microrelief. However, the copious calculations, high sample density and specialized applicability to 1-dimensional data detract from its value as a general applicable method for landing-site certification.

A basic approach to LEM site selection was developed by Byrne et al (1964). It has been especially valuable as an outline of the factors which constitute a doctrine of APOLLO landing strategy. This work necessarily involved many broad assumptions concerning the nature and distribution of lunar surface parameters; in this context, the present report is an investigation of methods for obtaining the stochastically defined properties of the surface, which are needed to validate the proposed strategy, and to establish reasonable values of these properties for various surface types.

D. ORGANIZATION OF REPORT

Two parallel studies involving different approaches to evaluation of terrain surfaces were undertaken. The first step in each was to develop a methodology for statistical treatment of sample data, followed by exercises to implement and evaluate these techniques. Raw data in each instance were obtained from field surveys or taken from very large-scale contour maps which were assumed to coincide with real surfaces. Results of these studies are described in Chapters II and III.

Another investigation addressed the problem of extrapolating terrain properties from one region to another on the basis of gross appearance. Preliminary assessment of this problem indicated a possibility that this could be accomplished by optical data processing techniques performed directly on the terrain photo images without a need for comparing some derived factor(s) or measurements. Chapter IV presents progress made on this work.

Conclusions and recommendations for further work are presented at the end of each chapter.

E. REFERENCES CITED

- Byrne, C.J. et al, 1964, An analysis of lunar site survey by the unmanned program: Bellcomm, Inc., Washington, D.C., Jan. 31, 56 p.
- Carr, D.D. and J. R. Van Lopik, 1962, Terrain quantification, phase I— surface geometry measurements: AFCRL, Contract AF 19(628)-481, Project 7628, Texas Instruments, 85 p., 348 annotated ref.
- Carr, D.D., R.E. Becker and J. R. Van Lopik, 1963, Terrain quantification, phase II — playa and miscellaneous studies: AFCRL, Rpt. AFCRL-63-793, Contract AF 19 (628)-2786, Project 7628, Texas Instruments, Oct. 6, 73 p.
- Kosofsky, L.J. and G.C. Broome, 1965, Lunar Orbiter — a photographic satellite: NASA Langley Research Center (Hampton, Va.), presentation at Spring Convention of Motion Picture and Television Engineers, Los Angeles, Calif., Mar. 28-Apr. 2.
- Kozin, F., L.G. Cote and J.L. Bogdanoff, 1963, Statistical studies of stable ground roughness: Rpt. 8391, U.S. Army Tank-Automotive Center, Warren, Mich., Nov.
- Stone, R.O. and J. Dugundji, 1963, A study of microrelief— its mapping, classification and quantification by means of a Fourier analysis: Univ. of S. Calif., Waterways Experiment Station Contract DA-22-079-eng-261, 161 p.
- Van Deusen, B.D. and C.H. Hoppe, 1965, A study of the vehicle ride dynamics aspect of ground mobility: Chrysler Corp., Waterways Experiment Station Contract Rpt. 3-114, v. IV, Contract DA-22-079-eng-403, Apr.

CHAPTER II

SITE EVALUATION FROM CONTOUR MAPS AND PHOTOGRAPHS

A. GENERAL APPROACH TO PROBLEM

The general problem is to devise a scheme for estimating the probability that a LEM will land safely in a specified area. In this chapter methods for obtaining tipping and impalement probabilities from contour maps and photographs are developed and illustrated by example data. These involve specification of required map scales, contour intervals, and sampling procedures. Fundamental to these approaches is the assumption that exceedingly high-resolution photography is available from which maps of the landing areas can be made which illustrate the requisite detail; it is recognized that the photographic system requirements on which these methods depend may be exceedingly difficult to satisfy.

A sampling technique which employs a circular template is suggested by geometry of the LEM landing gear. Scaled diameter of the template is set by the pad-spacings and a circle drawn through their centers. Contour-interval specifications must be sensitive to the permissible tilt over the template distance and also provide enough data points to make unambiguous determinations of landing safety. The principal map scale requirement, beyond that required to show the requisite contour lines clearly, is that it will be large enough to accommodate the template sampling scheme. A 1-cm template circle would thus require 1:800 map scale, since the circle diameter is the scaled equivalent of 8 meters.

No restrictive assumptions concerning the source of protuberance measurements are made in the analysis. A large percentage of bottoming hazards will be associated with crater rims, otherwise classified as slope hazards. However, the contouring process is not particularly sensitive to discrete objects of boulder-size dimensions and will not reveal the existence of bumps with heights less than the contour interval, if the bumps should occur in a vertical interval between two contour lines. Conceivably, shadow measurements made from lunar photographs could provide data on locations and dimensions of protuberances. Given large-scale photography, proper illumination and suitable control data on sun angle and photo orientation, the ACIC system described by Ruffin (1965) for automatic computation of lunar relative heights should serve this purpose. Limited protuberance coverage will be generated, at least, by Surveyor television photography. If these obstacles can be identified on photographs, their positions can be plotted on the contour sheets. In order to provide example data for this analysis, it was necessary to actually locate/measure boulders in the field by contact mapping procedures; 1:12000-scale contact prints proved to be worthless for this purpose.

B. STATISTICAL TREATMENT OF SLOPES AND PROTUBERANCES

The work reported in this subsection has the following objectives:

- To determine a map contour interval for use in certifying a LEM landing site
- To determine a probability of safe (i. e., nontipping and nonimpaled landing in a given area)
- To propose a mechanical method for determining the probability of a safe landing in a given area and estimating its "confidence"
- To define and examine the variation in "confidence" when maps with differing contour intervals are used

1. LEM Measurements

The following data are assumed:

R = LEM landing circle radius (in meters) = 4 m

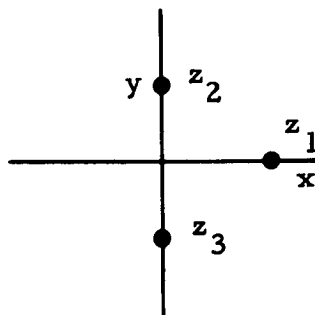
h = LEM bottoming height (in meters) = 50 cm = $1/2$ m

τ = LEM permissible tilt (in degrees) = 12°

It is very simple to express the parameters required for the subsequent analysis directly in terms of R , h , and τ ; explicit evaluations of these derived parameters based on the above numerical values for R , H , τ will be given in each instance.

2. Slope Conditions and Derivation of Contour Interval

Let z_1 , z_2 , and z_3 be the elevations of the three LEM legs which will determine the slope.



The locations of these points can be given by

$$z_1 : (x = R, y = 0)$$

$$z_2 : (x = 0, y = R)$$

$$z_3 : (x = 0, y = -R)$$

and a plane $z = ax + by + c$ passing through these points must satisfy

$$z_1 = aR + b \cdot 0 + c$$

$$z_2 = a \cdot 0 + bR + c$$

$$z_3 = a \cdot 0 + b(-R) + c$$

where a is the slope of the plane in the x direction and b is the slope of the plane in the y direction.

The true slope of the plane m (the angle the normal makes with the vertical) can be expressed as $m^2 = a^2 + b^2$.

The solution for a and b in terms of the z 's results in

$$m^2 = \left| (z_1 - z_3)^2 + (z_1 - z_2)^2 \right| / 2R^2$$

so that

$$m^2 \leq (z_H - z_L)^2 / R^2$$

where $(z_H - z_L)^2$ is the maximum of the above two elevation differences. It follows that

$$m \leq (z_H - z_L) / R.$$

Thus, if we can insure that in a disc of radius R the maximum deviation in elevation between any two points is less than $R \tan \tau^0$ then the center of the disc is a safe landing point regarding the slope conditions.

Suppose a contour map is available with contour interval κ . We will now examine a single point (x_0, y_0) on the map corresponding to the center of a hypothetical landing circle. The points (x, y) of interest on the map are those points "visible" to the critically descending LEM vehicle, namely the points (x, y) satisfying.

$$(x - x_0)^2 + (y - y_0)^2 \leq R^2.$$

Let $S(x_0, y_0)$ denote this set of points. Clearly this set of points can be defined in practice by those points covered by a circular template of radius R (according to the map scale) centered at the point (x_0, y_0) . The template may cover

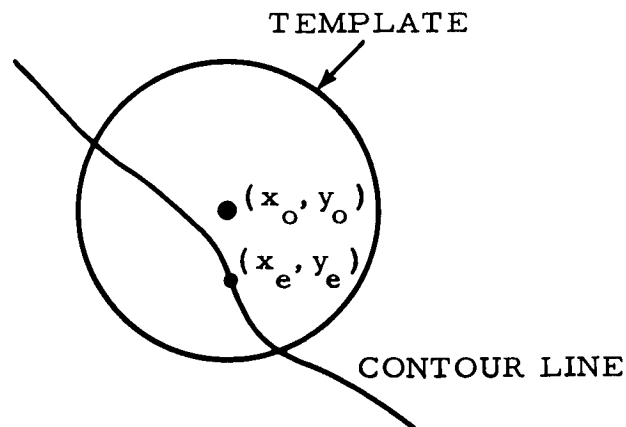
0, 1, of the contour lines. If no contour lines are covered, then it is known that

$$|H(x_1, y_1) - H(x_2, y_2)| < \kappa$$

for any two points (x_1, y_1) , (x_2, y_2) in the set $S(x_0, y_0)$, where $H(x, y)$ is the elevation at the point (x, y) . Thus if we let $\kappa = R \tan \tau^0$, the problem is theoretically solved because any two of the landing pads will correspond to points of $S(x_0, y_0)$ and therefore will not deviate in elevation more than $R \tan \tau^0$. The point x_0, y_0 can be classified as satisfying the slope criteria, and the ratio of the area of points similarly classified to the total area of interest will provide a conservative estimate of the probability of a successful LEM landing regarding the slope criterion. The reason we say conservative is that the centers of discs covering one or more contour lines may actually be safe landing points but these centers would not be allowed in the safe area described above. Thus the conservative estimate of the probability is less than the true probability of safe landing. The above method does not serve as a good practical method because of the high degree of conservatism. If the surface is a smooth plane of angle $< \tau^0$, there still will be contour intervals although perhaps sparse. All points within a distance R of each contour interval would be excluded from the safe region and therefore the probability of safe landing could be estimated by a very low value when the true probability is one.

This unfortunate situation can be remedied by just contouring at $\kappa = \frac{R \tan \tau^0}{2}$ and classifying as safe the centers of discs which cover none or one contour line.

Of course the center of a disc which covers no contour line is safe for the same reasons as before. Suppose the (x_0, y_0) is a center of a disc which covers one contour line.



Let (x_e, y_e) be a point on the covered contour line interior to the disc and $(x_1, y_1), (x_2, y_2)$ be any two points interior to the disc. Then

$$\begin{aligned} |H(x_1, y_1) - H(x_2, y_2)| &\leq |H(x_1, y_1) - H(x_e, y_e)| \\ &\quad + |H(x_2, y_2) - H(x_e, y_e)| \\ |H(x_1, y_1) - H(x_2, y_2)| &\leq \frac{R \tan \tau^0}{2} + \frac{R \tan \tau^0}{2} = R \tan \tau^0 \end{aligned}$$

and it follows that (x_o, y_o) is again a safe landing point.

The foregoing developments can be extended to the typical sampling situations shown in Figures II-1 and II-2, through resort to more intuitive arguments. These sketches are representative of a large proportion of the conditions which one may encounter in the application of the sampling template concept to large scale topographic maps. Where more than one dashed profile line is shown, it is intended to demonstrate a condition of critical importance.

In Figure II-1, for a contour interval $\kappa = \frac{R \tan \tau^0}{2}$:

a. Sketch A-A' shows the template circle uncrossed by any contour line; the maximum elevation difference between any two points (x, y) on the circle perimeter is therefore $\leq \frac{R \tan \tau}{2}$ corresponding to a safe slope.

b. Sketch B-B' shows the template circle crossed by one contour line; the maximum elevation difference between any two points (x, y) on the perimeter is thus $\leq 2 \left(\frac{R \tan \tau}{2} \right)$ corresponding to a safe slope.

c. Sketches C-C' and D-D' show template circles' crossed by two contour lines. The maximum elevation difference in each is $\geq \frac{R \tan \tau}{2}$ $\leq 3 \frac{R \tan \tau}{2}$. If the spacing between lines is $\geq R$, the slope is safe; otherwise it is uncertain. An auxillary 4m circle as shown will serve to distinguish these conditions. C-C' is safe, whereas D-D', ruled uncertain, is actually unsafe as drawn. This could be resolved with certainty only by precision photographic analysis. However this condition would only be unsafe if the landing pads, upon touching down, were oriented with diagonal pairs respectively parallel and normal to the maximum slope gradient and the elevation difference between any adjacent pads is $\geq 2 \frac{R \tan \tau}{2}$. This circumstance might result in the fourth pad being suspended above the ground. The contour spacing for such a condition can be detected by an auxillary 4-m diameter circle. Since there is less than 50 percent probability that such orientation would occur, the condition may be classified safe without strongly biasing results.

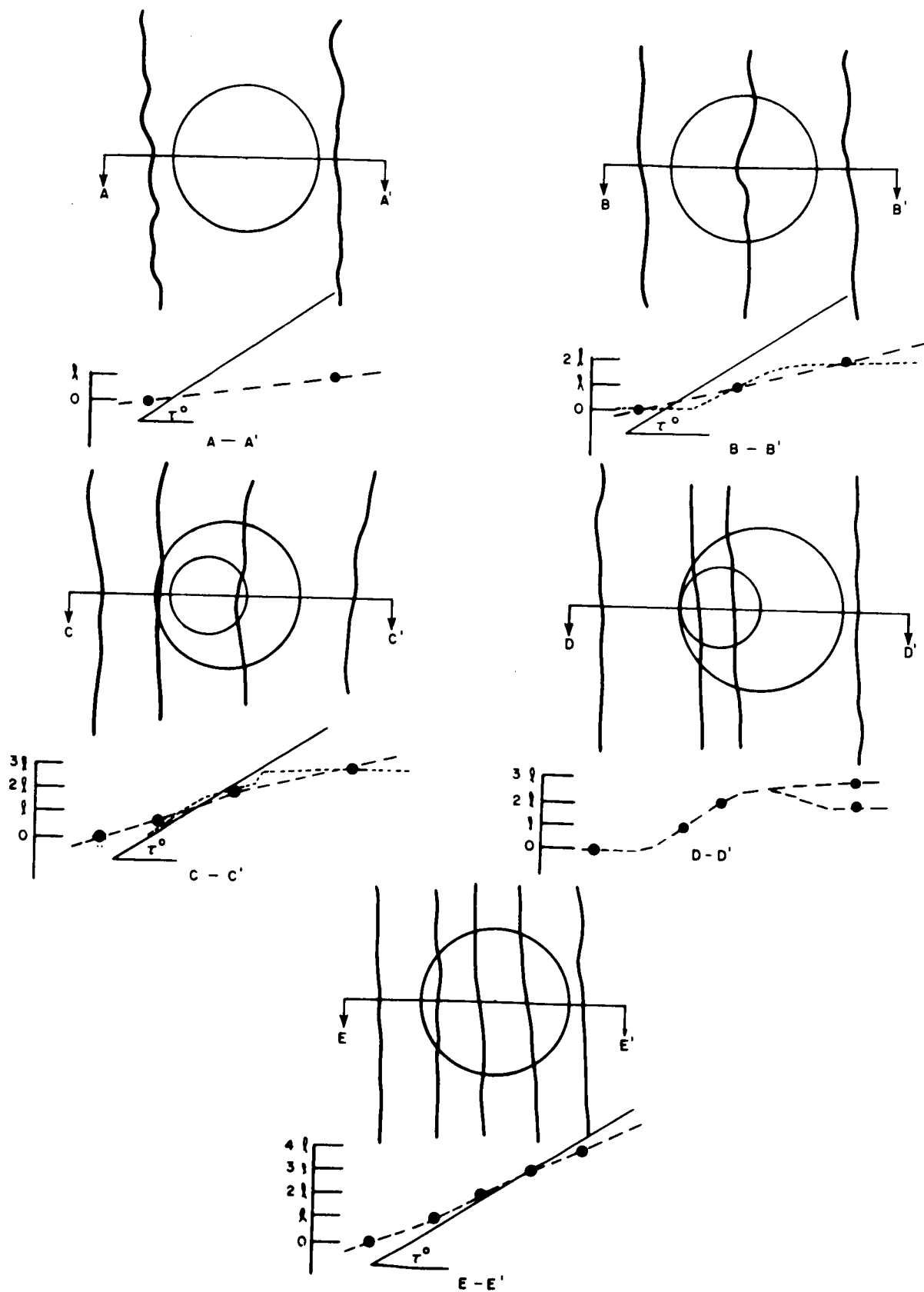


Figure II-1. Template Conditions for a Map with Contour

$$\text{Interval } \kappa = \frac{R \tan \tau}{2} = 0.4158 \text{ m}$$

d. Conditions denoted by three contour lines crossing the 8m circle as shown by section E-E' are also ambiguous. However, if three contour lines cross a 4m circle, the condition is clearly unsafe. If the previous case involving two contour lines crossing an 8m circle is ruled unconditionally safe, all cases involving three lines secant to an 8m circle should be ruled unsafe.

e. When four or more contour lines cross the circle, the minimum elevation difference is greater than $2 R \tan \tau$, thus indicating an unsafe condition.

NOTE: Contour lines in the foregoing discussions are assumed to increase or decrease monotonically. Judgment, care, and common sense must be used in applying these theorems. Cases in which alternating contour lines occur at the same elevations - the "rub-board" condition - are obvious exceptions.

Preparation of accurate lunar topographic maps with this contour interval may be an insurmountable task — it is desirable to relax this specification, if the resultant uncertainty can be resolved by some other means. To this end, the following conditions pertinent to a contour interval, $(0.83 \text{ m}) R \tan \tau^0$, as deduced by the same reasoning employed above are illustrated in Figure II-2:

aa. Sketch A-A'. When no contour lines cross (or touch) the 8-m template circle, the maximum elevation difference between any two points on the circle is less than $R \tan \tau$ corresponding to a safe slope. Areas where physical slopes qualify them in cases a and b above will meet this criterion as well.

bb. Sketch B-B'. When one contour line crosses the template circle, the maximum elevation difference is $< 2 R \tan \tau$. A plane described by three of the four pads could exceed 12° , thus causing an unsafe tilt as well as suspension of one pad above the surface. In the absence of other knowledge concerning the true nature of the surface, such a condition must be classified as uncertain. However, it is shown in subsection II. B-7 that such a condition has an extremely low probability of occurrence.

cc. When two contour lines cross the template, the elevation difference between two points on the template is the range between $R \tan \tau$ and $3 R \tan \tau$. The same argument as that immediately preceding requires this to be considered uncertain; the likelihood of hazard is certainly greater for this condition than that for a single line. An uncertain case and a clearly unsafe condition are shown by sketches C-C' and D-D' respectively.

dd. When three or more contour lines cross the circle, the slope is obviously unsafe. This is shown in sketch E-E'.

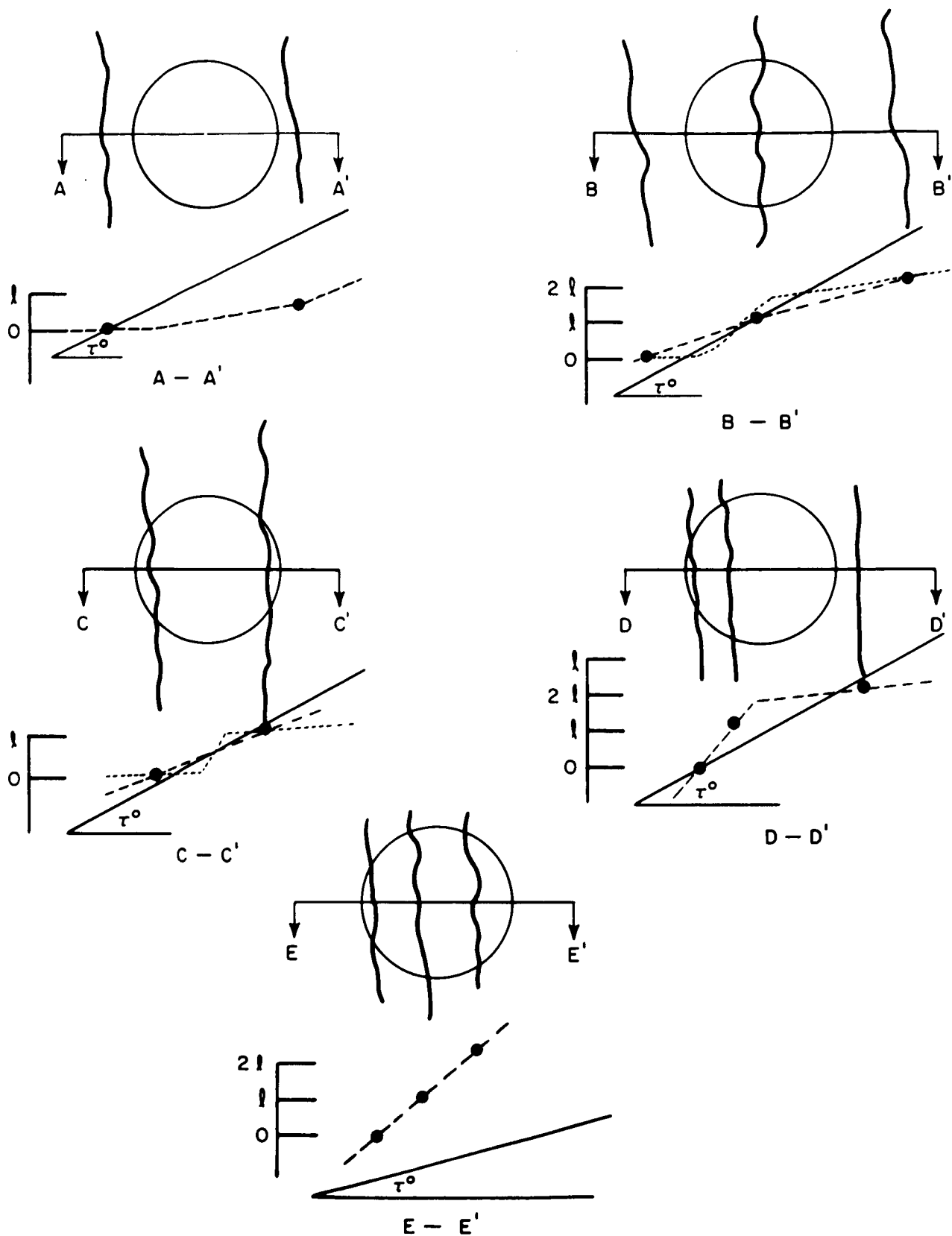


Figure II-2. Template Conditions for Map with Contour Interval $\kappa = R \tan \tau = 0.83 \text{ m}$

According to condition bb, the existence of any contour lines on a map whatsoever will result in a large percentage of the area being classed as uncertain, even if the surface is a smooth monotonic slope of only a few degrees. The only case for which such a condition is actually unsafe is when an inflection point in the profile occurs in the vicinity of the contour line, and the LEM is oriented with opposing pairs of pads respectively parallel and normal to the direction of maximum gradient. On the other hand, there is a much higher likelihood that condition cc is actually unsafe regardless of LEM orientation. In the absence of any better decision criterion, it is proposed that condition bb be ruled safe, and condition cc be ruled unsafe.

Again, referring to condition bb, this is most likely to be an unsafe condition when associated with the rims of shallow craters. The additional knowledge needed to make a stronger decision will be available if the crater outlines are plotted on the maps, or if the contours are closed and roughly circular. An expedient means of producing such maps would be to overprint contours on orthophotographs (maps in this format are commonly produced for tactical military use).

Case cc can be resolved unambiguously if the two contour lines in question are less than the template distance R apart. In this situation, there will be some position of the template for which both lines fall on the same sides of the template center.

Finally, the usual subjective criteria for evaluating terrain slopes from contour maps, such as inference of profile shapes from systematic changes in contour spacings, are valuable aids to mechanical schemes which can be expected to bias the results strongly in the direction of truth. For instance, if the trend of certain contour spacings indicates that a rising slope is flattening near its crest, and the highest contour line in the sequence reflects this trend, it is intuitively correct to assume that abrupt departures from the trend which would cause a large variation between the true and measured slope distributions will not occur between these contour lines.

3. Extraction of Nontipping Landing Probability from a $\kappa = 0.83164$ meter Contour Map

Let T be a given area on such a map. Then, define

$$\text{Probability of a safe} \left. \begin{array}{l} \text{landing in the area T} \end{array} \right\} = \frac{\text{number of times a LEM, dropped at} \\ \text{random into the area T, lands safely}}{\text{number of times the LEM is} \\ \text{dropped into the area T}}$$

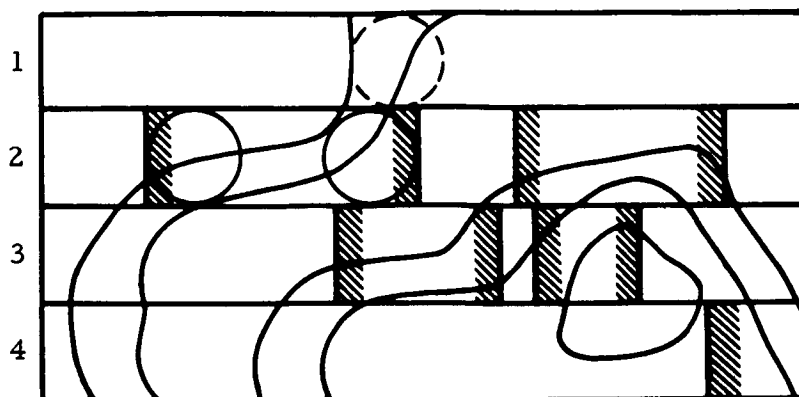


Figure II-3. Application of Template Test to Contour Map with $\kappa = R \tan \tau$

According to this definition, the area into which the LEM is allowed to drop must be specified clearly in advance. If it is found that the LEM has a certain probability of safe landing in a given area T and then, if T is enlarged (or made smaller), the probability of a safe landing in the new area will, in general, be different from that for the original T . The problem now can be formulated exactly: Given an area T on a topographic map where the contour levels are at κ m intervals, what is the probability that the LEM will land without tipping in T ?

In the previous section it was shown that a landing point on a 0.83164-m contour map may be categorized as safe, uncertain, or unsafe, depending on the number of contour lines intersected by a 4-m-radius circle about the point.

<u>Lines</u>	<u>Condition</u>
0	safe
1	slightly uncertain
2 (spacing > R)	uncertain
2 (spacing < R)	unsafe

The following mechanical process serves to determine the probability and illustrates the recommended method for assignment of uncertain conditions, based on intuitive arguments. A transparent circular template is prepared having radius R_m according to the map scale. The center is clearly marked and parallel tangent lines are cut on opposite sides of the circle. Orthogonal sets of grid lines spaced $2R$ apart are drawn on the map, and the template circle is swept across the map between each set of parallel lines. Whenever the template encounters two contour lines within a distance $< R$ apart, (in other words, two lines crossing a common radius between the circle center and perimeter) the leading edge of the template is placed on the leading contour line, and a line is drawn along the trailing tangent line. As long as the template continues to expose three or more contour lines, or two lines which cross a common radius, the vertical line is drawn in. When the trailing edge of the template becomes tangent to the trailing line of a terminal set, a vertical line is drawn along the leading edge of the circle which serves to bound a line of centers through an unsafe region.

When the entire area has been swept over in one direction, the total linear distance swept and the total linear distance blocked out are measured. The estimate of tipping probability is thus

$P_{tip} = \frac{B}{T}$ where B is the distance blackened out and T is the total area sampled.

The vagaries of contour lines make it advisable to perform the test in orthogonal directions. Results of the two independent tests may be combined by the geometric mean of probabilities, $P = \sqrt{P_x \cdot P_y}$.

It is apparent from the dashed circle in row 1 that the average slope defined by the two contour lines crossing the circle is less than 12° because they are more than a distance R apart. It is of course true that some peculiar curve could be fitted through these points, such as a "stairstep" profile, which would pose an unsafe condition, but such a possibility is unlikely.

By extending the limits of unsafe areas at least a distance R beyond the bounding contour lines (and somewhat more where the bounding contour interval is very steep) uncertainty covering the upper or lower limit of the unsafe slope is taken into account. On a slope trending downhill this practice has the effect of including too much in the unsafe area, but in the cases tested the amount of bias was slight. It could be improved by marking the circle diameter instead of an edge. On uphill slopes the procedure is reasonably correct.

4. Impalement

Let T be a specified area and assume that the LEM is going to land somewhere in T . Recall that h is the bottoming height of the LEM. The following parameter for T is required:

$b(h)$ = average number of boulders of height $\geq h$ m per unit area in T .

The following general theorem is pertinent to the impalement problem:

THEOREM I

Let \mathcal{A} be the σ -ring of Borel-measurable sets in some finite-dimensional Euclidean space E^n and let $\mu(A)$ denote the Lebesgue measure of $A \in \mathcal{A}$. Let ξ be a random variable on \mathcal{A} taking only nonnegative integral values, and assume:

- 1) The distribution of $\xi(A)$ depends on only the measure of A .
- 2) $\text{Probability}\{\xi(A) = 0\} \neq 1$
- 3) If $A_1 \cap A_2 = \emptyset$, then $\xi(A_1 \cup A_2) = \xi(A_1) + \xi(A_2)$
- 4) $\lim_{\mu(A) \rightarrow 0} \frac{\text{Prob}\{\xi(A) \geq 1\}}{\text{Prob}\{\xi(A) = 1\}} = 1$

Then,

$$\text{Prob}\{\xi(A) = k\} = e^{-\lambda \cdot \mu(A)} \frac{[\lambda \cdot \mu(A)]^k}{k!}$$

where

$$\lambda = E\left[\xi(A) / \mu(A)\right].$$

This theorem has been proved by L. Takács (1962).

Theorem I is now applied. For each Borel-measurable subset $A \subset T$, let $\xi(A)$ = number of boulders of height $\geq h$ m in A

and define

$$\begin{aligned} \left\{ \begin{array}{l} \text{Probability of non-} \\ \text{impaled landing} \end{array} \right\} &= \left\{ \begin{array}{l} \text{Probability that there is no boulder of} \\ \text{height } \geq h \text{ m in the landing disc } \Delta \end{array} \right\} \\ &= \text{Probability}\{\xi(\Delta) = 0\} \end{aligned}$$

Under the conditions of Theorem I which roughly state that the boulders

are fairly uniformly distributed over the entire T, it follows that

$$\text{Prob } \{ \xi(\Delta) = 0 \} = e^{-b(h) \cdot \mu(\Delta)}$$

In the case of the LEM, $\mu(\Delta) = \pi R^2$

so, $\text{Prob } \{ \text{nonimpaled landing the LEM in T} \} = e^{-\pi R^2 b(h)}$

For the current LEM measurements, $R = 4$ and $h = \frac{1}{2}$, so that

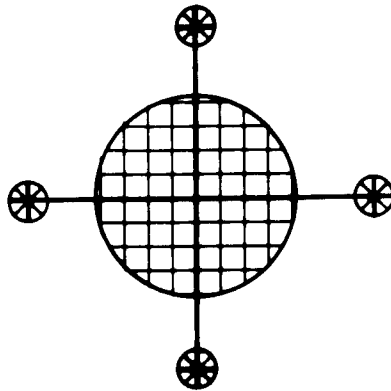
$$\text{Prob } \{ \text{nonimpaled landing for LEM in T} \} = e^{-16\pi b(\frac{1}{2})}$$

Computational Notes

- 1) In determining $b(h)$, which is $E [\xi(A)/\mu(A)]$, the procedure is to sample the given terrain T at random. For each sample A, compute $\xi(A)/\mu(A)$ and then average these ratios.
- 2) Count only boulders of height $\geq h$ m to κ m where κ is the contour interval used on the terrain map. The larger boulders automatically are accounted for in the contour lines. In particular, for the current LEM and the above specified contour map, only boulders of height $\frac{1}{2}$ m to 0.83 m should be counted.
- 3) As remarks 1) and 2) show, one can define $b(h)$ to be the number of protuberances of height $\geq h$ m per unit area in T and the analysis goes through exactly as before. Basically, one counts only those significant altitudes or depressions in $b(h)$ that are too small to merit a contour line on the map.

The above probability of nonimpaled landing in T is fairly conservative, as shown in the following diagram:

The landing configuration is



It is the body circle that is relevant, not the circle formed by the landing pads. Nevertheless, the body circle has been taken to be R m. Clearly, the smaller the body radius, the larger the probability of non-impaled landing.

5. Derivation and Application of "Confidence" in Safe Landing Probability Estimation

THEOREM II

Let μ be the Lebesgue measure in E^n and let $B \subset E^n$ be a fixed measurable set of finite positive measure. Let φ be a measurable real-valued function on B and let r be any fixed real number. Let

$$|\varphi \geq r| = \{x \in B \mid \varphi(x) \geq r\} \subset B$$

and assume that $\mu(|\varphi \geq r|) \neq \mu(B)$.

Choose any real number β , $0 < \beta < 1$, and let

$$N = \frac{\log(1 - \beta)}{\log \mu(|\varphi \geq r|) - \log \mu(B)}$$

Finally, let $|N|$ be the smallest integer larger than N . Then, in a random sample of $|N|$ points of B , the probability that at least one of them is NOT in $|\varphi \geq r|$ is greater than or equal to β .

PROOF

One has

$$\text{Prob} \{x \in |\varphi \geq r|\} = \frac{\mu(|\varphi \geq r|)}{\mu(B)} = P$$

The probability that in a random sample of M points, all of them belong to $[\varphi \geq r]$ is P^M . The probability that at least one of them is NOT in $[\varphi \geq r]$ is, therefore, $1 - P^M$. Since $P^M \rightarrow 0$ as $M \rightarrow \infty$, there is a value N such that $\beta = 1 - P^N$; then, $P^N = 1 - \beta$ so $N = \log(1 - \beta) / \log P$. Using the integer $[N]$, one finds $1 - P^{[N]} \geq \beta$, and the proof is complete.

In the mechanical process shown, let the blackened region be devoted by B . If the linear measure of B is taken as a valid estimate of all parallel sweeps in a zone bounded by $\pm R$, then the area denoted by B is a valid estimate of the unsafe area in that zone. Thus the region B can be taken to have the following significance:

Let $a(x)$ denote the altitude at the point x and, for each $x_0 \in T$,
let

$$\varphi(x_0) = \max \{ |a(y) - a(x_0)| \mid \text{all } y \text{ at a distance } \geq R \text{ m to } x_0 \}$$

Then, the black region B is exactly

$$B = \{ x \in T \mid \varphi(x) \geq 2 \kappa \} = \varphi \geq \kappa$$

Theorem II now can be applied. If $0 < \beta < 1$ is any given real number and if

$$N = \log(1 - \beta) / [\log \mu(B) - \log \mu(T)]$$

there is then a probability β that in $[N]$ landings one of them will not be centered at a point of $B = \varphi \geq \kappa$ (that is, one of them will be nontipping).

The factor β is defined to be the "confidence" of a safe landing in these $[N]$ trials. Therefore it is seen that, with confidence β , the probability of a nontipping landing in the area T is

$$\frac{1}{N} = \frac{\log \mu(B) - \log \mu(T)}{\log(1 - \beta)}$$

Since a safe landing is by definition a nontipping and nonimpaled landing, it is determined that:

With confidence β , the probability of a safe landing in a given area T is

$$P = \frac{\log \mu(B) - \log \mu(T)}{\log(1 - \beta)} \cdot e^{-\pi R^2 b(h)}$$

Using the measurements of the LEM given in subsection B.1, this formula is

$$P = \frac{\log \mu(B) - \log \mu(T)}{\log(1 - \beta)} e^{-16 \pi \cdot b(\frac{1}{2})}$$

For example, using the measurements of the LEM given in subsection B.1, assume that

$$b(\frac{1}{2}) = 1/16 \pi \text{ and } \mu(B) = \frac{1}{2} \mu(T) \text{ for a given area } T.$$

Then,

- With confidence $\beta = \frac{1}{2} = 50$ percent, the probability of a safe landing in T is

$$\frac{\log \frac{1}{2}}{\log \frac{1}{2}} e^{-1} = 0.36$$

- With confidence $\beta = 3/4 = 75$ percent, the probability is 0.18
- With confidence $\beta = 1/4 = 25$ percent, the probability is 0.88

One can introduce refinements in the above formula for P by considering that a boulder of sufficient height to tip the LEM may appear under a landing pad, even on flat ground. This has not been done in the analysis, since it appears that the above probabilities already are fairly conservative.

6. Use of the Above Results to Partition Maps

Suppose it is decided in advance that one wants landings to have a probability P (for example, $P = 0.90$) of being safe. Then, one can assign to any given region T the confidence with which this probability is assured. This will be

$$\beta = 1 - e^{\frac{1}{P} [\log_e \mu(B) - \log_e \mu(T)] \cdot e^{-\pi R^2 b(h)}}$$

For example, assume it is decided one wants $P = 0.90$ always. Then, in the example of subsection B.5, the confidence in the region T would be

$$\beta = 1 - e^{\frac{+1}{.9} \left[\log_e \frac{1}{2} \right] e^{-1}} = 0.24$$

Once one decides on the a priori P , then he can carve up a map as follows:

Given any point x_0 of the map, let T_{x_0} be the region of possible landing when the LEM is pointed at x_0 (for example, T_{x_0} may be the CEP with center x_0). Using the area T_{x_0} , compute the confidence $\beta(x_0)$ for T_{x_0} . In this way, a function $\beta(x)$ defined at each point of the map is obtained. For each point x , the number $\beta(x)$ is the confidence that there will be a proportion P of safe landings when the LEM is directed toward x . Now, one can partition the map according to the values of $\beta(x)$; for example, the map may be divided into the ten regions

$$T_n = \{x \mid \frac{n}{10} < \beta(x) < \frac{n+1}{10}\}, \quad n = 0, 1, \dots, 9$$

where, of course, some of the T_n may be empty.

If the blacking-out process described in subsection B.3 is first performed on the entire map, then the function $\beta(x)$ can be obtained easily as follows: If B is the black region, then

$$\beta(x) = 1 - e^{\frac{1}{P} \left[\log_e \mu(B \cap T_x) \right]} e^{-\pi R^2 b(h)}$$

7. Use of Different Contour Intervals and Probability of Tipping When One Contour Line is Exposed

The process given in B.3 is based on using a map with the contour interval $\kappa = R \sin \tau$, so that $\kappa = 0.83164$ in for the current version of the LEM. The effect of using larger contour intervals and the probability of tipping when a single contour line is exposed on a 0.83164-m C. I. map, will be considered here. (The considerations will be almost entirely heuristic; however, they do lead to a fairly reasonable formula that indicates the deterioration in the confidence of a nontipping landing with increasing contour interval.)

It is now evident that even if one or less contour line is exposed, a tipping landing may be possible. It is the probability of this latter event that is to be estimated.

Let ℓ be the map contour interval. Since the circle cuts at most one-contour line, a sectional view of the terrain along a diameter of

the template would give a curve $y(t)$ such as



which is defined in $0 \leq t \leq 2R$ and satisfies $0 \leq y(t) \leq 2l$ in that interval.

Now, let Y be the set of all absolutely continuous real-valued functions defined in $[0, 2R]$ such that $y(0) \in [0, 2l]$ and $y(2R) \in [0, 2l]$. Because the following considerations will be heuristic, it shall not be required that the curve satisfy $0 \leq y(t) \leq 2l$ in the interval $[0, 2R]$, so that the big peaks and troughs are allowed.

For any $y \in Y$, the average slope is

$$y'_{av} = \frac{1}{2R} \int_0^{2R} y'(t) dt = \frac{y(2R) - y(0)}{2R}$$

so that

$$\left(y'_{av} \right)^2 = \left[\frac{y(2R) - y(0)}{2R} \right]^2$$

Now, assume that $y(0)$ and $y(2R)$ each are independently, uniformly distributed in $[0, 2l]$; then, for the ensemble average over Y one finds

$$\overline{y'_{av}} = 0$$

$$\overline{y'_{av}^2} = \frac{1}{(2R)^2} \int_0^{2l} \int_0^{2l} (\xi - \zeta)^2 \frac{d\xi}{2l} \cdot \frac{d\zeta}{2l} = \frac{l^2}{6R^2}$$

Now, consider the random variable $|y'_{av}|$ on ξ . Because the value is always non-negative, it is fairly reasonable to assume that $|y'_{av}|$ has the Rayleigh distribution.

$$P(r) = \frac{r}{\sigma^2} e^{-r^2/2\sigma^2}$$

so that

$$\text{Prob}(r \geq \xi) = e^{-\xi^2/2\sigma^2}$$

where

$$2\sigma^2 = \text{second moment of } |y'_{av}| = \overline{(y'_{av})^2} = \ell^2/6R^2$$

Finally, assume that the LEM can effect a nontipping landing whenever $|y'_{av}| \leq \tan \tau$. Then,

$$\begin{aligned} Q = \text{Prob} \left\{ \begin{array}{l} \text{tipping when at most} \\ \text{one-contour line is} \\ \text{exposed by template} \end{array} \right\} &= \text{Prob}\{|y'_{av}| \geq \tan \tau\} \\ &= \exp\left(\frac{-6R^2 \tan^2 \tau}{\ell^2}\right) \end{aligned}$$

which is a rough estimate and neglects the fact that the curve will not peak above the level 2ℓ nor drop below the level 0 in a properly constructed contour map.

This formula for Q does show that as the contour interval is increased, the confidence in nontipping (when the template crosses at most one-contour lines) decreases fairly rapidly at first and then, for large values of ℓ , becomes relatively insensitive to further increases.

Using this formula with the LEM measurements so that $R = 4$ and $\tau = 12^\circ$, one obtains

$$Q = \exp -4.337/\ell^2$$

In case ℓ is the contour interval 0.83164 m, one obtains $Q = e^{-6} \approx 0.002$ which is not too far removed from the correct value, zero. Thus, despite the assumptions made in obtaining the formula, nevertheless it is a fairly reasonable (and conservative) value for the probability of tipping in the known case.

If $\ell = 1$ m, one finds $Q = e^{-4.337} \approx 0.01$ and, if $\ell = 10$ m, then $Q \approx 0.97$.

By using the above formula for Q , one can obtain a probability of a safe landing in a given area T when the contour map is assumed to have contour interval ℓ . In fact, using the mechanical process (described in subsection B.3) on the given map, the formula for the probability of a safe landing in the area T with confidence β becomes

$$P \cdot (1 - Q)$$

and then, in the formula of subsection B.5, for β , the entire exponent is multiplied by $(1 - Q)$.

8. Map Inaccuracy

To consider possible inaccuracies in the position of the contour lines on a given 0.83 m contour map, the circular template might consist of a clear circle C of radius $(R + 2)$ m (according to the map scale) on which is drawn a smaller concentric circle c of radius R m. Then, when the larger circle C covers not more than one contour line, the LEM can land safely in the smaller circle c . In the blacking out process discussed in subsection B.3, the small circle is swept through the map and the small circle diameters are drawn in whenever the large circle covers two or more contour lines.

In cases where the criterion for an unsafe area is that two contour lines cross the template circle within a distance Δx less than R apart, an additional distance $R + (R - \Delta x)$ is added in the scan direction to account for the possibility of abrupt slope change near the next contour level. Since this provides a quite conservative measure of safe landing probability, a circle of radius $(R + 2)$ m was not adopted for the map example tested.

C. FIELD EXPERIMENTS AND DATA ANALYSIS

1. Topographic Map and Aerial Photograph Requirements

a. Site Selection Criteria

Ideally, tests of this system should be conducted for terrain surfaces which meet the following criteria:

- Existence of slopes ranging from level to more than 12° , measured at the scale of the LEM
- Surface conditions ranging from smooth bare soil to boulders of heights exceeding the 50-cm criterion
- Accessibility for field checking and verification
- Map coverage at scales and contour intervals adequate to measure 12° slopes from trough to crest within an 8-m distance, if present
- Recent aerial photographic coverage at a scale large enough to identify boulders and other surface irregularities somewhat smaller than the contour interval (down to about 40 cm in order to assure high confidence in identification of all 50-cm bumps)

These conditions proved virtually impossible to fulfill in a single area within the limitations of existing map and photo coverage. Consequently, the work reported in this section is a composite approach to field testing.

b. Map Scale Selection

The 0.83-m contour interval specification derived in Section B effectively limits the range of horizontal scales which can be adopted for the map format. If a small scale is used, an impossibly complex bunching of contour lines will result and significant errors may be introduced by inaccuracies in the template circle, the finite width of contour lines and instability in the cartographic base material. On the other hand, if a convenient working scale is adopted to minimize these sources of error, the resulting map for an entire landing site will be extraordinarily large. A compromise, therefore, must be adopted in order to use the desired contour interval, produce a map of manageable dimensions, and yet cover a large enough area so that significant testing can be undertaken.

A scale of 1 in. = 50 ft (or 1:600) proved satisfactory for those areas which were mapped in the field. At this scale, the template diameter was 0.584 in. Even at this scale, coverage of an entire landing

site results in an exceedingly large map; consequently, the demonstration areas mapped were somewhat smaller.

c. Acquisition of Aerial Photographs

Existent large-scale aerial photographs were sought for desert and semiarid regions which would illustrate the various surface phenomena described in paragraph C. 1. a. and which could be mapped at appropriate scale and contour interval by ground methods if suitable contour maps were not available. The index map and photo files of the U.S. Geological Survey, Map Distribution Branch, Washington, D.C., were searched with no success and several commercial concerns contacted in Los Angeles were unable to provide the desired large-scale data from their open files. Finally, photo coverage at a scale of 1:600 was obtained through the State of California, Division of Highways, for two sites which afforded the desired ranges of slopes, surface features and accessibility.

The photographs available were of areas that necessarily had a major road or highway and where the terrain generally would permit economical road construction. Furthermore, it was necessary to select areas that had been flown within the past year or two. Otherwise, modification of the topography by erosion and deposition would not have permitted valid comparison with the topographic maps prepared in 1965. For example, extremely good photographs of an ideal area of dunes and alluvial fans in Death Valley as well as some superb dunes and a boulder-strewn dry-wash area in the Colorado Desert could not be utilized because both areas had been flown 8 or 10 years previously. Previous experience on these areas has shown that dune migration and the effects of desert floods are capable of changing the configuration of the areas and the distribution of "bottoming hazards" to such a degree that photointerpretation techniques related to the prepared maps could not be undertaken.

Four sets of photography flown at the Pisgah lava flows in the Mojave Desert, Southern California, were obtained at a scale 1:2500, 1:3700, 1:7300, and 1:20000. Attempts to map protuberances by photointerpretation techniques were disappointing because the complexity of the flow surface which generally does not allow one to separate discrete features at the scale of interest. Of course, even at the largest scale 1:2500, a 25-in. diameter boulder appears only 0.01-in. wide. The problem was compounded by the generally low highlights and poor contrast over the roughest portions of the area, especially on the smaller scale photography. Radial lens distortion also was apparent in the largest scale photographs. A reconnaissance of the site showed conclusively that detailed ground mapping was virtually impossible; even with close-up inspection the coalescing, tortuous and fractured character of the surface materials defied identification of discrete protuberances in many instances. In effect, one would designate areal patches of bottoming hazards rather than point locations.

2. Field Mapping and Testing

a. Contour Mapping Techniques

Two areas were selected that appeared appropriate and for which photo coverage of recent vintage could be obtained. These areas were the Neenach Ranch area (paragraph C.3.a), which is traversed by a dry wash, and the Covina Knolls (paragraph C.3.6), an area of rolling hills and mature dissection. The chosen areas were mapped at a scale of 1 in. = 50 ft by the plane table method, using the alidade and stadia rod. Surveyed points were plotted directly on the map in the field, permitting the most economic distribution of effort. Weather conditions during the survey were far from ideal: there were winds of 30 knots and heat-induced refraction effects that limited long sights. By keeping individual sight lines under a maximum of 300 yd and usually considerably less, a high degree of accuracy in both position and elevation were maintained. Particular emphasis was placed on the definitions of slopes, minor topographic relief features and the occurrence of boulders and depressions which would prove troublesome to hypothetical LEM landings. Field maps were returned to the office, were carefully recontoured and final-inked maps prepared.

b. Additional Map Coverage

In addition to the two topographic maps acquired by field methods, other map coverage at usable scales and contour intervals were obtained. These included four areas in the Pisgah lava flow, California, measuring 1000-ft square which were mapped by photogrammetric techniques by Aero Service Corporation for the Space Systems Division, North American Aviation Incorporated, Downey, California. These areas are shown in Plates I through IV. Also tested was a map of the Ranger VII impact area prepared for NASA by the Astrogeology Branch, U.S. Geological Survey, by photometric techniques (Plate V).

c. Slope Classification Measurements

Determination of average slope on topographic maps has been examined by several investigators. Probably the most familiar technique is that of Wentworth (1930). In this simplified method of determining the average slope of land surfaces, an accuracy may be obtained up to the limit of the map. The Wentworth system consists of the following steps:

- 1) Lay out an east-west, north-south grid of not less than 3 lines each way and of such size as to involve not less than 100 to 200 contour intersections

- 2) Count all crossings and tabulate, thus, determining the average number of crossings per mile
- 3) Repeat the first two steps with an oblique grid, covering substantially the same area
- 4) Average the results and divide the product of the contour crossings per mile and the contour interval in feet by the constant 3361 (which is 5280 x the mean value of the sin θ)
- 5) Determine the tangent of the average slope of declivity using the equation:

$$\frac{I \times M}{K}$$

I = contour interval
 where M = average number of crossings
 per mile
 K = 5280 x mean value of sin θ = 3361

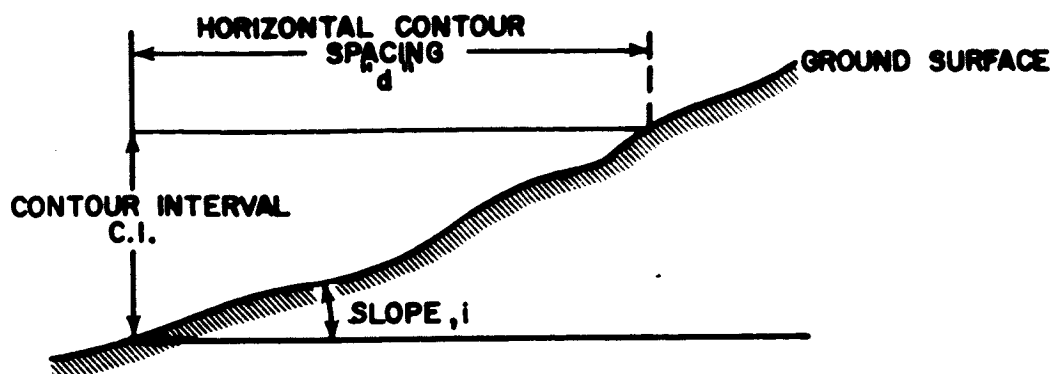
Wood and Snell (1959) applied the Wentworth system to arrive at the average slope angle, but made random traverses rather than applying a grid system to determine the number of contours crossed per mile. A third method is that of Finsterwalder (1890) whose approach was to determine the average slope by multiplying the sum of the total lengths of contour lines contained in a given area by the contour interval (reduced to like units) and dividing by the map area under study.

All of these methods are useful tools, but in this particular application a restricted range of slopes, greater or less than 12° , is the major concern. Furthermore, the noted analyses were developed for small-scale maps with measurements made in miles; whereas, in this study, large-scale maps of restricted areas are considered.

Three classes of slopes are recognized on the slope maps (Plates VI and VII), namely:

- Slopes less than 6°
- Slopes between 6° and 12°
- Slopes in excess of 12°

Classes of slopes were determined for the Neenach Ranch and Covina Knolls topographic maps (Plates VI and VII) in order to eliminate from detailed consideration areas which were obviously unsuitable. This was accomplished by determining the contour line spacings according to the following relations:



A contour interval of 2.7 ft (0.83 m) was applied for area A, Neenach Ranch; whereas, a contour interval of 2.5 ft was utilized in area B, Covina Knolls. The latter contour interval resulted by mistake, but its use in the steeper terrain at this site is slightly conservative. The limits in the computation are presented on the following chart.

Slope i	$\tan i$	d (Neenach) CI = 2.7 ft	d (Covina) CI = 2.5 ft
6°	0.1051	25.68 ft	23.78 ft
12°	0.2126	12.69 ft	11.76 ft

On these two plates, slopes less than 6° are plain, areas with slopes between 6° and 12° are shaded and those areas in which the slopes are in excess of 12° are cross-hatched. A cursory examination of the maps permits a rapid evaluation of areas which are totally unsuitable for LEM landings and for areas which are suitable (in terms of slopes) for potential landings.

d. Detailed Tests of Landing Probability

Areas which contained 6° - 12° slopes, and flatter areas bounding those having slopes greater than 12° were tested against the LEM effective slope criterion. For each of the maps a template consisting of an inked circle on transparent acetate film was prepared, and three sides of a bounding square were cut tangent to the circle, in order to facilitate marking of the maps.

Slope zones greater than 12° were obvious, but adjacent transitional areas in which the LEM could assume an unsafe attitude, either by landing with only three pads touching the surface, had to be defined. It was also required to map in more detail those areas within the 6° - 12° zones which, by virtue of closely spaced contours exceeded 12° , or were transitional to areas the slopes of which exceeded 12° .

The process used for accomplishing this deviated from that employing parallel scan zones, in that movement of the template circle followed contours which bounded clearly unsafe areas. In some instances areas interior to the 6 - 12° zones were tested, also by moving the circle tangent to selected contours. Boundaries of unsafe areas were marked tangent to the circle as previously discussed; i. e., whenever two contour lines fell within the circle on the same side of the center point, or when the circle crossed three contour lines. These criteria serve to bound safe/unsafe zones in up- and down-slope directions. Lateral limits — where close contour lines widen sufficiently to indicate slopes flatter than 12° — were established by marking a circle diameter approximately normal to the contours at locations where the lateral transitions occurred.

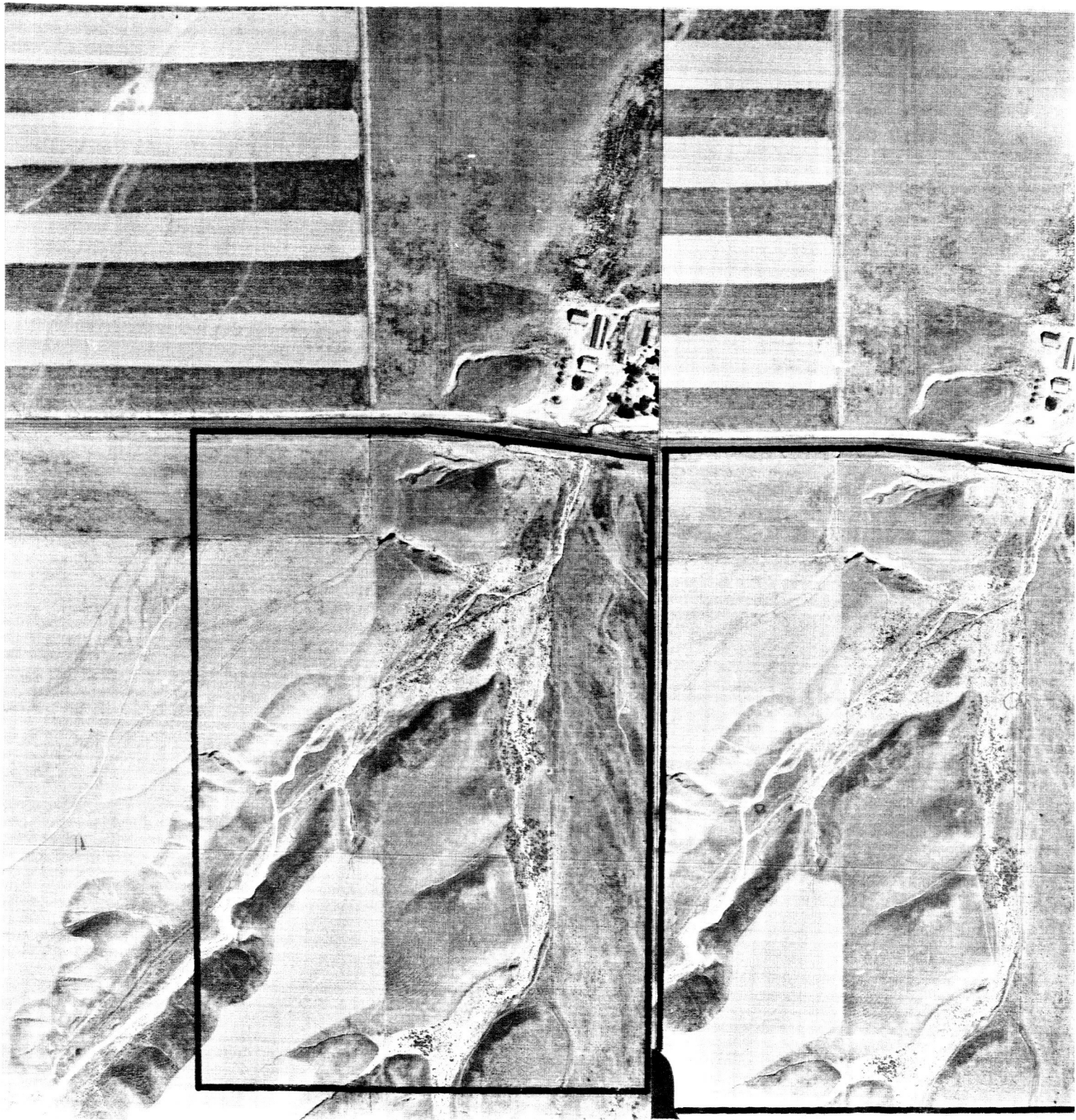
3. Area Descriptions and Test Results

a. Neenach Ranch, California

The Neenach Ranch area was the first of two areas in Southern California selected for detailed topographic mapping (Plate VI) to permit testing of the landing site analysis system. This particular area was chosen because of the topographic character of the terrain as well as the availability of high-quality aerial photographic coverage. The terrain is a dissected alluvial fan dry-wash complex with a considerable range of slopes. The lines of both a projected freeway and the Feather River aqueduct fall close to the surveyed area; thus, very large scale aerial photographs were available. A stereo set of three air photos (ASC-587), 1-2, 1-3 and 1-4, at a scale of 1:6000 was obtained and is shown in stereogram form as Figure II-1.

1) Location and General Setting

The mapped area shown in Figure II-2 is 60 mi northwest of Los Angeles and approximately 8 mi west of Gorman, the closest town. It is on the southern slope of the Antelope Valley, the extreme western extension of the Mojave Desert, between the San Gabriel and Tehachapi Mountains. The San Andreas Fault runs in a northwest-southeast direction



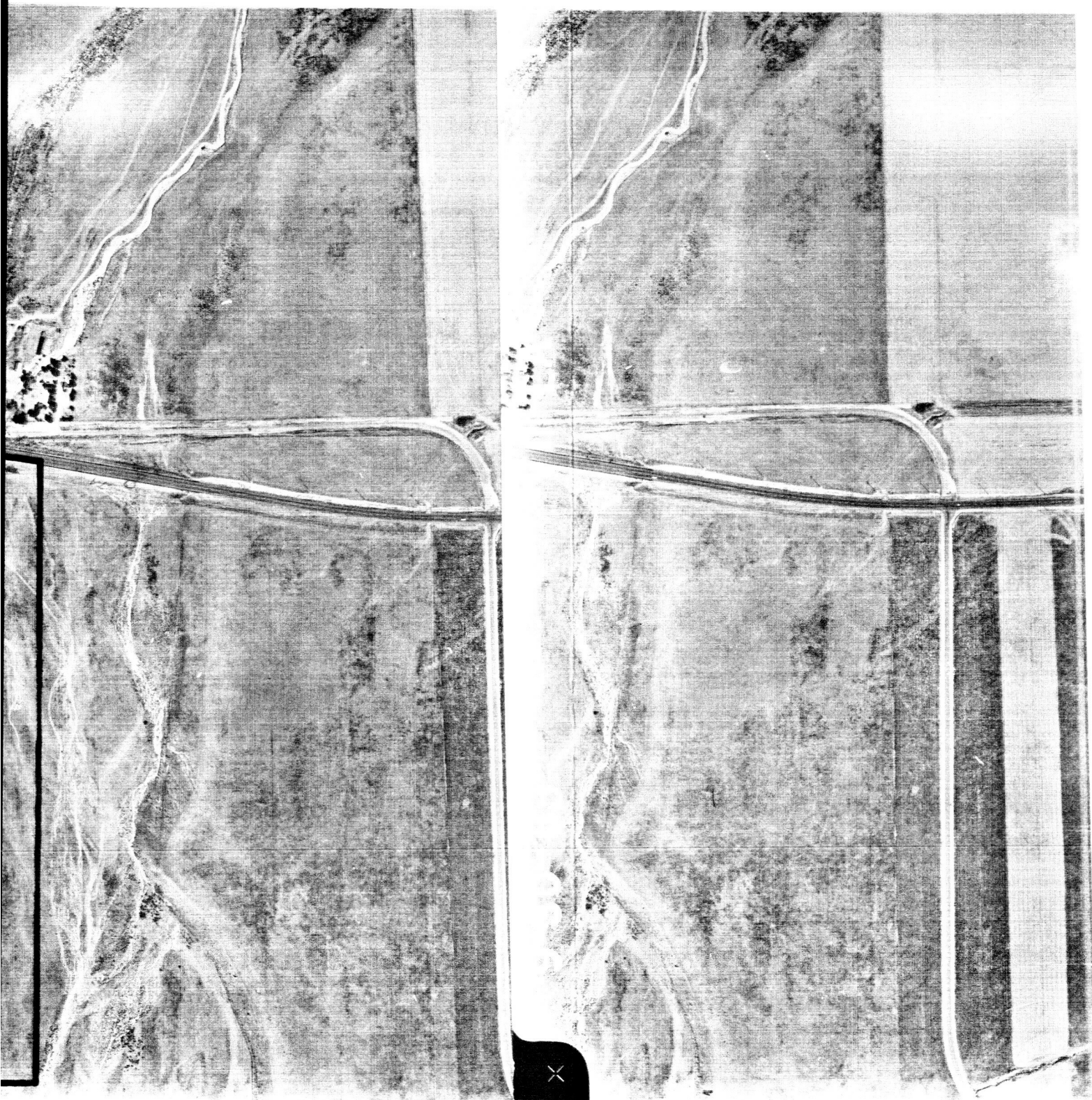


Figure II-4. Stereogram of Neenach Ranch Test Area

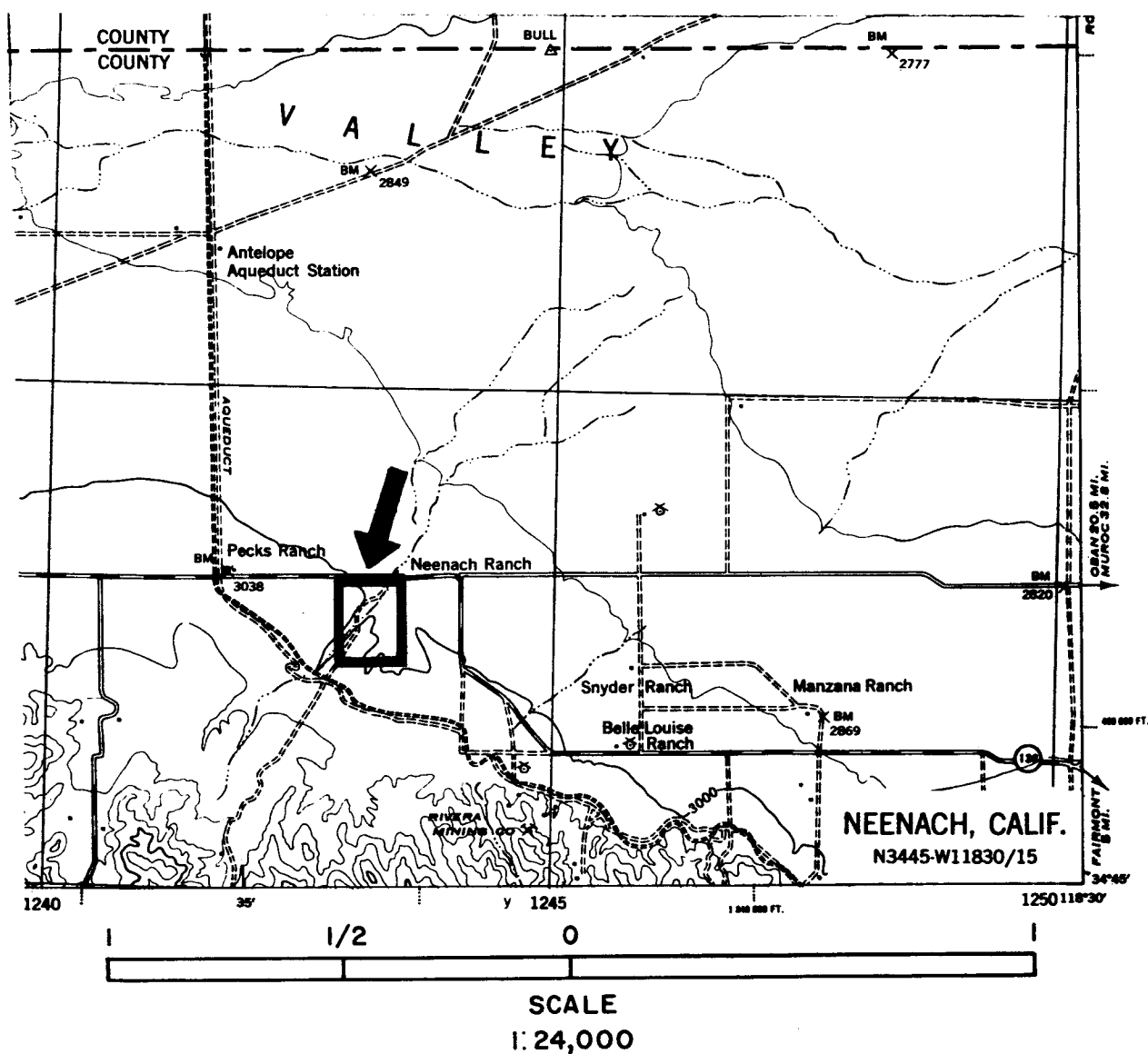


Figure II-5. Location Map, Neenach Ranch Test Area, Neenach Quadrangle, 15-Min Series (California)

less than 2 mi south of the mapped area. California State Highway 138 forms the northern limit of the survey area and permits ready access.

2) Geology and Topography

Two generations of fluvial deposition and erosion created the geologic formations which directly influence the topography in the area of study. The hills consist of a Late Pleistocene Early Recent continental deposit of poorly consolidated sands and gravels. Both the composition of the material and its obvious slight dip away from the nearby mountain front suggest its local derivation as an alluvial fan from the Western San Gabriels. The valleys and dry washes are filled with a contemporary generation of alluvium, probably all reworked from the surrounding older material.

3) Discussion of Test

The Neenach area map (Plate VI) is at a horizontal scale of 1 in. = 15.24 m (1 in. = 50 ft) and is contoured at 0.828 m or 2.74 ft. A testing template of a radius of 0.62 in. and a diameter of 0.584 in. was used to perform the testing. Areas unsuitable for LEM landings are outlined by a shaded border. Ridges along the dry wash, which trends diagonally across the map, are excessively steep for safe landings; whereas, the zones of low relief and gentler slopes bordering the wash, as well as itself, are acceptable landing sites.

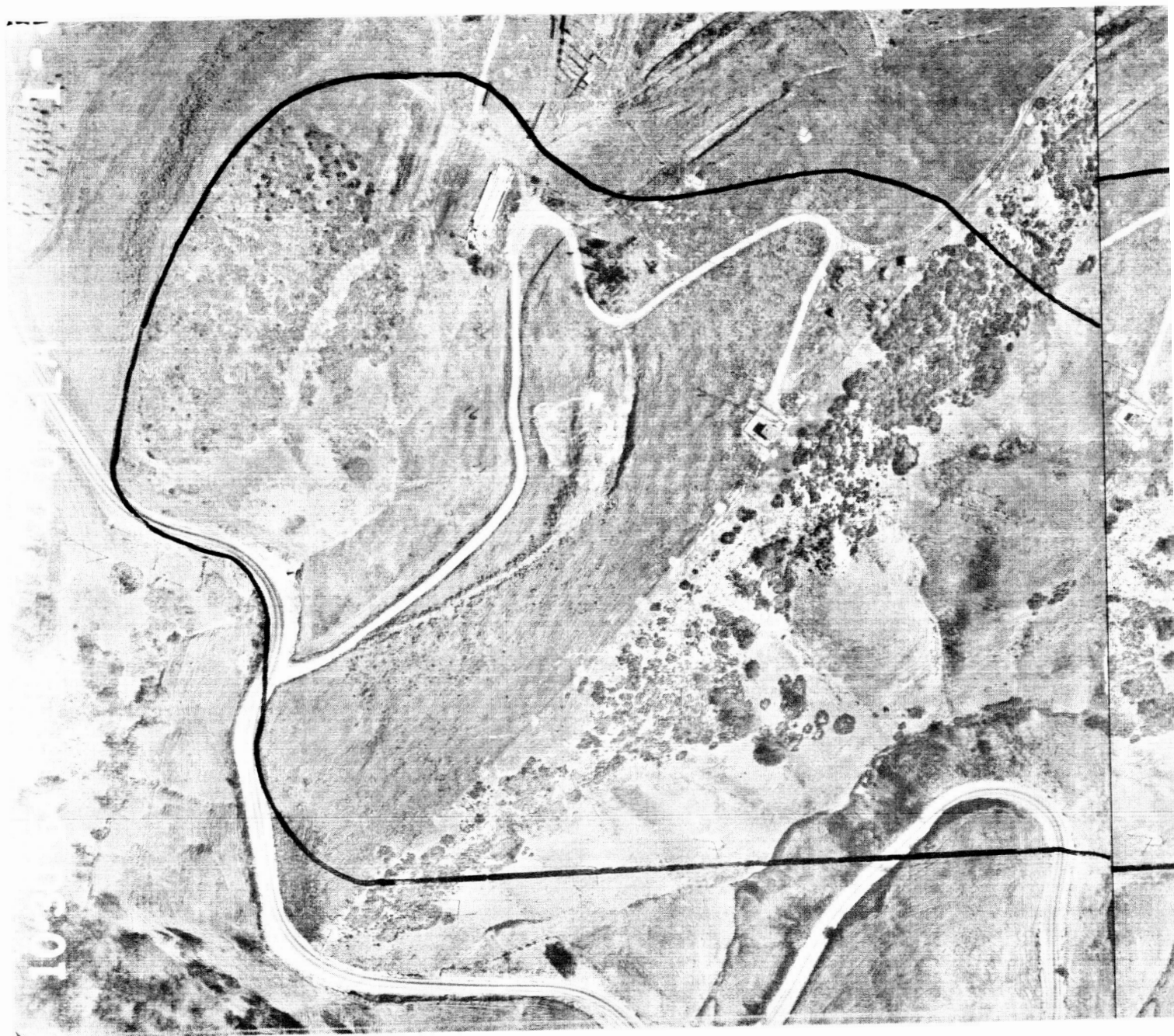
The mapped area is considered to be a random sample of this terrain type discussed. The probability of safe landing based on slopes which do not exceed 12° in the Neenach Ranch test area is 0.80.

b. Covina Knolls, California

A portion of the Covina Knolls of Southern California was the second area for which a detailed topographic map was prepared by plane-table mapping (Plate VII). Large-scale photographs, scale 1:3000, with stereo coverage (ASC-648-38) were obtained. Of the series of photographs available, 1-1, 1-2 and 1-3 were utilized and are shown as a stereogram in Figure II-3. This area was selected because, although some LEM landings may be accomplished successfully, the presence of many slopes in excess of 12° provides a strong contrast to the Neenach Ranch site.

1) Location and General Setting

The Covina Knolls are a portion of the San Jose Hills, a minor topographic high rising above the alluvial plains of the Los Angeles Basin. A location map is shown as Figure II-4. The Knolls are approximately 30 mi east of Los Angeles and are readily accessible by means of U.S. Highway 99.



31

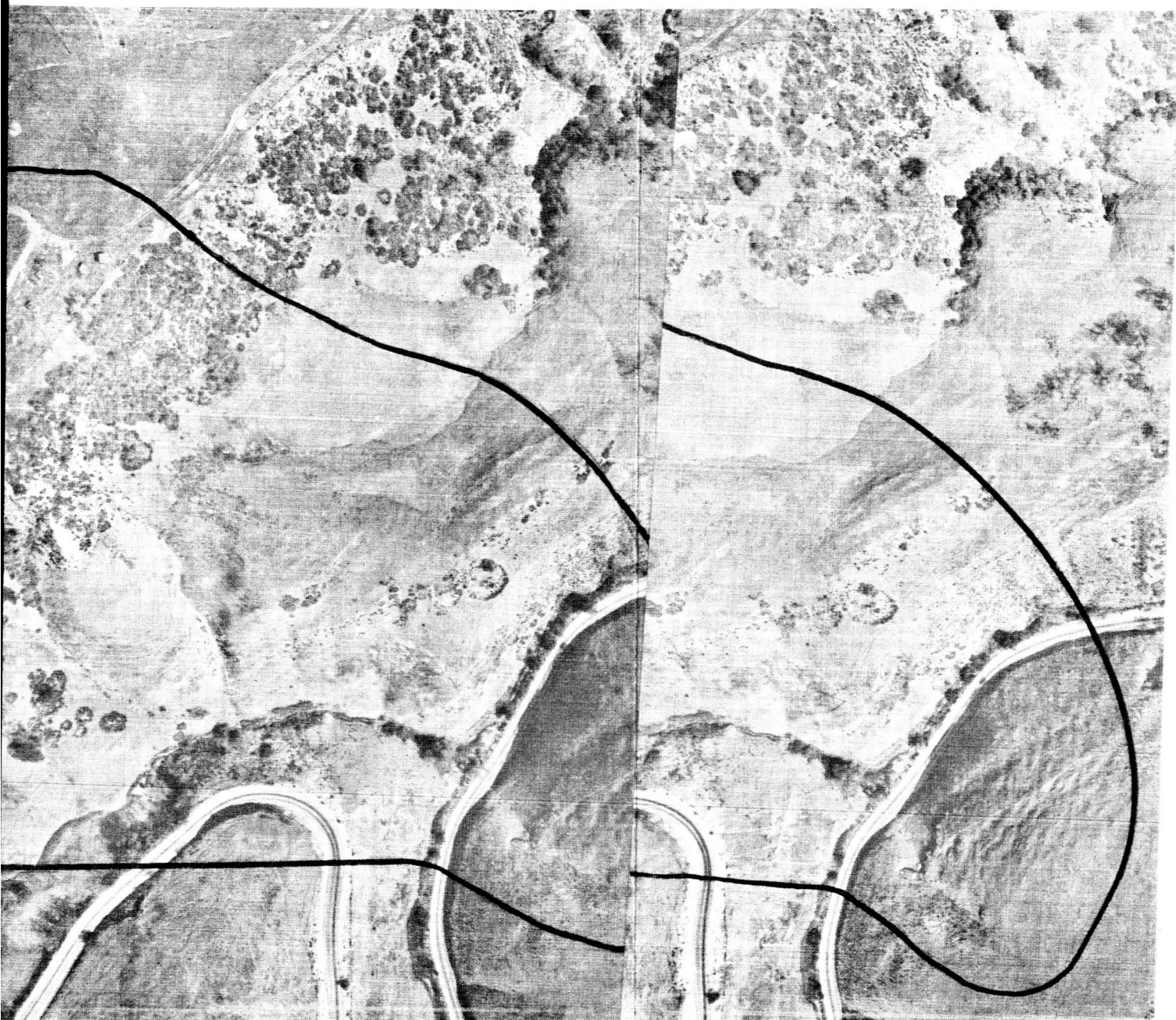


Figure II-6. Stereogram of Covina Knolls Test Area

2) Geology and Topography

The Covina Knolls are predominantly folded marine sedimentary rocks of Miocene and Pliocene age. In the surveyed area, the surface rocks principally are shales and sandy shales with lesser amounts of sandstone, conglomerate (locally called "puddingstone") and siliceous shales and diatomite. Where sandstone or conglomerate crop out, bold cliffs have formed due to the greater resistance of these rocks than the more prevalent shaley beds.

Maturely eroded low-rounded hills and intervening rounded gulleys typify the area. The terrain largely consists of slopes and relief is highly variable. The rocks are dipping about 12° in a northerly direction. Almost all of the topography has been formed by stream erosion, although rainwash and rillwash have contributed to landform development. On some of the steeper slopes, gravity slumping and hillside creep also have contributed to shaping the topography. The mapped area is considered to be a random sample of this terrain type discussed. The probability of safe landing based on slopes which do not exceed 12° in the Covina Knolls test area is 0.078.

3) Discussion of Tests

Template tests were made on the Covina Knolls map which was prepared at a scale of 1 in. = 15.24 m and contoured at 0.81 m. A template diameter of 0.584 in. was used to perform the testing. Almost the entire area is composed of excessively steep slopes, making the bulk of the area unacceptable for LEM landing sites. However, the system did resolve several restricted areas where safe landings could be made.

c. Pisgah Lava Field

1) Location and General Setting

Pisgah Crater, in the Mojave Desert, is near the central portion of San Bernadino County, California (Figure II-5). It is 41 mi east of Barstow and is accessible by means of U. S. Highway 66. A paved road 2 mi long, owned and maintained by the Santa Fe Railroad Company, leads south from the highway to the cinder cone.

2) Geology and Topography

The Pisgah Crater and lava flows lie in the bottom of a northwest-trending trough between Cady Mountains to the north and Lava Bed Mountains to the south. Lavic Lake appears originally to have been part of a large valley that drained northwestward to the Lower Mojave Valley near Newberry Spring, but the lava flows cut off the upper part of the valley and formed a closed basin. Excellent preservation of the volcanic landforms, the lack of significant erosion (especially on the cinder cone), the small

amount of alluvial covering due to wind-blown sand and encroaching alluvial fans indicate a probable Pleistocene-to-Recent age of eruption. The flows are dominantly black augite and olivine basalts (Roth, 1962).

Three types of volcanic material form the present Pisgah landscape: volcanic cinders, pahoehoe flows and aa flows (Esmilla, 1965). Two periods of flow can be recognized from aerial photographs, the first dominantly of pahoehoe and the second of aa. The pahoehoe, being more mobile and less viscous, are more extensive than the aa flows. Roth (1962) estimates the pahoehoe constitutes 85 percent of the total lava flows at Pisgah. A diversity of geomorphic features are developed in the pahoehoe.

a) Pahoehoe Surfaces

The surface of the pahoehoe generally is smoother than that of the aa flows, but may range from a raspy, corrugated texture to that of an elephant-skin texture which is characterized by pockmarks, small tumuli, pits, and shrinkage cracks. Larger geomorphic features are pressure ridges, collapsed sinks and lava tubes. The gross form of the flow units commonly is lobate. Upbowings of lava crust (termed tumuli), attributed to hydrostatic pressure of mobile subcrustal lava, and pressure ridges are prevalent. Tension cracks along the crests of these features commonly occur.

b) Aa Field

Aa lava flows at Pisgah can be distinguished from the pahoehoe by darker photographic tone and much more rugged topography. Under the stereoscope the surface looks rough and clinkery. A few circular pits are observed in the aa field. Pressure ridges with associated crustal tension cracks also are noted in the aa flow, but are less common and less smooth than those developed in the pahoehoe.

3) Discussion of Tests

Two of the four Pisgah Crater plates were used for testing. These maps have a horizontal scale of 1 in. = 44.5 ft and are contoured at 25-cm intervals. The maps were recontoured at approximately an 0.83-m interval, and old contours were eliminated from the presentation (Plates VIII and IX). The maps were scanned systematically in two directions and the limits of areas classified unsafe with respect to tipping were noted by hachured bars, with the hachures pointing towards the unsafe areas. For area A (Plate VIII) the probability of tilting was determined as 23.4 percent in the horizontal scanning direction, and 22.6 percent in a vertical direction. The geometric mean value is thus 23 percent. The safe landing probability is therefore

$$P_s = 1 - 0.23 = 0.77$$

For area C (Plate IX) the probability of tilting was 0.015 in a horizontal direction and 0.023 in a vertical direction. The geometric mean is 0.019. The safe-landing probability is therefore,

$$P_s = 1 - 0.019 = 0.981$$

d. Mare Cognitum

A test was performed on a topographic map of a small area of the Moon's surface in Mare Cognitum (Plate V). The map was prepared by the U. S. Geological Survey in cooperation with the National Space and Aeronautics Administration in 1964 based on Ranger VII photography P-979 and represents the only lunar topographic coverage available which shows sufficient detail for this purpose. The contour interval of the map is 10 cm, the horizontal scale is 1:80, and the template diameter at this horizontal scale is 1.914 in.

This map was selected to demonstrate an analysis based on use of an 0.4158-m contour interval. The map was recontoured by extrapolating between the original 10-cm contour lines, to produce 0.42-cm contour intervals. Only the new contour lines are shown on the map for the sake of clarity.

Areas were classified as safe, uncertain, and unsafe, with respect to tipping only. The map was scanned non-systematically, using 8-m and 4-m diameter circles, according to criteria shown in Figure II-1. The mapped areas constitute locii of the 8-m circle center point for the specified conditions. It was found that this technique requires considerably more judgment in interpretation than the 0.83-contour systematic and non-systematic methods. This was largely due to the need to distinguish between uphill and downhill contours in ascertaining whether a three-legged landing is possible in the uncertain case involving two contours crossing a 4-m template. Uncertainty results when two contours cross a 4-m circle, thus indicating a possible elevation greater than the highest contour value. Thus the total elevation distance over a four-meter distance could approach a maximum value of $3R \frac{\tan \tau}{2}$, whereas a difference of $2R \frac{\tan \tau}{2}$ is critical for a three-legged landing. But when a 4-m template circle is used, the position of the LEM center corresponds to some point on the circumference; if the template is placed on the uphill side of the lowest of two contour lines, the area bounded by the template above the higher contour line will be the locus of uncertain LEM landing center points.

The percent of unsafe area, corresponding to the minimum tipping probability is 6.34 percent. Uncertain areas comprise 17.7 percent of the total.

e. Death Valley, California (Treatment of bottoming hazards)

The topographic map studies described in the previous paragraphs were not suitable for treatment of bottoming hazards such as boulders below the map contour interval; therefore, a statistical approach to predict these hazards was developed. In order to acquire realistic data which could be used in the analysis, field surveys were conducted in Death Valley, California, where barren, boulder-strewn outwash surfaces adjacent to a block-faulted mountain range provided the desired range of obstacles.

Large-scale contour maps for the two locations tested were not available nor were any made, since the only intent was to map the distribution of boulders greater than 50 cm high. The two surfaces studied were selected because they appeared exceedingly uniform in slope. The A-series plots were made on an alluvial fan having a maximum slope of 5° as measured by a Brunton compass clinometer; while the B-series surface (a nearby Pleistocene lake terrace) measured 8° . A location map is shown as Figure II-6.

The field survey party selected the plots at random by vigorously throwing a beverage can over one's head and starting the survey at the point where the can landed. Borders of each plot were determined by a 50-sq ft traverse which was carried clockwise with an initial leg along the axis of the can. Distances were taped and directions were measured by the Brunton compass. The field data is tabulated in Table II-1; a sample survey plot is illustrated as Figure II-7. An analysis of data follows:

1) A-Series (Alluvial Fan in Death Valley)

- Number of boulders (protuberances): 53
- Area examined: 200 x 225 sq m (Assumes that from an average of every 20 areas, each of 225 sq m, only one is found to contain boulders)
- $\lambda(\frac{1}{2}) = \frac{53}{200 \times 225}$
- $\frac{53 \times 50.26544}{200 \times 225} = \frac{2664.06832}{45000} = 0.05920$
- $e^{-0.05920} = 0.942 = \text{probability of nonimpaled landing}$

Assume now that $\frac{\mu(B+)}{\mu(B)} = 0.05$ so that of the 45,000 sq m, a nontipping landing on an area of 2.250 m cannot be made.

The confidence in a safe landing with probability = 0.9 in the area B where B is a given area on the 0.83-m contour map.

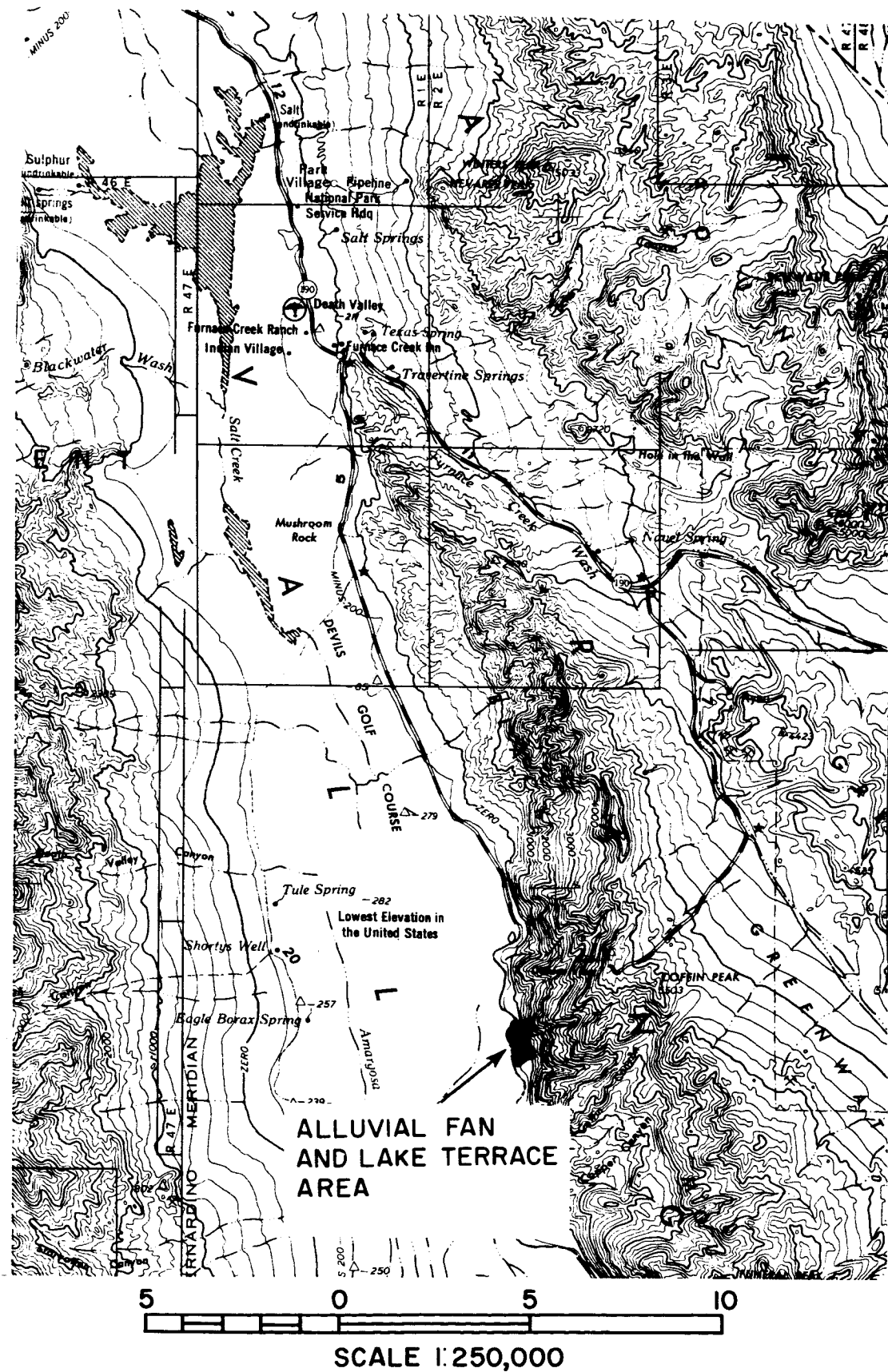


Figure II-9. Location Map of Death Valley, California

TABLE II-1

BOULDER MEASUREMENTS
Death Valley, California

Boulders measured on fan South of Badwater Slope with Brunton 5°											Boulder No. Ht. L W Trend of long axis						
Boulder No.	Ht.	L	W	Trend of long axis		Boulder No.	Ht.	L	W	Trend of long axis							
A-1	1	61	160	95	N10E	A-7	1	50	90	55	N22W		6	55	85	65	NS
	2	55	125	95	N38E			2	55	80	55	NS		7	90	150	90
A-2	1	95	210	135	N5E		3	50	100	45	N83W		8	55	85	60	N64E
	2	90	220	115	N80E	A-8	1	60	170	160	N67W		9	75	110	85	N46E
A-3	1	95	140	50	N15E			2	55	70	50	N8W		10	80	115	100
	2	110	125	115	N11E		3	60	90	50	N20W		11	85	135	110	N49W
	3	85	110	65	N20W		4	90	95	85	N3E		12	80	130	95	N87E
	4	70	80	80			5	50	70	50	N32W		13	55	85	75	N27E
	5	53	50	45	N25W		6	65	100	70	N23E	B-3	14	135	165	145	N25W
	6	53	90	65	N30W	A-9	1	70	135	90	N73W		1	75	140	95	N43W
	7	90	135	80	N10W			2	60	105	75	N26W	2	60	115	105	N35E
	8	55	90	85	N45E		3	50	120	60	N32W	3	65	95	75	N50E	
Depressions							4	100	180	180	N15E	4	95	130	115	N26E	
A'	-55	350	175		N65E	A-10	1	55	115	80	N8E	5	85	95	85	N37W	
A''	-60	275	100		N50E			2	50	90	55	N15E	6	70	105	100	N72W
A-4	1	90	120	115	N86E		3	110	265	145	N15E	7	70	140	120	NS	
	2	85	120	70	N35E		4	55	85	80	N65E	Slope with Brunton 8°					
	3	100	105	75	N70W		5	85	165	125	N38W	B-4	1	95	165	145	N52W
	4	50	100	45	N40W		6	60	85	60	N85W		2	50	85	60	N22E
	5	55	70	65	N40W	Boulders measured on Manly Terrace Basalt porphyry Slope with Brunton 8°							3	50	75	55	N22E
	6	65	200	170	N50W								4	50	80	80	
	7	50	120	95	N74E	B-1	1	75	160	120	N80E	5	95	220	160	N38E	
	8	95	130	90	N63W			2	55	90	80	N80E	6	60	95	90	N55W
	9	65	100	60	N87W		3	80	160	115	N77E	7	55	125	105	N51W	
	10	60	300	150	N60E		4	50	100	100		8	60	75	45	N78W	
A-5	1	85	225	105	N25E		5	50	100	70	N48E	9	50	70	60	N40W	
	2	55	80	60	N70W		6	65	120	85	N55E	10	65	85	65	N61E	
	3	75	175	75	N45E		7	50	95	75	N50E	11	85	155	115	N20E	
	4	105	110	100	N45E		8	75	135	100	N50E	Slope with Brunton 6°					
	5	70	170	75	N70W		9	130	170	125	N75W	B-5	1	55	80	50	N80E
	6	80	200	180	N15W	B-2	1	60	100	70	N65E		2	80	145	120	N47E
A-6	1	135	260	200	N27W			2	50	100	55	N57E		3	70	95	70
	2	52	75	55	N20W		3	80	95	85	N12W		4	105	135	100	N87W
	3	70	235	125	N15E		4	70	100	85	N22E		5	50	55	55	
	4	120	185	110	N12W		5	50	70	45	N52E		6	50	60	50	N22W
Slope measured with Brunton 7°													7	55	80	60	N25E
													8	55	60	45	N69W
													9	75	115	80	N30E
													10	50	70	60	EW

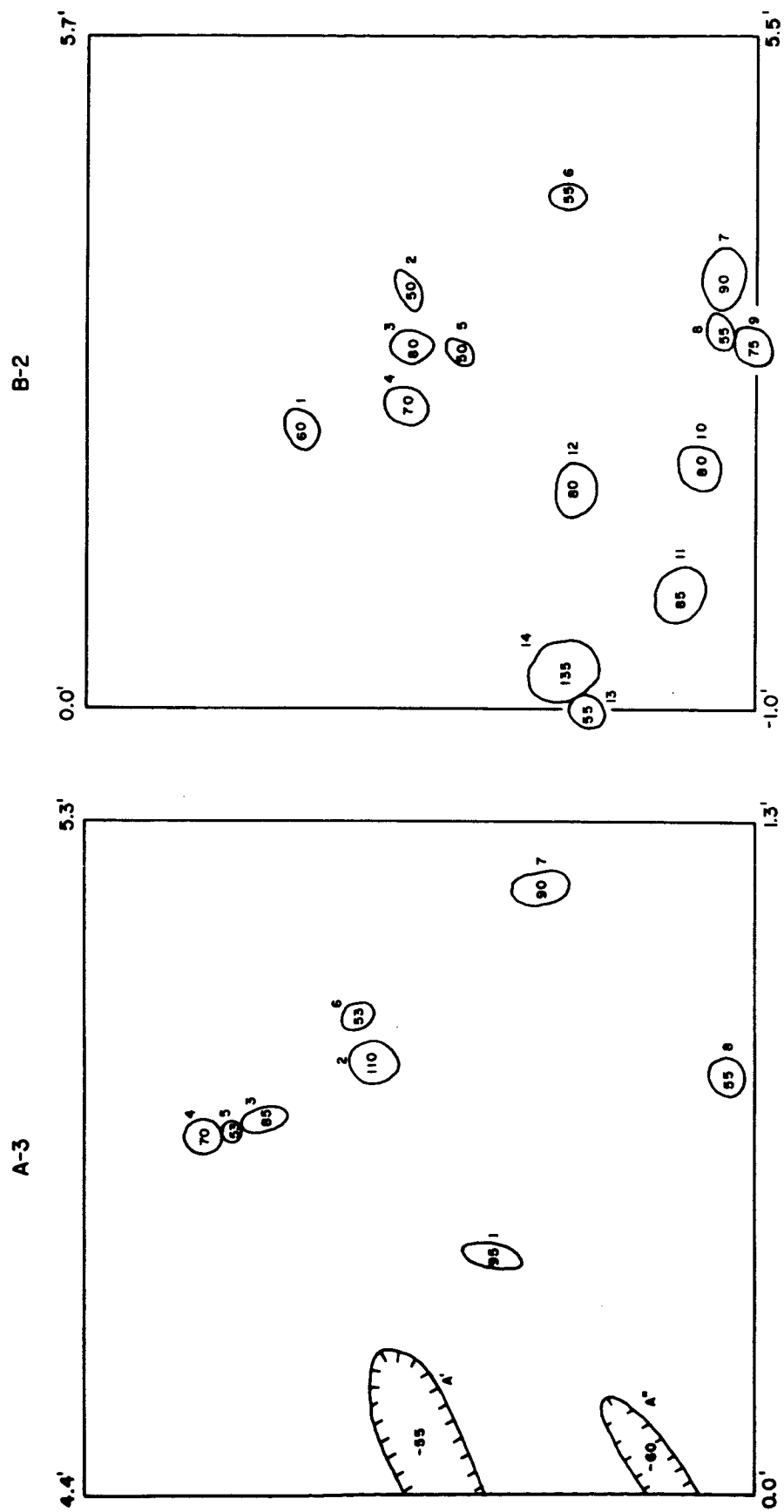


Figure II-10. Sample Survey Plots

$$1 - e^{-\frac{1}{0.9} \times 2,99573 \times 0.942} = 1 - e^{-2.99573 \times (1.05)} = 1 - 0.043 = \underline{0.957}$$

The confidence in a safe landing with 1 as the probability in area B is

$$1 - e^{-2.99573 + 0.942} = 1 - 0.06 = 0.94$$

2) B-Series (Pleistocene lake terrace)

- Number of boulders: 51
- Area examined: 225 x 5 x 15 (i.e., from an average of 15 areas examined, only one was found to have boulders or protuberances greater than 50 cm)
- $\lambda(\frac{1}{B}) = \frac{51}{225 \times 5 \times 15}$
- $\frac{51 \times 50.26544}{225 \times 75} = \frac{2563.53744}{16875} = 0.15191$
- $e^{-0.15191} = 0.859 = \text{probability of a nonimpaled landing}$

Assuming $\frac{\mu(B+)}{\mu(B)} = 0.05$ so that out of the 16,875 sq m there are 843 sq m where a landing will tip the LEM.

The confidence in 0.9 being the probability of a safe landing in the area is

$$\beta = 1 - e^{-\frac{1}{0.9} \times 2.99573 \times 0.859} = 1 - e^{-2.86} = 1 - 0.057 = \underline{0.943}$$

The confidence in that 1 is the probability of a safe landing in the area is

$$\beta = 1 - e^{-2.5733} = 1 - 0.076 = 0.92$$

D. REFERENCES

- Esmilla, A. B., 1965, Geomorphic forms of Pisgah Crater, San Bernadino County, California: Unpub. Rpt., Univ. of So. Cal., 11 p.
- Finsterwalder, S., 1890, Uber mittleren Boschungewinkel und das wahre Areal siner topographischen Flache, Stizber, K. Ak. der Wiss: Math. -Phys. Kl., v. 20, p. 35-82.
- Roth, E.S., 1962, Mt. Pisgah and Sunshine Crater lava fields: Unpub. Rpt., Univ. So. Calif., 35 p.
- Ruffin, B. W., 1965, Automatic computation of lunar relative heights from shadow-measurements: USAF, Aeronaut. Cht. and Info. Cntr., Lunar and Planetary Branch St. Louis, Mo., Mar., 6 p.
- Takács, L., 1962: Stochastic Processes, New York, 40 p.
- Wentworth, C. K., 1930, A simplified method of determining the average slope of land surfaces: Am J. Sci., v. 220, p. 184-194.
- Wood, W. F. and J.B. Snell, 1959, Preliminary investigations of a method to predict line-of-sight capabilities: Res. Study Rpt. EA-10, Quartermaster Res. and Eng. Center, Natick, Mass., 16 p.

CHAPTER III

STATISTICAL PROPERTIES OF TOPOGRAPHIC SURFACES

A. APPROACH TO PROBLEM

One must conclude from evaluation of the Orbiter photographic system and mission plans (Kosofsky and Broome, 1965) that the degradations in accuracy which accompany generalization of a surface by contouring may be intolerable for landing site analysis because the system appears to be designed for performance at a threshold level with respect to resolution of small elevation differences (Chapter V). Furthermore, manual methods for extraction of the required data from contour maps cannot be extended easily to an automatic process. Consequently, the approach described in this chapter was undertaken to make direct use of elevation data in rectangular matrix format without the intermediate contour mapping requirements. This treatment would lend itself most conveniently to data from a variety of automatic system outputs including microphotometer traces and automatic map compilation systems as described by Bertram (1965), Williams and Rosenberg (1958), Williams (1960), and others.

The basic approach of this chapter is to consider the elevation Z at a point x, y in the plane of interest to be a random variable. Extending this concept to all points x, y in the plane of interest, the surface $Z = Z(x, y)$ is considered a random surface or a two-dimensional random variable. The LEM landing problem is specified in terms of surface conditions satisfying certain criteria. The success or failure of the landing at a given point depends on surface elevations over a very small radius of surrounding points. It is the purpose of this chapter to describe a method of expressing the probability of success in terms of statistical parameters which represent the surface. Under certain stringent assumptions, this probability can be expressed by a very simple function of these statistical parameters. Relaxing the assumptions still allows solution of the problem through a numerical integration. Section B gives the development of this statistical method with the necessary assumptions. In Section C, the method is illustrated on actual grids of elevation data for several areas of interest. Finally, in Section D, the validity of the assumptions is examined.

B. DEVELOPMENT OF STATISTICAL PROCESS

1. Introductory Comments

A rectangular coordinate system (x, y, z) has been introduced to describe the problems associated with topography. The x and y axes are in a horizontal plane and z is the altitude of a point on the surface. Any given topographic map yields a deterministic functional relation $z = f(x, y)$. The reference datum $z = 0$ can be anything, but it will be convenient in the following discussion to choose the plane so that the average elevation $\langle z \rangle$ for the map is zero.

The correct statistical point of view is to consider any given map covering a fixed area as a single sample chosen from a population of maps of similar properties. From the given map, one endeavors to infer the relevant statistical parameters that govern the statistical population. Once these parameters are found, one can make statements of a probabilistic nature about any map drawn from the population, and, in particular, can make statements about the original map from which the statistical parameters were inferred.

The comments in the preceding paragraphs are important for they enable one to answer criticisms of the following nature. It is commonly argued that if one has at hand a topographic map $z = f(x, y)$, every quantity of interest such as the maximum slope is determined uniquely and there is no place or need for statistical statements.

The most simple question of a statistical nature that one may ask about a topographic surface is "What is the probability that the elevation z at any randomly selected point satisfies the relationship $h \leq z \leq h + \Delta h$?" One may state this question mathematically by introducing a function $P_1(x, y, z)$ such that

$$\int_{h_1}^{h_1 + \Delta h_1} P_1(x, y, z) dz = \text{probability that } h_1 \leq z \leq h_1 + \Delta h_1 \text{ at the point } (x, y) \quad (\text{III-1})$$

Of course, if one has only one map, this function is integrated over all (x, y) to give a function $\bar{P}(z)$ such that

$$\int_{h_1}^{h_1 + \Delta h_1} \bar{P}(z) dz = \text{probability that } h_1 \leq z \leq h_1 + \Delta h_1 \text{ for any point on the map} \quad (\text{III-2})$$

This function $\bar{P}(z)$, which is designated the frequency function, has been computed, for example, for the topography of the entire surface of the earth (Defant, 1961). The function $\bar{P}(z)$ may be computed readily for any map by taking a large number of sample values z_i from a regular distribution of sample points (x_i, y_i) .

The next most simple question that one may ask relates to the probable altitudes at two points on the map. Thus, one considers a frequency function $P_2(x_1, y_1, z_1; x_2, y_2, z_2)$ such that

$$\int_{h_1}^{h_1 + \Delta h_1} dz_1 \int_{h_2}^{h_2 + \Delta h_2} P_2(x_1, y_1, z_1; x_2, y_2, z_2) dz_2 = \text{probability}$$

that $h_1 \leq z < h_1 + \Delta h_1$ at the point (x_1, y_1)

and $h_2 \leq z < h_2 + \Delta h_2$ at the point (x_2, y_2) (III-3)

simultaneously. It is evident that P_2 is a function of six variables so that it will be necessary to obtain a large amount of sampling to determine the nature of the function and to arrive at a suitable analytic approximation.

One can proceed to define higher-order probability functions by a simple extension of Equations (III-1) and (III-3). These higher-order functions are necessary if one wishes to make any statements about confidence limits, but they can be determined only with a very large amount of sampling and computations.

2. Assumptions Regarding Frequency Functions of Topography

In view of the extreme paucity of information on the statistical properties of topographic surfaces, it is desirable to introduce some assumptions in order to reach the goals of the analysis in a reasonable time. As statistical data accumulate, these assumptions can be re-examined and, ultimately, must be substantiated with quantitative arguments or replaced by more realistic assumptions.

A frequency function $P_1(x, y, z)$ was introduced in Equation (III-1). If one divided a topographic map of the United States into regions such as the area west of the Continental Divide, the Mississippi River Valley, etc., one would expect to get a different function P_1 in each of these areas. However, if one restricted his consideration to a limited area of uniform physiography such as Florida, one would find that as this area was further subdivided, $P_1(x, y, z)$ no longer changed with the successive subdivisions. Although these ideas can be stated more explicitly, it is hoped that this simplified account will give to the reader a sufficiently clear idea of what is meant by the statement that the function $P_1(x, y, z)$ is independent of (x, y) .

Similarly, if one restricts the size of the map under consideration, it may result that the function $P_2(x_1, y_1, z_1; x_2, y_2, z_2)$ introduced in Equation (III-3) depends on only the differences $x_2 - x_1$ and $y_2 - y_1$. A more restrictive assumption, but one that may hold true in many areas, is that P_2

depends on only the distance $\rho = \sqrt{(x_2 - x_1)^2 + (y_2 - y_1)^2}$ between the points (x_1, y_1) and (x_2, y_2) , but not on the orientation of the line joining them.

At the present time it will be assumed that

$$P(x_1, y_1, z_1; x_2, y_2, z_2) = \bar{P}_2(x_2 - x_1, y_2 - y_1; z_1, z_2) \quad (\text{III-4})$$

This is a form of stationarity for maps and is the analog of stationarity for time series. In the following equations the bar will be omitted from \bar{P}_2 for convenience. If a regional topographic trend exists, it must be removed before the data can be considered stationary. The effect of regional trends is considered in Subsection B. 7.

The following statement is demonstrated in subsection B. 3. If the topographic surface can be approximated by an inclined plane in the neighborhood of some point, the slope of this plane can be determined readily from the apparent slope in two orthogonal directions at that point. This means that one can make the initial sampling on profiles and thereby avoid the more-complicated problem of sampling entire maps. It is therefore assumed that statistical conclusions based on orthogonal profile samples are valid.

The next assumption is that the frequency function appearing in Equation (III-1) is Gaussian. The relevant statistical justification is the following theorem, an exact statement of which is given and proved by Doob (1953). If one knows the first and second moments of a statistical distribution, one can find a Gaussian process which has the same first and second moments. Thus, if one knows only the first and second moments, there is a Gaussian process which fits all of the known facts about the data. The decisive advantage of the Gaussian distribution is that all of the higher-order moments are determined uniquely from the first and second moments.

There are two justifications for introducing the a priori assumption of a Gaussian distribution. First, it gives one a mathematical model so that one can continue with the problem of analyzing maps and making probabilistic statements. Secondly, there is no lost motion, since any sampling that is in connection with the Gaussian assumption can be used, whatever the true distribution function is.

When one assumes that the distribution of topography is Gaussian, one assumes (Rice, 1944) that

(III-5)

$$P_2(x_2 - x_1, y_2 - y_1; z_1, z_2) = \frac{1}{2\pi\sqrt{\mu_{11}\mu_{22} - \mu_{12}^2}} e^{-\frac{\mu_{22}z_1^2 - 2\mu_{12}z_1z_2 + \mu_{11}z_2^2}{2(\mu_{11}\mu_{22} - \mu_{12}^2)}}$$

where the quantities μ_{ij} which are defined by

$$\mu_{11} = \langle z_1^2 \rangle, \quad \mu_{22} = \langle z_2^2 \rangle, \quad \mu_{12} = \langle z_1 z_2 \rangle \quad (\text{III-6})$$

are functions of $(x_2 - x_1)$ and $(y_2 - y_1)$.

If the integrals

$$\int_{-\infty}^{+\infty} P_2 dz_2 \quad \text{and} \quad \int_{-\infty}^{+\infty} P_2 dz_1 \quad (\text{III-7})$$

are evaluated, one gets the frequency function for z_1 and z_2 , respectively.

By virtue of the arguments given in the first paragraph of this section and the symmetry of the expression in the right member of Equation (III-5), one concludes that μ_{11} and μ_{22} are equal and independent of $x_2 - x_1$ and $y_2 - y_1$.

Further, the standard deviation σ is defined by

$$\sigma = \sqrt{\mu_{11}} = \sqrt{\mu_{22}} \quad (\text{III-8})$$

and the correlation coefficient τ is defined by

$$\tau = \frac{\langle z_1 z_2 \rangle}{\sqrt{\langle z_1^2 \rangle \langle z_2^2 \rangle}} = \frac{\mu_{12}}{\sqrt{\mu_{11} \mu_{22}}} = \frac{\mu_{12}}{\mu_{11}} \quad (\text{III-9})$$

Equation (III-5) becomes

$$P_2(x_2 - x_1, y_2 - y_1; z_1, z_2) = \frac{1}{2\pi\sigma^2\sqrt{1 - \tau^2}} e^{-\frac{z_1^2 - 2\tau z_1 z_2 + z_2^2}{2\sigma^2(1 - \tau^2)}} \quad (\text{III-10})$$

3. Relation Between True Slope and Apparent Slope

Suppose that one has an inclined plane of slope θ as illustrated in Figure III-1 and that the apparent slopes θ_1 and θ_2 are measured in two orthogonal directions \vec{OA} and \vec{OC} . It is shown in Equation (A-8), Appendix A, that

$$\tan^2 \theta = \tan^2 \theta_1 + \tan^2 \theta_2 \quad (\text{III-11})$$

Hence, if one can make probabilistic statements about the apparent slopes θ_1 and θ_2 , one can make the corresponding statements about θ .

4. Statistical Properties of the Slope Along a Profile

Suppose that for a fixed sampling interval $\Delta x = x_2 - x_1$ one defines the apparent* slope θ_1 by

$$\tan \theta_1 = \frac{z_2 - z_1}{\Delta x} \quad (\text{III-12})$$

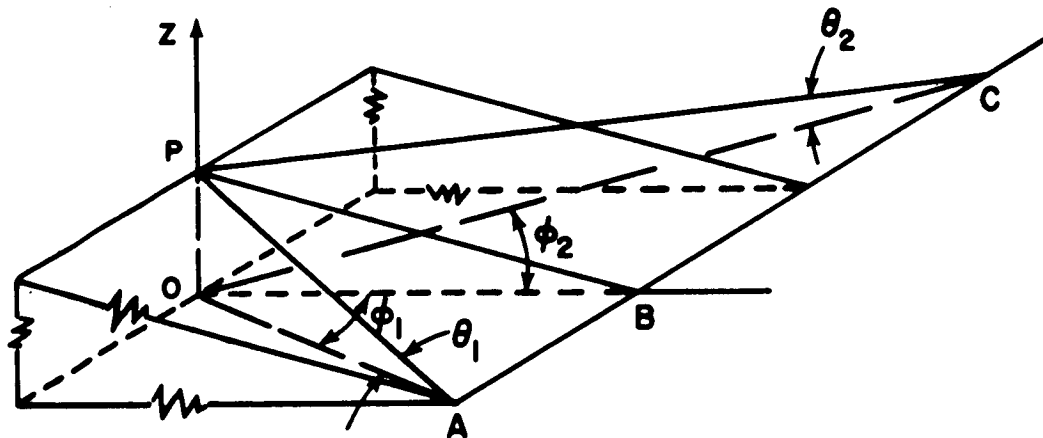


Figure III-1. Relationship Between True Dip and Apparent Dip

*"Apparent" is used instead of "average" so that the word average can be reserved for statistical averages. Even in the limit as $\Delta x \rightarrow 0$, θ_1 is not the "true" slope, since the x-axis may not be oriented parallel to the direction of steepest slope. The y component θ_2 must be considered as in Equation (III-11).

The average or expected value of $\tan \theta_1$ is defined as

$$\langle \tan \theta_1 \rangle = \frac{1}{\Delta x} \iint_{-\infty}^{+\infty} (z_2 - z_1) P_2(\Delta x; z_1, z_2) dz_1 dz_2 \quad (\text{III-13})$$

It is shown in Appendix B (Section A) that this is zero, as one would expect. Since the altitudes are distributed symmetrically about the reference plane $z = 0$, then $\langle z_1 \rangle = \langle z_2 \rangle = \langle \tan \theta_1 \rangle = 0$.

The average value or expected value of $\tan^2 \theta_1$ is defined as

$$\langle \tan^2 \theta_1 \rangle = \frac{1}{(\Delta x)^2} \iint_{-\infty}^{+\infty} (z_2 - z_1)^2 P_2(\Delta x; z_1, z_2) dz_1 dz_2 \quad (\text{III-14})$$

It is shown in Appendix B (Section B) that

$$\langle \tan^2 \theta_1 \rangle = 2 \left(\frac{\sigma}{\Delta x} \right)^2 (1 - \tau) \quad (\text{III-15})$$

This formula agrees with one's intuitive ideas. The smoother the surface, the smaller the dispersion of the altitudes and the smaller the θ_1 . The larger the separation Δx , for a fixed correlation coefficient τ , the smaller the apparent slope θ_1 . Finally, if the elevation z_2 at x_2 is highly correlated positively with the elevation z_1 at x_1 , $\tau \cong 1$ and the slope θ_1 must be small, as indicated by Equation (III-15). Further, if the separation Δx is such that τ is negative, the average value of $\tan^2 \theta_1$ will be larger than for the corresponding positive value.

One has computed the mean values of $\tan \theta_1$ and $\tan^2 \theta_1$. The next problem of interest is the probability that the slope has a value less than any predetermined value. This probability, which is called the distribution function, can be determined as follows. Consider the two-dimensional Cartesian coordinate system displayed in Figure C-1, Appendix C, where z_1 is the abscissa and z_2 is the ordinate. For a fixed separation Δx , any point $Q(z_1, z_2)$ in this plane can be characterized according to whether it falls above or below the line

$$z_2 = z_1 + \Delta x \tan \alpha_1 \quad (\text{III-16})$$

If the point Q falls above this line, the slope θ_1 defined by Equation (III-12) is greater than α_1 . However, if Q falls below this line, θ_1 is less than α_1 . If one lets S be the part of the (z_1, z_2) plane below the line defined by Equation (III-16), then the probability that $\theta_1 < \alpha_1$ is the probability that Q falls in S. This probability can be stated analytically by virtue of Equation (III-10).

If one defines a distribution function

$$F(\alpha_1) = \text{probability that } \theta_1 < \alpha_1, \quad (\text{III-17})$$

one has

$$\begin{aligned} F(\alpha_1) &= \iint_S P_2(\Delta x; z_1, z_2) dz_1 dz_2 \\ &= \frac{1}{2\pi\sigma^2 \sqrt{1-\tau^2}} \iint_S e^{-\frac{z_1^2 - 2\tau z_1 z_2 + z_2^2}{2\sigma^2(1-\tau^2)}} dZ_1 dZ_2 \end{aligned} \quad (\text{III-18})$$

This integral is evaluated in Appendix C where it is shown that the natural variable to use is not the slope angle α_1 , but the \tan of α_1 . If we introduce a new variable t_1 defined by

$$t_1 = \tan \alpha_1$$

it is shown in Appendix C that the distribution of t_1 is Gaussian and that one has the frequency function

$$P(t_1) = \frac{1}{\sqrt{2\pi} \sigma_t} e^{-t_1^2 / 2\sigma_t^2} \quad (\text{III-19})$$

where

$$\sigma_t = \frac{\sigma}{\Delta x} \sqrt{2(1-\tau)} \quad (\text{III-20})$$

The dispersion σ_t shows the correct dependence on the three physical parameters σ , τ and Δx . This can be seen by reviewing the arguments given on pages III-6, 7, and 8.

5. Statistical Properties of the True Slope

The discussion in the preceding subsection was devoted to the statistics of the apparent slope as measured along a profile. The question of relevant interest is the slope θ as measured along the direction of greatest decrease of altitude, i. e., the local direction of dip. It was demonstrated in Equation (III-11) that θ can be determined from θ_1 and θ_2 . One has seen already how θ_1 can be described for any profile. It is only necessary to combine the statistical distributions for θ_1 and θ_2 to get a distribution for θ .

To carry the analysis further, the following assumption was made: That at any point on the map, the apparent slope θ_1 in any direction, e. g., the x direction, was statistically independent of the apparent slope θ_2 in the perpendicular direction, e. g., the y direction. This assumption appears valid after one has removed regional trends, but no effort was made to find a proof. The importance of this assumption for the following analysis is that it enables one to write down the probability of finding simultaneously, at any point, a slope θ_1 along the x axis and a slope θ_2 along the y axis. It will simply be the product of the respective probabilities.

Let

$$t_1 = \tan \theta_1$$

$$t_2 = \tan \theta_2$$

One can apply Equation (III-19) to t_1 and t_2 , each with suitable values of σ_t and τ_1 and τ_2 . The parameter σ_t should be the same for each profile, but τ_1 and τ_2 can differ easily.

To carry the analysis further, assume that $\tau_1 = \tau_2$. This is equivalent to the assumption that the map is isotropic. In this case, one can define $P(t_1, t_2)$ as the joint frequency function for the two slopes and can write, by virtue of the assumption of statistical independence,

$$P(t_1, t_2) = P(t_1) P(t_2) = \frac{1}{2\pi\sigma_t^2} e^{-\frac{t_1^2 + t_2^2}{2\sigma_t^2}} \quad (\text{III-21})$$

where σ_t is defined by Equation (III-20).

The pairs of values (t_1, t_2) can be represented in a Cartesian plane and, by virtue of Equation (III-11), one sees that the slope θ at any point exceeds some critical value θ_c , if the point (t_1, t_2) falls outside the circle of radius $\tan \theta_c$, i. e., if

$$t_1^2 + t_2^2 > \tan^2 \theta_c \quad (\text{III-22})$$

This is illustrated in Figure III-2. Hence, the probability P that $\theta > \theta_c$ is given by

$$P = \frac{1}{2\pi\sigma_t^2} \iint_{\substack{\text{area} \\ \text{outside circle}}} e^{-\frac{t_1^2 + t_2^2}{2\sigma_t^2}} dt_1 dt_2 \quad (\text{III-23})$$

This can be evaluated readily by introducing polar coordinates

$$\begin{aligned} t_1^2 + t_2^2 &= r^2 \\ t_2/t_1 &= \tan \theta \end{aligned} \quad (\text{III-24})$$

This gives

$$P = \frac{1}{\sigma_t^2} \int_{\tan \theta_c}^{\infty} e^{-\frac{r^2}{2\sigma_t^2}} r dr \quad (\text{III-25})$$

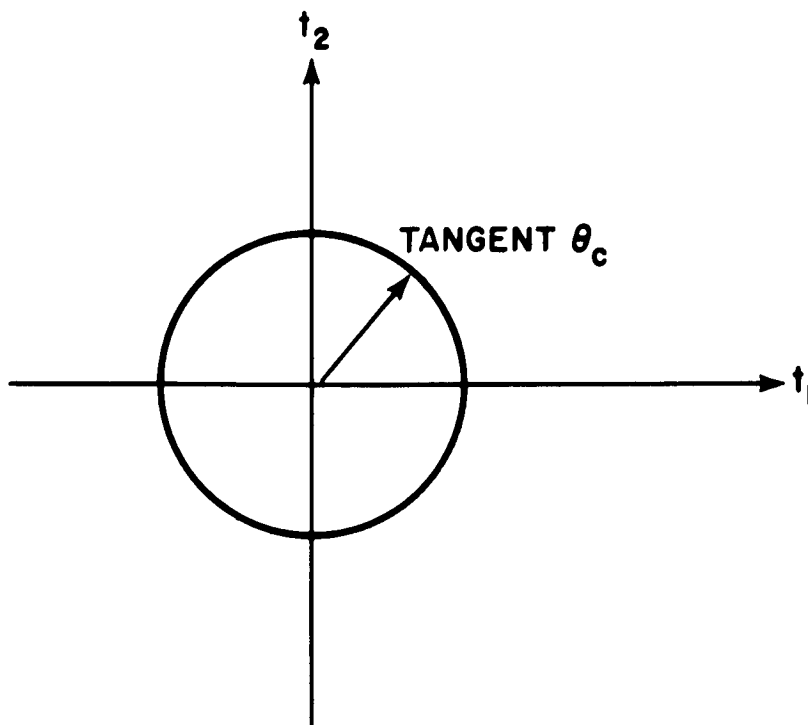


Figure III-2. The (t_1, t_2) Plane

or

$$P = e^{-\frac{\tan^2 \theta_c}{2\sigma_t^2}} \quad (\text{III-26})$$

One can assess immediately the probability that $\theta > \theta_c$ when Δx is chosen and σ and τ (a function of Δx) are known for the map.

6. Probability Evaluation

The probability given by Equation (III-26) can be obtained numerically from a grid of elevation data in the following way. Let Z_{ij} be the elevation data at the point ij where the sampling interval is Δx . Then the σ^2 and τ can be estimated by

$$\hat{\sigma}^2 = (MN)^{-1} \sum_{j=1}^M \sum_{i=1}^N Z_{ij}^2$$

$$\hat{\tau}_x = \left([N(M-1)]^{-1} \sum_{j=1}^{M-1} \sum_{i=1}^N Z_{ij} Z_{i,j+1} \right) / \hat{\sigma}^2$$

$$\hat{\tau}_y = \left([M(N-1)]^{-1} \sum_{j=1}^M \sum_{i=1}^{N-1} Z_{ij} Z_{i+1,j} \right) / \hat{\sigma}^2$$

$$\hat{\tau} = \left(\hat{\tau}_x + \hat{\tau}_y \right) / 2$$

where there are N rows and M columns of the matrix Z_{ij} of data. These estimates of $\hat{\sigma}^2$ and $\hat{\tau}$ can be used in Equation (III-20) to obtain an estimate of σ_t which in turn can be used in the expression for the probability given by Equation (III-26). The evaluation of these quantities is carried out numerically in Section C-2 for several different areas.

7. Effect of Regional Trends

If the sample of the topographic map available is limited in size, one may find it necessary to remove a regional trend before making the statistical calculations outlined above. Any conclusions about critical slope probability must be corrected for these regional trends. Presumably, one can devise a suitable correction for any specific regional trend.

If the map has random fluctuations superimposed on uniformly dipping plane, it is easy to prescribe the procedure that should be used. Select the x and y axes so that the +x axis points up the slope and the y axis is parallel to the strike of the planar surface. The topographic cross-section parallel to the x axis will look like that shown in Figure III-3.

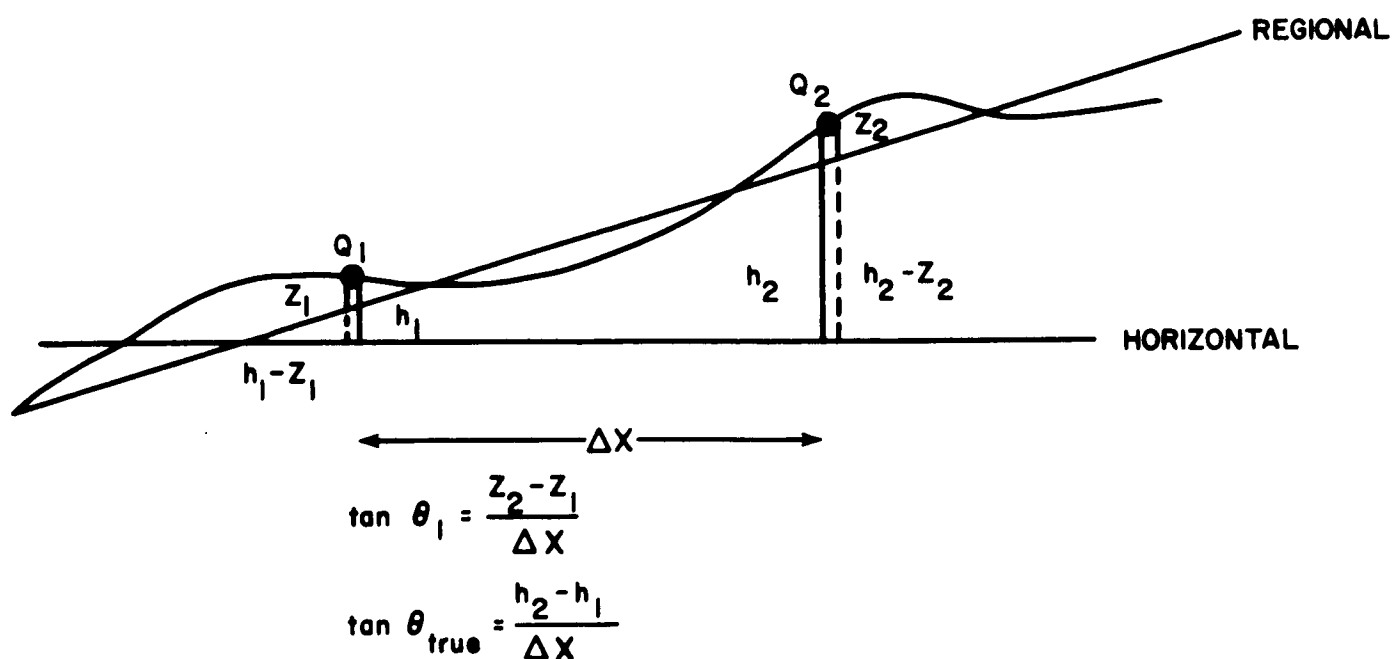


Figure III-3. Topographic Cross-Section Parallel to the X-Axis

Let

z_1, z_2 = elevations relative to the regional trend

h_1, h_2 = elevations relative to the horizontal

θ_1 = apparent slope relative to the regional trend

θ_{true} = apparent slope between Q_1 and Q_2 relative to the horizontal

θ_{reg} = slope of regression plane (regional trend)

The angle θ_1 is still the quantity obtained when the statistical analysis is applied to the map after the planar regional trend is removed.

One sees from Figure III-3 that

$$\tan \theta_{\text{true}} = \frac{h_2 - h_1}{\Delta x} = \frac{z_2 - z_1}{\Delta x} + \frac{(h_2 - z_2) - (h_1 - z_1)}{\Delta x}$$

or

$$\tan \theta_{\text{true}} = \tan \theta_{\text{reg}} + \tan \theta_1 \quad (\text{III-27})$$

Returning to Equation (III-4), one must replace $\tan^2 \theta_1$ by $\tan^2 \theta_{\text{true}}$. Thus, if one wants to have $\theta > \theta_c$, one must have

$$(\tan \theta_{\text{reg}} + \tan \theta_1)^2 + \tan^2 \theta_2 > \tan^2 \theta_c \quad (\text{III-28})$$

in place of Equation (III-22).

Thus, the integral of Equation (III-23) still is evaluated for points outside a circle of radius $\tan \theta_c$, but the center of the circle has been shifted from the point (0, 0) to $(-\tan \theta_{\text{reg}}, 0)$. Since the integrand in Equation (III-23) has its maximum value at the origin and decreases monotonically with distance from the origin, it is evident that any shift in the center of the circle increases the probability that $\theta > \theta_c$, as one would expect.

The probability P can be simply approximated in the following way.

$$P = \text{Prob} \left\{ \left(\frac{\tan \theta_{\text{reg}} + t_1}{\sigma} \right)^2 + (t_2/\sigma)^2 > \tan^2 \theta_c / \sigma^2 \right\}$$

Under the assumption of normality, independence of t_1 , t_2 and homoscedasticity (equal variance) of t_1 and t_2 , it follows that

$$P = \text{Prob} \left\{ \chi_{1,0}^2 + \frac{\tan^2 \theta_{\text{reg}}}{\sigma^2} > \tan^2 \theta_c / \sigma^2 \right\}$$

$$= \text{Prob} \left\{ \chi_{2, \lambda}^2 > \tan^2 \theta_c / \sigma^2 \right\}$$

where $\chi_{i, \lambda}^2$ is a non-central chi-squared random variable with i degrees of freedom and noncentrality parameter λ . The approximation is thereby obtained as a result of Patnaik (1949) that

$$\chi_{v, \lambda}^2 \approx S \chi_u^2$$

where u, S are given in terms of v, λ

$$u = (2 + \tan^2 \theta_{\text{reg}} / \sigma^2)^2 / 2(1 + \tan^2 \theta_{\text{reg}} / \sigma^2)$$

$$S = 2(1 + \tan^2 \theta_{\text{reg}} / \sigma^2) / (2 + \tan^2 \theta_{\text{reg}} / \sigma^2)$$

Thus the probability P can be expressed

$$P \approx \text{Prob} \left\{ \chi_u^2 > \tan^2 \theta_c / S \sigma^2 \right\} \quad (\text{III-29})$$

One can obtain a numerical value for P by estimating $Q = \tan^2 \theta_c / S \sigma^2$ and u from the elevation data since u and S are both functions of θ_{reg} and σ^2 . Using arguments Q and u , one then finds P from a table of cumulative chi-square distribution as given in standard statistics texts.

8. Summary of the Method

The following listed assumptions allow the probability of safe LEM landing to be expressed as a simple function of statistical parameters.

- (a) Elevation values can be considered as a two-dimensional, stationary, isotropic random process after removing the effect of regional trends.
- (b) The distribution of the elevation at any point in the plane is Gaussian

(c) Conclusions based on orthogonal profile samples are valid

These assumptions will be discussed in more detail in a later section after presentation of some numerical results.

C. APPLICATION OF THE METHOD TO THE MT. PISGAH AREAS

The following paragraphs apply the foregoing analysis. The analysis was applied to sample data from the Mt. Pisgah (California) lava flow; this area was selected because it was the only area for which extremely large-scale contour maps were available and it had been studied quite extensively under other NASA programs as a possible lunar analog. Use of contour maps to generate this data is incidental to demonstration of the method; however, the tedious task of interpolating many elevation points between contours was a practical limitation on the sample density which could be processed and served to emphasize the unsuitability of contour maps as source materials for detailed LEM site analysis.

1. Acquisition of Data

The analysis was applied to the Mt. Pisgah (California) crater area, considered analogous to predicted lunar terrain. Data available were contained in four contour maps of statistically different areas. The scale and contour interval were the same for each map and were 1 in. = 44.5 ft and 25 cm. Areas were designated D, B, A, and C, Plates I through IV, in the order of increasing roughness, with roughness having an intuitive definition, implying closeness of spacing and irregularity of contour lines.

A sampling grid of 29 x 29 lines 10.3 m apart was applied to the maps (which were oriented with north at the top). Elevations were read at each of the grid-line intersections. Unfortunately, intersections usually did not occur on contour lines, necessitating interpolation. Hence, at worst, data were accurate to within one-half contour interval (except for area C which already contained a matrix of data points). The computer (IBM 7040) input was a square matrix of 841 elevations.

In order to consider the effect of any regional trend, a simple least-square analysis was performed on each matrix to determine the plane which most closely approximated it. Then this plane was subtracted from the data points. The result was a matrix of elevations which contained no regional trend, at least on a large scale, and whose mean value was zero. An expanded discussion of the trend plane removal is given in Appendix D.

Later work utilized a larger (in the sense of number of sampled points) grid of 57 x 57 lines 5.15 m apart for the areas D and B with the purpose of testing the variability of statistical parameters with grid spacing. Areas A and C were not tested because the time required to read

3249 elevations for each map was excessive and preliminary results for areas D and B indicated testing was not necessary.

The trend plane parameters are given in Table III-1 for the six matrices analyzed.

Table III-1
TREND PLANE PARAMETERS

Parameter	29 x 29					57 x 57	
	D	B	A	C		D	B
a	+0.0207	-0.0372	-0.00192	-0.000234		+0.0202	-0.0374
b	-0.0217	+0.00957	+0.00291	+0.000540		-0.0215	+0.00962
c	-892	-114	-114	+7.00		-875	-120
Parameters for trend plane equation $z = a x + by + c$							

Figure III-4 shows the maximum dip of the trend removed from each of the 29 x 29 matrices plotted to scale as an aid in visualization.

2. Calculations

A number of statistical parameters were evaluated for each of the four areas from the resultant data matrices. These were the standard deviation σ , the variance σ^2 (standard deviation squared), the x-autocorrelation coefficient τ_x , the y-autocorrelation coefficient τ_y , the autocorrelation coefficient τ , the x-dispersion σ_{tx} , the y-dispersion σ_{ty} , and the dispersion σ_t . These parameters are discussed in Sections A and B and are defined in the following manner:

The variance and standard deviation have the customary definitions

$$\sigma^2 = \frac{1}{MN} \sum_{j=1}^M \sum_{i=1}^N z_{ij}^2 \quad (\text{III-30})$$

$$\sigma = \sqrt{\sigma^2} \quad (\text{III-31})$$

where the subscript i denotes matrix row and j denotes matrix column (Figure III-5).

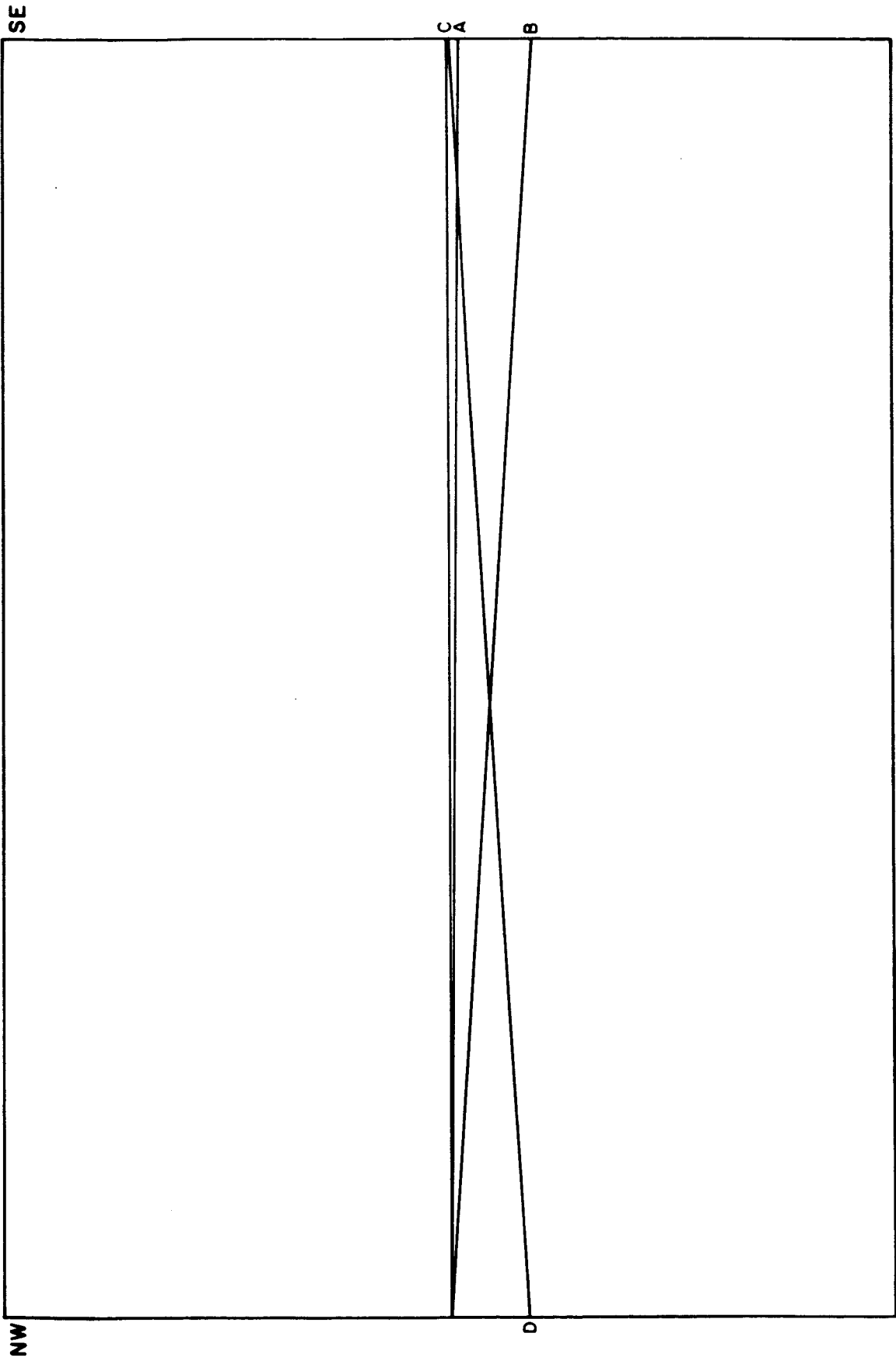


Figure III-4. Maximum Dip of Trend

$$\begin{array}{ccccccc}
 z_{11} & z_{12} & z_{13} & \cdots & z_{1j} & \cdots & z_{1M} \\
 z_{21} & & & & & & \\
 z_{31} & & & & & & \\
 \vdots & & & & & & \\
 z_{i1} & & z_{ij} & z_{i,j+1} & & & \\
 \vdots & & z_{i+1,j} & z_{i+1,j+1} & & & \\
 \vdots & & & & & & \\
 z_{N1} & & & & z_{NM} & &
 \end{array}$$

Figure III-5. Matrix Representation of Elevation Point Data

The x-autocorrelation coefficient is the normalized value of the average of all elevations multiplied by the adjacent (in the x direction) points. That is,

$$\tau_x = \frac{\frac{1}{(M-1)N} \sum_{j=1}^{M-1} \sum_{i=1}^N z_{ij} z_{i,j+1}}{\sigma^2} \quad (\text{III-32})$$

Similarly,

$$\tau_y = \frac{\frac{1}{M(N-1)} \sum_{j=1}^M \sum_{i=1}^{N-1} z_{ij} z_{i+1,j}}{\sigma^2} \quad (\text{III-33})$$

and

$$\tau = \frac{\frac{1}{(M-1)(N-1)} \sum_{j=1}^{M-1} \sum_{i=1}^{N-1} z_{ij} z_{i+1,j+1}}{\sigma^2} \quad (\text{III-34})$$

Note that the correlation distance for τ is not the same as for τ_x and τ_y . It is $\sqrt{2}$ 10.3 or 14.5 m. This form of τ was used in lieu of that given on page III-11 in order to investigate the sensitivity of P to Δx vs Δr .

The x dispersion is the evaluation of Equation (III-20)

$$\sigma_{tx} = \frac{\sigma}{\Delta x} \sqrt{2(1 - \tau_x)} \quad (\text{III-35})$$

where Δx is the grid-line spacing 10.3 or 5.15 m. Similarly

$$\sigma_{ty} = \frac{\sigma}{\Delta y} \sqrt{2(1 - \tau_y)} \quad (\text{III-36})$$

and

$$\sigma_t = \frac{\sigma}{\Delta r} \sqrt{2(1 - \tau)} \quad (\text{III-37})$$

where $\Delta r = \sqrt{2}$ 10.3 m or 14.5 m.

The results provided by the computer are given in Table III-2.

Table III-2
CALCULATED STATISTICAL PARAMETERS

Parameter	29 x 29				57 x 57	
	D	B	A	C	D	B
σ	457	177	122	21.9	451	196
σ^2	209,000	31,400	14,900	478	203,000	38,400
τ_x	0.923	0.805	0.658	0.641	0.971	0.707
τ_y	0.842	0.758	0.719	0.617	0.931	0.699
τ_{avg}	0.883	0.782	0.688	0.629	0.951	0.653
τ	0.815	0.649	0.529	0.542	0.916	0.668
σ_{tx}	0.174	0.107	0.0983	0.0180	0.211	0.292
σ_{ty}	0.250	0.120	0.0892	0.0186	0.325	0.296
σ_{tavg}	0.215	0.114	0.0937	0.0183	0.268	0.294
σ_t	0.191	0.102	0.0813	0.0144	not calculated	

The Equation (III-29) can be readily evaluated using the results of Table III-2. The results of this calculation are given in Table III-3 and the last line of this table shows the probability of a successful LEM landing for each of the four areas considered.

Table III-3
EVALUATION OF EQUATION III-29

	D	B	A	C
σ	0.215	0.114	0.0937	0.0183
$\tan^2 \theta_{\text{reg}}$	0.0008994	0.0014754	0.0000122	0.0000035
u	2.0000186	2.0057871	2.0000009	2.0000597
S	1	1	1	1
$\tan^2 \theta_c$	0.897	3.193	4.727	123.917
$S\sigma^2$				
P	0.37	0.79	0.90	1.0

Note: Equation (III-26) would give the same values of P. The effect of the regression plane is, therefore, unimportant for the present data, after the determination of the σ 's.

D. EXAMINATION OF ASSUMPTIONS

The present section presents some calculations from elevation data for two areas. These calculations are intended to test the hypothesis that the elevation distribution is normal. A correlation analysis of the Pisgah data is also presented to indicate whether the assumptions of space stationarity and isotropy are warranted for this data.

1. Gaussian Assumption from Kerrville Data

A theory for the distribution of slopes on a topographic surface was developed in the previous section, on the basis of an assumption regarding the statistical distribution satisfied by samples of the elevation. It was shown that if the first- and second-order distributions of the elevation were Gaussian, the average slope over a fixed distance, Δx , would also satisfy a Gaussian distribution. This theory was tested on a sample of topography from near Kerrville, Texas.

The first-order distribution of elevation samples sufficiently satisfy the Gaussian distribution. The calculated distribution of slopes for $\Delta x = 1$ mi did not deviate markedly from a Gaussian distribution. This implies, according to the theoretical analysis, the the second-order distribution of elevations is approximately Gaussian.

The U. S. Geological Survey Quadrangle Map for Kerrville, Texas, of scale 1:125,000 and contour interval 50 ft was used for a test. Read in a square pattern 20 mi x 20 mi were 441 samples of elevation. The distance between each sample was one mile and the square was oriented north-south and east-west. Elevations were interpolated linearly between contours to the nearest 10 ft. To simplify the numerical work, the elevation was recorded in tens of feet and Δx was treated as unity. These choices for the units will have no effect on questions of statistical distributions.

When the elevation samples were read, it was found that they could be fitted approximately by a plane surface dipping to the northeast with a dip of 2.83 ft/mi. The properties of this mean plane were found rather simply by forming averages in the four quadrants. The elevation values read from the map were corrected by subtracting the elevation of this northeast dipping plane. All future statements refer to these corrected elevations expressed in tens of feet.

The elevation range was divided into class intervals of five and a count was made of the number of elevations that occurred in each interval. Standard techniques were used to calculate the mean and the dispersion of these values. The result was

$$\begin{aligned}\bar{z} &= 0.80 \text{ tens of ft} \\ \hat{\sigma}^2 &= 226.2 (\text{tens of ft})^2\end{aligned}\tag{III-38}$$

In order to illustrate the distribution, the observations were expressed as the percentage of the totals that were less than z and the results were plotted on probability graph paper in Figure III-6. It is apparent that the first-order probability distribution follows the Gaussian distribution very closely. Further, the straight line corresponding to $\langle z \rangle$ and σ quoted in Equation (III-38) fits the data quite well.

In order to test the distribution of slopes, the elevation difference Δi between adjacent sample points on east-west lines was formed for every pair of points on the square grid. This gave 420 elevation differences, each of whose statistical distribution was calculated. The sense of each difference was chosen so that it would be positive when the slope was upwards to the east. These elevations could be converted to slope $\tan \theta$ by dividing by 528 tens of ft (1 mi).

The range of elevation differences was divided into class intervals of four and a count was made of the number of elevation differences that fell in each interval. This analysis yielded the following values for the mean and the dispersion:

$$\begin{aligned}\bar{\Delta} &= 1.54 \text{ tens of ft} \\ \sigma_{\Delta}^2 &= 69.24 (\text{tens of ft})^2\end{aligned}\tag{III-39}$$

Figure III-7 is a plot of the percentage of the total samples that yielded an elevation difference less than the amount shown on the ordinate.

In order to use Equation (III-20) as developed in Section B, one must calculate the correlation coefficient τ . The results of the calculation for a displacement Δx of 1 mi to the east are

$$\hat{\tau} = 0.804$$

$$\sqrt{1 - \hat{\tau}^2} = 0.443$$

When one substitutes the values in Equation (III-20) of subsection B.5, to predict the dispersion of the elevation differences, one finds

$$\hat{\sigma}^2_{2(1-\hat{\tau})} = 9.42 \text{ tens of ft}$$

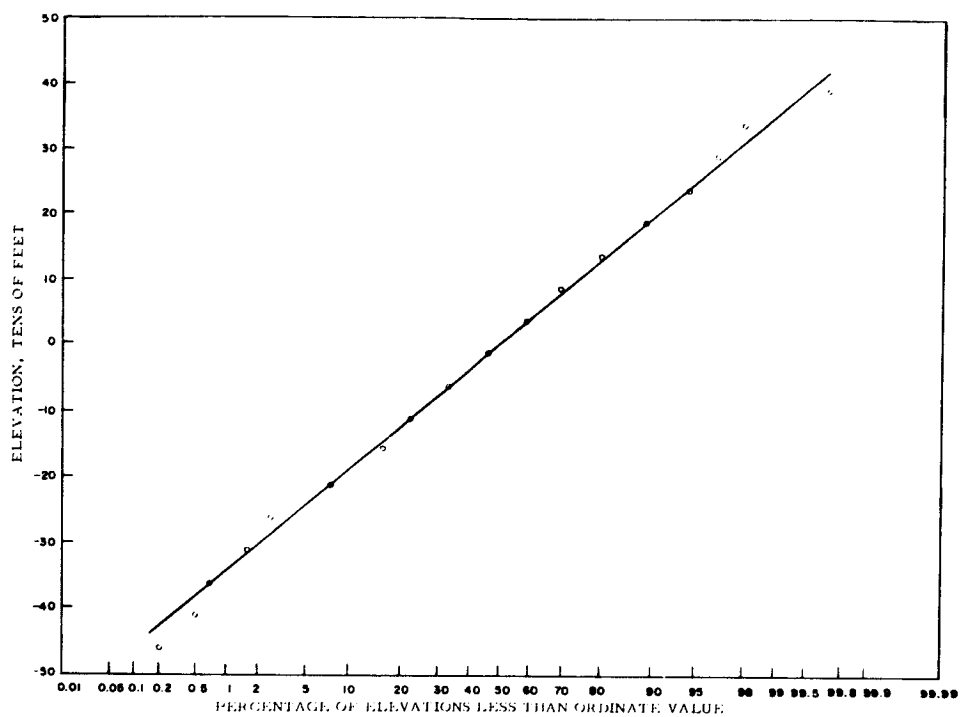


Figure III-6. Distribution Function of Elevations

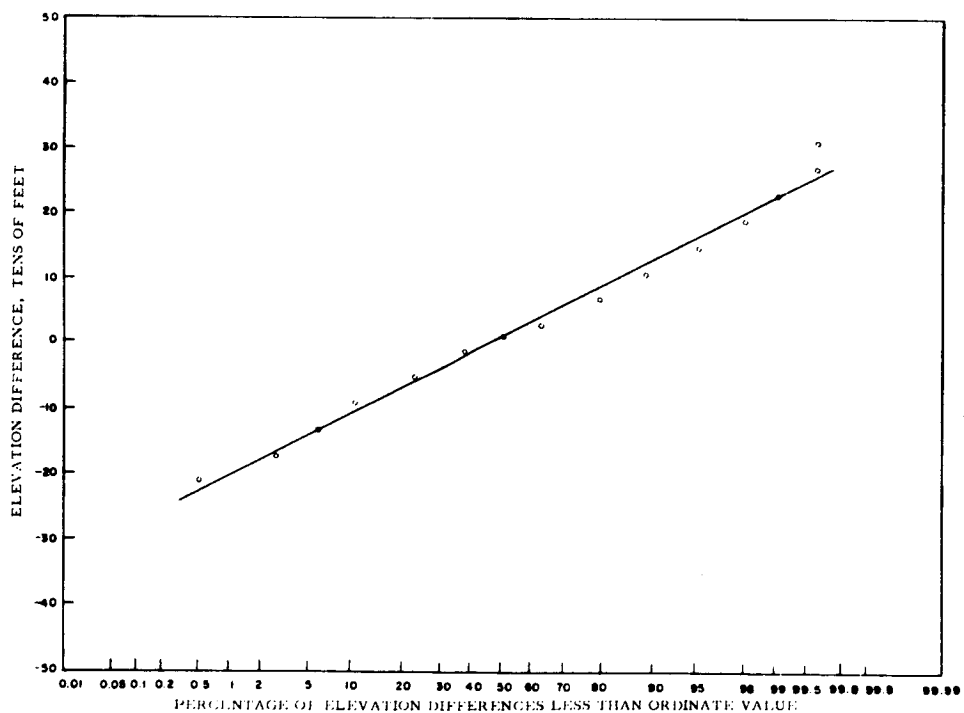


Figure III-7. Distribution Function of Elevation Differences

A straight line corresponding to this value of the dispersion is plotted in Figure III-7. One can see that the gross fit is good, but the detailed fit is poor.

The error introduced by using the Gaussian assumption in the numerical evaluation of the probability that elevation differences are in a specified interval is nevertheless seen to be very small.

2. Gaussian Assumption from the Mt. Pisgah Data

In order to test the validity of the assumption of Gaussian distribution of elevations for the Mt. Pisgah areas, the frequency distribution of elevations was calculated for each of the four areas. Increments were 5 cm, since accuracy of the readings could have been no better for the 25-cm contour intervals. The results are plotted in Figure III-8 and are replotted on a probability scale in Figure III-9. On such a scale, a Gaussian distribution would manifest itself as a straight line. Obviously, only B approaches the Gaussian form.

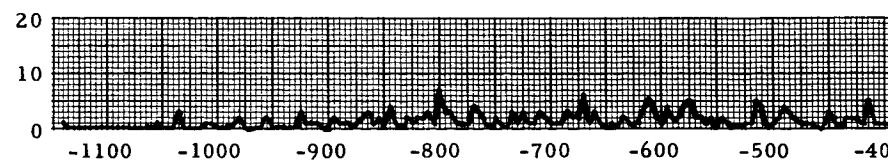
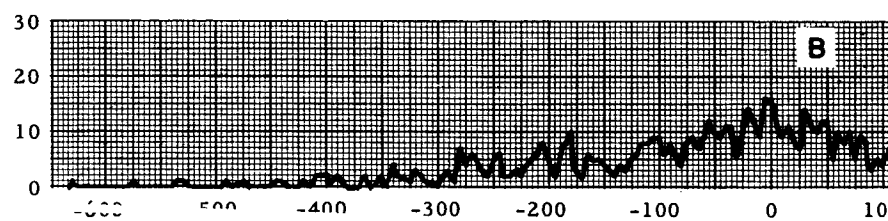
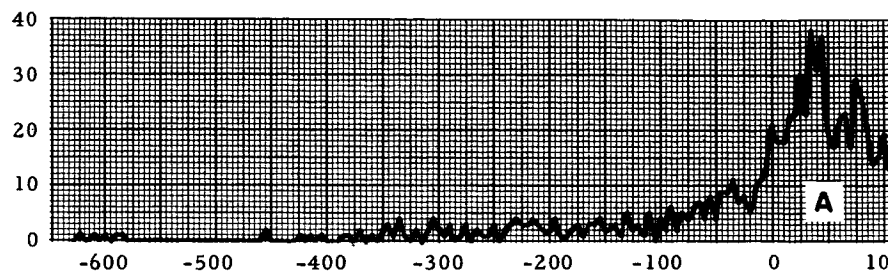
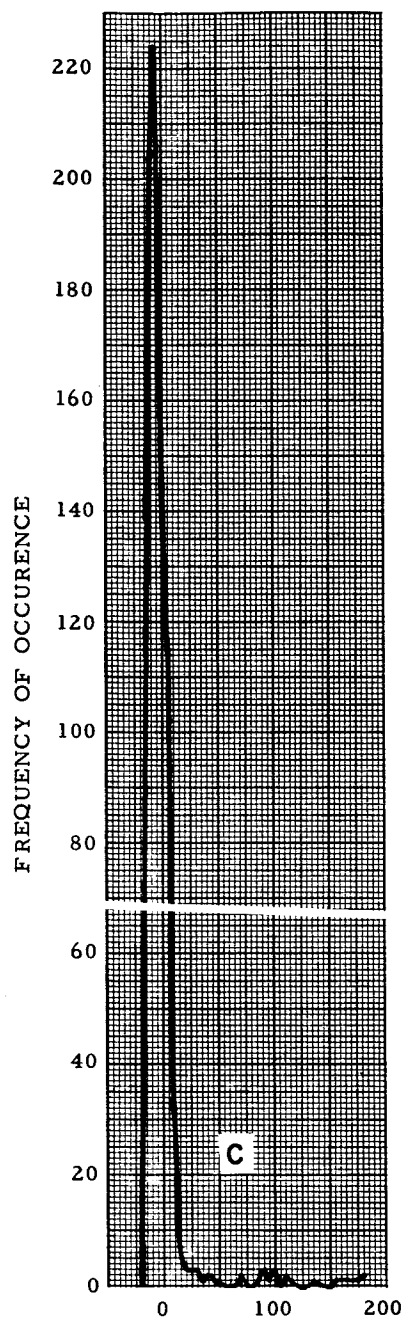
Previous work in the field of terrain quantification (Tanner, 1959, 1960) suggested the possibility that the distributions could be fitted by Pearson curves of Type I or IV. The method of fitting, according to Kendall (1947) and Elderton (1927), is discussed in Appendix E. It requires the calculation of the first four moments of the distribution in question where the n-th moment is defined

$$\mu_n = \frac{1}{M} \sum_{i=1}^M (x_i - \bar{x})^n \quad (\text{III-40})$$

From the first four moments, a parameter κ is calculated which determines the type of Pearson distribution. For Type I, $\kappa < 0$ and for Type IV, $0 < \kappa < 1$. The κ 's calculated for areas D, A and C indicated Type I distribution, whereas, for area B the κ 's indicated Type IV. The first four moments of the distributions and the associated κ 's are given in Table III-4.

Table III-4
CALCULATED MOMENTS AND PEARSON κ

	D	B	A	C
μ_1	0	0	0	0
μ_2	209,000	31,400	14,900	478
μ_3	-47,100,000	-958,000	-3,480,000	58,300
μ_4	93,100,000,000	3,140,000,000	1,630,000,000	8,860,000
κ	-0.0831	0.0825	-2.32	-10.4
First four moments and κ for each elevation distribution				



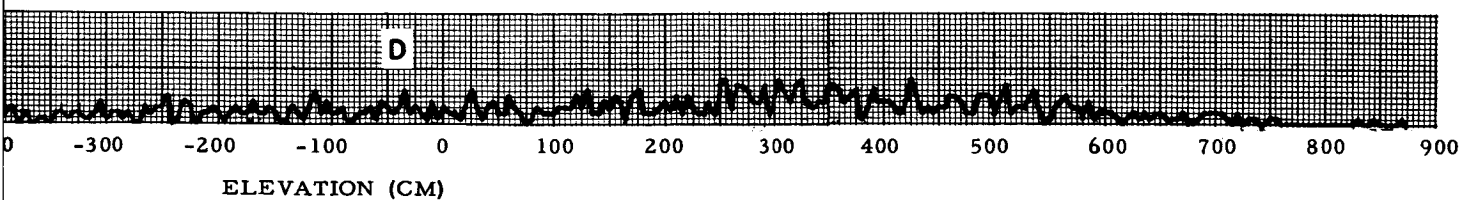
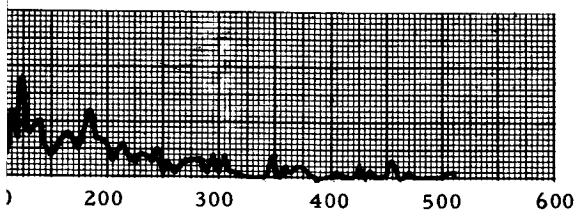
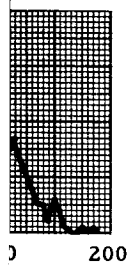


Figure III-8. Frequency Distribution of Elevations
for Areas A, B, C, and D

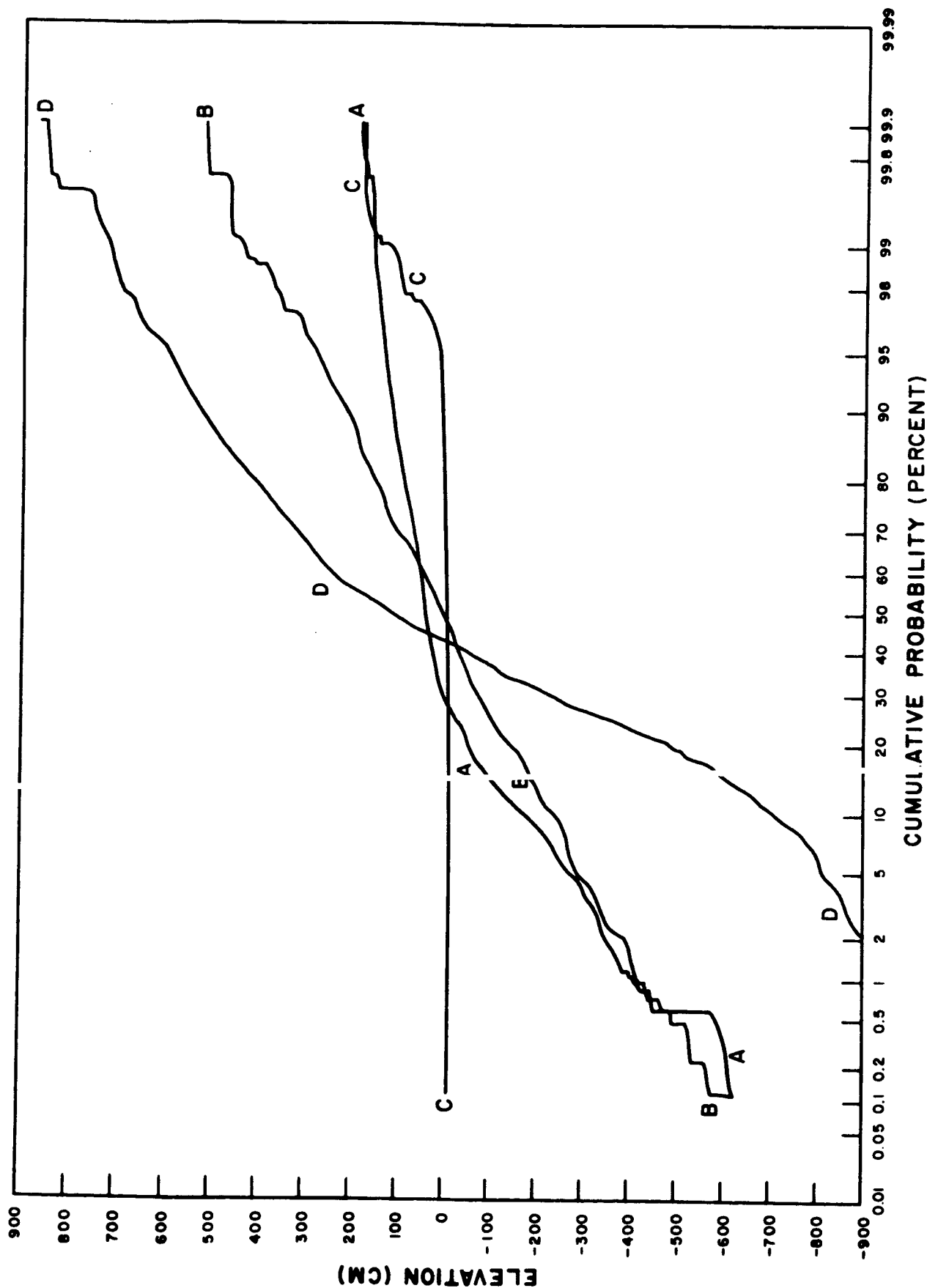


Figure III-9. Probability Scale for Frequency Distribution of Elevations (Areas A, B, C, and D)

Pearson's Type I curve is of the form

$$f_I(x) = k \left(1 + \frac{x}{a_1}\right)^{m_1} \left(1 - \frac{x}{a_2}\right)^{m_2} \quad (\text{III-41})$$

where $-a_1 \leq x \leq a_2$ and $\frac{m_1}{a_1} = \frac{m_2}{a_2}$

Type IV is

$$f_{IV}(x) = k \left(1 + \frac{x}{a}\right)^2 e^{-m - \nu \tan^{-1} \frac{x}{a}} \quad (\text{III-42})$$

The constants m_1 , m_2 , a_1 , and a_2 were calculated for the Type I distributions. For each area, however, one of the exponents calculated was negative. According to Elderton (1927), a negative exponent indicates a singularity. No singularities are present in the actual curves, except possibly that of area C, as Figure III-8 clearly shows. Consequently, it must be concluded that either an error exists in the application of Elderton's analysis to the problem or the curves are not Pearson's type I or type IV.

In order to evaluate the probability integral of Equation (III-17), it is necessary to know the frequency distribution of the slopes at the sampling points. This can be approximated by calculation of the frequency distribution of differences between adjacent elevations. These difference distributions are given in Figures III-10 to III-13. They are plotted on a probability scale in Figures III-14 to III-16.

Again, unfortunately, the distributions were not Gaussian. In view of the negative results obtained for the elevation distributions, no attempt was made to fit the difference distributions.

3. Correlation Analysis

a. Introduction

For a continuous sample of infinite length, the autocorrelation function is defined

$$c(\tau) = \lim_{T \rightarrow \infty} \frac{1}{T} \int_{-\frac{T}{2}}^{\frac{T}{2}} x(t) \cdot x(t + \tau) \cdot dt \quad (\text{III-43})$$

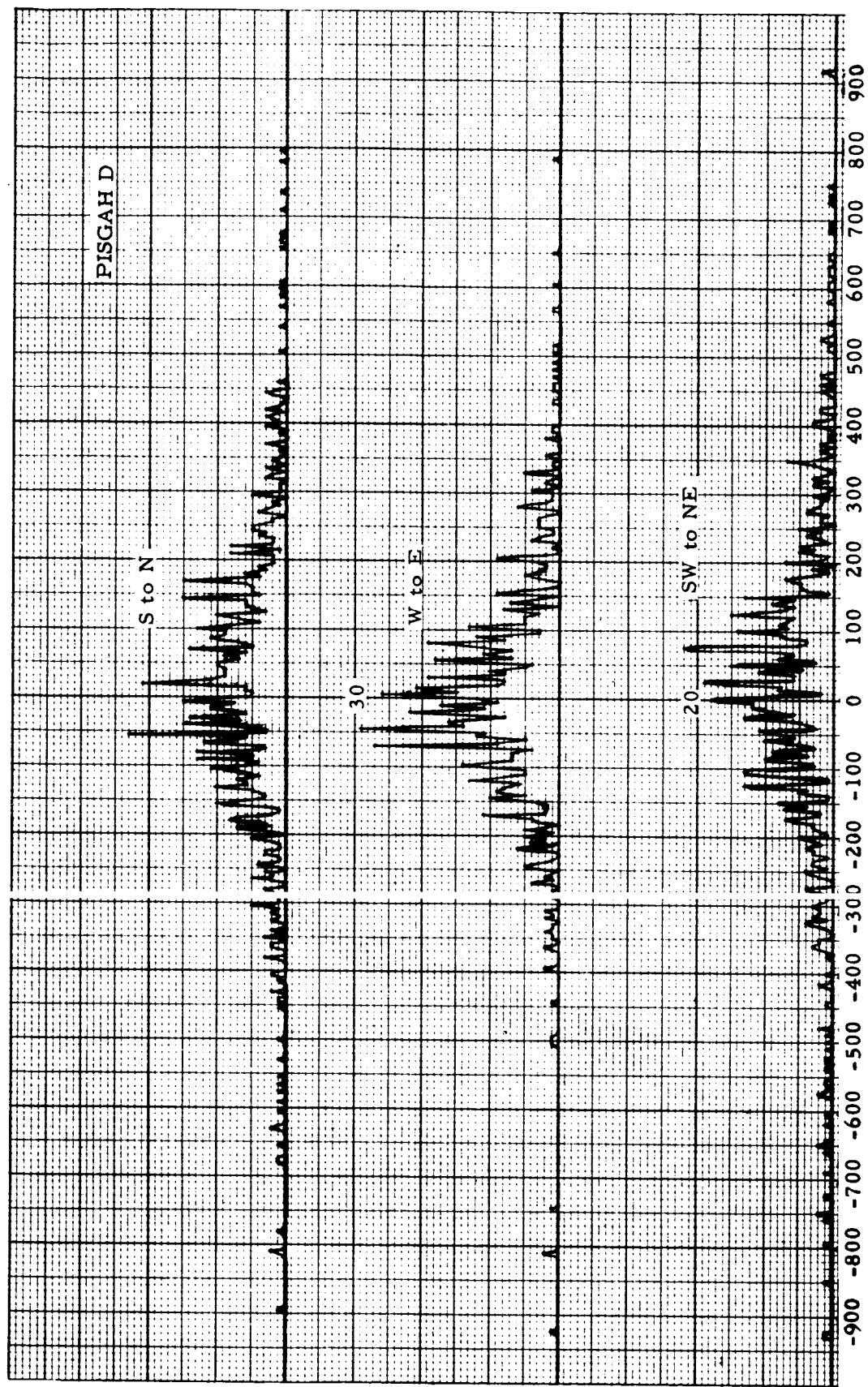


Figure III-10. Frequency Distribution of Elevation Differences (Area D)

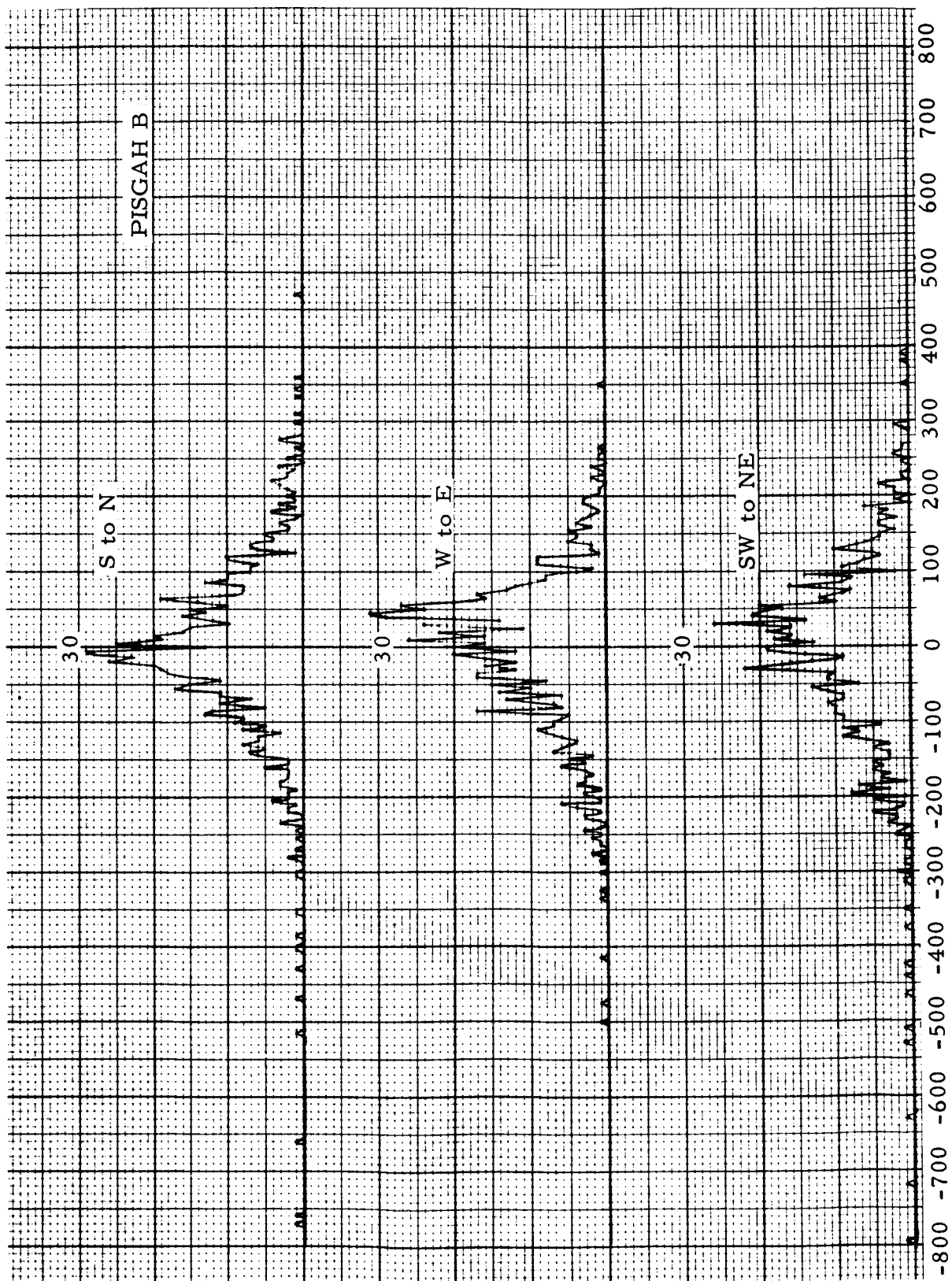


Figure III-11. Frequency Distribution of Elevation Differences (Area B)

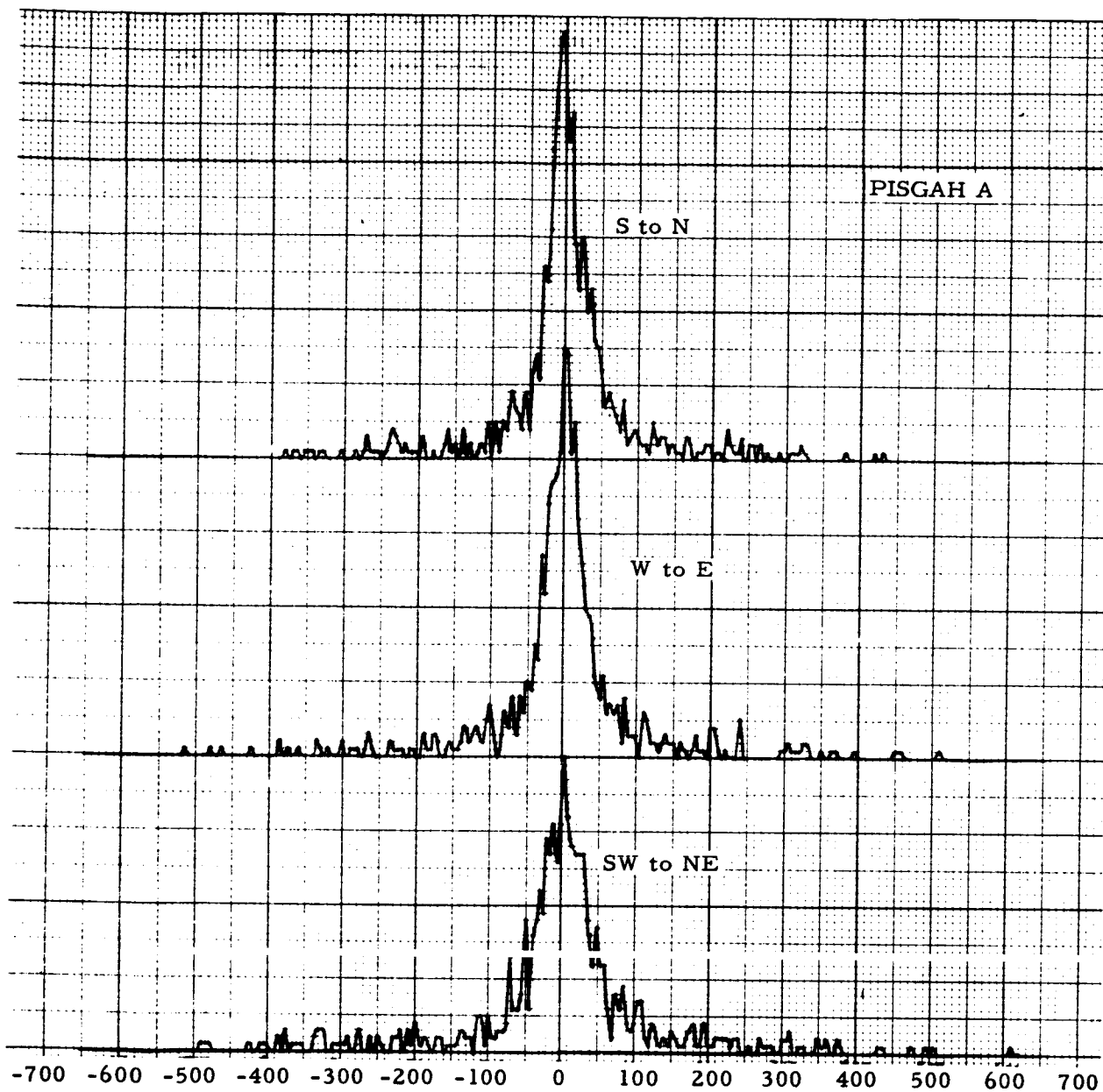


Figure III-12. Frequency Distribution of Elevation Differences (Area A)

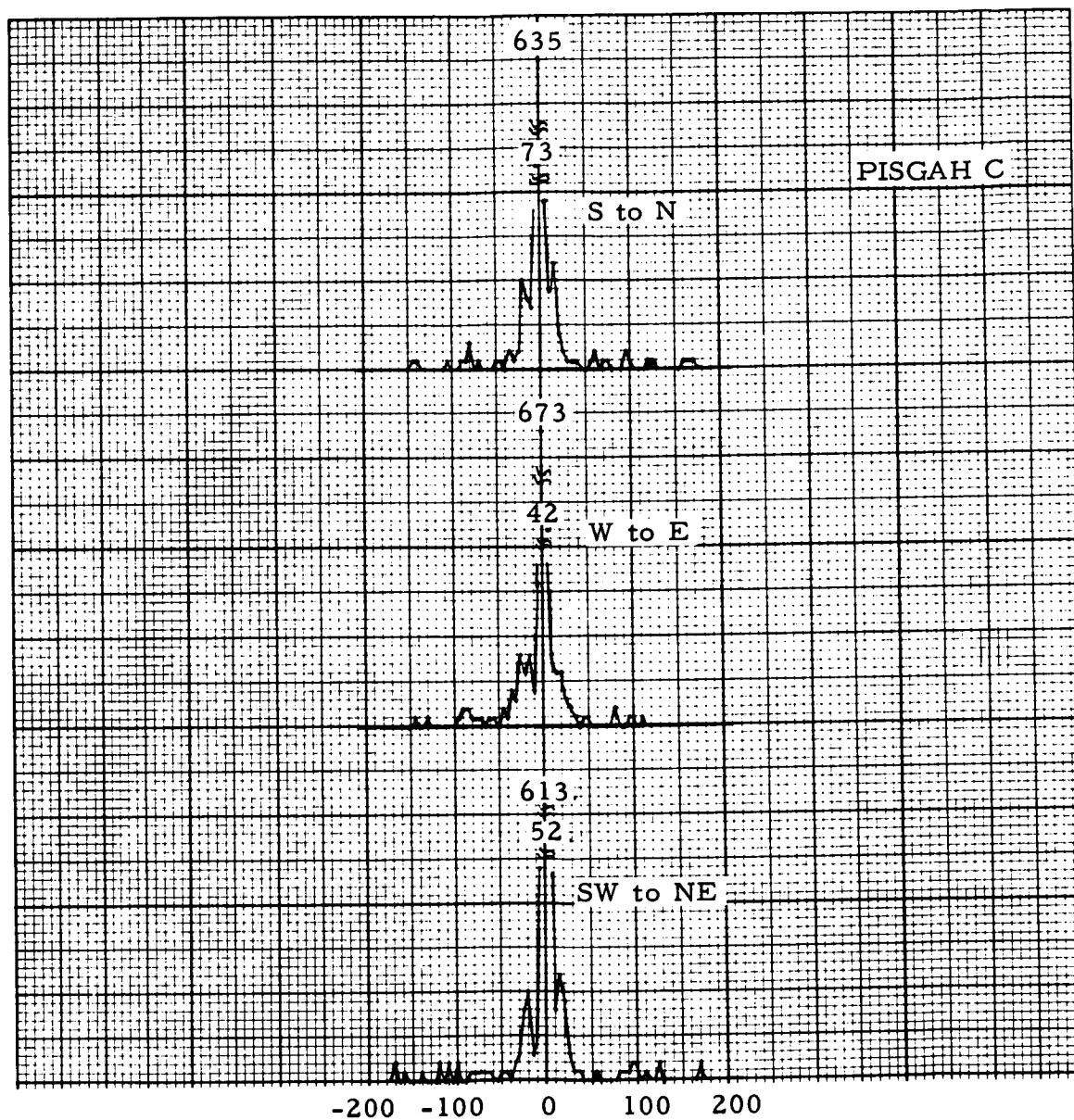


Figure III-13. Frequency Distribution of Elevation Differences (Area C)

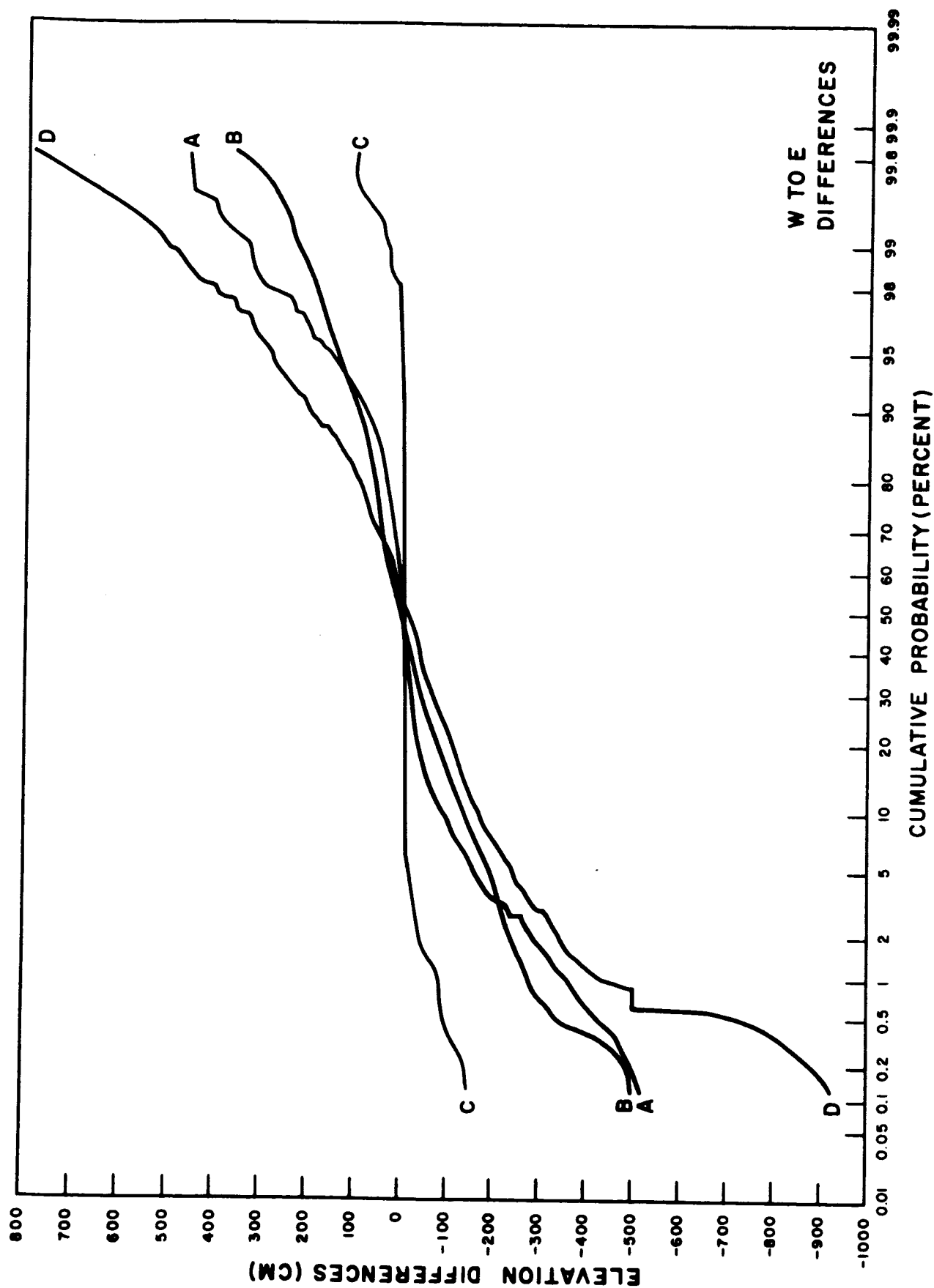


Figure III-14. Frequency Distribution of Elevation Differences (West to East) on Probability Scale

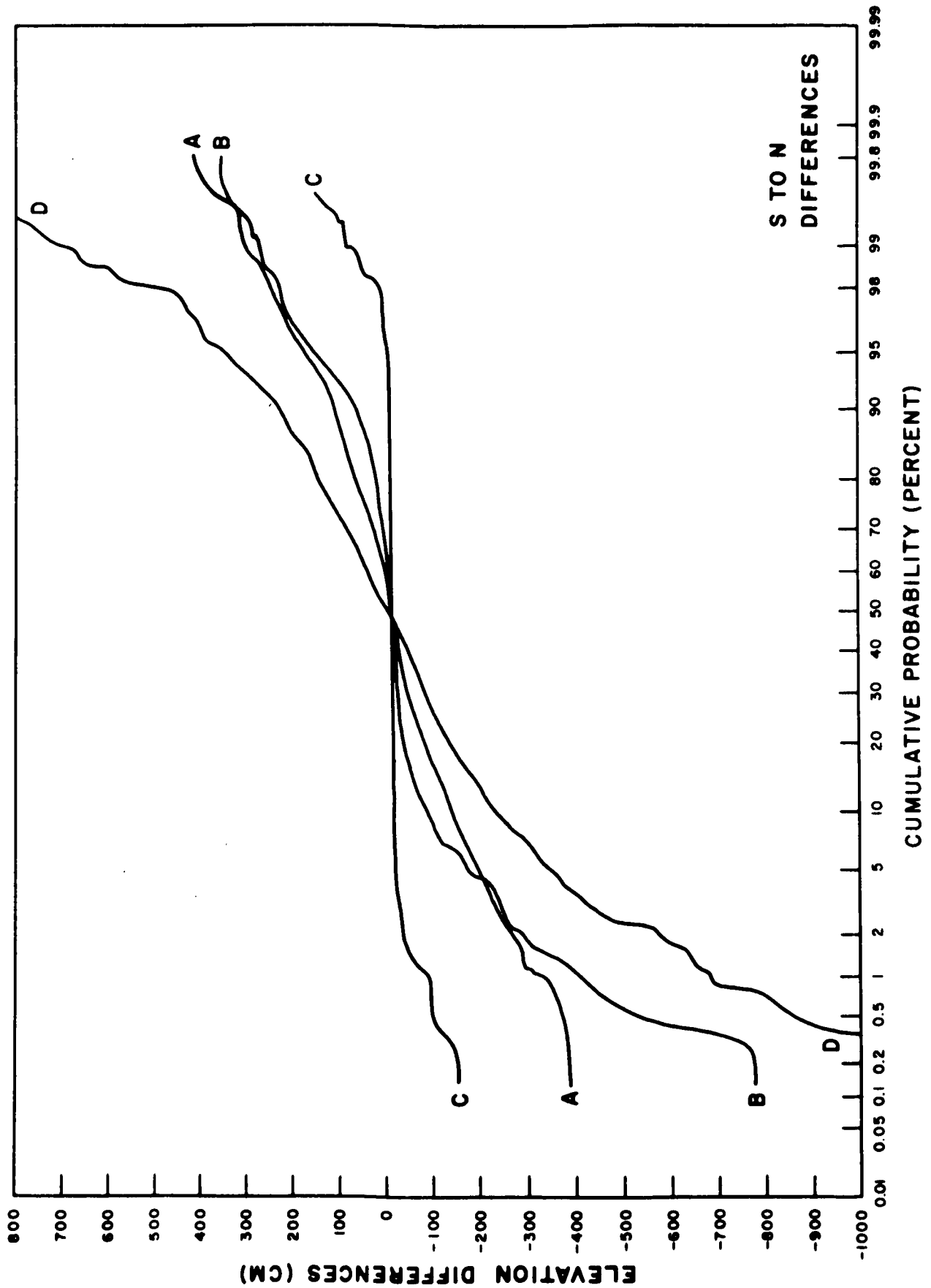


Figure III-15. Frequency Distribution of Elevation Differences (South to North) on Probability Scale

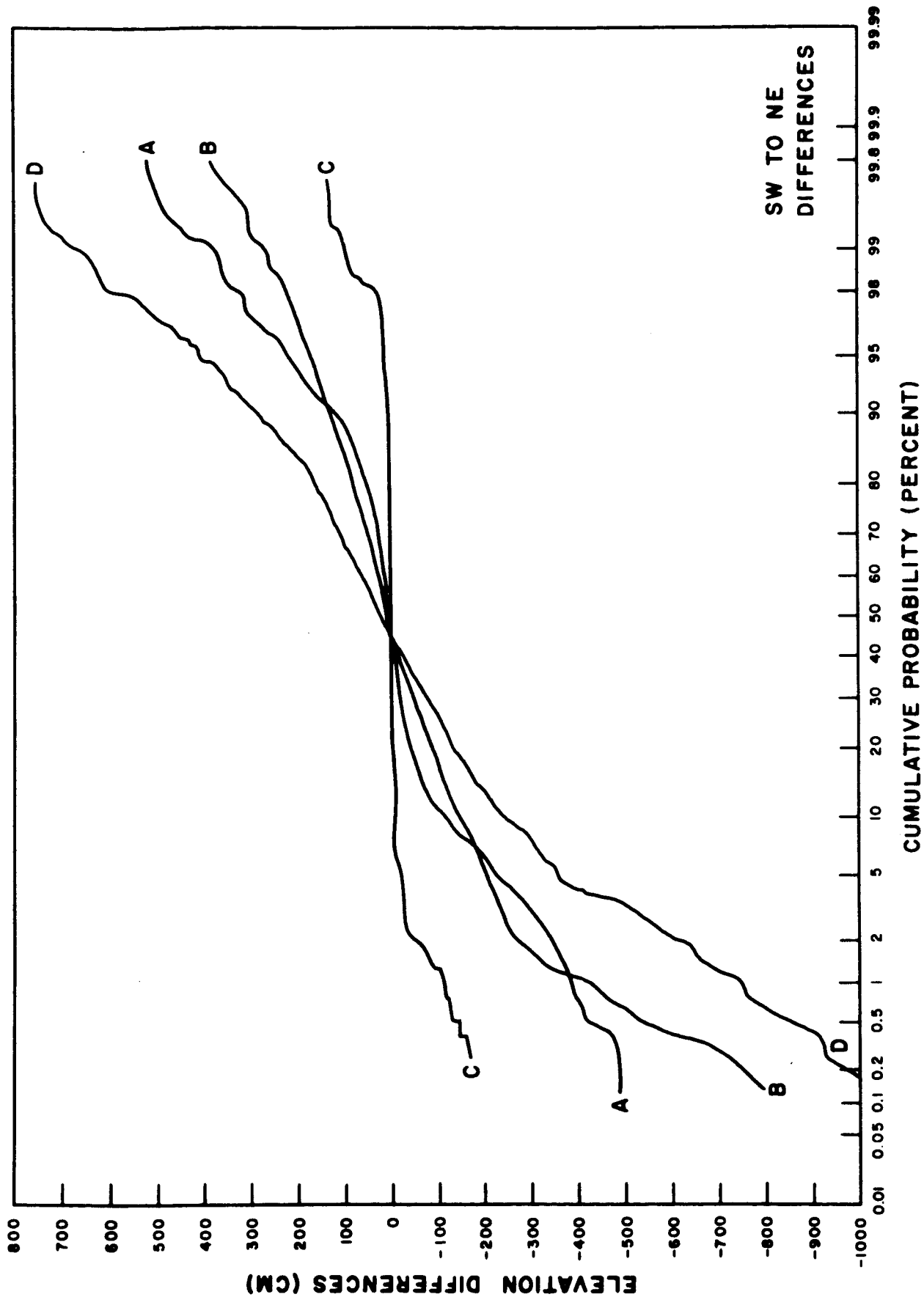


Figure III-16. Frequency Distribution of Elevation Differences (Southwest to Northeast) on Probability Scale

where τ is the lag distance and $\bar{x} = 0$. The power spectrum is the Fourier transform of the autocorrelation function

$$P(f) = \int_{-\infty}^{\infty} C(\tau) \cos 2\pi f \tau d\tau \quad (\text{III-44})$$

Unfortunately, in reality one never has a continuous sample of infinite length. Of necessity, the length must be finite. The effect is that the autocorrelation function $C(\tau)$ is multiplied by a lag window.

Furthermore, in this problem, the sample is not continuous but equispaced, causing the autocorrelation function $C(\tau)$ to be multiplied by an infinite series of Dirac delta functions (comb function).

One of the properties of Fourier transformation is that upon transformation, convolution becomes multiplication and multiplication becomes convolution. Consequently, the power spectra of interest will be convolved with the transform of the comb function (itself, a comb function of different spacing) and also convolved with the transform of the spectral window. These are discussed briefly in Appendix F.

b. Autocorrelation Function

The calculated autocorrelation functions $C_x(n\Delta\tau)$ and $C_y(n\Delta\tau)$ are

$$C_x(n\Delta\tau) = \frac{1}{(M-n)N} \sum_{j=1}^{M-n} \sum_{i=1}^N Z_{ij} Z_{i,j+n} / \sigma^2 \quad (\text{III-45})$$

and

$$C_y(n\Delta\tau) = \frac{1}{M(N-n)} \sum_{j=1}^M \sum_{i=1}^{N-n} Z_{ij} Z_{i+n,j} / \sigma^2 \quad (\text{III-46})$$

where $n = 0, 1, \dots, m$, $\Delta\tau$ is the grid-line spacing 10.3 m (5.15 m for the larger matrix) and $M = N = 29$ (57 for the larger matrix). The value of m was limited to 18 (39 for the larger matrix) so that the autocorrelation function always would be the average of at least 300 points. Division by the variance σ^2 makes $C_x(n\Delta\tau)$ and $C_y(n\Delta\tau)$ the normalized autocorrelation functions in which the maximum value, which always occurs at zero lag, equals one. Note that the entire matrix, not just a single row or column, was employed for calculation of the autocorrelation functions. This was one method of reducing the two-dimensional analysis to a simpler one-dimensional analysis. (Another method would have been to average data from randomly oriented sample lines.)

1-1

The autocorrelation functions calculated from the smaller matrices for the four areas are given in Figure III-17. The differences in the east-west (x) functions and the north-south (y) functions can be attributed to oriented power. To obtain a single function for each area, the x and y values were averaged. The results are shown in Figure III-18.

The autocorrelation function of an infinite, perfectly smooth surface would be one for any lag. That of an infinite, perfectly rough surface would be a Dirac delta function of magnitude one centered at zero lag. Consequently, one would expect that as the surface became smoother, the autocorrelation function would have dropped from one to zero (and would have remained there, ideally) at a smaller lag distance. Observe, however, that exactly the opposite occurred. The autocorrelation function dropped to zero for area C at a smaller lag than for area D.

Since larger matrices were available for areas D and B, autocorrelation functions were calculated again and compared to the original values (Figure III-19). The strong similarity of the curves indicates that appreciable power of wavelengths 5.15 m to 10.3 m is not present in the two areas.

c. Power Spectrum Analysis

The actual power spectra of the four areas were somewhat masked by the effects noted earlier. These were calculated in an attempt to explain the peculiar autocorrelation coefficient behavior, where the estimated contributions to the power spectra were removed (Figure III-20). The power spectrum of an infinite, perfectly smooth surface would be a Dirac delta function centered at zero frequency; that is, all of the power is concentrated at the frequency whose associated wavelength is infinite. The power spectrum of an infinite, perfectly rough surface would be one for any frequency; that is, the power is divided evenly among all frequencies associated with all wavelengths. Again note that the results are the antithesis of those expected (as one should anticipate from the autocorrelation function results). The roughest surface spectrum is a sharp peak centered at zero frequency; the smoothest is a more evenly distributed function.

d. Discussion of Results

Explanation of these results presented a problem to which only one satisfactory explanation has been found. Obviously, some roughness power is present in area D, causing it to be classified as the roughest surface. For purposes of discussion, assume it to be power of wavelength λ_0 . (It is more likely to be within a wavelength range $\lambda_0 + \Delta\lambda$.)

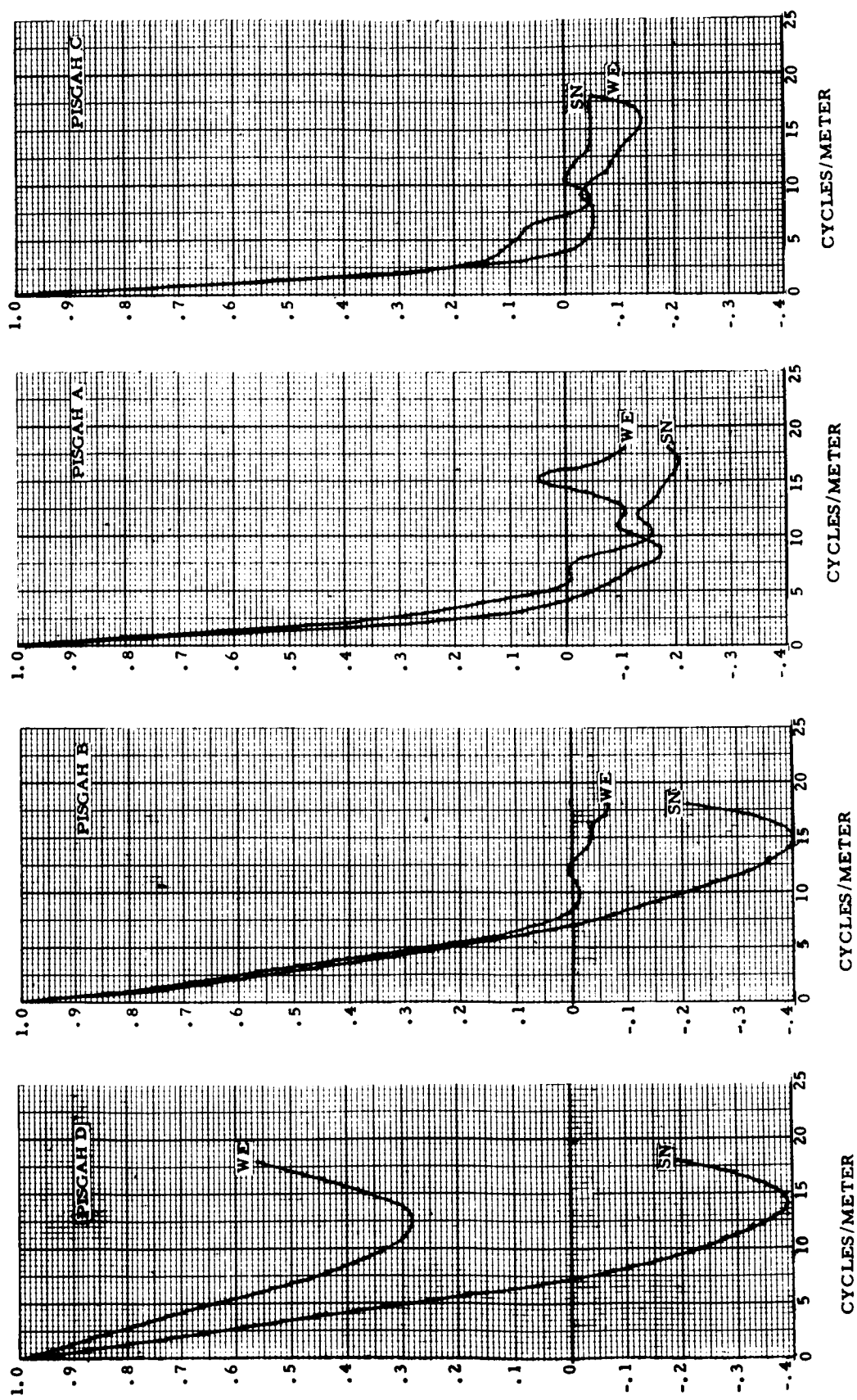


Figure III-17. Autocorrelation Functions

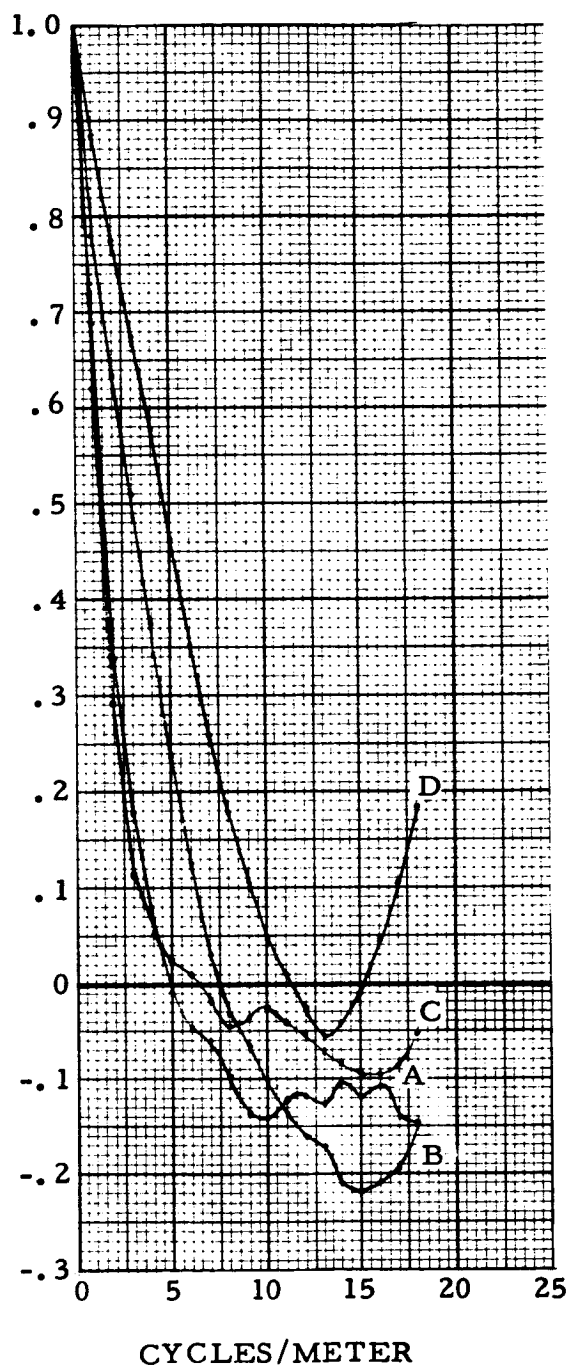


Figure III-18. Averaged Autocorrelation Function for All Areas

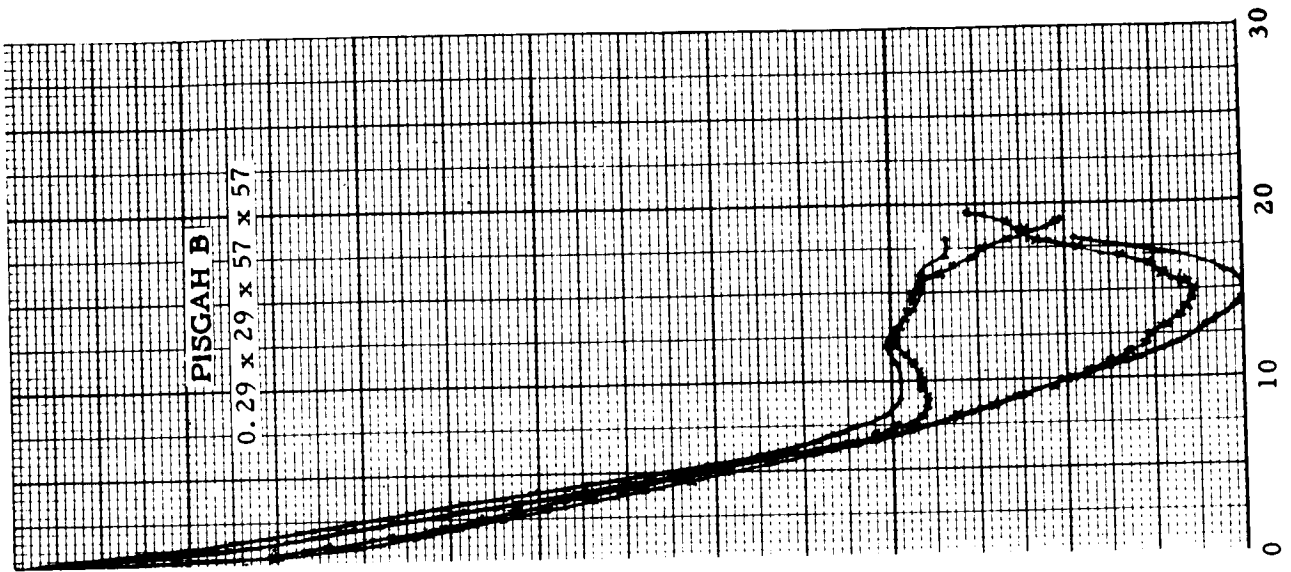
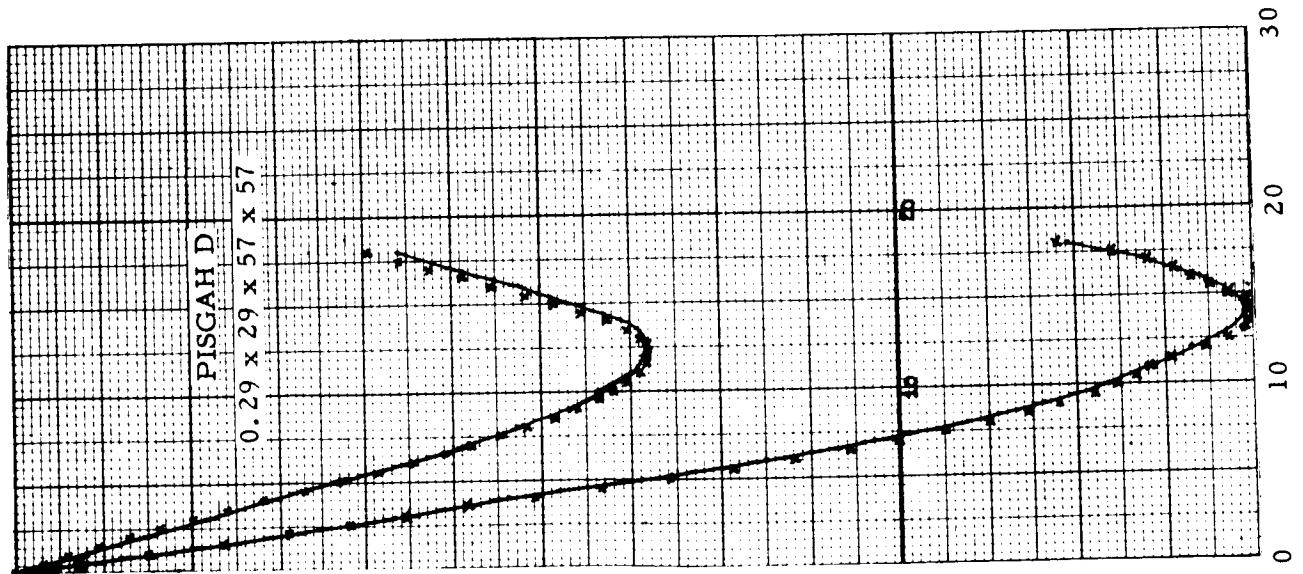
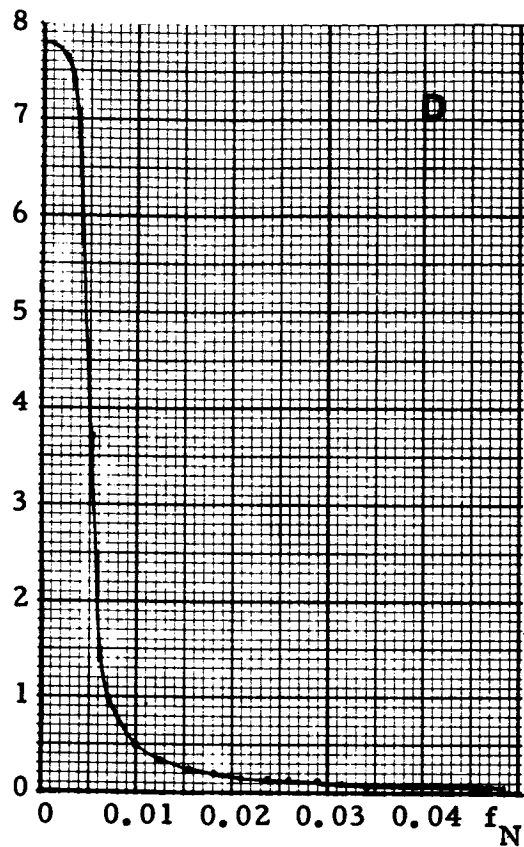
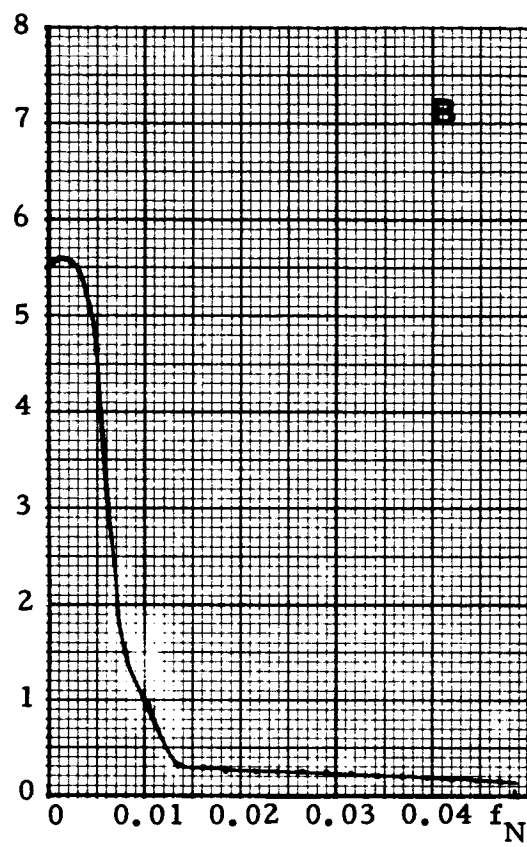


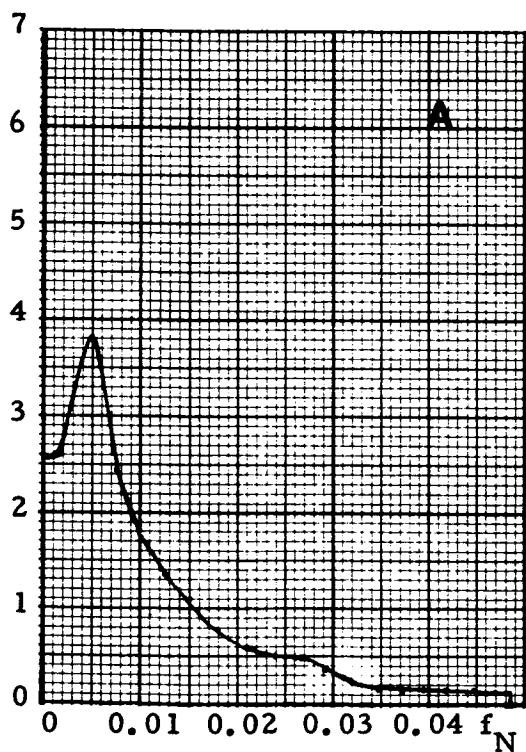
Figure III-19. Autocorrelation Function Based on Multiples of 10.3 Meters Lag and 5.15 Meters Lag (Area D)



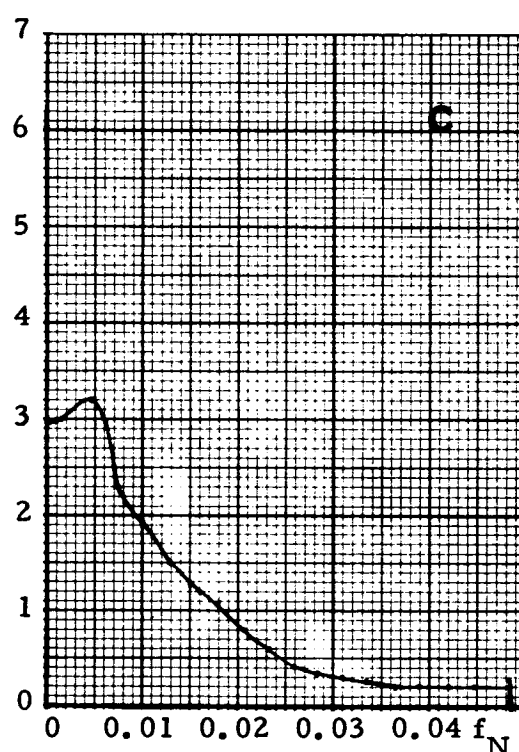
CYCLES/METER



CYCLES/METER



CYCLES/METER



CYCLES/METER

Figure III-20. Power Spectra

The analysis presented here can detect energy only within a given range of frequencies. The highest frequency is the Nyquist or folding frequency f_N which is determined by the grid-line spacing Δt

$$\begin{aligned} f_N &= \frac{1}{2\Delta t} \\ &= \frac{1}{2(10.3 \text{ m})} \\ &= 0.0485 \text{ cycles/m} \end{aligned}$$

This corresponds to energy whose wavelength is 20.6 m. Nothing can be said about energy whose wavelength is shorter than this. Furthermore, the limited size of the areas analyzed decreased the accuracy of the spectral estimates possible, especially at the frequencies approaching the Nyquist frequency (at the shorter wavelengths).

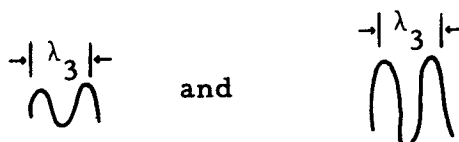
A much better analysis could have been performed had the maps represented areas 3000 m x 3000 m rather than the available 300 x 300 m. To increase the Nyquist frequency and, thereby, determine energy content at shorter wavelengths, one would have had to shorten the grid-line spacing. However, doing so without also having sampled a larger area would have been useless. The signal of interest (energy content at the shorter wavelengths) would have been buried in the noise caused by the finiteness of the sample. The lowest frequency (longest wavelength) which could be detected is zero theoretically. Practically, however, the trend plane removal already has removed low-frequency energy, but it is of little interest in classifying the surfaces. The actual limit is on the order of 0.000833 cycles/m (wavelength 1200 m).

It is proposed that the energy present which causes one to classify area D as the roughest is of frequency higher (wavelength shorter) than can be detected with this analysis. Horton* expresses this in a different way:

"It is my opinion that in a given rock type, the factor that limits topography is the maximum slope. So in order to have relief of large magnitude, the topographic features must have large wavelength. Regions of small relief will have features of short wavelength. Thus in a given region (i. e., rock type) one can have



but not



Now in case (a) where the relief is small, a shift of 10.3 meters will be far enough in terms of the average wavelength λ_1 that the new sample z_2 will tend to 'forget' the value of the original sample so there will be a lower coefficient of correlation. On the other hand in case (b), λ_2 is larger so that the same displacement, 10.3 meters, is a smaller fraction of the wavelength and the 'memory' is better."

The data available were insufficient for a proper power spectrum analysis. It is considered important to explain the apparent discrepancy in the trend of the autocorrelation function with respect to the intuitive roughness classification. A more accurate power spectrum analysis would verify or disprove the proposed explanation of high high-frequency content. Such an analysis, however, would require much larger maps of the Pisgah areas than were available for this contract, as well as closer sampling, i. e., shorter grid-line spacing.

4. Summary

Correlation functions along different profiles are expected to be equal if the assumption of isotropy is valid. In Figure III-17, correlation functions along orthogonal profiles are given for areas D, B, A, and C. Those of A, B, and C support this assumption for small lag values. This assumption does not appear valid for area D. This surface evidently has unusual properties compared to the other Pisgah areas studied as evidenced by the non-Gaussian character.

*Personal communication of Dr. C.W. Horton to Martha Fowler, 11 March 1965.

Formal tests of the Gaussian assumption show that the elevation data considered in the present report are not Gaussian. However, it is apparent from Figures III-7 and III-9 that for certain areas the Gaussian assumption will result in only small errors. The error made will be in a conservative direction. In all areas examined, there are more elevations or elevation differences in the neighborhood of zero than would be expected under the Gaussian assumption.

The power of this method certainly rests in the simple relation expressed in Equation (III-26) for the probability derived under the Gaussian assumption. Many statistical procedures are known to be "robust" under this assumption of normal data. This means that although the input data deviates from normality, the procedure still will accomplish the purpose for which it was intended. In this sense the statistical procedure outlined in the present chapter might serve as a preliminary measurement for many area's resulting in a quantitative value for the probability of success for each area and thereby indicating a relatively small number of areas which should be more closely examined.

The data sampling grid distance should be approximately equal to the LEM pad separation distance. The essential formula to examine for sensitivity of this procedure to grid sampling interval is Equation (III-37) of Section C-2. From Figure III-17 it can be seen that the quantity $1-\tau = ax$ in the neighborhood of the value $x = \text{LEM pad separation}$ of $n = 1$. Thus,

$$\sigma^2 \propto \frac{1-\tau}{x^2} = \frac{a}{x}$$

which is insensitive to changes in x , small in comparison with x . This can be observed numerically in Table III-2 by comparing σ_t ($\Delta x = 1.45 \text{ m}$) with σ_{tx} and σ_{ty} ($\Delta x = 10.3 \text{ m}$) for the areas A, B, C, D. The large increase in x produces a small decrease in the value of σ_t .

Also in Table III-2, the 57x57 matrix analysis shows that a large decrease in Δx from that given by the 29x29 matrix produces a large increase in the standard deviations.

This method may best be utilized for rank ordering several areas according to their suitability as LEM landing sites. For purposes of ranking areas, the data sampling grid distance should be approximately the LEM pad separation distance and constant for all areas.

E. REFERENCES

- Bertram, S., 1965, The universal automatic map compilation equipment: Photogrammetric Eng., v. XXXI, no. 2, Mar, p. 244-260.
- Blackman, R. B. and J. W. Tukey, 1959: The Measurement of Power Spectra from the Point of View of Communication Engineering, Dover Publications, Inc., N. Y.
- Defant, A., 1961, Physical Oceanography: Pergamon Press, Oxford, v. I, p. 14.
- Doob, J. L., 1953, Stochastic Processes: John Wiley & Sons, N. Y., p. 72.
- Elderton, W. P., 1927: Frequency Curves and Correlation, Charles & Edwin Layton, London, 2nd ed., p. 36-73.
- Kendall, M. G., 1947: The Advanced Theory of Statistics, Charles Griffin & Co., Ltd., London, 3rd ed., v. I, p. 137-145.
- Kosofsky, L. J. and G. C. Broome, 1965, Lunar Orbiter: a photographic satellite: NASA Langley Research Center, Hampton, Va., Presentation at Spring Convention of Motion Picture and Television Engineers, Los Angeles, Calif., Mar 28- Apr 2.
- Patnaik, P. B., 1949, The non-central X^2 -F-distributions and their applications: Biometrika, v. 36, p. 202-232.
- Rice, S. O., 1944, Mathematical analysis of random noise: Bell System Tech. J., 23, Sec. 2.9, p. 282-332.
- Tanner, W. F., 1960, Numerical comparison of geomorphic samples: Science, v. 131, p. 1525-1526.
- Tanner, W. F., 1959, Examples of departure from the Gaussian in geomorphic analysis: Am. J. of Sci., v. 257, p. 458-460.
- Williams, C. W., 1960, Study of a digital method for an automatic map compilation system: USAERDL, Ft. Belvoir, Va., Contract DA-44-009-eng-4205, IBM Corp., 36 p.
- Williams, R. E. and P. Rosenberg, 1958, Automatic map compilation system: experimental study of profiles and match error curves: USAERDL, Contract DA-44-009-eng-3154, Paul Rosenberg Associates, 96 p.

CHAPTER IV
APPLICATION OF OPTICAL DATA
PROCESSING TO LEM LANDING SITE SELECTION

A. GENERAL APPROACH TO PROBLEM

1. The Role of Optical Computers

The program's overall objective is to determine the suitability of any portion of the lunar surface for LEM landing. Input data for this evaluation will consist of lunar surface photographs, most of which will be taken at long range. A limited number of photographs will be taken at low elevation and with great detail. From the close-range photographs, it will be possible to map with considerable reliability the portions of the surface which do not have a slope greater than 12° and protuberances less than 50 cm in height and hence are suitable for landing. Deductions from photographic work about one limited area may be confirmed further by landing a suitable unmanned vehicle.

The amount of territory which may be explored in such detail, therefore, is limited. However, it is desirable to evaluate as much of the lunar surface as possible so that a best selection may be made, alternate landing sites selected and the magnitude of areas suitable for any landing given. Therefore, a technique which could evaluate areas from long-range photographs with speed and confidence is desirable. Since the basic input data are photographic, it is worthwhile to examine optical data processing and evaluate its effectiveness for gross evaluation of fairly large regions. Optical data processing affords a way to recognize features through the use of Fourier transforms and suitable filters at the frequency plane. Cross- and autocorrelation operations in two dimensions also are possible. It is conceivably possible to compare two regions on a quantitative basis by appropriate statistical parameters based on these functions. Such numerical comparisons, which can be performed arithmetically by digital computers, also can be done reliably with optical techniques.

The objective of this portion of the study is to identify optical data processing techniques that can compare two surfaces from their photographic images on a slope-cumulative area basis and to determine a degree of correlation for this comparison. Such a technique would be useful in examining large areas rapidly in order to preselect those promising areas to which other detailed measurements could be applied later. Further, it is desirable to find those features of the lunar surface that could be used to compare two regions, one of which is photographed with high resolution and the other with lower magnification.

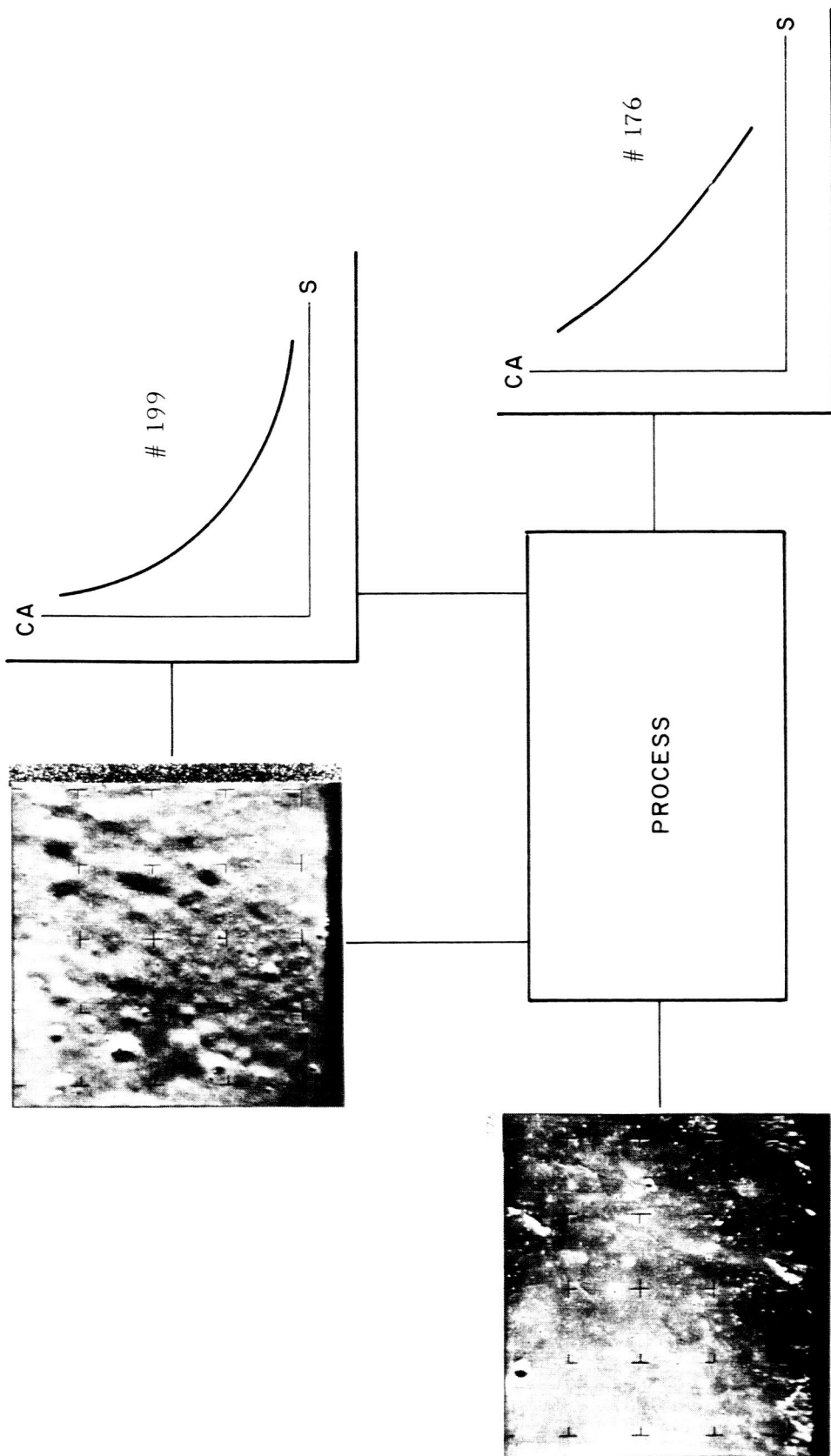
Optical data processing experiments were performed on the Ranger series photographs and Pisgah Crater photographs. This report describes the work accomplished to date. The objective is illustrated in Figure IV-1. Ranger VII photograph 199 illustrates a short-range lunar surface for which the cumulative area vs slope is assumed known, and Ranger VII photograph 176 is a typical long-range surface to be evaluated. Required is a process for operating on these data to predict the cumulative area vs slope for the area in photograph 176. It is assumed that, once this curve is available for this area, other computations will suffice for calculating the probability that a LEM will not tilt upon landing randomly in this area. These latter computations are not within the scope of the optical data processing investigations performed to date.

2. The Search for a Comparison Criterion

Before proceeding to apply the optical techniques, a visual evaluation of Ranger VII photographs (NASA, 1965) was made in an attempt to find a guide to the approach to be taken. Consider the series selected from photographs 199 to 151 and presented in Figure IV-2. What happens to the small-scale detail observed in short-range photograph 199 as the magnification decreases with the increasing photographing distance? Do any characteristics appear to persist in 199, as one observes the series of photographs taken at increasing photographing distance, that can be used to characterize the area of which photograph 199 is a portion?

The answer to the first question is that as the distance increases, the craters observed in photographs 199 gradually disappear; in photograph 193, only the large craters observed in photograph 199 are visible. As one proceeds through photographs 185, 176 and 151, the large craters eventually disappear; in 151, the details of 199 are no longer recognizable. Therefore, one concludes that the small details alone would not necessarily be the criterion on which to evaluate an area; some other criterion must be sought.

To seek an answer to the second question, one observes in photo 197 that photo 199 is found in the upper right-hand quadrant as a group of small craters. Other similar groups of craters are present. Further, ignoring the position and comparing photos 199, 197 and 193, one observes that the distribution in dimension of the craters appears the same. Large-dimension photographs of the craters in one plate are replaced in another plate by craters having the same dimension on the photograph. Similarly, for the small-dimension craters on the photograph and for those sizes in between, this same constancy of pattern is markedly observed by comparing photos 197 and 193, and it persists through photo 151; i. e., the size-frequency distribution of the craters appears to characterize the lunar area, and it might be the criterion for comparing to lunar surfaces.



OBJECTIVE

Figure IV-1. Objective of the Optical Data Process

RANGER VII

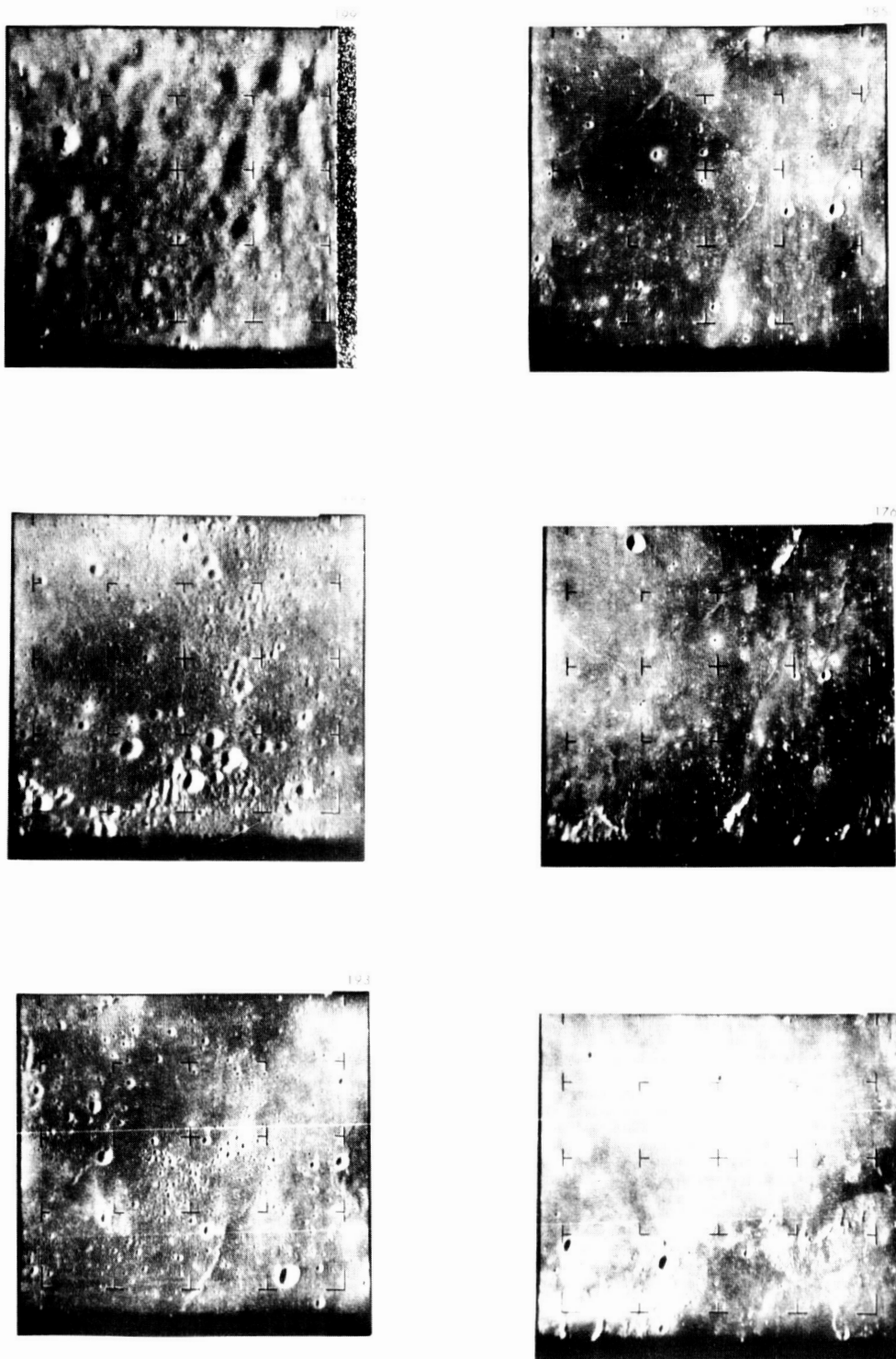


Figure IV-2. Search for Criterion

How well does the crater size-frequency distribution characterize the lunar surface? Dodd, Salisbury and Smalley (1963) find that, from earth-based observations, the cumulative frequency crater size may be represented by an expression

$$F = AD^B$$

where

F = cumulative frequency

D = crater diameter

A, B = constants for a selected lunar area

In Figure IV-3, two plots based on this equation show a good fit to observations.

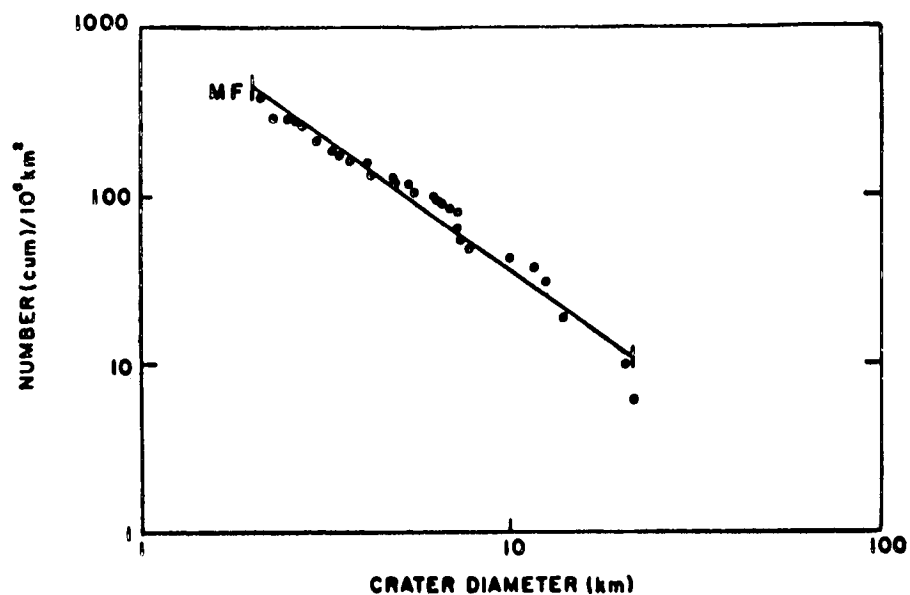
For any lunar area, a set of values for A and B may be selected. For a different lunar area, a new set of values may be found. Their summary for 10 lunar areas is presented in Table IV-1, which shows that each lunar area is characterized by its own crater frequency-size distribution. Extension of earth-based observations to the Ranger VII photographs by Kuiper et al (1965) showed that, for at least the one area, the data may be extended with reasonable agreement over a crater diameter range of three orders of magnitude. Kuiper's data are reproduced in Figure IV-4.

There is, therefore, reasonable confidence that any given lunar surface is characterized by the crater frequency-size distribution, that this distribution persists over a considerable range in crater diameters and that two territories may be compared on the basis of this distribution. No other basis for comparison has yet been found.

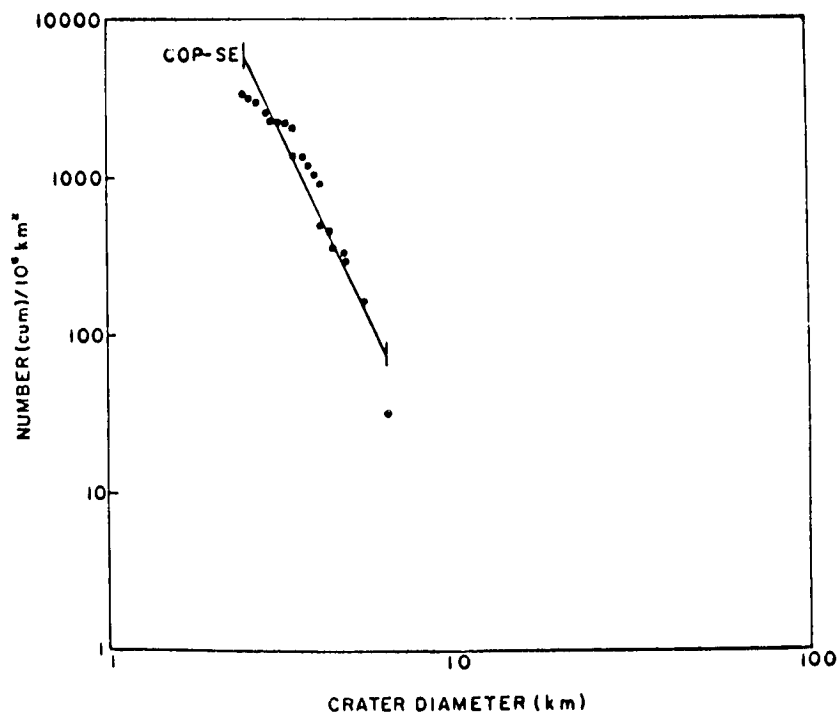
B. EXPERIMENTAL STUDIES

1. The Optical Fourier Transform

Having decided to use the frequency-crater size distribution to compare two areas, one desires a step which recognized the craters regardless of their position on the photograph or number. Examining the Range VII photographs, one sees that the craters appear as circular areas; one semicircle is dark, the other bright. These craters are dispersed in a grey area. A synthetic crater was constructed and a photographic copy made in two ways. In the first, only a single crater was copied using a single lens; in the other, a multiple copy (1400 in this study) was made using a "Fly Eye" camera. These two copies are presented in Figure IV-5(A) and (B). Using these copies, each in turn on optical Fourier transform equipment, Fourier transforms of these two copies as shown in Figure IV-5 were also obtained. On the single copy, the crater has a 1/4-in. dia; in the multiple copy, each crater had a 0.02-in. dia.



(A) Mare Frigoris



(B) Area Southeast of Copernicus

Figure IV-3. Crater Frequency (Cumulative) as a Function of Crater Diameter. Data and computed curve are shown (after Dodd, Salisbury and Smalley, 1963)

Table IV-1

LUNAR SURFACES ON WHICH CRATERS HAVE BEEN COUNTED

Surface	Symbol (Fig. IV-3)	Area (km ²)	A*	B*	R ² *
Mare Frigoris	MF	1.6 x 10 ⁴	1299.0	-1.545	0.969
Mare Serenitatis	MS	3.4 x 10 ⁴	641.7	-1.707	0.977
light portion	MS-Light	2.6 x 10 ⁴	561.6	-1.702	0.959
dark portion	MS-Dark	8.5 x 10 ⁴	581.2	-1.535	0.939
Northern Mare Imbrium	NMI	4.7 x 10 ⁴	1172.6	-1.776	0.985
Apenninian debris	AD	1.3 x 10 ⁴	9661.8	-2.103	0.989
Central Crater Province	CCP	3.4 x 10 ⁴	49 687.0	-2.085	0.943
Ptolemaeus	PT	1.3 x 10 ⁴	5072.3	-2.118	0.961
NE of Copernicus	COP-NE	3.5 x 10 ⁴	488 317.0	-4.804	0.956
SE of Copernicus	SOP-SE	3.1 x 10 ⁴	439 110.0	-4.629	0.918

* A and B are constants in the expression relating diameter and crater frequency; R² is the correlation coefficient (squared) for the computed diameter-frequency curves.
(after Dodd, Salisbury and Smalley, 1963)

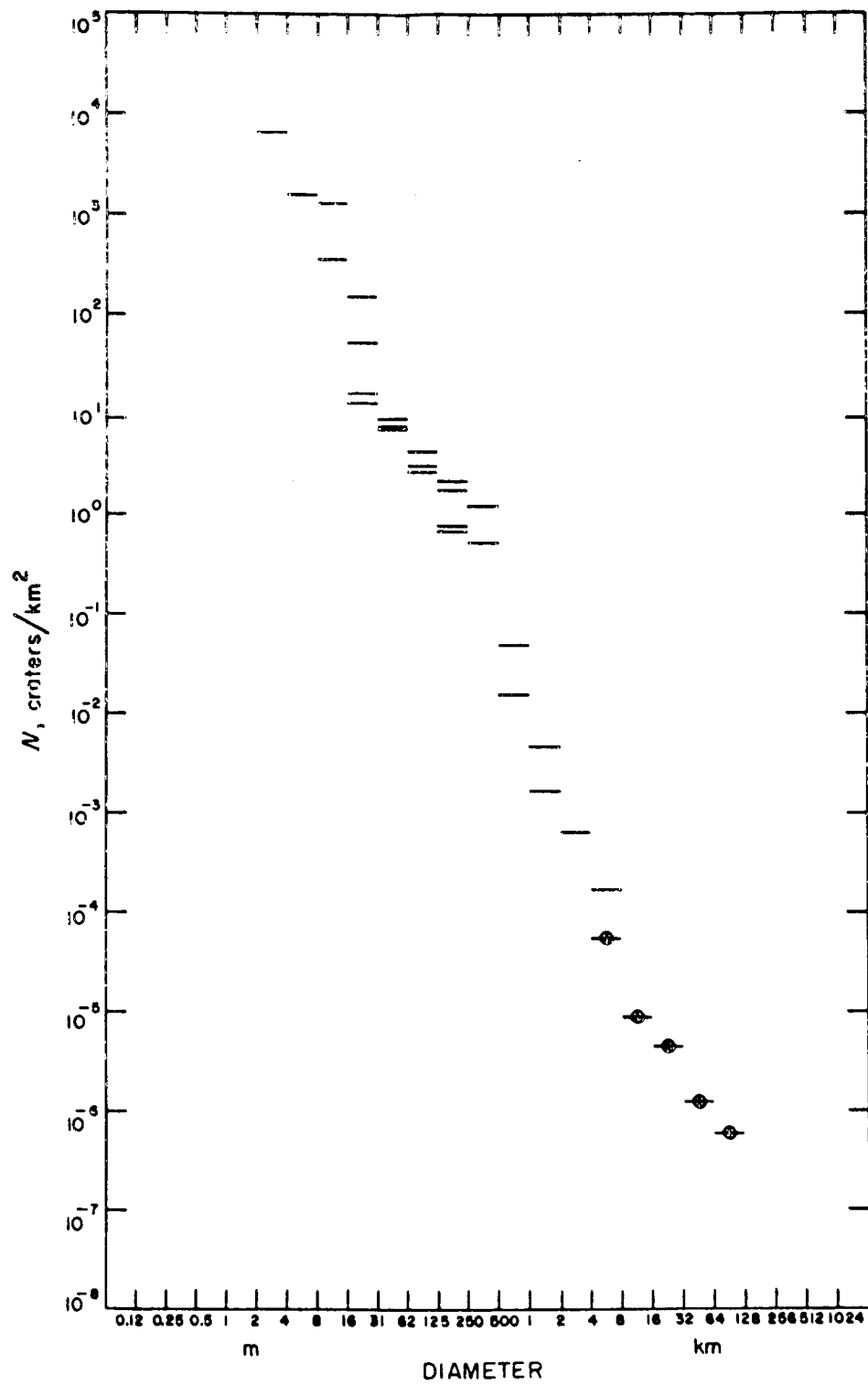
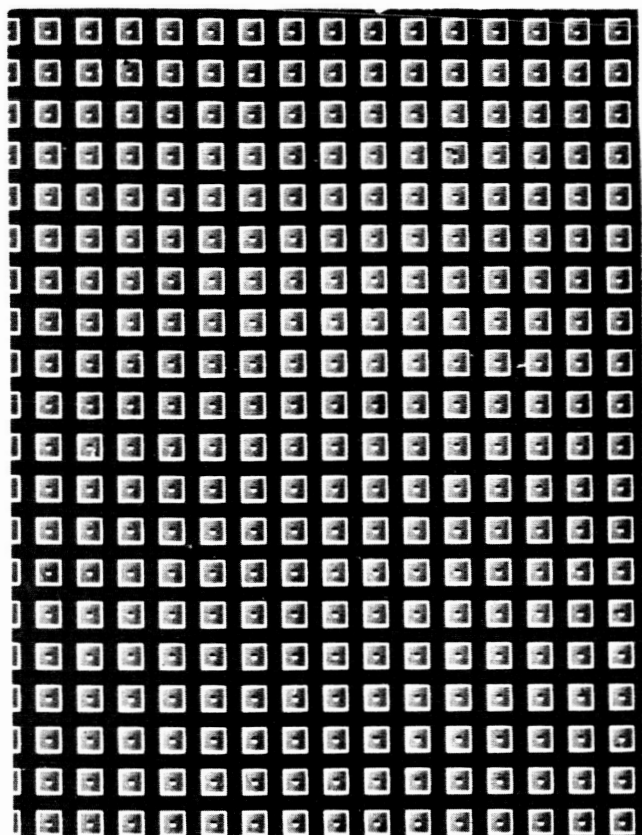


Figure IV-4. Post-Mare Diameter Distribution of Lunar Craters from Earth-Based and Ranger Photographs (Hartmann)

(A)



(B)

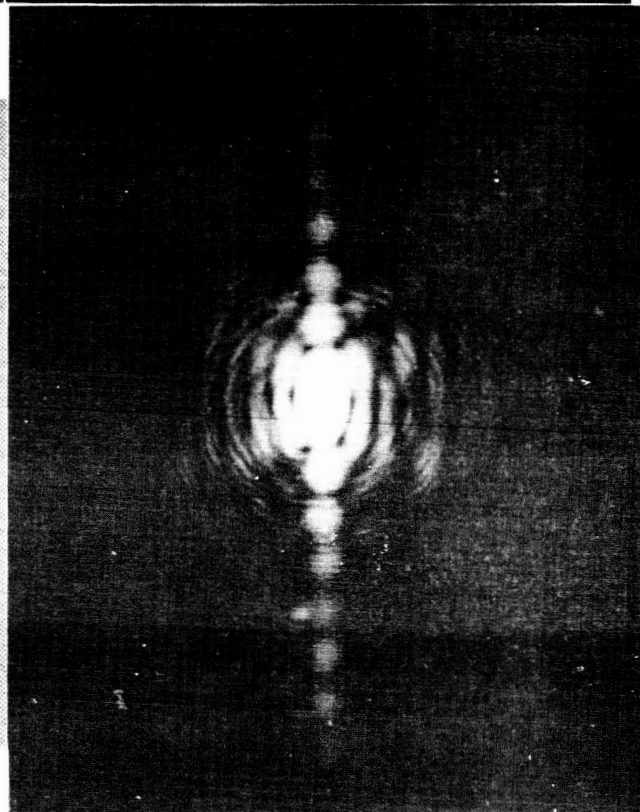
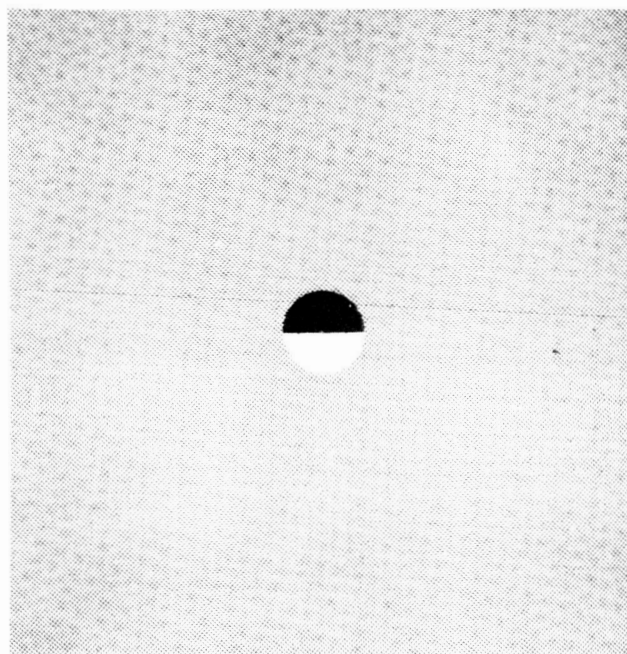
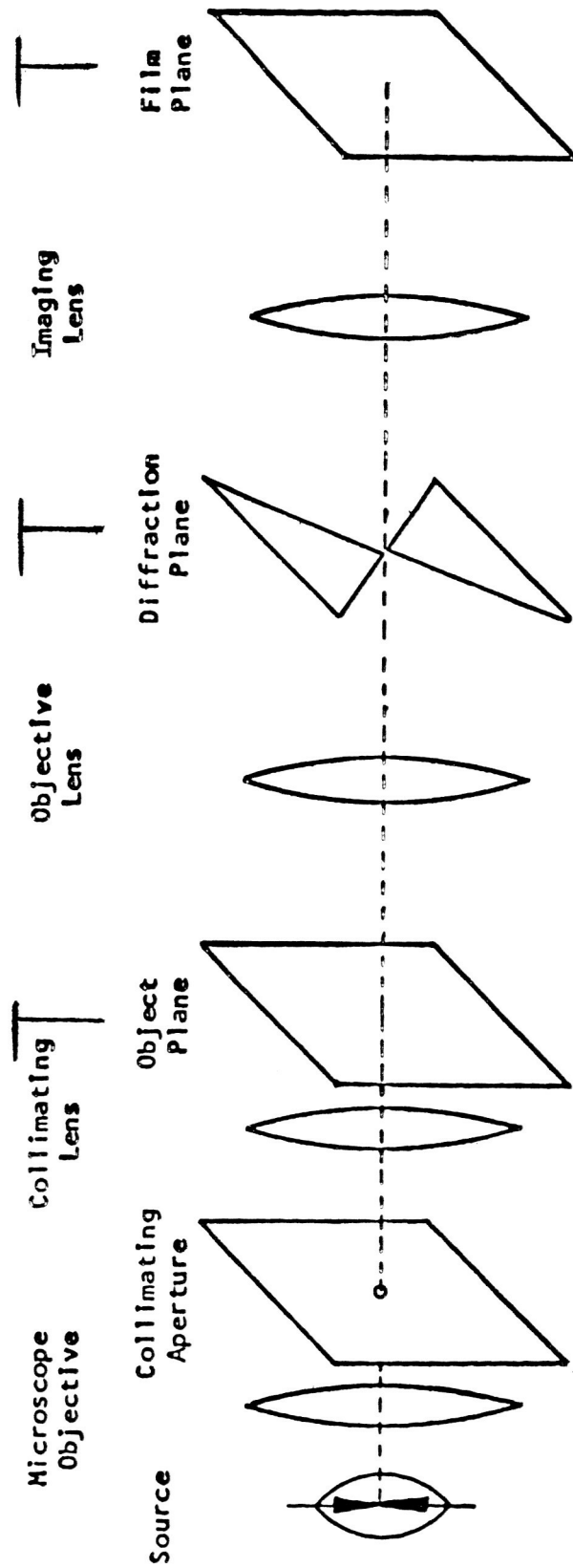
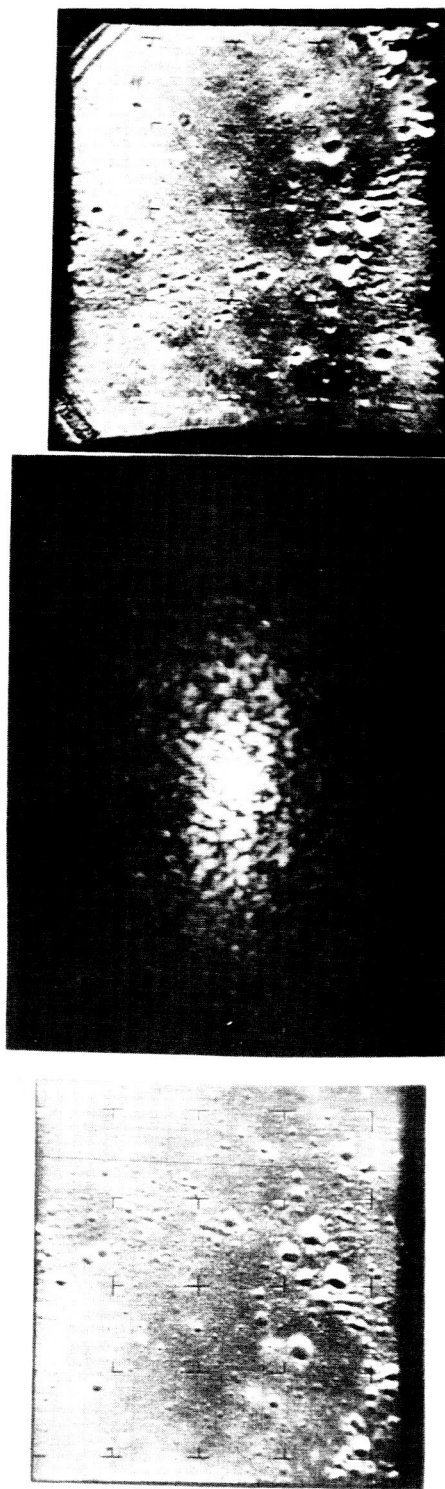


Figure IV-5. Constancy of Fourier Transform

The optical equipment was modified to take these size differences into account. Then, by final magnification in the enlarger, the Fourier transforms were obtained having comparable dimension. Comparing these two transforms, one can recognize the similarity in the two patterns. The features of Fourier transform do not depend on the position of the craters or their number. The large number of craters in Figure IV-5 (B) produces a Fourier transform having a large number of dots. If, in the densitometer, one chose the slit of correct dimension, one would obtain similar traces regardless of the Fourier transform densitometered. Therefore, the Fourier transform suppresses the position of the crater but retains a feature that characterizes the crater feature regardless of the number. It is, therefore, a useful tool in the process for comparing the lunar surfaces.

There are a number of reports on optical methods for obtaining the Fourier transforms (Cutrona et al, 1960; O'Neill, 1956; Vander Lugt, 1964, Preston, 1965). The system used in this study is illustrated in Figure IV-6. Each of the lenses has a focal length of 57.3 cm. Such a system as illustrated gave Fourier transforms too small to be useful. Consequently, a 2-cm focal-length negative simple lens was added between the diffraction plane and the object plane to enlarge the transform image. This resulted in a small recovered image. To check that the simple lens did not deteriorate the quality of the optics, another negative lens of comparable focal length was placed before the film plane. The recovered image had dimensions comparable to the original object (Range VII photograph 197), and no serious loss in detail, even with the introduction of some "pincushion" effect, was incurred. Fourier transform and recovered image, along with the corresponding mathematical function, are illustrated in Figure IV-6. The recovered image was not used in the study but served as a check on equipment performance. It is to be noted that the photograph records the light amplitude squared only, i. e., $|F(\xi, \eta)|^2$, thereby losing the information stored in the phase portion of the propagated wave. Therefore, the Fourier transform so recorded in this study is not unique but, since only lunar data are used, application and use should not be thereby invalidated.

The Ranger VII series contains photographs of one lunar surface at large and small magnification. To a lesser extent so do the VIII and IX series. These photographs are ideally suited for this study since, for example, the short- and long-range photographs of Ranger VII may be processed with the long-range frames of Ranger VIII, and an estimate of this performance in predicting the short-range surface characteristics of VIII can be made by actual comparisons with the short-range photograph of VIII. A similar comparison using IX may be made.



$$f(x, y) \quad F(\xi, \eta) =$$

$$\frac{I}{\lambda} K \iint f(x, y) \exp \left[\frac{-2\pi i}{f \lambda} (x \xi + y \eta) \right] dx dy$$

$$F(\xi, \eta)^2$$

Figure IV-6. Equipment

The photographs were obtained from William Cunningham, Ranger project manager, NASA headquarters, Washington, D.C. Unfortunately, they were not received in similar format. The Ranger VII series was received in 16-mm form as a movie, VIII was received as 35-mm positives while IX was received as 35-mm negatives. In addition, it was decided to investigate photographs of Pisgah Crater, San Bernardino County, California, for which topographic maps and photographs were available. For this study, it is desirable to have all input data in the same form, preferably as 35-mm positives. The condition in which the Ranger series and Pisgah Crater data were received required additional photographic processing to reduce them to a common form. These photographic steps introduced differences in contrast and graininess which, coupled with the nature of the optical Fourier transform step, produced perturbations not anticipated initially.

In preparation for the next step, Fourier transforms of selected shots from the Ranger VII, VIII, IX, and the Pisgah Crater were obtained. Figure IV-7 illustrates the shots from Ranger IX and their respective transforms.

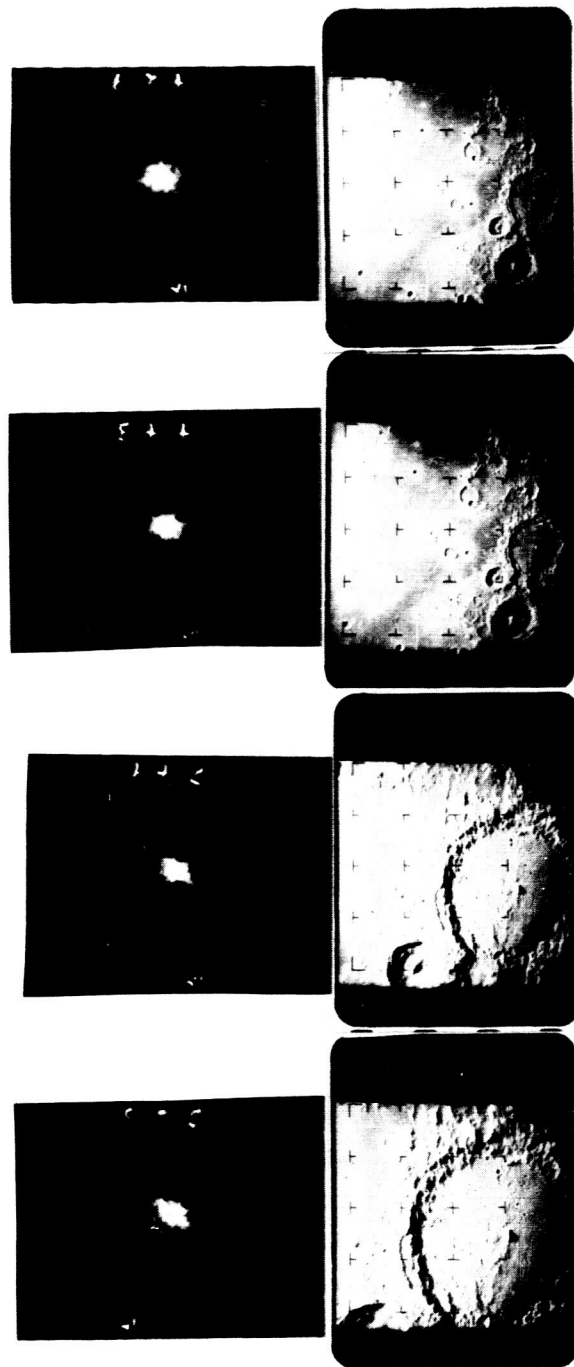
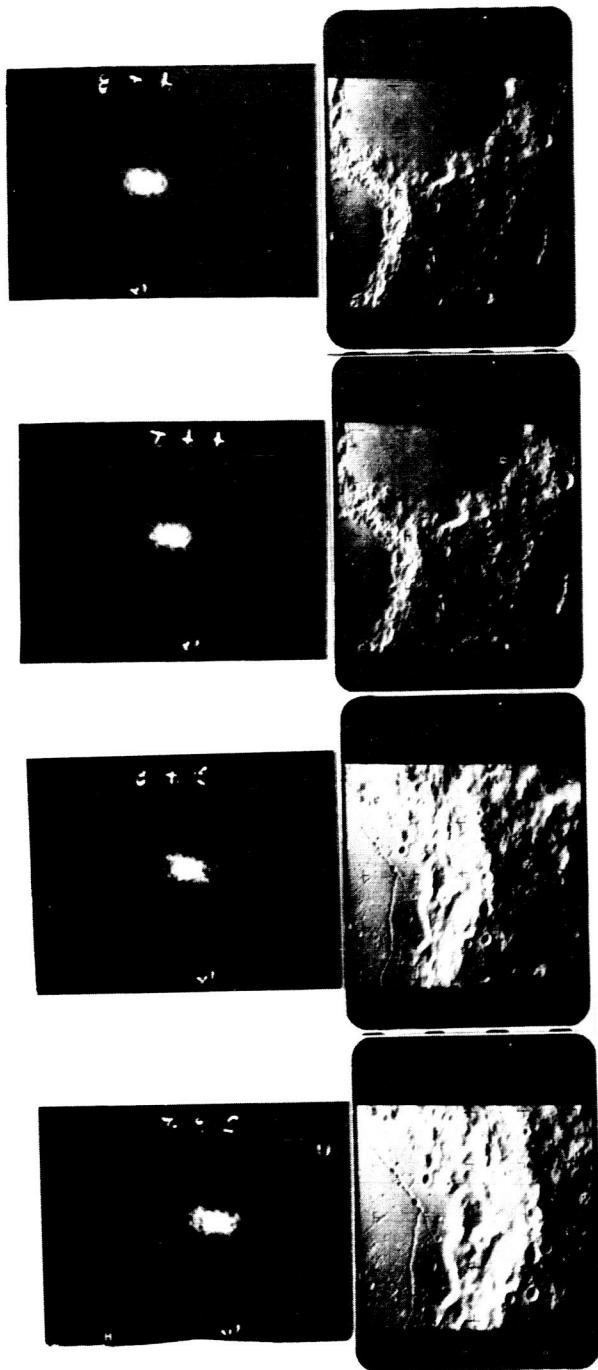
2. The Correlation Step

One would like to compare any two transforms in a quantitative way, and correlation processes suggest a means to be considered. Of course, these same correlation processes may be applied directly to the original images as well as to the transforms. A hazard in this approach is that, while good correlation may be observed, features such as mountain ranges, which are not of interest, may be involved; hence, an approach not involving the Fourier transform was not considered.

Consider the contribution that the correlation process will contribute in the following way. The crosscorrelation in a single variable is represented by (Lee, 1960).

$$\frac{1}{2X_i} \int_{-X_i}^{X_i} f_1(x) \cdot f_2(x + \xi) dx = \phi_{12}(\xi) \quad (\text{IV-1})$$

The graphical method for determining the crosscorrelation between the two functions consists of determining and summing the values of the areas overlapped by the two functions as ξ covers the range from $-X_i$ to X_i and dividing by $2 X_i$.



73

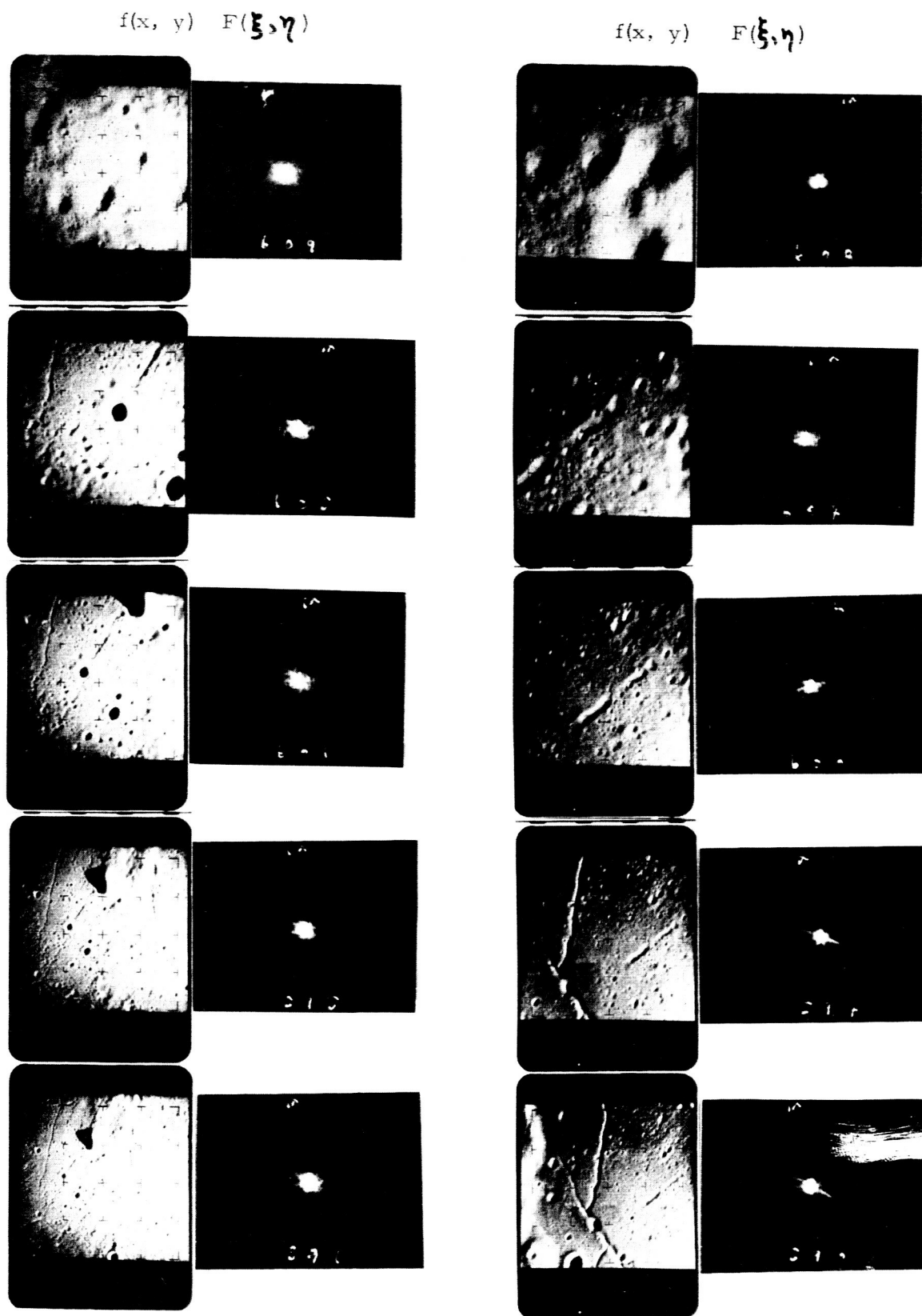


Figure IV-7. Fourier Transforms Ranger IX

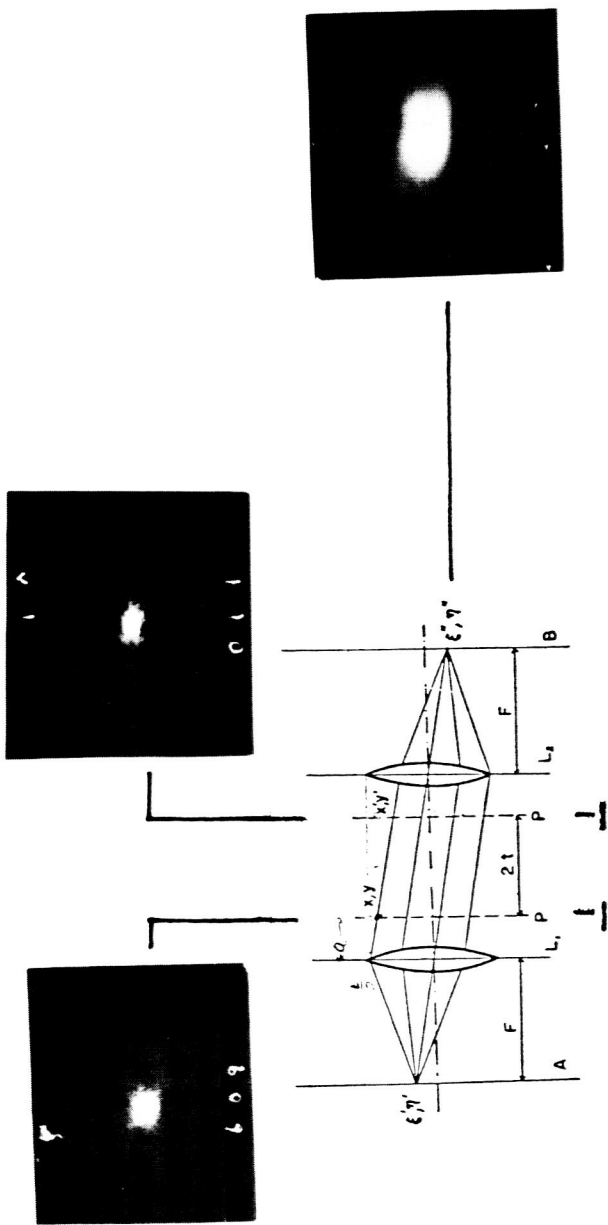
In Figure IV-8, Equations (IV-2) to (IV-5), let $f_1(x)$ be represented by the same segment of a triangle. In Equation (IV-2), let $f_2(x)$ be a triangle wider than f_1 ; in Equation (IV-3), $f_2(x) = f_1(x)$; in Equation (IV-4), $f_2(x)$ is a triangle narrower than $f_1(x)$. Equation (IV-3) is an autocorrelation. If an unknown function $f_2^i(x)$ has a crosscorrelation φ^j with $f_1(x)$ such that $\varphi^j = \varphi^2$, one concludes that $f_2^j(x) = f_1(x)$. Now, if the functions $f_1(x, y)$ and $f_2(x, y)$ are the Fourier transforms of the Ranger series, one has a means of recognizing two similar regions by comparing the crosscorrelations of $f_1(x, y)$, a close-range shot, and $f_2(x, y)$, a long-range shot, with the autocorrelation of $f_1(x, y)$. The degree to which crosscorrelation departs from the similarity to the autocorrelation may be used in calculating the degree to which the lunar surface was used to generate $f_2(x, y)$ differs from the lunar surface that is known and used to generate $f_1(x, y)$. The comparison of lunar surfaces by the crosscorrelation of their Fourier transforms thus may be placed on a quantitative basis.

The optical correlation was done with a system as described by Kovasznay and Arman (1957) using the same lenses as for the Fourier transform. It is illustrated in Figure IV-9 which shows the two lunar photographs, their Fourier transforms and the crosscorrelation. The mathematical representation of the behavior also is given.

The optical system was checked by replacing $f_1(x, y)$ and $f_2(x, y)$ with two identical Ronchi rulings and obtaining their expected autocorrelation, which is Figure IV-10.

a. Ranger IX Series

Figure IV-11 shows a set of crosscorrelations of the Fourier transforms obtained optically for the Ranger IX series where $f_1(x, y)$ (the close-range shot 609) and $f_2(x, y)$ were the other shots used each in turn. One notes that the first three shots present surfaces, the features of which resemble those of photograph 609 and, likewise, these correlation functions are similar. As mountain features appear in the succeeding shots, the crosscorrelation changes dimension. The crosscorrelation for photographs 609 and 604 may be taken to be almost equivalent to the autocorrelation of 609 or 604 since these two surfaces were taken almost at the same height.



$$\varphi_{12} = \frac{I_0}{A} \iint_A f_1(x, y) \cdot f_2(x + \xi, y + \zeta) dx dy$$



Figure IV-9. Correlation Optics

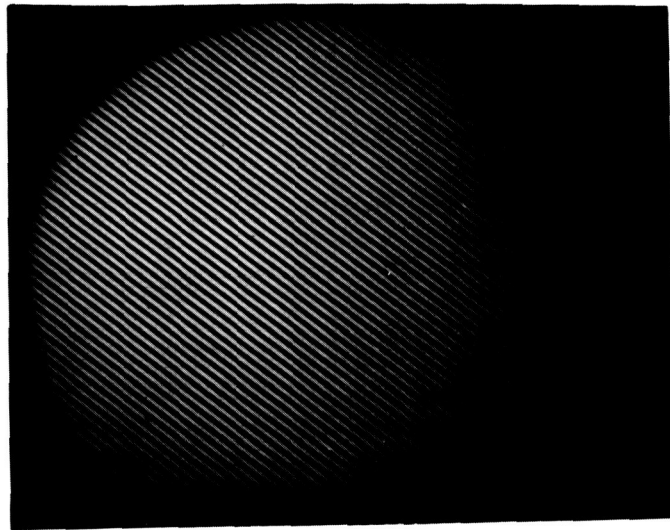
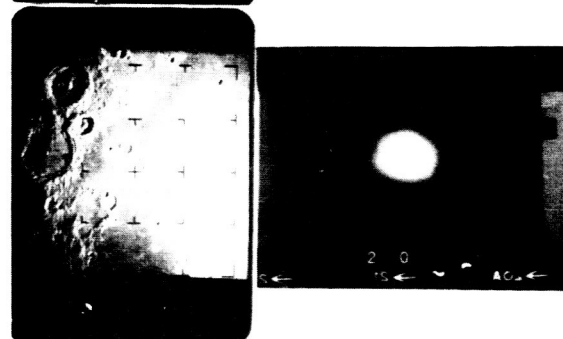
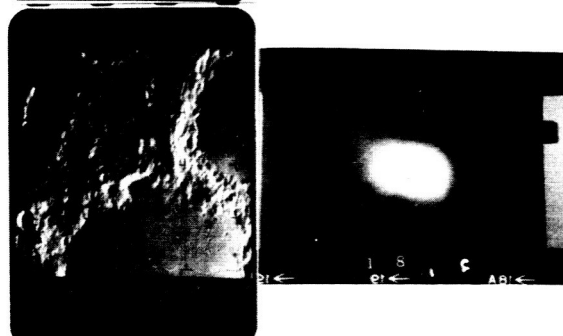
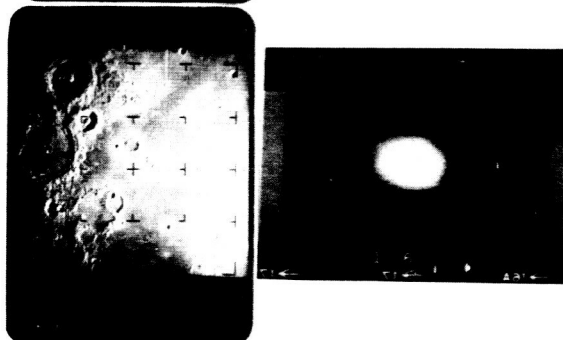
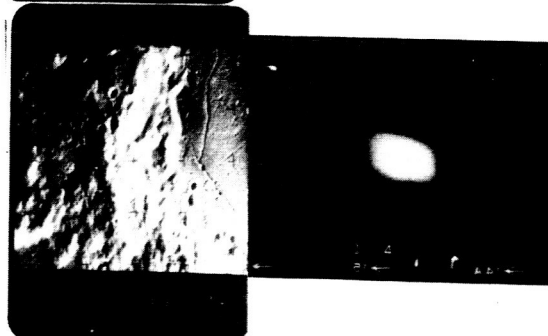
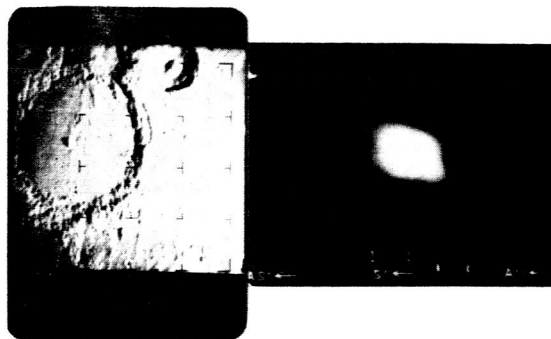


Figure IV-10. Equipment Check, Autocorrelation of Two Ronchi Rulings



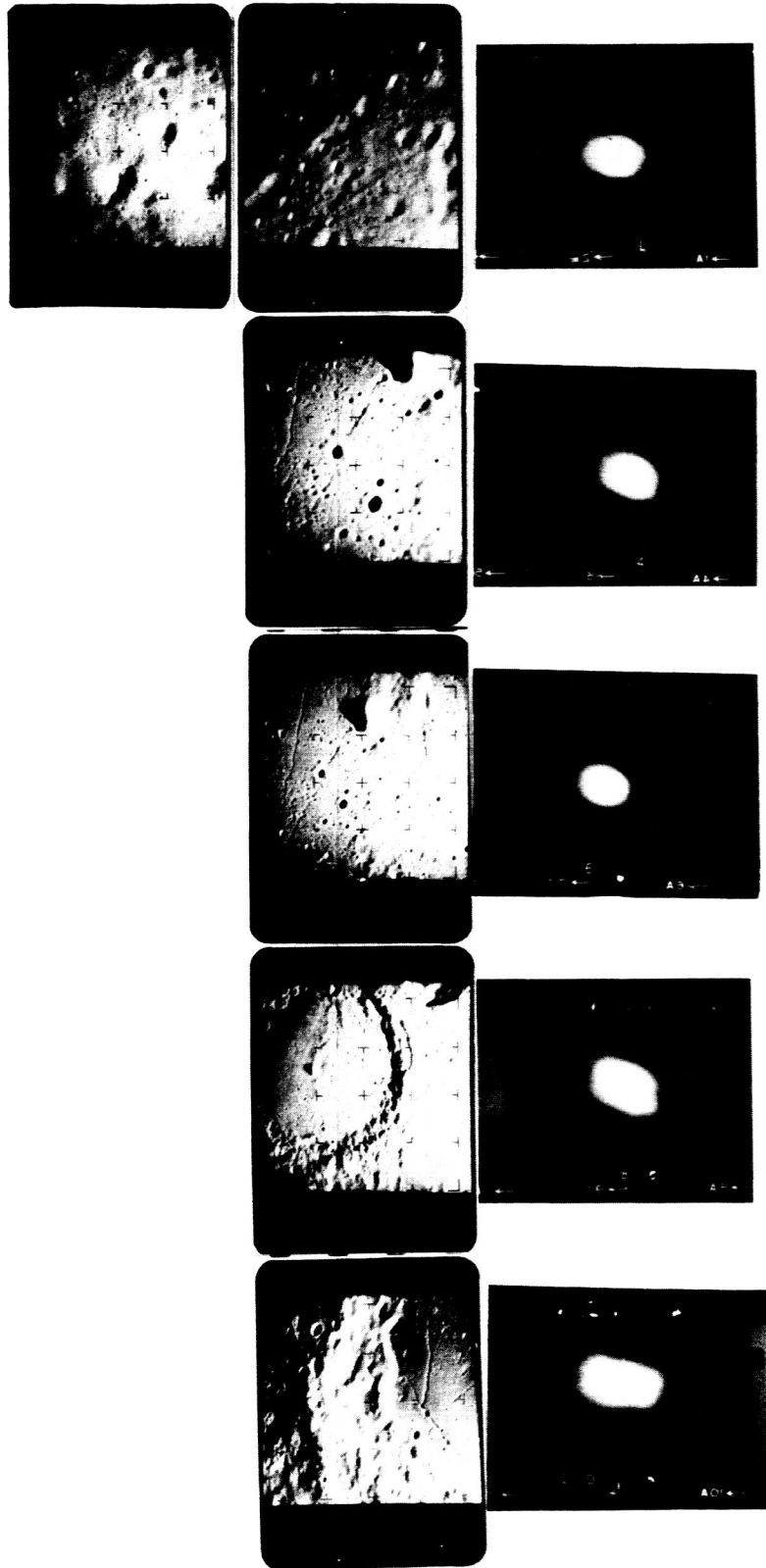


Figure IV-11. Crosscorrelation of Fourier Transforms, Ranger IX

In comparison, the crosscorrelation of photographs 609 and 562 is much larger. The amount by which it is larger could be determined by placing a mask, which is a negative of the autocorrelation of 609, at the point in the optical system where this crosscorrelation of 609 and 562 is formed and by measuring electronically the amount of light that still passes through. The greater the amount of light passing through, the less is the examined area similar to that of 609. Very little light would have passed when the crosscorrelation was with 595, in which case one concludes that 595 is similar to 690 as it appears to be. Thus, the comparison could be placed on a quantitative basis.

Finally, knowing the probability of a successful LEM landing on 609, P_{609} (from other means), the probability of successful landing on 595, P_{595} , would be some function F:

$$P_{595} = F(P_{609} \times C_{609}^{595}) \quad (\text{IV-6})$$

where C_{609}^{595} is the degree of similarity of 595 to 609 on the basis of the crosscorrelation of the Fourier transforms from the optical data process procedure.

The nature of the function F, which will be examined for its validity, is discussed in section C, subsection 2, a. It must be appreciated that the optical data approach is only at the initial phase when the equipment has been assembled and placed into operation. A qualitative evaluation is all that is possible during this time. A full evaluation of the potential of the optical data processing is yet to be done.

b. Pisgah Crater Series

A crosscorrelation of the Fourier transforms was made (Figure IV-12) using photographs of the Pisgah Crater. Photograph 372 shows rough terrain; consequently, there would be many high-frequency components in the frequency domain — the Fourier transform. The autocorrelation of photograph 372 is large. The crosscorrelation of photographs 372 with 376 is large for the same reason. Photograph 398 shows flat terrain and much less area having high-frequency components, so the crosscorrelation is smaller.

c. Crosscorrelation of Pisgah Crater with Ranger Series

Here, the Fourier transforms of two of the Pisgah Craters were crosscorrelated with the close Ranger shots from the VIII and IX series (Figure IV-13). If the topography of Pisgah is known, a prediction of these Ranger areas can be attempted. The crosscorrelations did not show the difference anticipated.

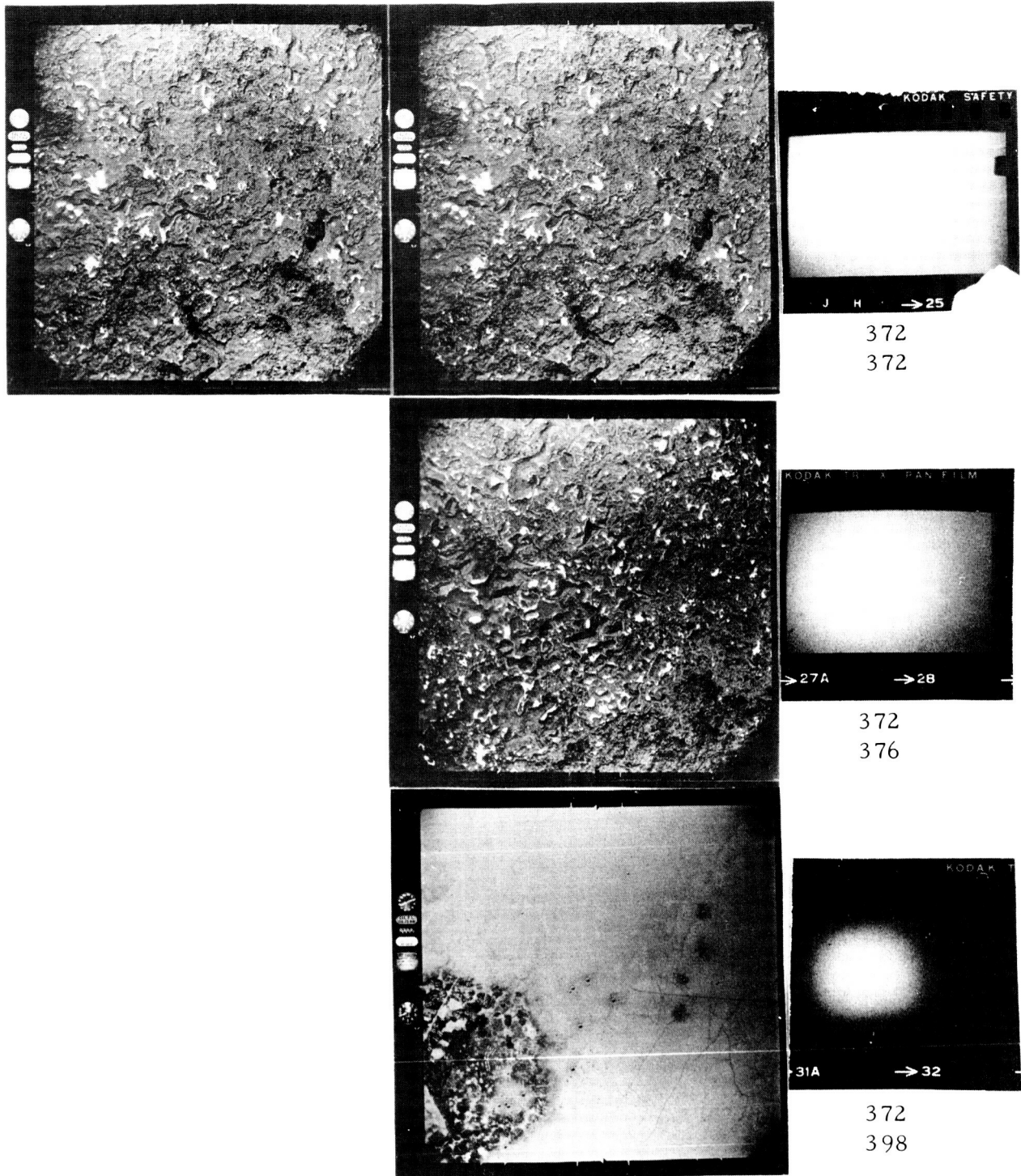


Figure IV-12. Crosscorrelation of Fourier Transforms Using Pisgah Crater Photographs

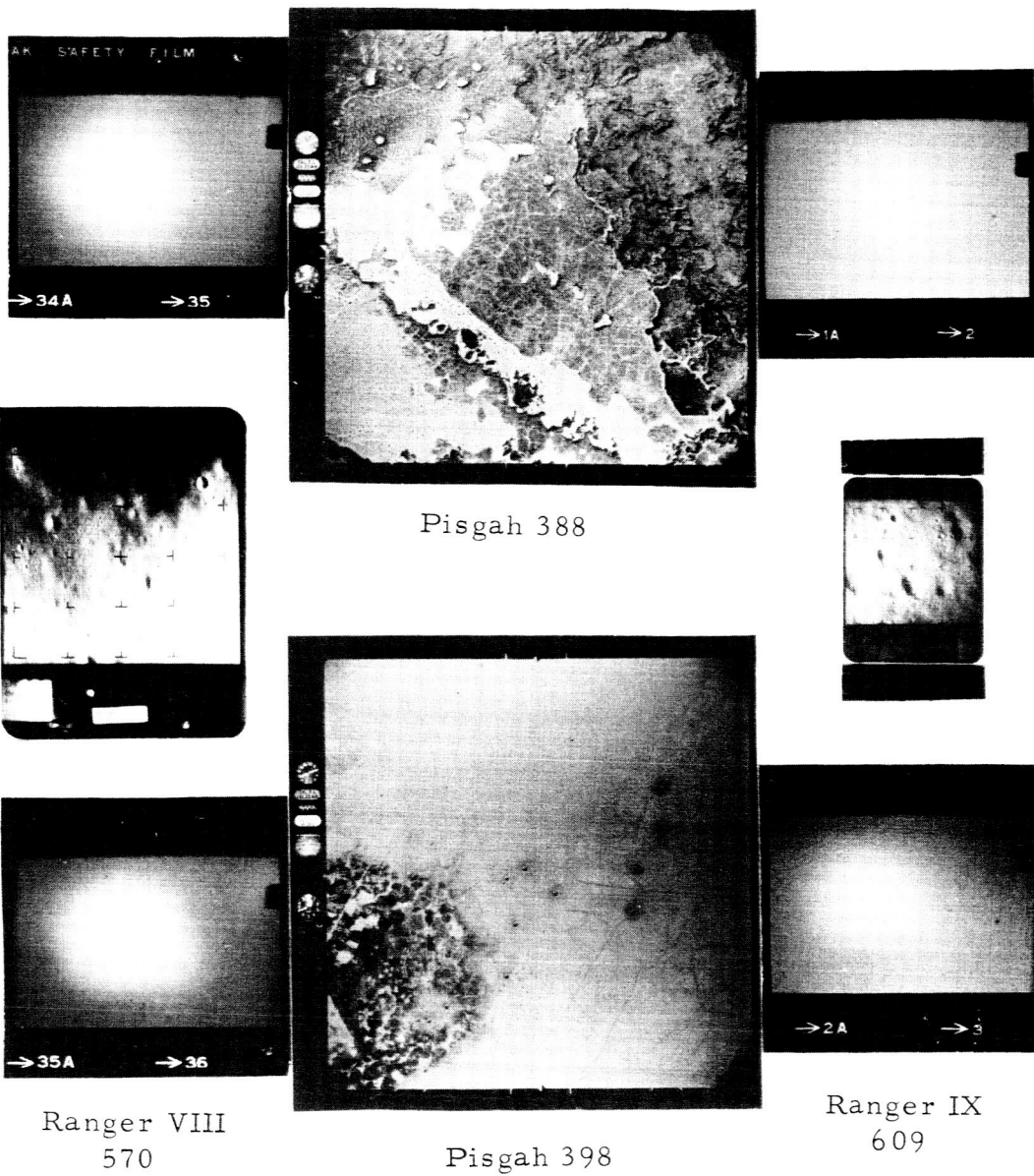


Figure IV-13. Crosscorrelation of Fourier Transforms, Pisgah Crater with Ranger Close-Range Shots

First, the crosscorrelation of Ranger IX photograph 609 is smaller than that of VIII series photograph 570, although it was expected that the corresponding ones would be comparable. A possible explanation is that the two Ranger shots were used through different processes, the VIII series being received as positives and the IX as negatives. Since there was no attempt to duplicate the emulsion gamma, this could form a difference in the final result. Other work with these photographs showed differences that could be attributed to this cause.

Second, a difference in the crosscorrelations was expected between Pisgah photographs 388 and 398 and each of the Ranger shots because of the difference of the appearance in the Pisgah terrains. No explanation is offered, although one possibility is that the sun and observation angles of the Ranger and Pisgah shots were too different.

It can at least be concluded that considerable attention must be paid to the photographic procedures when applying the optical data processing approach.

C. CONCLUSIONS AND RECOMMENDATIONS

1. Summary of Current Findings

Optical data processing techniques are being applied to industrial applications such as analysis of seismograms, recognition of alphanumerics and military applications in target recognition. Because of the equipment's simplicity and the speed with which complex mathematical computations may be performed by the optical data processing technique, it was examined for its application to the problem of LEM landing-site selection.

The Ranger VII photographs were examined visually to select a criterion that characterizes a lunar area regardless of the magnification. It was found that the crater size-frequency characteristic is a suitable criterion, and confirmation of this criterion was found in the literature. Preliminary tests showed that the Fourier transform of a crater maintains a constant shape regardless of the position and number on the photograph. The optical system for obtaining Fourier transforms was set up and used to obtain transforms of the Ranger series and Pisgah photographs. It was observed that similar terrains showed similar transforms, while the appearance of a new feature such as a mountain introduced changes in the transform.

It was shown that crosscorrelation of the transform permits recognition of similar features. The optical system for obtaining cross- and autocorrelations was set up and applied to the transform. Again, it was observed that similarity and differences were recognizable on the transforms of the Ranger series and Pisgah Crater.

To date, the work has been qualitative in nature. It is believed that it can be placed on a quantitative basis and that lunar surfaces may be classified rapidly into two groups: one which has a probability of safe LEM landing greater than some figure; the other, a probability less than this figure. The approach to this quantization is discussed in the following subsection.

Optical data processing has a further advantage. The quantitative comparison of terrains does not require conversion to topographic maps by the photometric method, thus eliminating a step which may introduce the degradation of the fine features. It is the nature of the Fourier transform that fine features are recorded over a large film area and that consequently their information content is not lost in the photographic steps. To take advantage of this fact requires standardization and careful film processing control when comparing different images.

2. Other Proposed Approaches

The optical data processing approach to examination of lunar surfaces for LEM landing-site evaluation was introduced near the end of this contract period when the limitations of other methods became evident. Hence, it was not possible to conduct a complete evaluation of all possible techniques. Nevertheless, the work accomplished suggested other possible methods of evaluating selected lunar surfaces by means of an optical data processing system.

a. Crosscorrelation and Cumulative Area-Slope Calculations

The nature of the function used in Equation (IV-6) will now be examined. Consider the case when the lunar surfaces, both the unknown and the known, have planar surface characteristics. Suppose that photographic data and physical contact permit determination of the cumulative area-slope characteristic of the known area as given in Figure IV-14. Using the photographs of the known, the searched and a plane area, one obtains the respective Fourier transforms. Using these transforms, one obtains the following correlations:

CC (kn. searched):	crosscorrelation between the searched and known areas
AC (kn.):	the autocorrelation of known area
CC (kn. plane):	crosscorrelation between known and plane area
AC (plane):	autocorrelation of the plane

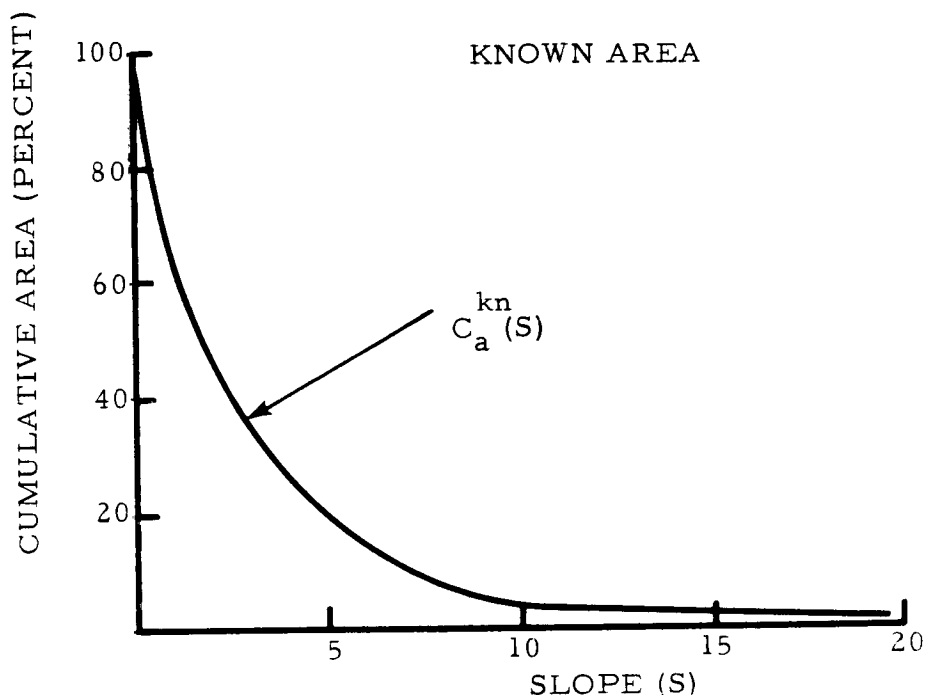


Figure IV-14. Cumulative Area-Slope Characteristic of the Known Area

For the known area, one reads from the curve (Figure IV-14) the value of the cumulative area $C_a^{kn}(S_i)$ for any slope (S_i). Then, for the searched area, the value of the cumulative area $C_s^{srch}(S_i)$ for any slope (S_i) is given by

$$C_a^{srch}(S_i) = \left[1 - \frac{CC(kn. searched) - AC(kn)}{CCC kn. plane - AC(plane)} \right] C_a^{kn}(S_i) \quad (IV-7)$$

In this way, for different values S_i , the cumulative area-slope curve may be determined for the searched area point-by-point as illustrated in Figure IV-15.

If the searched lunar area has mountainous features, Equation (IV-7) should be replaced by

$$C_a^{srch}(S_i) = \left[1 - \frac{CC(kn. searched) - AC(kn)}{AC(mountain) - CC(kn. mountain)} \right] C_a^{kn}(S_i) \quad (IV-8)$$

Equations (IV-7) and (IV-8) are a proposed approach, the validity of which would have to be established by application to known areas such as may be obtained using terrestrial data.

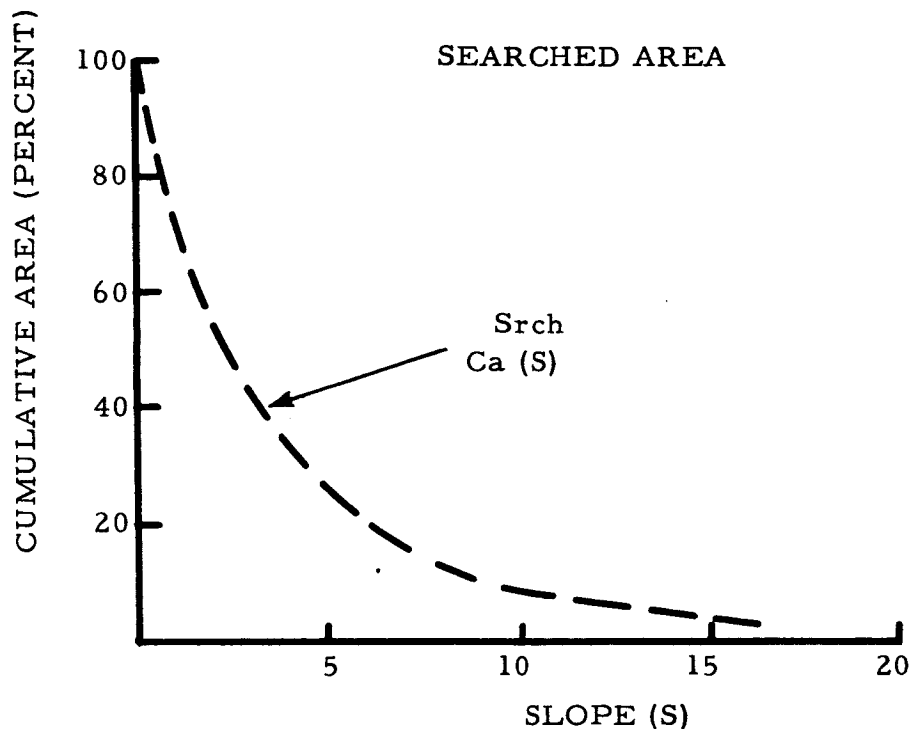


Figure IV-15. Cumulative Area-Slope Characteristic for Searched Area Computed by Equation IV-7

If one knows the cumulative area-slope characteristics with an accuracy whose standard deviation is σ , it is assumed that, for any given area, the probability of a successful LEM landing can be computed with a degree of confidence determined by σ . It is not intended that the optical data processing make this calculation of the probability but rather provide the data used in the calculation. If these calculations show that 97 percent of the area has slope less than 12, the probability is 95 percent that the LEM will make a successful landing. Then, the optical data processing would permit a rapid comparison technique for selecting those areas that have a probability of 95 percent or better for a successful landing.

As stated earlier, this is a proposed approach which requires further study but which appears to be well-defined.

b. Cumulative Area-Slope from the Fourier Transform

The photometric technique for measuring lunar slopes relies on the fact that the brightness of any element of the lunar surface depends on the albedo, the angle of incidence of the sunlight on the surface and the angle of observation (Wilhelms, 1962; Shoemaker, 1965). By knowing the instrument and the photographic factor and by repeated microdensitometric scanning in the proper direction, one may obtain the cumulative area-slope characteristic for the whole area represented in the photograph. Since the Fourier transform contains the same terrain information as the original photograph (if the phase information is also included), there is the possibility of existence of a process which would give the cumulative area-slope characteristics of the area from the Fourier transform by means of only a few densitometer traces and fewer calculations. The exact direction and number of densitometer traces can only be determined experimentally, but the scheme is illustrated in Figure IV-16.

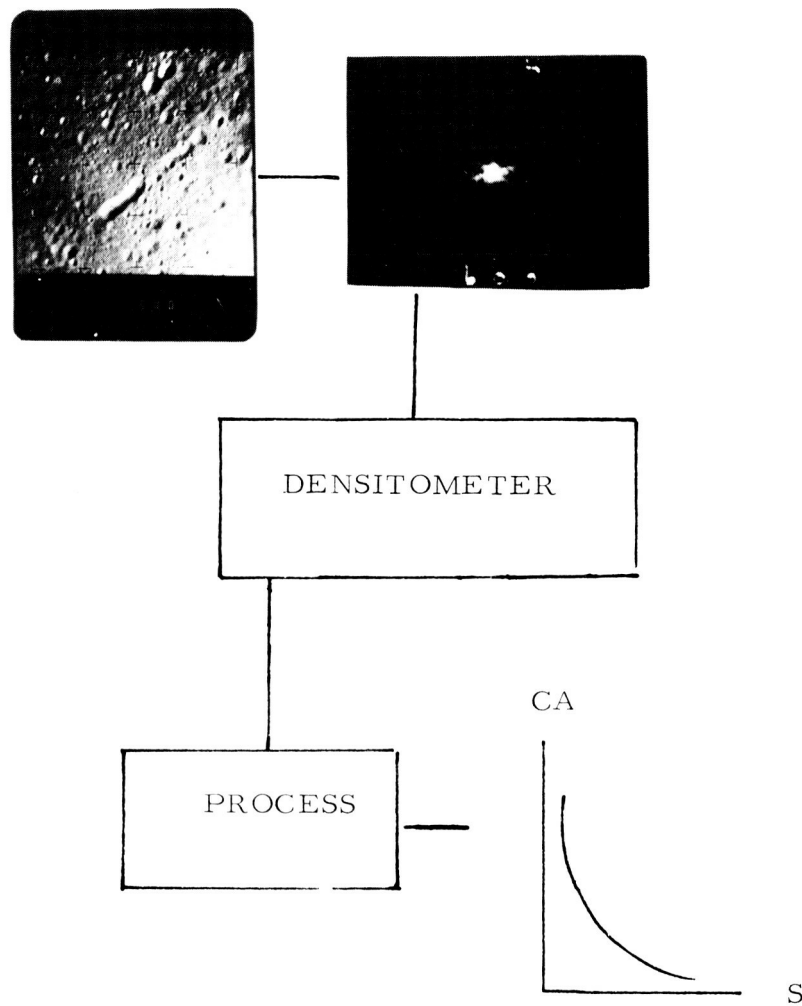


Figure IV-16. Cumulative Area-Slope from the Fourier Transform

When the cumulative area-slope is known, one would then calculate the probability that the LEM will not tilt as mentioned in the previous subsection C.2. a.

c. Enlargement Step

This step suggests itself if one desires to evaluate a small segment of the searched area that appears suitable for landing. As illustrated in Figure IV-17, this segment is enlarged and subjected to either or both processes discussed in subsection C. 2. a and b, to obtain the cumulative area-slope characteristic. As before, if one knows this characteristic, one will know the probability of a successful LEM landing from studies prepared in advance.

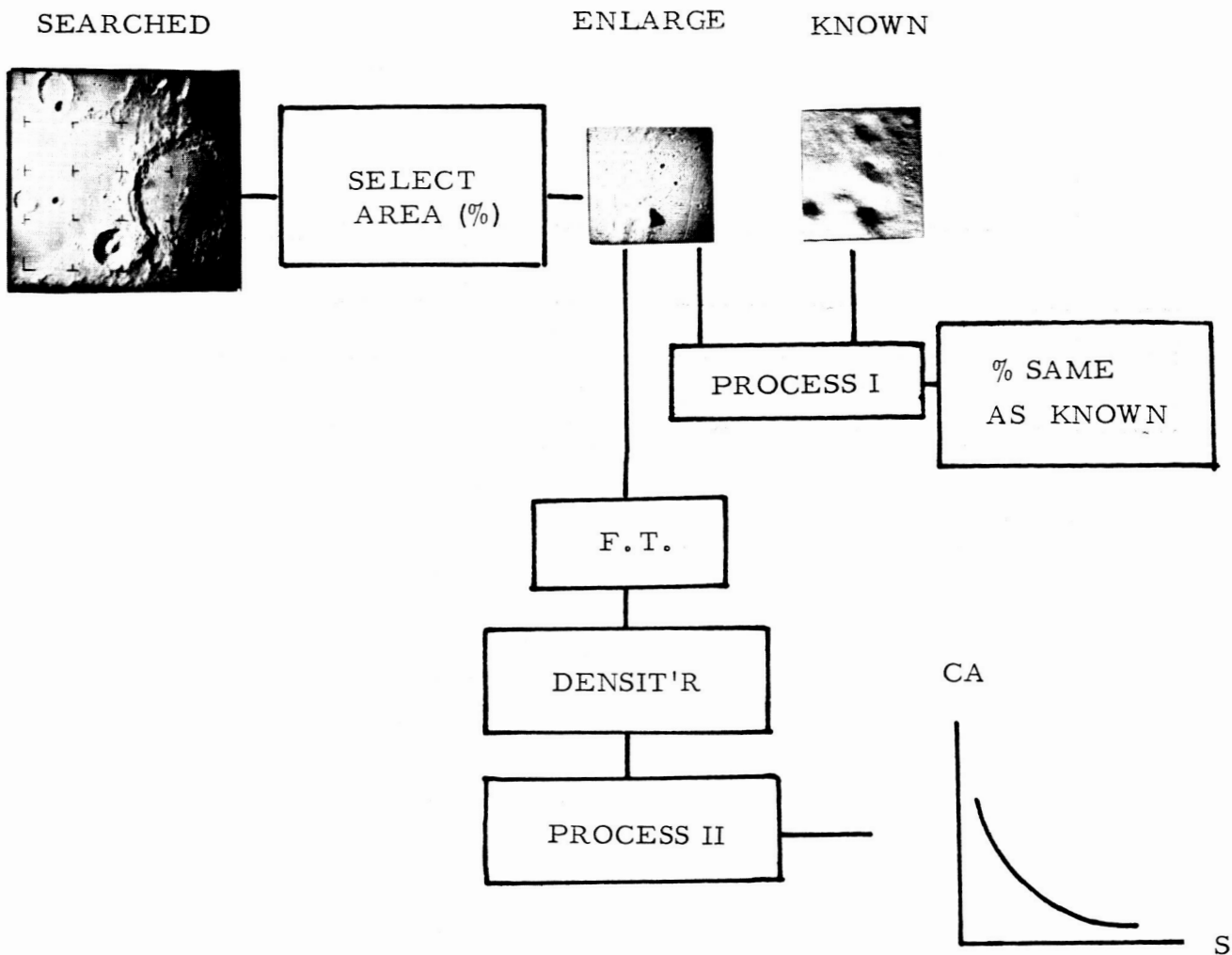


Figure IV-17. Enlargement Step

d. Pattern Recognition Step

Spatial filtering in optical systems finds application in detecting "signal" in the presence of "noise" and in problems of shape or pattern recognition (Preston, 1965; Vander Lugt, 1964; Kelly, 1965).

The pattern recognition step may be applied in two ways. The first way would be applied in evaluating regions which are essentially plains but have small mountains. Treating the mountains as "noise" will obtain from the original a second photograph in which the "noise" is eliminated. This photograph then may be treated in the techniques of subsection C.2. a or b, to obtain the cumulative area-slope curve and thence the probability of successful landing in the plain area. This approach is presented in Figure IV-18. The second way would be for recognition of protuberances, for then all features other than protuberances are treated as "noise" and eliminated. The protuberances or "signal" then would be recorded on a second photograph.

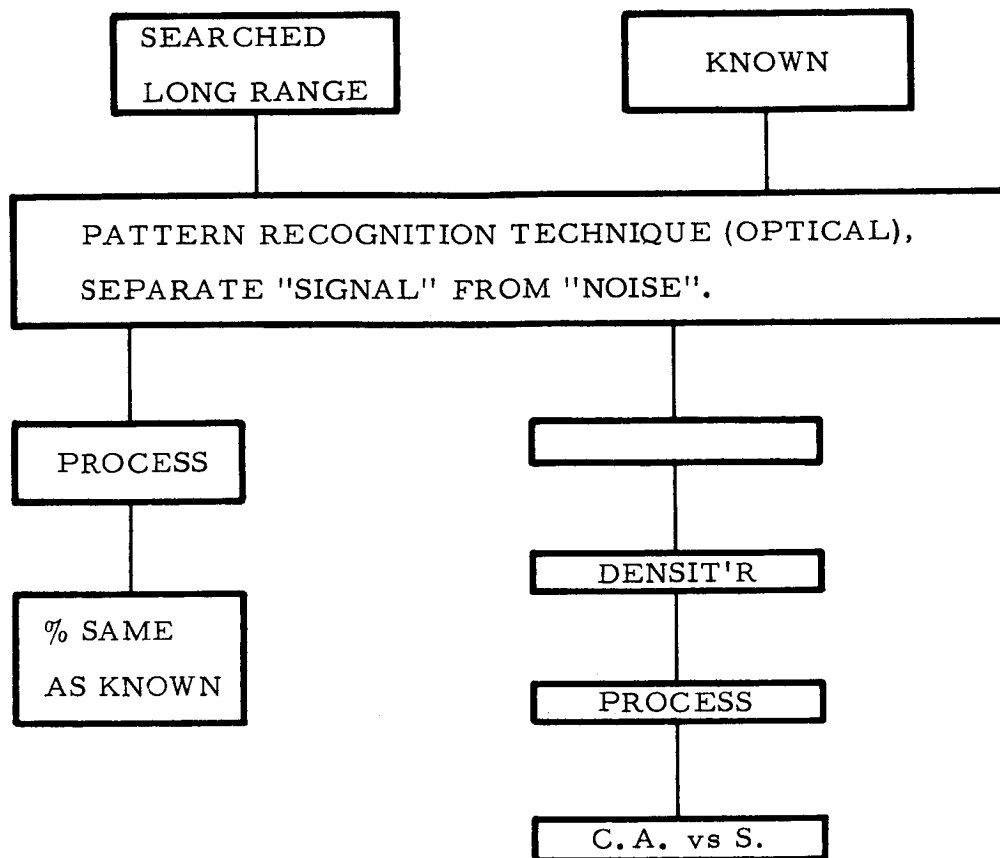


Figure IV-18. Pattern Recognition Step

D. REFERENCES

- Cutrona, L.J., E.N. Leith, C.J. Palermo, and L.J. Procello, 1960, Optical data processing and filtering systems: IRE Trans. on Info. Theory, v. II-6, June., 386.
- Dodd, R. T., Jr., J. W. Salisbury and V. G. Smalley, 1963, Crater frequency and the interpretation of lunar history: Icarus, 2, 5, 466.
- Heacock, R.L., G. P. Kuiper, E.M. Shoemaker, H.C. Ure, and E. A. Whitaker, 1965, Ranger II, pt. II, experimenter's analysis and interpretations: Tech. Rpt. 32-700, JPL, Cal. Tech., Pasadena, Calif., Feb.
- Kovaszny, L.S.G. and A. Arman, 1957, Optical autocorrelation measurement of two-dimensional random patterns: Rev. Sci. Instr., 28, 2, Oct., 793.

- Kozma, A. and D. L. Kelly, 1965, Spatial filtering for detection of signals submerged in noise: Applied Optics, 4, 4, Apr., 387.
- Lee, Y. W., 1960: Statistical Theory of Communication, John Wiley & Sons Inc., New York.
- National Aeronautics and Space Administration, Scientific and Technical Div., 1965, Ranger VII photographs of the moon, pt. II, camera B series: NASA SP-62, Washington, D. C., Feb.
- O'Neill, E. L., 1956, Spatial filtering in optics: IRE Trans. on Info. Theory, v. II-2, Jun., 56.
- Preston, K., 1965, Computing at the speed of light: Electronics, Sept. 6, 72.
- Radar Lab. Inst. Sci. and Tech., Univ. of Mich., Ann Arbor, Mich., Optical spatial filtering techniques for automatic target recognition: Proj. 4144, Task 414408, A. F. Avionics Lab., Wright-Patterson AFB, Ohio (CONFIDENTIAL).
- Shoemaker, E. M., 1965, Preliminary analysis of the fine structure of the lunar surface in Mare Cognitum: Tech. Rpt. 320700, JPL, Cal. Tech., Pasadena, Calif., Feb.
- Vander Lugt, A., 1964, Signal detection by complex spatial filtering: IEEE Trans. on Info. Theory, Apr., 139.
- Vander Lugt, A., 1964, Signal detection by complex spatial filtering: IEEE Trans. on Info. Theory, Apr., 140.
- Wilhelms, D. E., Photometric technique for measurement of lunar slopes: Astrologic Studies, Part D, Studies for Space Flight Program, Annual Progress Rpt., U.S. Geol. Survey, Interior Dept., Aug. 24, 1962, to Jul. 1, 1963, 1.

CHAPTER V

PHOTOGRAPHIC MEASUREMENTS

A. APPROACH TO PROBLEM

The confidence with which one predicts the bottoming hazard probability for a given area is strongly dependent on the reliability of detection and measurement of the objects in question. It was previously noted that contour mapping is a smoothing process, and that physical dimensions of map format and finite width of contour lines limit the amount of data which can be shown by contours; the higher-order geometric perturbations are lost. Therefore, it must be concluded that features at the scale associated with 50-cm protuberances will be lost in a contour mapping process, and information concerning their presence must be obtained by direct examination of the photographs, possibly in conjunction with spot photogrammetric elevation differences. The studies described in this section were therefore undertaken to identify and evaluate critical factors which influence interpretability of Lunar Orbiter photography.

One can develop an estimate of system performance by identifying the various elements of the system, noting their relationships to each other and analyzing the behavior of an input signal as it is cascaded through each element. The quality of the final answer is, of course, dependent on the accuracy of the assumptions made about behavior of each system element. Data were not available to analyze in detail the basis for design of the Orbiter camera system, but there was available a performance specification for the high-resolution (1:75,000 scale) camera by Kosofsky and Broome (1965) which serves as a starting point for the discussion that follows. As stated by Kosofsky and Broome:

"For the purpose of evaluating Lunar Orbiter performance, the ground resolution is defined in terms of the photometric detection of a standard shape; i. e., a circular cone $\frac{1}{2}$ meter high with a 2-meter base diameter. When this is photographed under the operational illumination conditions and transmitted through all of the data links and picture reconstruction equipment and, subsequently, scanned by a densitometer having a scanning aperture of effective $\frac{1}{2}$ -meter diameter, the resulting signal-to-noise ratio must be at least 1 in order to demonstrate a 1-meter ground resolution."

B. IMAGE INTERPRETABILITY

Despite the sophistication which has been achieved in photogrammetric instrumentation and analysis, the problems posed by detection of microterrain features near the resolution threshold are, to a large extent, qualitative, involving human physiological parameters such as discernment of photographic tone, discernment of resolved detail, discernment of parallax, and mental acuity. Excellent treatments of these factors are presented by Saltzman (1949) and Blackwell (1946). A number of approaches to quantitative evaluation of picture quality have been undertaken including work by Linfoot (1964), Higgins, Wolfe and Lamberts (1956) and many others, but virtually, all are complex, experimental and not well suited for predictive use.

From the trigonometric relationship between flight altitude (46 km) and 24-in. focal length of the high-resolution camera, it is determined that one meter on the ground corresponds to 1/76-mm on the film, or one line pair. A frequently stated criterion for the smallest detectable feature on the ground is that its size is no smaller than one line or one space ($1/2 R$ where R , the resolving power, stated in line pairs/mm). However, Itek (1962) investigators noted that "most observers agree that, for visual recognition, an object must be imaged at a size approximately five times that great; $5/2 R$ millimeters." In the case of the 24-in. Orbiter camera photographs, this equals $2\frac{1}{2}$ m on the ground. This criterion is related to visual recognition only, and does not apply to microdensitometer scanning which has no recognition ability. Nevertheless, this $2\frac{1}{2}$ -m dimension is somewhat larger than the 2-m dia cone which was cited as a detection standard for the high-resolution camera system; thus, it is important to note carefully the implications in "detection" (implying only that an object — a "blob" — can be distinguished from its background) and "recognition" (implying that enough detail can be "recognized" in the outline or texture to place it in a class of objects).

In order for an object to be "detected" on a photograph, there must be a suitable tone difference between the object and its background as well as some minimum physical dimension. The concept of edge gradient is frequently used with reference to probabilities for detection and recognition of objects. Edge gradient refers to the abruptness of tone or color change between the edge of a photographic image. Colwell (1952) says: "The absolute detectable tone range ... has been reported to be as low as 2 percent of the range from jet black to pure white." As image sharpness increases, edge gradients are steepened so that the tone contrast required for detection increases. On the other hand, as tone contrast increases beyond the detection threshold, edge gradients also steepen. This can be generalized by the statement that tone is the primary factor governing detection, while image sharpness governs recognition.

The amount of contrast between an image and its background determines the number of cones in the human eye which must be activated by illuminance changes in order to detect an edge gradient. Thus, it is found (Macdonald, 1951) that the eye can resolve up to 73 lines/mm for a very high contrast test target, but fewer than 5 lines/mm of a very low-contrast target. It is safe to assume that low contrast images will predominate in Lunar Orbiter photography, especially at high sun angles as demonstrated by the model studies performed by Eastman Kodak Company (1965). The low contrast inherent in images of any small area of the moon is attributed to a generally prevailing dust layer of uniform reflecting properties; thus, sharp edge gradients depend mainly on shadows cast by topographic relief. Even though the ground-reconstructed high-resolution photos will have 7x enlargement (to about 11 lines/mm), there may be insufficient contrast to resolve the smallest features of interest with high confidence. (It is suggested that an analysis of Eastman's data showing object height vs sun angle for various photo system resolving powers may yield a useful empirical relationship based on barely detectable shadow lengths of relative contrast vs visual resolving power.)

A gross assessment of picture quality for various geometric patterns can be made by means of a factor called shade relief (Herriman, Washburn and Willingham, 1963). The shade relief associated with a sharp-crested ridge (in crystallographic terms, a dome) having base width, slopes and height corresponding to the standard cone of Kosofsky and Broome was investigated. Its axis is oriented in the direction of the luminance meridian (Figure V-1).

Shade relief is defined by the relationship

$$\frac{\varphi_1}{\varphi_2} = (2)^{\frac{s}{2}}$$

where φ_1 , φ_2 are photometric functions of adjacent slope elements, and s is the shade relief.

From the chart for the lunar photometric function of φ vs α (Figure V-2), with the phase angle g as a parameter (Figure V-2), the following values are obtained for the geometry illustrated:

Horizontal surface	$\varphi_0 = 0.22$
= -27° (toward sun)	$\varphi_1 = 0.28$
= $+27^\circ$ (away from sun)	$\varphi_2 = 0.03$

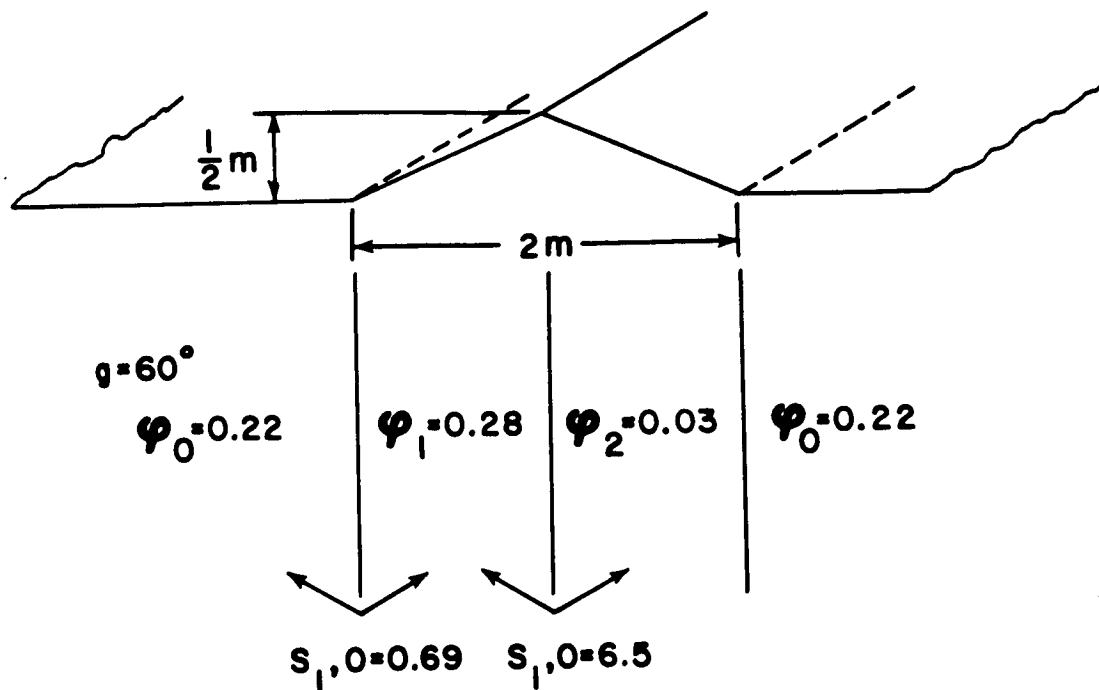


Figure V-1. Hypothetical Ridge

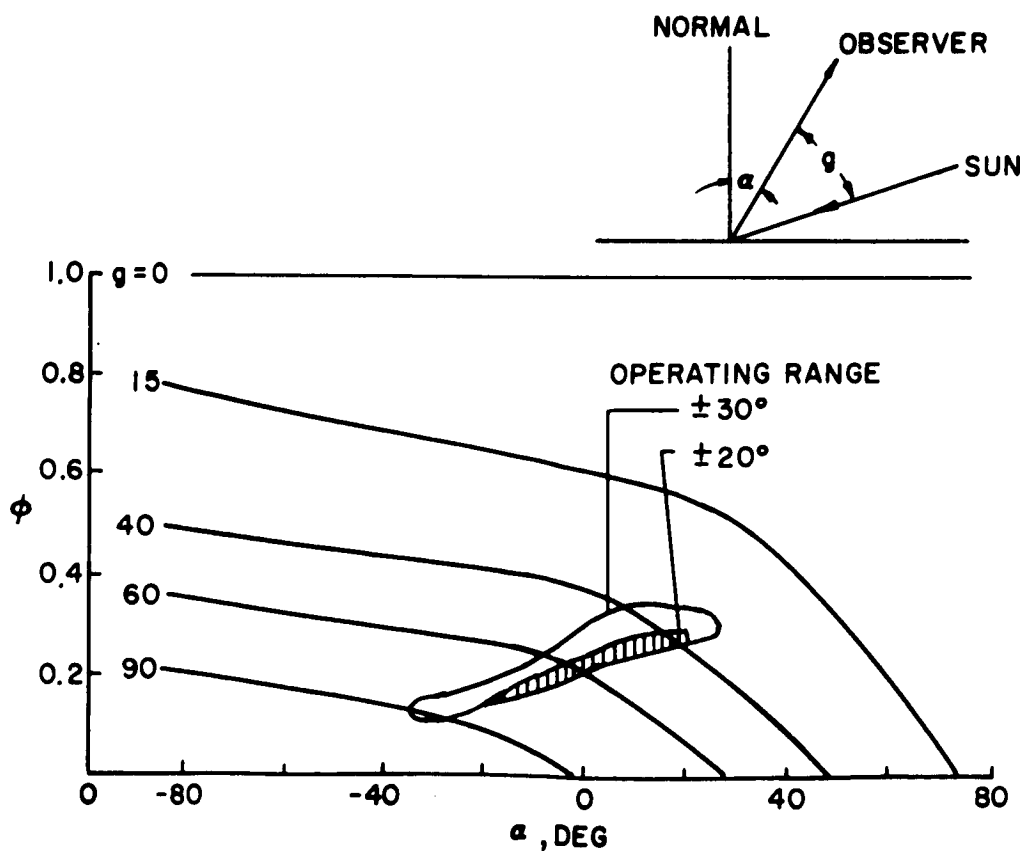


Figure V-2. Lunar Photometric Function of ϕ Vs α

Thus

$$\frac{\varphi_1}{\varphi_0} = \frac{0.28}{0.24} = 1.27 \quad S_{1,0} = 0.69$$

$$\frac{\varphi_1}{\varphi_2} = \frac{0.28}{0.03} = 9.34 \quad S_{1,2} = 6.5$$

$$\frac{\varphi_0}{\varphi_2} = \frac{0.22}{0.03} = 7.32 \quad S_{0,2} = 5.75$$

It has been reported by Herriman, Washburn and Willingham (1963) that pictures having shade relief greater than 4 are considered good; the higher the shade relief, the higher the information content. Shade relief of 2 is borderline, while below 1 there is almost no information content. The values determined may be taken as a qualitative indication of the difficulty involved in making interpretive conclusions about the terrain micro-relief. This illustration indicates that the boundary of the foreslope toe will be poorly defined. However, these dimensions are too small to be resolved with high confidence as will be shown in a succeeding paragraph.

Thus, it is illustrated that for lunar conditions at the limit of resolution, although "detection" may be achieved, "recognition" may be impossible.

C. PHOTOGRAMMETRIC CAPABILITIES

The cartographic function of Orbiter is handicapped severely by lack of an established vertical datum and selenodetic control points. Under these conditions, a great deal of reliance must be placed on orbital parameters and proper orientation of the camera axis. Errors can be minimized by interior adjustment of photogrammetric triangulation within the areas covered so that systematic errors, referenced to a true datum, should not be more than a small fraction of a degree.

Errors of this magnitude, although important to selenodesists, are of little consequence for selection of LEM landing sites. Good relative heighting accuracy over short distances is of extreme importance, however, for the classification of slopes and protuberances.

Assuming adequate control to establish flatness of the stereo model parallel to the mean regional gradient, the contouring efficacy of various stereo plotters can be examined by means of their respective

C-factors. The C-factor is an empirical value which serves to determine the minimum contour interval attainable with a given photogrammetric system such that 90 percent of the points in the resulting map will be within $\pm \frac{1}{2}$ -contour interval of their true elevations (in this case, referred to the assumed model datum), and all points will lie within one contour interval. If contour interval and C-factor are specified, the maximum flight altitude to achieve this contour interval within U.S. National Map Accuracy Standards can be determined as the product (contour interval x C-factor). Conversely, it can be used to specify the minimum contour interval which a specified flight altitude and photogrammetric system will produce.

Duane Lyon (1965) points out that, despite its vulnerability to factors inherent in the stereo equipment, operation skill, quality of photography, topographic relief, condition of the ground surface, established production rates, and adequacy of photogrammetric control, the C-factor is nevertheless the best guess regarding contouring accuracy.

Some example C-factors for operational plotting systems include the following estimates, described as "optimistic" by Skidmore (1965):

Multiplex	1000 (a more reasonable estimate: 750)
High Precision	1500
A-7	1800
A-9	1500

The highest C-factor which can be achieved under operational conditions by any first-order stereo plotter is probably about 2200. Based on these figures, the minimum contour intervals which can be adopted for a model flown at 46 km, to meet the stated contour criterion with 90 percent confidence for the above systems, are:

Multiplex	46 m (more realistically: 61 m)
High Precision	31 m
A-7	26 m
A-9	31 m

The so-called anaglyph plotters are limited to use with photography having base height ratios greater than 0.4, because the projectors touch at minimum settings; however, "universal" instruments such as the Autograph A-7 and Stereoplanigraph C-8 can simulate a zero base condition (Theis, 1965).

Production of contours from a stereo model involves establishing a floating mark at some position corresponding to the desired contour at that elevation. If accurate measurements of elevation differences between points in the model are required, the floating mark is placed precisely on one point, then raised and moved laterally as required until it rests precisely on the other point. In either case, precision of the elevation measurements between positions in the model depends on the ability to detect the individual points in question. If the smallest reliably detectable point in the photograph is limited to $\frac{1}{2R}$, where R is resolution of the final photographic image in lines/mm, this will also be the reliability of each elevation measurement; the reliability of measurement between two points will accordingly be $\frac{\sqrt{2}}{2R}$.

These limiting values provide a basis for estimating minimum height differences which can be measured from Orbiter photographs by stereoscopic systems.

Coverage in the high-resolution, high-repetition mode will only achieve 5 percent overlap between successive exposures, thus defining a strip 210 m x 16,400 m on the ground. A standard formula for minimum detectable elevation difference is

$$\Delta H = \frac{H}{b} \cdot \frac{H}{f} \Delta P \quad (V-1)$$

where

H = flight height above the target, 46 km

b = base distance between exposures, 3.99 km

f = focal length of camera (246 in. = 0.61 m)

ΔP = minimum detectable parallax, taken as

$$\frac{1}{2R} = \frac{1}{2 \times 76 \text{ lines/mm}}$$

then

$$\Delta H = \frac{(46,000 \text{ m})^2}{3990 \text{ m} \times 0.61 \text{ m} \times 152 \text{ d/mm}} = 5.71 \text{ m}$$

The reliability of heighting measurement was shown to be of the order of $\frac{\sqrt{2}}{2R}$; thus, the minimum detectable height is known within $\pm 0.71 \text{ m}$ in terms of ground elevation. Lyon (1965), however, assumes

that parallax differences smaller than $2/R$ are not photographically recorded with 90 percent confidence. The implication of this assumption is that, to assure 90 percent confidence in relative height measurements, one would need to increase the computed ΔH 's by four times.

The minimum detectable height for the medium resolution (1:600,000 scale) system with 3-in. lens can be determined in the same manner (it is demonstrated by Kosofsky and Broome's data that the 3-in. camera system has the same resolving power as the 24-in. system):

$$H = 46 \text{ km}$$

$$b = 18 \text{ km}$$

$$f = 6.62 \text{ cm}$$

thus

$$\Delta H = \frac{(46,000)^2}{18,000 \times 0.61 \times 152} = 10.15 \text{ m}$$

D. RELATIONSHIP OF CONTOUR ACCURACY TO CONFIDENCE IN SLOPE PROBABILITY MEASUREMENT

The confidence in the predicted probability of unsafe slope class occurrence will obviously depend on the accuracy of the height measurements used for drawing the contour lines. Consider an area which contour line spacing has shown to be unsafe. This area will include and be separated from the safe-landing area by at least two contour lines designating a slope of at least 12° . Let the standard deviation of the error in height measurement be determined to be σ . Then there is 95.4 percent confidence that true height of any line is within $\pm 2\sigma$. From Figure V-3 there is, then, 95.4 percent confidence that the area unsafe due to tilting is within that determined:

$$U \pm \frac{2\sigma}{\tan 12^\circ} \cdot P \quad (V-2)$$

where P is the perimeter of the unsafe area. For a given area U , the perimeter is a minimum when U is circular. Consider this circular case.

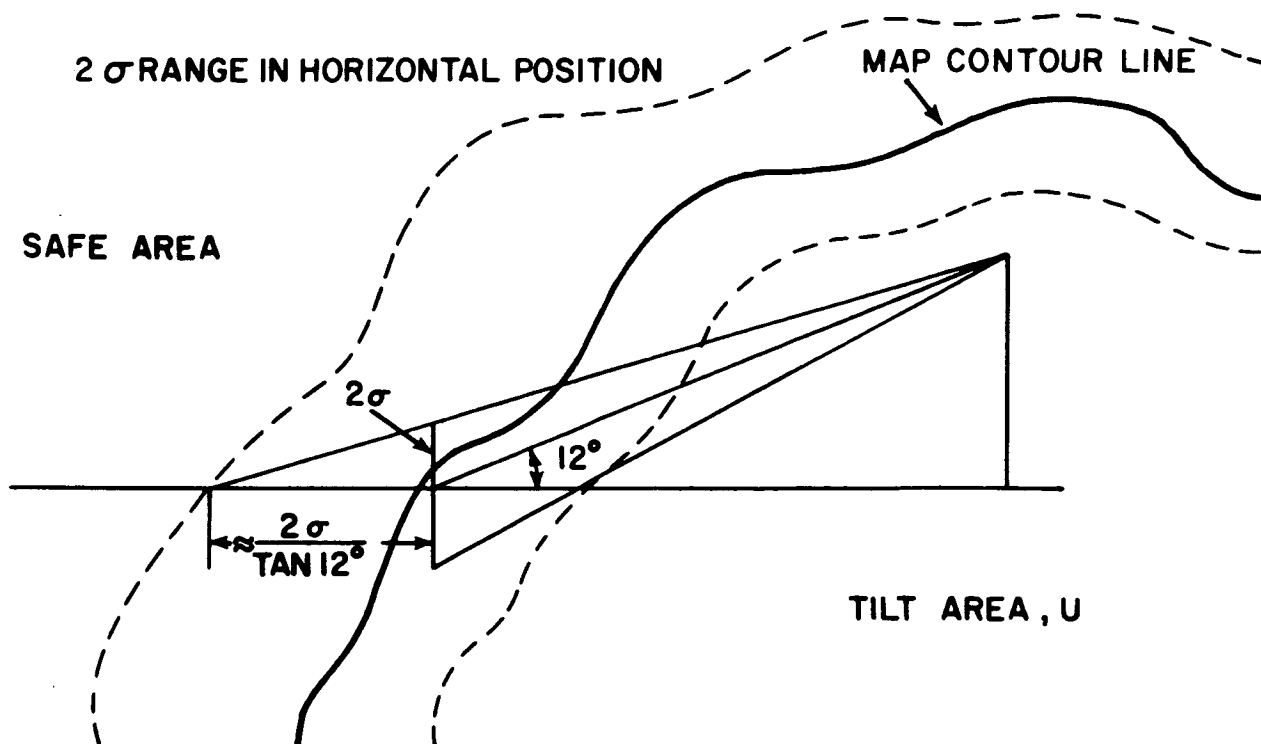


Figure V-3. The Uncertainty in Position of Boundary of Tilt Area As a Function of the Standard Deviation σ in Height Accuracy

Let $U = fT$ where T is the total area examined for landing and $0 < f < 1$

Therefore, one can say with 95.4 percent confidence, that the uncertainty in U is

$$E_{\min} = \pm \frac{2\sigma}{\tan 12^\circ} \cdot 2\pi \sqrt{\frac{fT}{\pi}}$$

The probability of safe landing in T is then

$$P_{\text{safe}} = 1 - f \pm \frac{4\pi\sigma}{T \tan 12^\circ} \sqrt{\frac{fT}{\pi}}$$

with 95.4 percent confidence.

Consider now the case where, for the same accuracy in height determination, the unsafe area has the same value, i. e., $U = fT$ as before, but the unsafe area now consists of n circles of radius r_c each such that

$$fT = U = n\pi r_c^2$$

$$r_c = \sqrt{\frac{fT}{n\pi}}$$

and the total perimeter now is

$$\begin{aligned} P_c &= n2\pi r_c \\ &= n2\pi \sqrt{\frac{fT}{n\pi}} \\ &= 2\pi \sqrt{\frac{fT}{\pi}} \cdot \sqrt{n} \end{aligned} \quad (V-3)$$

The uncertainty in the unsafe area U with 95.4 percent confidence is

$$E_c = \pm \frac{2\sigma}{\tan 12^\circ} \cdot 2\pi \sqrt{\frac{fT}{\pi}} \cdot \sqrt{n} \quad (V-4)$$

The probability of safe landing in T is then, with 95.4 percent confidence

$$P_{\text{safe}}^c = 1 \left\{ -f \pm \frac{4\pi\sigma}{T \tan 12^\circ} \sqrt{\frac{fT}{\pi}} \cdot \sqrt{n} \right\} \quad (V-5)$$

That is, for exactly the same accuracy in height determination and safe landing area, the certainty in the probability of safe landing has deteriorated by a factor \sqrt{n} , where n is the number of equal circular segments that the unsafe area consists of.

It is now possible to generalize. Let the contour lines be determined from height measurements having a standard deviation σ . Let the unsafe area due to tilt be determined to be $U = fT$. Let the perimeter of this area be P . Then, one can say with 95.4 percent confidence that the probability of safe landing is

$$P_{\text{safe}} = 1 - \left[f \pm \frac{2\sigma}{T \tan 12^\circ} \cdot P \right] \quad (\text{V-6})$$

The uncertainty has a minimum value when $P = 2\pi \sqrt{\frac{fT}{\pi}}$, being the perimeter of a circle.

The confidence in the predicted safe landing probability requires not only a knowledge of accuracy (σ) of the height measurements but the shape of the unsafe landing area as well. A similar consideration would apply when the position of contour lines are obtained from a slope analysis (e.g. photometric techniques), in that the confidence in the safe landing probability would depend on the accuracy of contour position σ_c and perimeter P of the unsafe area.

E. MICRODENSITOMETRIC ACCURACY

Since it is contemplated that measurement of small protuberances and craters is to be performed by microdensitometric-scanning techniques, an exercise was undertaken to simulate this process as a means of examining possible error sources.

The $\frac{1}{2}$ -m cone of Kosofsky and Broome was adapted as a model protuberance. Figure V-3 illustrates the cone geometry and conditions of illumination. The sun angle for this experiment was selected to provide grazing illumination on the back of the cone in the sun-observer plane, or "brightness equator."

By means of spherical trigonometric formulae, the emission angle between the observer (camera) and average surface normal for each 10° section of the cone was projected into the brightness equator plane, and the resulting angle α was determined. Subsequently, the lunar photometric function for each zone was obtained from the photometric chart (Figure V-2) for the various α 's, with the phase angle $g = 63.6^\circ$ as a parameter. Exposure in meter-candle-seconds is numerically equal to surface brightness in meter-lamberts.

The effect which a given element has in terms of film density can be evaluated if the exposure in meter-candle-seconds and the characteristic curve for the film in question are known.

A relationship has been derived for the exposure level.

$$Q = \frac{E_s \rho \varphi T \Delta t}{4 \cdot (f\text{-no})^2} \cdot 10.75 \quad (\text{V-7})$$

where

Q is in meter-candle-sec

E_s = Solar constant = 1.31×10^4 lu/ft²

φ = photometric function

T = transmission of lens

Δt = exposure, sec

ρ = albedo

For the surfaces computed in the preceding, assuming $f/\text{no} = 5.6$, 1/25-sec exposure time, optical transmittance ~ 1.0 , and normal albedo 7 percent.

$$Q = \frac{1.31 \times 10^4}{4} \times \frac{0.07}{5.6^2} \times \frac{1}{25} \times 10.75 \frac{\text{ft}^2}{\text{m}^2} \times \varphi$$

$$Q = 3.14 \varphi$$

The film density D corresponding to any exposure value can be read directly from a sensitometric curve for the corresponding film, exposure and processing conditions. In this example, a curve for SO-243 film, D-19 developer at 68°F and 20-min development time was used (Figure V-5). Values of φ , Q and D for each 10° sector are listed in Table V-1.

The objective of this exercise is to predict the microdensitometer response to an image of the $\frac{1}{2}$ -m cone as the densitometer aperture integrates the range of film densities at each of several positions along its diameter. For this purpose, densities were computed for seven positions as shown in Figure V-4. A circular aperture of $\frac{1}{2}$ -m-scale dia was assumed as specified by Kosofsky and Broome.

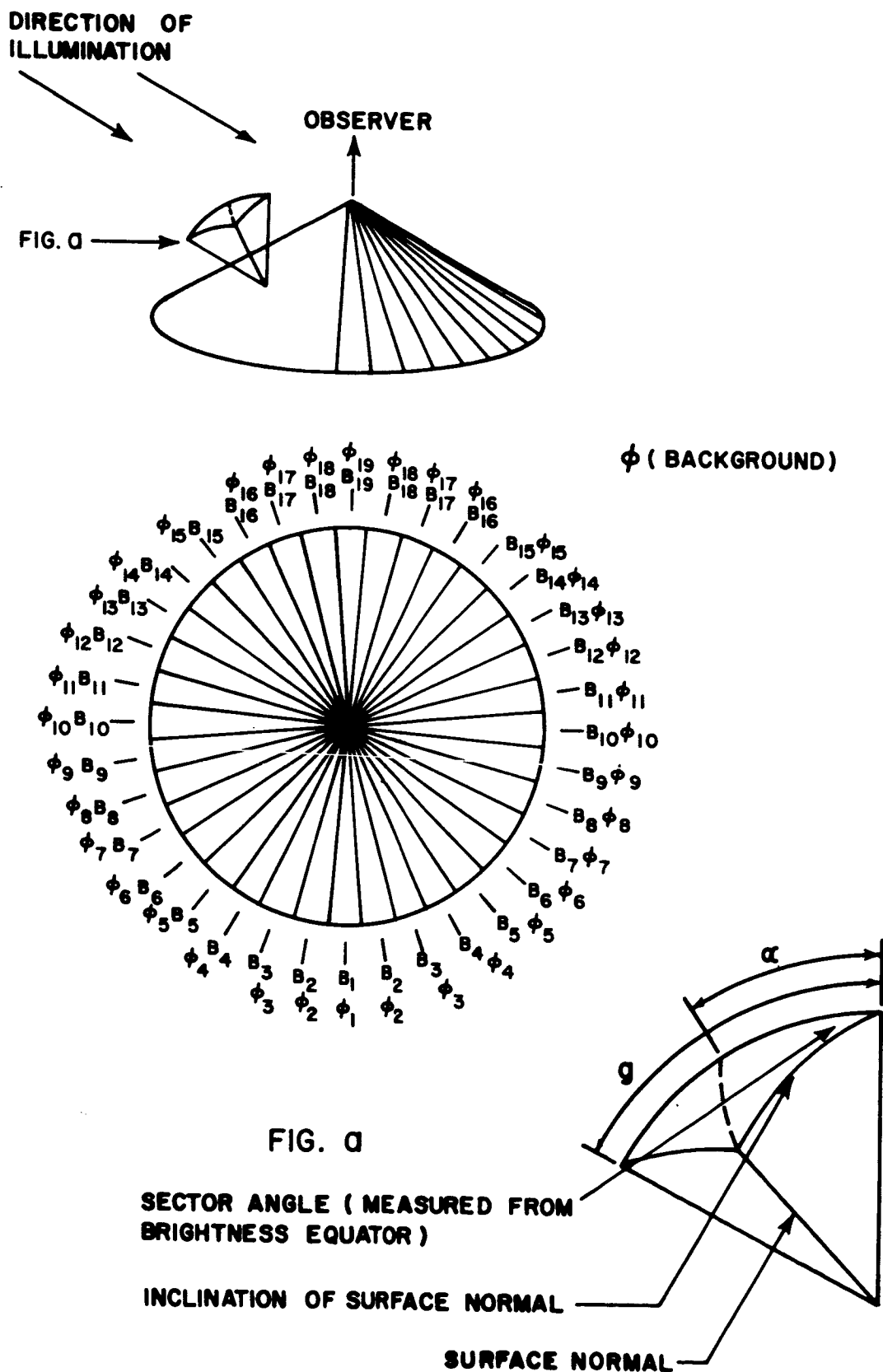


Figure V-4. Cone Geometry and Condition of Illumination

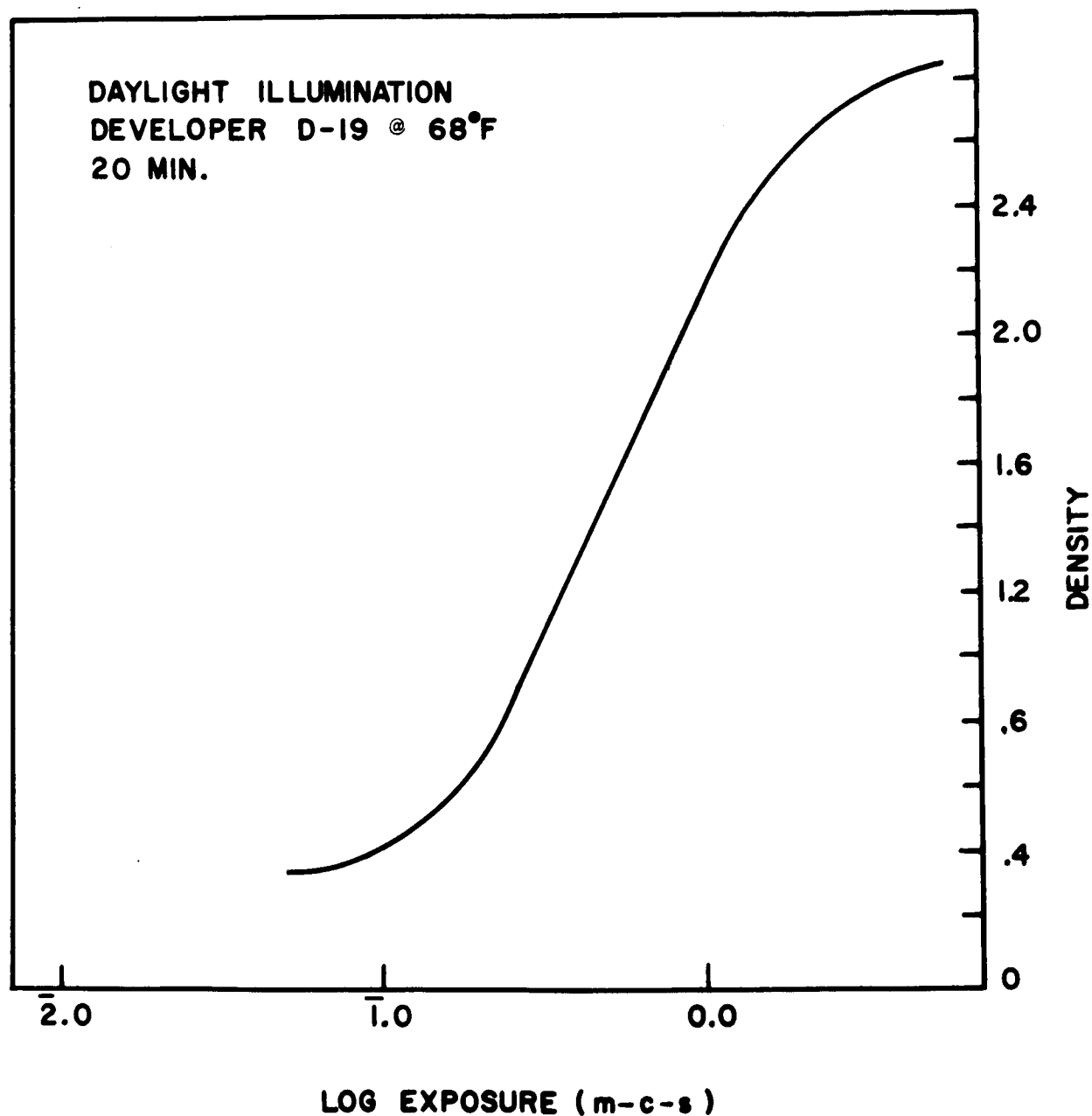


Figure V-5. Characteristic Curve Film SO-243

Film density is now defined as

$$D = \log_{10} \frac{P_o}{P_T}$$

where

P_o = power incident

P_T = power transmitted

thus,

$$P_T = \frac{P_o}{10^D}$$

The total power transmitted through the circular aperture for position x ($= 1, \dots, 7$) is

$$P_x = \sum \frac{a_n}{a_t} P_{tn} \quad (V-8)$$

where

a_n = incremental area corresponding to the n^{th} segment

a_t = total area of sensitometer scanning aperture

P_{tn} = power transmitted through the n^{th} segment

If P_o = total incident power at the input side of the densitometer, the measured density will then be

$$D_x = \log \left[\sum_{n=S_i}^{S_j} \frac{P_o}{\left(\frac{a_n}{a_t}\right) P_{tn}} \right] \quad (V-9)$$

as each n^{th} segment of the image transmitted with a density $D_n = \log \frac{P_o}{P_{tn}}$ through the densitometer aperture (of area a_t).

S_i denotes the i^{th} segment shown in Figure V-3. Note that, as the densitometer aperture moves from (a) the outer edge at the bottom of the protuberance image, (b) through the center, (c) through the inside edge, and finally (d) the outer edge on the top, the densitometer covers (a) none of the segments of the protuberance image, (b) all the segments, (c) segments B_{17} , B_{18} and B_{19} (and their counterparts in the unlabeled half circle), and finally, (d) none of the segments.

To aid in the computations, Equation (V-9) was transformed into

$$D_x = \sum_{n=S_i}^{S_j} D_n - \log \sum_{a_t} \frac{a_n}{a_t} 10^{\left(\sum_{S_k=S_i}^{S_i} D_{S_k} \right) - D_n} \quad (V-10)$$

since the density D_n of the n^{th} segment in the image is known from its photometric function of the protuberances and photographic emulsion as calculated and listed in Table V-1.

Thus, the density obtained when scanning this image with a $\frac{1}{8}$ -m dia selected densitometer aperture was computed for each of the seven positions shown in Figure V-6. Results are tabulated in Table V-2. Using this computation, the degradation in the information content of the image due to such a microdensitometric step is shown in Figure V-7.

The microdensitometric step required in the transmission of the image to earth degrades the fine details needed in recognizing impaling protuberances.

Table V-1

CALCULATION OF DENSITY PROFILE OF PHOTOGRAPHIC IMAGE OF THE
STANDARD PROTUBERANCE (BY SEGMENTS)

Phase Angle $g = 63^\circ$

Segment Number, B_i	Angle α° (Calculated)	Photometric Function ϕ	Q Reflected Energy (MCS)	D Film Density
(Lunar Surface)	0.0	0.20	0.581	1.61
1	-26.6	0.27	0.848	2.2
2	-26.36	0.27	0.848	2.2
3	-25.24	0.26	0.816	1.97
4	-23.28	0.25	0.785	1.93
5	-21.06	0.23	0.723	1.87
6	-18.08	0.225	0.707	1.83
7	-13.58	0.225	0.707	1.84
8	- 9.74	0.21	0.66	1.75
9	- 5.04	0.205	0.644	1.72
10	0.00	0.20	0.581	1.61
11	5.04	0.17	0.534	1.60
12	9.74	0.12	0.377	1.23
13	13.58	0.10	0.314	1.05
14	18.08	0.06	0.189	0.63
15	21.06	0.03	0.095	0.42
16	23.28	0.015	0.047	0.33
17	25.24	0.00	0.00	0.32
18	26.36	0.00	0.00	0.32
19	26.6	0.00	0.00	0.32

F. METHOD FOR DETERMINING SAFE LANDING PROBABILITY
(PROTUBERANCES) FROM SURVEYOR SAMPLE AREA AND
ORBITER PHOTOGRAPHS

The foregoing considerations indicate a strong possibility that photography from the proposed Orbiter system will not yield adequate resolution or heighting accuracy for measurement of protuberances within the requisite confidence limits. The only alternative, short of redesigning the system or relaxing specifications, appears to demand increased reliance on statistical estimates.

Limited, extremely detailed terrain coverage exists from the Ranger series missions and will be forthcoming from the Surveyor program. In conjunction with Orbiter photography, it may prove feasible

Table V-2

CALCULATED DENSITY OBTAINABLE BY SCANNING THE IMAGE OF THE
STANDARD 2-M BASE DIAMETER PROTUBERANCE WITH A
DENSITOMETER APERTURE EQUIVALENT TO $\frac{1}{2}$ -M DIAMETER

Densitometer Aperture Position (See Figure V-4)	Image Segments Scanned	Density (Calculated)	True Density
0	None (lunar surface)	1.61	1.61
1	Lunar surface plus Nos. 1 and 2	1.80	2.2
2	Nos. 1, 2 and 3	2.12	2.2
3	Nos. 1 through 9	1.98	2.2
4	Nos. 1 through 19	0.86	2.2
5	Nos. 11 through 19	0.40	0.32
6	Nos. 17, 18 and 19	0.32	0.32
7	None (lunar surface)	1.61	1.61

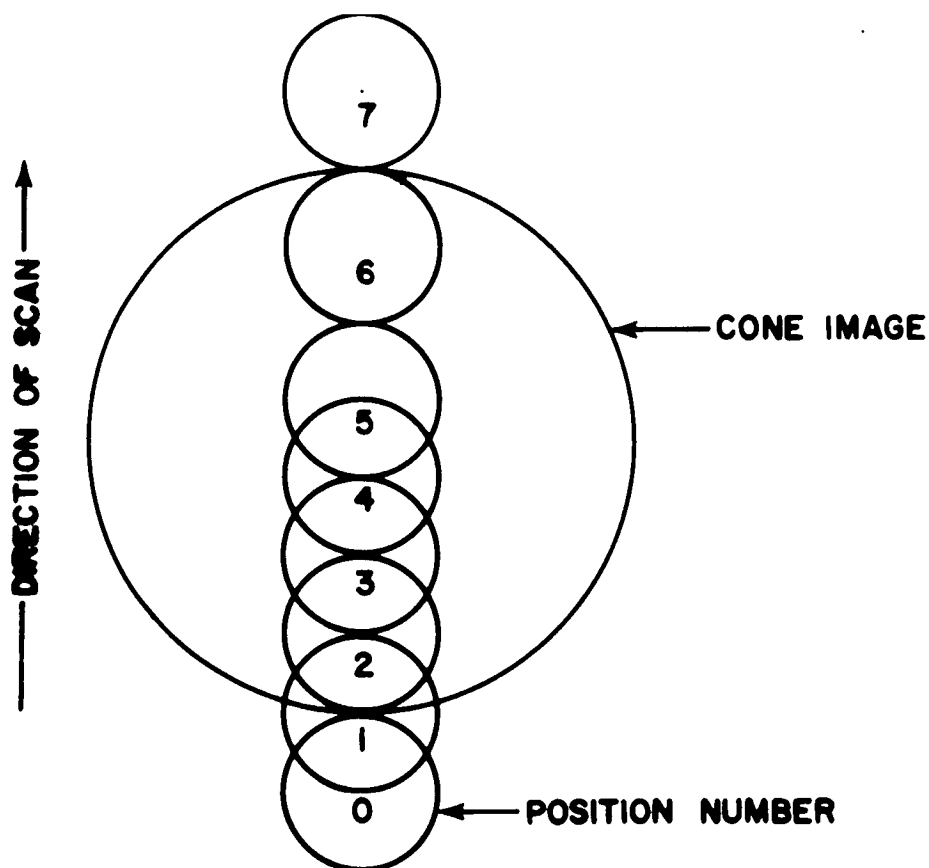


Figure V-6. Aperture Positions for Which Density Was Computed

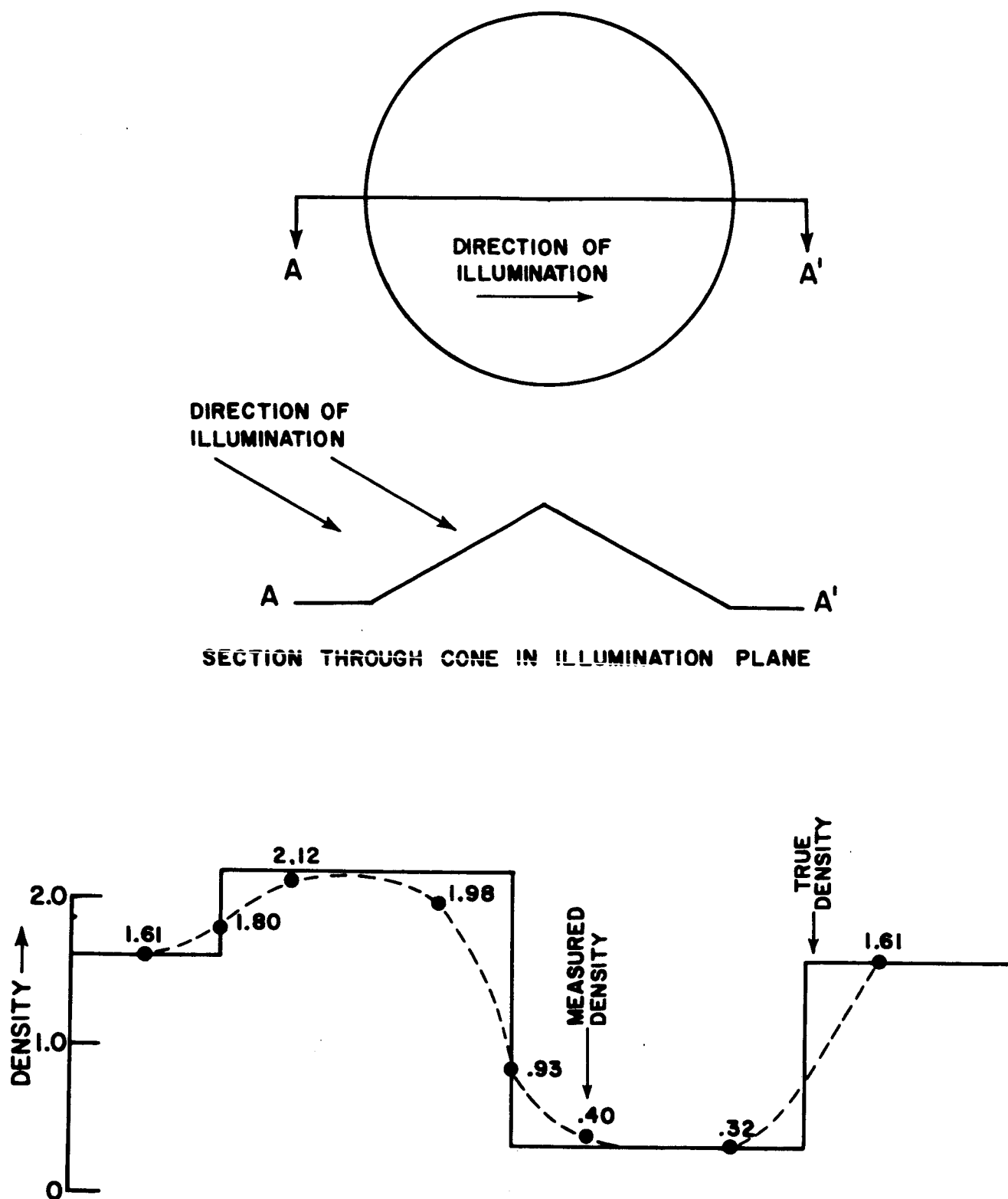


Figure V-7. Comparison of Microdensitometered Density with True Density

to extrapolate protuberance incidence from very limited samples over larger areas by the following method. This method is based on the fact that all discrete lunar features in the size range of interest — that is, objects which are large enough to detect but too small to identify on high-resolution Orbiter photography — constitute a binominal population of craters and protuberances. One can, indeed, note, on the last Ranger IX frame, protuberances about 1 m across on the floor of Alphonsus which appeared only as bright spots, indistinguishable from small craters, in earlier frames.

It is assumed, then, that Surveyor landing sites will be located within relatively homogeneous areas of large enough extent to enclose one or more LEM landing areas of 1.6-km diameter. Surveyor will provide a capability to detect and map, with high incidence, craters and protuberances over a restricted sample area, which will range in size from those that can be distinguished on Orbiter pictures to subdetection size. It is further assumed that objects which cannot be detected on Orbiter pictures are too small to constitute bottoming hazards.

The only discrete objects in the Surveyor photographs will be craters and protuberances. These craters and protuberances constitute a sample from a larger population of objects which extends throughout the homogeneous area of interest. Within this area, an assumption can be made that the same proportion of protuberances to total objects will exist if the objects have some common origin such as secondary crater ray material, mare surfaces, etc.

From the Survey sample data, one determines the following:

n_c = number of craters

n_p = number of protuberances

$n_{p>50}$ = number of protuberances > 50 cm

$p_{p>50}$ = proportion of protuberances > 50 cm

$$= \frac{n_{p>50}}{n_p + n_c}$$

Thus, all objects of interest for LEM protuberance studies are present and accounted for within the sample area scanned by Surveyor.

There is substantial evidence that the Orbiter high-resolution monoscopic photography will enable identification and measurement of protuberances somewhat larger than 50 cm, but will only afford detection of objects — "blobs" — some of which may be protuberances in the critical range around 50 cm. It is assumed that, if an object can be measured, it can be classified with 100 percent confidence as a crater or protuberance. Thus, it is desired to make a statistical estimate of the proportion of objects in the range of detection, but below the range of identification, which are protuberances greater than 50 cm.

Therefore, by available photointerpretive and photographic techniques, one identifies with a high degree of confidence — 100 percent — those protuberances which are large enough to be measured. From the Surveyor data, one eliminates from further consideration any craters and protuberances which could be positively identified in the Orbiter photographs. This total population, consisting of unidentifiable craters and protuberances, can be counted on the Orbiter photographs.

The probability of making a safe landing can now be estimated with some preassigned confidence level.

Let $N = N_p + N_c$ be the number of "objects" observed for a given area of interest with the Orbiter data. Thus, N is known, but the proportions of N_p or N_c remain to be estimated since the class of detected objects which are unidentifiable is being considered exclusively.

Now the Surveyor data provides a sample of the total number of objects N which can be partitioned as $n = n_p$ where n_p , n_c and n are measured. It is desired to estimate N_p by \hat{N}_p where \hat{N}_p will be some function of the sample values n , n_p , n_c . Assuming that n is a random sample of the N objects, the distribution of n_p is given by

$$p\left(n_p; N_c, N_p\right) = \frac{\binom{N_p}{n_p} \binom{N_c}{n_c}}{\binom{N}{n}} \quad (V-11)$$

and the best estimate of N_p is given (Cochran, 1953) by

$$\hat{N}_p = n_p \frac{N}{n}$$

with variance

$$N_p N_c (N - n) / [n (N - 1)] \quad (V-12)$$

From the method presented in Chapter II, B, the critical number of protuberances to yield bottoming probability $P_{.05}$ for an area designated on the Orbiter coverage can be determined. The value of $P_{.05}$ is such that, if $N_p = P_{.05}$, the probability of a nonimpaled landing is 95 percent.

Therefore, a landing decision can be made by testing the hypothesis $H_0: N_p \leq P_{.05}$ against the alternative hypothesis that $H_A: N_p > P_{.05}$. The possible outcomes of such a test can best be described by the following diagram:

		Decision	
State of Nature	H_0	Correct Decision	α
	H_A	β	Correct Decision

Clearly, one decides $N_p \leq P_{.05}$ if $n_p \leq C$ where C is, for the present, an undetermined constant. If $n_p > C$, then the correct decision of $N_p > P_{.05}$. Either of the errors α or β can be forced to a predetermined choice at the cost of having to fit the constant C . Suppose the error β is "controlled" by specifying that the probability of deciding $N_p \leq P_{.05}$ when, in fact, $N_p > P_{.05}$ is to be less than or equal to 0.9 (any arbitrary value may be assumed). This determines the constant C from the relation

$$\sum_{n_p=0}^C p(n_p, N, P_{.05}) = 0.9$$

One could tailor this method to a more restrictive condition involving selection of only protuberances greater than 50 cm in height as the sample: then the foregoing estimate of \hat{N}_p is multiplied by a factor $\frac{n_p}{n_{p>50}}$

At the present state of lunar knowledge, it may be advisable to treat all protuberances as hazards until the likelihood and amount of sinkage can be determined.

G. CONCLUSIONS AND RECOMMENDATIONS

It is concluded that present state-of-the-art photogrammetric or photometric measurements will not yield sufficiently accurate results from the contemplated Lunar Orbiter photography to satisfy the rigid requirements for certification of safe landing sites with respect to bottoming hazards.

A statistical process was outlined which may yield valid results based on detection of objects near the photographic resolution threshold in conjunction with higher resolution measurements and interpretation from Ranger and Surveyor coverage.

This technique should be critically appraised by detailed examination of its underlying assumptions and experiments involving Ranger photography at various scales or model studies. The most fundamental uncertainty concerns the assumption that a common origin for craters and protuberances implies a constant ratio of protuberances to craters within the domain of interest.

The principal shortcoming of the high-resolution camera system stems from lack of overlapping stereo coverage and insufficient base-height ratio. It appears that both these shortcomings could be overcome by adoption of a wide-base convergent photographic mode, as shown in Figure V-8. The minimum height which can be resolved by such a system is computed by the equation

$$\Delta H = \frac{H}{4fR \sin \frac{\phi}{2}} \quad (V-13)$$

where

H = flight height

f = focal length

R = resolution lines/mm

ϕ = convergence angle

Taking $\phi = 60^\circ$, $f = 0.61$ m, $R = 76$ lines/mm, $H = 4600$ m

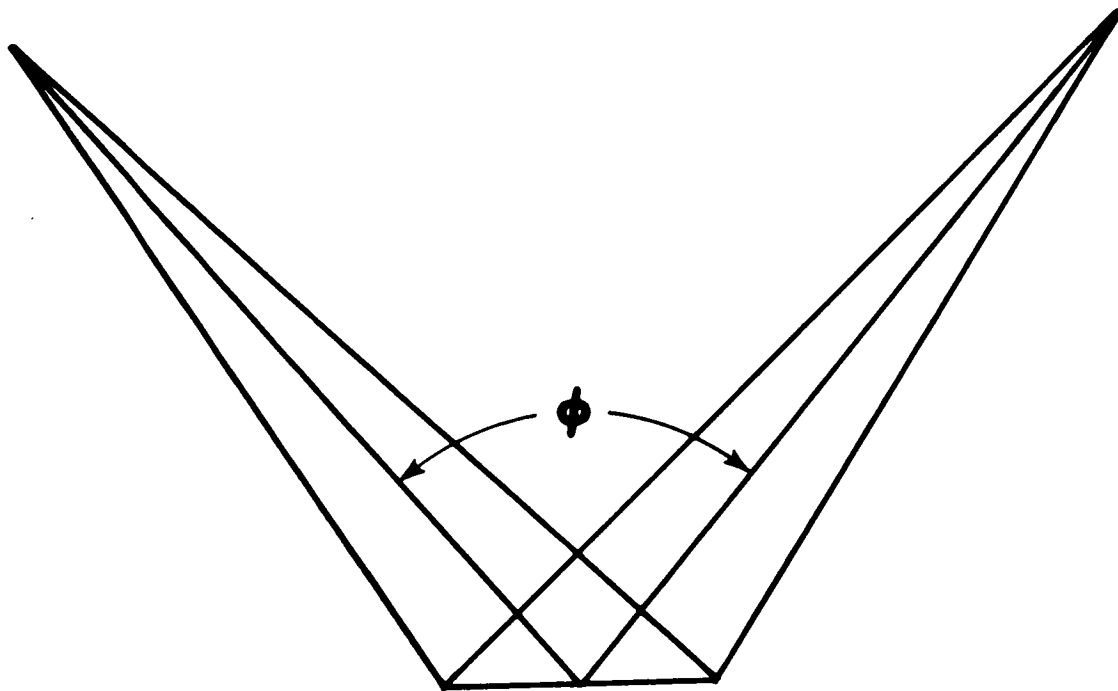


Figure V-8. Geometry for Wide Base Convergent Photography

$$\Delta H = \frac{46,000}{4 \times 0.61 \times 76 \times 0.5}$$

$$\Delta H = 0.49 \text{ m}$$

This is quite a reasonable figure, compared with those previously computed for vertical overlapping photography.

It appears that the existing camera system could be modified without undue difficulty as illustrated by the conceptual system in Figure V-9. The camera axis is aligned horizontally and utilizes a hinged mirror looking downward in front of the lens. The mirror is equipped with a motor-activated position selector so that the camera can look forward and backward in consecutive exposures. Image motion compensation is provided by rotating cams, which also serve as position stops for the mirror.

A price is paid, of course, for stereo coverage utilizing this system, in that complete high-density monoscopic coverage is sacrificed for stereo coverage of alternate areas on the ground. Also, slight

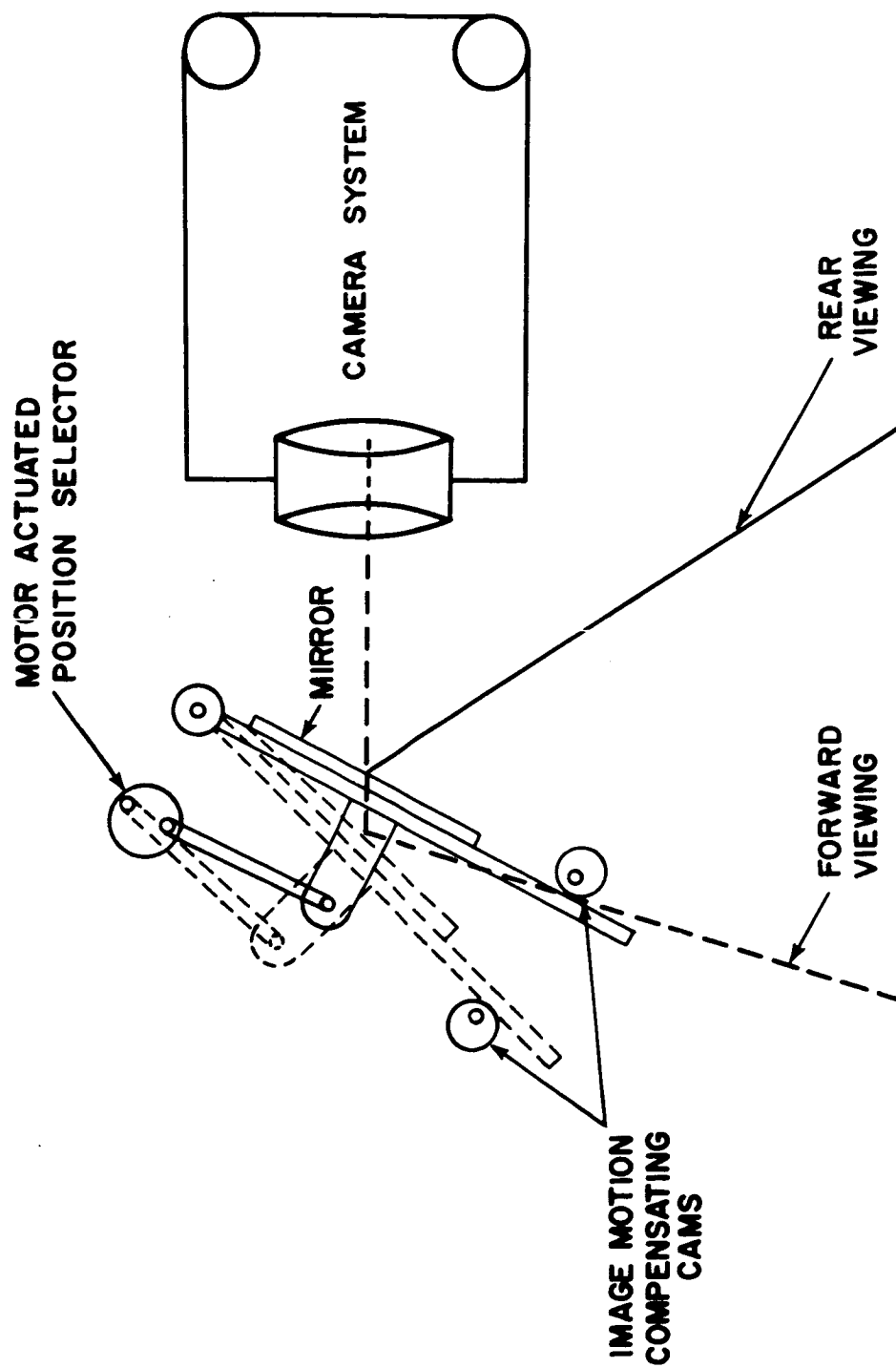


Figure V-9. Conceptual Camera System

degradation of resolution may result from the mirror. Nevertheless, it is believed that such a tradeoff would be advantageous since it would provide greater accuracy in differential elevation measurements, due to the longer stereo base. These measurements could then be extrapolated over the adjacent gaps in high-resolution coverage.

H. REFERENCES CITED

- Blackwell, H.R., 1946, Contrast thresholds of the human eye: J. Dept. Soc. Am., v. 36 (11), p. 624-643.
- Cochran, W.G., 1953, Sampling Techniques: John Wiley & Sons.
- Colwell, R.N., 1960, Procurement of aerial photography: Ch. 2; Manual of Photographic Interpretation, An. Soc. of Photogrammetry, Washington, D.C., 868 p.
- Higgins, G.C., R.N. Wolfe and R.S. Lamberts, 1956, Relationship between definition and resolving power with test objects differing in contrast: J. Opt. Soc. Am., v. 46, Sept., p. 752-754.
- Itek Laboratories, 1962, Photographic and photogrammetric methods of terrain analysis for determination of aircraft landing sites: prepared for Geophysical Directorate, AFCRL Contract AF 19(628)-277, Jun. 8.
- Keene, G., 1965, Bi-monthly progress report no. 3: Contract NAS 9-3826, 1 Apr. — 1 Jun.
- Kosofsky, L.J. and G.C. Broome, 1965, Lunar Orbiter: A photographic satellite: NASA Langley Research Center, Langley Station, Hampton, Va., presented at the spring convention of the Soc. of Motion Picture and Television Engineers, Los Angeles, Calif., Mar. 28 — Apr. 2.
- Linfoot, E.H., 1965, Fourier Methods in Optical Image Evaluation: Pittman Press
- Lyon, Duane, 1965, Charting with lunar satellites: ACIC Tech. Paper TP-19, Sept.
- Macdonald, D.E., 1951, Calibration of survey cameras and lens testing: Photogrammetric Eng., v. 17 (3), p. 383-389.
- Saltzman, M.H., 1959, The factors in human vision applicable to photogrammetry: Photogrammetric Eng., v. 15 (4), p. 637-647.

Skidmore, J., 1965, Contour accuracy versus spot heights: Photogrammetric Eng., v. XXXI, n. 5, p. 828-830.

Theis, J.B., 1965, The mirror and the map: Photogrammetric Eng., v. XXXI, p. 791-795.

CHAPTER VI

ADDITIONAL READING

- Adams, J., J. Conel, A. Filice, Z. Kopal, A. Loomis, D. Nash, N. Nickle, R. Speed, and R. Steinbacher, 1964, Surveyor block II, phase 3: a study of lunar terrain assessment: JPL, Tech. Mem. 33-172, Calif. Inst. of Tech., Pasadena, Calif., Apr. 20, 179 p.
- Aeronautical Chart and Information Center, 1964, Cartographic reduction of Ranger VII mission: ACIC Tech. Paper 16, USAF, St. Louis, Mo., Dec., 11 p.
- Aeronautical Chart and Information Center, 1964, Ranger VII lunar charts RLC 1-5: Supt. of Doc., U.S. Govt. Printing Office, Washington, D.C.
- Aeronautical Chart and Information Center, 1964, Reduction of NASA's lunar orbital photography: Tech. Prop., Sept. 1, 20 p.
- Amdursky, M.E., 1964, Application of a photometric technique for mapping the lunar surface: Presentation at 3rd Symposium on Remote Sensing of Environment, Univ. of Mich., Bendix Corp., Systems Div., Ann Arbor, Mich., Oct. 14-16.
- Barrows, R.S., 1957, Factors affecting the recognition of small, low-contrast photographic images: Photo. Sci. and Eng., v.1, Jul. 1, p. 15-22.
- Beilock, M., 1964, Surveyor lander mission and capability: JPL, Preprint 64-8, Presentation before 10th Annual Meeting, Am. Astronaut. Soc., Calif. Inst. of Tech., Pasadena, Calif., May 4-7, 41 p.
- Bendat, J.S., 1962, Interpretation and application of statistical analysis for random physical phenomena: IRE Transactions on Bio-Medical Electronics, Jan., p. 31-43.
- Benson, M.A. and R.D. Williams, 1965, Description and flight analysis of the Ranger VII TV subsystem: JPL, Tech. Rpt. 32-680, Contract NAS 7-100, Calif. Inst. of Tech., Pasadena, Calif., Feb. 15, 18 p.
- Beswick, A.G., 1964, Instrumentation for investigating the physical properties: Preprint 16.1-4-64, Presentation at 19th Annual ISA Conference and Exhibit, NASA Langley Res. Center, New York, Oct. 12-15.

- The Boeing Company, 1964, The lunar orbiter: Aero-Space Div., Doc. for NASA Langley Res. Center, Oct., 34 p.
- Brock, G.C., 1961, The status and problems of air photography: Photo. J., v.101, Jun., p. 165-177.
- Byrne, C.J., 1963, Lunar photographic orbiter: lighting and viewing conditions: Bellcomm, Inc., Washington, D.C., Oct. 11.
- Carman, P.D. and R.A.F. Carruthiers, 1951, Brightness of fine detail in air photography: J. OSA, v.41, May 5, p. 305-310.
- Clapp, L.C. and H. Yilmaz, 1963, Optical information processing: Intl. Sci. and Tech., Jul., p. 34-98.
- Cutrona, L.J., E.N. Leith, C.J. Palermo, and L.J. Porcello, 1960, Optical data processing and filtering systems: IRE Transactions on Information Theory, Jun, p. 286-400.
- Dodd, R.T. Jr., J.W. Salisbury and V.G. Smalley, 1963, Crater frequency and the interpretation of lunar history: AFCRL, Bedford, Mass., Dec., 24 p. (16 illus.).
- Doyle, F.J., 1963, The absolute accuracy of photogrammetry: Photogrammetric Eng., v. XXIX, n. 1. Jan., p. 105-108.
- Eimer, M., 1963, Photography of the moon from space probes: JPL, Tech. Rpt. 32-347, Contract NAS 7-100, Calif. Inst. of Tech., Pasadena, Calif., Jan. 15, 21 p.
- Fairchild Camera and Instrument Corp., 1963, Study of scientific objectives and calibration requirements for the surveyor lander spacecraft TV camera system; scientific objectives, Task 1; system capability, Task 2: JPL, Final Rpt. SME-BA-130, Sys. Man. and Eng. Dept., Calif. Inst. of Tech., Pasadena, Calif., Dec. 30.
- Gardner, I.C., 1932, The optical requirements of airplane mapping: J. Res. NBS, v. 8, Feb., p. 445-455.
- Gondran, A.D. and R. M. Woolheater, 1964, An introduction to spectral calculations from digital records: Internal Rpt. R44-720, Ling-Temco-Vought, Inc., Military Electronics Div., Garland, Texas, Jan. 8.

- Hallert, B. P., 1963, Accuracy and precision in photogrammetry: Photogrammetric Eng., v. XXIX, n. 1, Jan., p. 108-112.
- Hapke, B. W., 1962, Second preliminary report on experiments relating to the lunar surface: CRSR 127, Cornell Univ., Jul., 41 p.
- Hayre, H. S. and R. K. Moore, 1961, Theoretical scattering coefficient for near vertical incidence from contour maps: J. Res. NBS, v. 65D, n. 5, Sept. -Oct., p. 427-432.
- Herriman, A. G., H. W. Washburn and D. E. Willingham, 1963, Ranger preflight science analysis and the lunar photometric model: JPL, Tech. Rpt. 32-384, Contract NAS 7-100, Calif. Inst. of Tech., Pasadena, Calif., Jan. 7, 38 p.
- Higgins, G. C. and F. H. Perrin, 1958, The evaluation of optical images: Photo. Sci. and Eng., v. 2, Aug. 2, p. 66-76.
- Horton, C. W., W. B. Hemphkins and A. A. J. Hoffman, 1964, A statistical analysis of some aeromagnetic maps from the Northwestern Canadian shield: Geophysics, v. XXIX, Aug. 4, p. 582-601.
- Hunt, M., 1965, Lunar geodesy...a problem in statistics: Research Review, OAR, v. III, Feb. 12, p. 19.
- International Business Machines Corp., 1963, Optimized digital mapping system: First Interim Rpt, Contract DA-44-009 AMC-111(X), Proj. 8 T35-14-001-07, U.S. Army Eng., Geod. Intell. and Mapping Res. and Dev. Agcy. May 30, 46 p.
- Itek Corporation, 1962, Photographic and photogrammetric methods of terrain analysis for determination of aircraft landing sites: Final Rpt., Contract AF 19(628)277, AFCRL-62-644, 9037, Geophys. Res. Directorate, OAR Palo Alto, Calif., Jun. 8, 168 p.
- Jackson, P. L., 1965, Analysis of variable-density seismograms by means of optical diffraction: Geophysics, v. XXX, Feb. 1, p. 5-23 (19 figs).
- Jastrow, R., 1960, The exploration of the moon: Sci. Am., v. 202, May 5, p. 61-68.
- Kay, I. and P. Swerling, 1964, Statistics of random surfaces: Radio Sci. J. of Res. NBS/USNC-URSI, v. 68D, n. 9, Sept., p. 1035-1047.
- Keene, G. T. and T. F. Kerwick, 1965, An analysis of photography from Ranger VII: Presentation at 97th Tech. Conf., Soc. of Motion Picture and Television Eng., Eastman Kodak Co., Rochester, N. Y., Mar. 29-Apr. 2.

- Kindt, D.H. and J.R. Staniszewski, 1965, The design of the Ranger television system to obtain high-resolution photographs of the lunar surface: JPL, Tech. Rpt. 32-717, Calif. Inst. of Tech., Pasadena, Calif., Mar. 1, 23 p.
- Lorens, C.S., 1963, Aspects of theoretical and experimental map-matching: IEEE Transactions on Aerospace and Navigational Electronics, Jun., p. 98-114.
- McGille, C.D. and B.P. Miller, 1962, Lunar surface roughness from crater statistics: J. of Geophys. Res., v. 67, n. 12, Nov., p. 4787-4794.
- Michael, W. H. Jr., R. H. Tolson and J. P. Gapcynski, 1962, Feasibility study of a circumlunar photographic experiment: NASA Tech. Note D-1226, NASA Langley Res. Center.
- Miller, Burton P., 1965, Distribution of small lunar craters based on Ranger 7 photographs: J. of Geophys. Res., v. 70, n. 9, May 1, p. 2265-2266.
- Miller, C.S., F.G. Parsons and I.L. Kofsky, 1964, Simplified two-dimensional microdensitometry: Nature, v. 202, Jun. 20, p. 1196-1200.
- Mueller, G.E., 1964, Apollo capabilities: Astronautics & Aeronautics, Jun., p. 1-7.
- National Academy of Sciences, 1964, Ranger VII photographic mission to the moon: IG Bull. 88, Oct., 24 p.
- National Aeronautics and Space Administration, 1965, Project Apollo pad-abort: NASA Press Release 65-202, Jun. 25.
- Newton, J.D. and H.F. Dodge, 1964, Digital fictitious data for automatic mapping research: TR 21.097, IBM Data Sys. Div., Kingston, N.Y., Jan. 30, 26 p.
- Pike, R.J., 1964, Some morphometric properties of the lunar surface... a preliminary investigation from lunar aeronautical charts: Internal Res. 86-141, CAL Rpt. VS-1985-C-1, Aug. 21, 112 p.
- Program Directive M-DE 8020.008 A, 1963, Requirements for data in support of Project Apollo: Issue III, Aug. 15, 5 p. (CONFIDENTIAL)
- Radin, H.W., 1964, Surveyor site certification study: Bellcomm, Inc., Washington, D.C., Jan. 31, 16 p.

- Roach, C.D., Application of power spectral density concept to terrain analysis: 6038, U.S. Army Transport. Res. Command, Fort Eustis, Va., 13 p.
- Rogers, J.R. and O.H. Vaughan Jr., 1964, Lunar environment; an interpretation of the surface of the moon and its atmosphere: NASA Tech. Mem. TM X-53124, Geo. C. Marshall Space Flight Center, Huntsville, Ala., Sept. 3, 118 p.
- Ruffin, B.W., 1965, Automatic computation of lunar relative heights from shadow measurements: USAF ACIC, Lunar and Planetary Br. Cartog. Div., St. Louis, Mo., Mar., 6 p.
- Russell, J.A.G., 1963, A precision flying spot film digitizer: Contract W-7405-eng-48, UCRL-7619, Livermore, Calif., Dec. 13, 10 p.
- Schloss, M., 1965, Quantifying terrain roughness on lunar and planetary surfaces: Presentation 65-389 at AIAA Second Annual Meeting, San Francisco, Calif., Bendix Corp., Jul. 26-29.
- Schurmeier, H.M., 1964, Ranger VII, Pt. 1, mission description and performance: JPL, Tech. Rpt. 32-700, Contract NAS 7-100, Calif. Inst. of Tech., Pasadena, Calif., Dec. 15, 89 p.
- Seamans, R.C. Jr., R.L. Bisplinghoff, H.E. Newell, G.E. Mueller, and O.B. Lloyd Jr., 1965, Background material and NASA FY 1966 budget briefing: NASA Press Release, Jan. 25.
- Shaw, R., 1962, The application of Fourier techniques and information theory to the assessment of photographic image quality: Photo. Sci. and Eng., v. 6, 5, Sept.-Oct., p. 281-286.
- Swerling, P., 1962, Statistical properties of the contours of random surfaces: IRE Transactions on Information Theory, p. 315-321.
- Taback, I. and E.A. Brummer, 1965, The lunar orbiter: Presentation at AIAA Unmanned Spacecraft Meeting, Los Angeles, Calif., NASA Langley Res. Center, Hampton, Va., Mar. 1-3.
- Tanner, W.F., No date, Possible Gaussian components of zigzag curves: Florida State Univ., Tallahassee, Fla.

- Toll, E., 1964, Comments on correlation functions and power spectral density functions: Rpt. NADC-AC-6408, Aeronaut. Computer Lab., Johnsville, Penn., May 18.
- Troeh, F.R., 1965, Landform equations fitted to contour maps: Am. J. of Sci., v. 263, Summer, p. 616-627.
- U.S. Dept. of Interior, 1961, Astrogeologic studies: Semiannual Prog. Rpt., Geological Survey, Feb. 26-Aug. 24, Mar., 137 p.
- Valencia, S.M., 1965, The pahoehoe/aa flows, southeast of Pisgah Crater: Unpub. Rpt., Univ. of Southern Calif., 22 p.
- Van Deusen, B.D., 1965, A study of the vehicle ride dynamics aspect of ground mobility: Summary Rpt. 3-114, Contract DA-22-079-eng-403, Chrysler Corp., WES, Vicksburg, Miss., v. 1, Mar., 71 p.
- Whitten, E.H.T., 1964, Process-response models in geology: Geol. Soc. of Am. Bull., v. 75, May, p. 455-464.
- Willey, R.L. and H.A. Pohn, Detailed photoelectric photometry of the moon: Contrib. 1254, Geol. Sci. Div., Calif. Inst. of Tech., Pasadena, Calif.
- Willingham, D., 1964, The lunar reflectivity model for Ranger block III analysis: JPL, Tech. Rpt. 32-664, Calif. Inst. of Tech., Pasadena, Calif., Nov. 2, 11 p.
- Wood, W.F., 1964, Statistical terrain analysis: Research Trends, CAL, Cornell Univ., Buffalo, N.Y., Summer-Autumn, p. 7-11.
- Wood, W.F. and J.B. Snell, 1959, Predictive methods in topographic analysis I; relief, slope, and dissection on inch-to-the-mile maps in the United States: Tech. Rpt. EP-112, Hq. Quartermaster, U. S. Army Res. & Eng. Command, Apr., 31 p.

APPENDIX A

DERIVATION OF TRUE SLOPES FROM APPARENT SLOPES

APPENDIX A DERIVATION OF TRUE SLOPES FROM APPARENT SLOPES

The following statements refer to Figure III-1. Let $H = \overline{OP}$, then

$$\tan \theta = H / \overline{OB} \quad (A-1)$$

$$\tan \theta_1 = H / \overline{OA} \quad (A-2)$$

$$\tan \theta_2 = H / \overline{OC} \quad (A-3)$$

Now

$$\cos \phi_1 = \overline{OB} / \overline{OA} \quad (A-4)$$

$$\cos \phi_2 = \overline{OB} / \overline{OC} \quad (A-5)$$

so (A-2) and (A-3) may be written

$$\tan \theta_1 = (H / \overline{OB}) \cos \phi_1 = \tan \theta \cos \phi_1 \quad (A-6)$$

$$\tan \theta_2 = (H / \overline{OB}) \cos \phi_2 = (H / \overline{OC}) \cos (90^\circ - \phi_1) = \tan \theta \sin \phi_1 \quad (A-7)$$

In the last equation it was assumed that \overline{OC} is perpendicular to \overline{OA} .

Upon squaring and adding Equations (A-6) and (A-7), one has the desired result

$$\tan^2 \theta_1 + \tan^2 \theta_2 = \tan^2 \theta \quad (A-8)$$

APPENDIX B

CALCULATIONS FOR DETERMINING AVERAGE VALUES

OF TANGENT θ_1 AND TANGENT² θ_1

APPENDIX B

CALCULATIONS FOR DETERMINING AVERAGE VALUES OF TANGENT θ_1 AND TANGENT² θ_1

A. THE EVALUATION OF EQUATION (III-13)

Equation (III-13) reads

$$\langle \tan \theta_1 \rangle = \frac{1}{\Delta x} \int_{-\infty}^{+\infty} \int_{-\infty}^{+\infty} (z_2 - z_1) P_2(\Delta x; z_1, z_2) dz_1, dz_2 \quad (\text{B-1})$$

with

$$P_2(\Delta x; z_1, z_2) = \frac{e^{-\frac{z_1^2 - 2\tau z_1 z_2 + z_2^2}{2\sigma^2(1-\tau^2)}}}{2\pi\sigma^2 \sqrt{1-\tau^2}} \quad (\text{B-2})$$

so

$$\langle \tan \theta_1 \rangle = \frac{I_1 - I_2}{2\pi\sigma^2 \Delta x \sqrt{1-\tau^2}}$$

with

$$I_1 = \int_{-\infty}^{+\infty} z_2 e^{-\frac{z_2^2}{2\sigma^2(1-\tau^2)}} dz_2 \int_{-\infty}^{+\infty} e^{-\frac{z_1^2 - 2\tau z_1 z_2}{2\sigma^2(1-\tau^2)}} dz_1$$

and

$$I_2 = \int_{-\infty}^{+\infty} z_1 e^{-\frac{z_1^2}{2\sigma^2(1-\tau^2)}} dz_1 \int_{-\infty}^{+\infty} e^{-\frac{z_2^2 - 2\tau z_1 z_2}{2\sigma^2(1-\tau^2)}} dz_2$$

When one examines the expressions for I_1 and I_2 , one sees that if the change of variables $z_1 \rightarrow z_2$, $z_2 \rightarrow z_1$ is made, I_2 becomes identical with I_1 and $\langle \tan \theta_1 \rangle$ becomes zero.

B. THE EVALUATION OF EQUATION (III-14)

When Equation (B-2) of this appendix is substituted into Equation (III-14), one has

$$\langle \tan^2 \theta_1 \rangle = \frac{I_3 - 2I_4 + I_5}{2\pi\sigma^2 (\Delta x)^2 \sqrt{1 - \tau^2}} \quad (\text{B-3})$$

with

$$I_3 = \int_{-\infty}^{+\infty} z_2^2 e^{-\frac{z_2^2}{2\sigma^2(1-\tau^2)}} dz_2 \int_{-\infty}^{+\infty} e^{-\frac{z_1^2 - 2\tau z_1 z_2}{2\sigma^2(1-\tau^2)}} dz_1 \quad (\text{B-4})$$

$$I_4 = \int_{-\infty}^{+\infty} z_2 e^{-\frac{z_2^2}{2\sigma^2(1-\tau^2)}} dz_2 \int_{-\infty}^{+\infty} z_1 e^{-\frac{z_1^2 - 2\tau z_1 z_2}{2\sigma^2(1-\tau^2)}} dz_1 \quad (\text{B-5})$$

$$I_5 = \int_{-\infty}^{+\infty} z_1^2 e^{-\frac{z_1^2}{2\sigma^2(1-\tau^2)}} dz_2 \int_{-\infty}^{+\infty} e^{-\frac{z_2^2 - 2\tau z_1 z_2}{2\sigma^2(1-\tau^2)}} dz_1 \quad (\text{B-6})$$

The same argument given above may be used to show that $I_3 = I_5$. The first step in evaluating I_3 and I_4 is to complete the square in the second integral.

$$z_1^2 - 2\tau z_1 z_2 = (z_1 - \tau z_2)^2 - \tau^2 z_2^2 \quad (\text{B-7})$$

So

$$I_3 = \int_{-\infty}^{+\infty} z_2^2 e^{-\frac{z_2^2 (1 - \tau^2)}{2\sigma^2 (1 - \tau^2)}} dz_2 \int_{-\infty}^{+\infty} e^{-\frac{(z_1 - \tau z_2)^2}{2\sigma^2 (1 - \tau^2)}} dz_1$$

The second integral, which is independent of z_2 , is well-known (Peirce and Foster, 1957). One has

$$I_3 = \sqrt{2\pi} \sigma \sqrt{1 - \tau^2} \int_{-\infty}^{+\infty} z_2^2 e^{-\frac{z_2^2}{2\sigma^2}} dz_2$$

This integral also is given by Peirce and Foster. One has

$$I_3 = 2\pi\sigma^4 \sqrt{1 - \tau^2}$$

When Equation (B-7) is substituted into (B-5), one obtains

$$I_4 = \int_{-\infty}^{+\infty} z_2^2 e^{-\frac{z_2^2}{2\sigma^2}} dz_2 \int_{-\infty}^{+\infty} z_1^2 e^{-\frac{(z_1 - \tau z_2)^2}{2\sigma^2 (1 - \tau^2)}} dz_1$$

Set $z_1 - \tau z_2 = u$ and get

$$I_4 = \int_{-\infty}^{+\infty} z_2^2 e^{-\frac{z_2^2}{2\sigma^2}} dz_2 \int_{-\infty}^{+\infty} u e^{-\frac{u^2}{2\sigma^2(1-\tau^2)}} du$$

$$+ \tau \int_{-\infty}^{+\infty} z_2^2 e^{-\frac{z_2^2}{2\sigma^2}} dz_2 \int_{-\infty}^{+\infty} e^{-\frac{u^2}{2\sigma^2(1-\tau^2)}} du$$

The first term vanishes while the second term is τI_3 . Hence

$$I_4 = 2\pi\sigma^4 \tau \sqrt{1-\tau^2}$$

Finally

$$\langle \tan^2 \theta_1 \rangle = \frac{2\sigma^2}{(\Delta x)^2} (1-\tau)$$

C. REFERENCE CITED

Peirce, B.O. and R.M. Foster, 1957: Short Table of Integrals, 4th Ed., Blaisdell Publishing Co., New York, n. 492.

APPENDIX C

TRANSFORMATION OF COORDINATE SYSTEM

APPENDIX C

TRANSFORMATION OF COORDINATE SYSTEM

A. EVALUATION OF EQUATION (III-18)

It is evident when one evaluates Equation (III-18) that the integral can be simplified if the coordinate system $z_1 z_2$ is rotated 45° to the coordinate system u, v , as shown in Figure C-1.

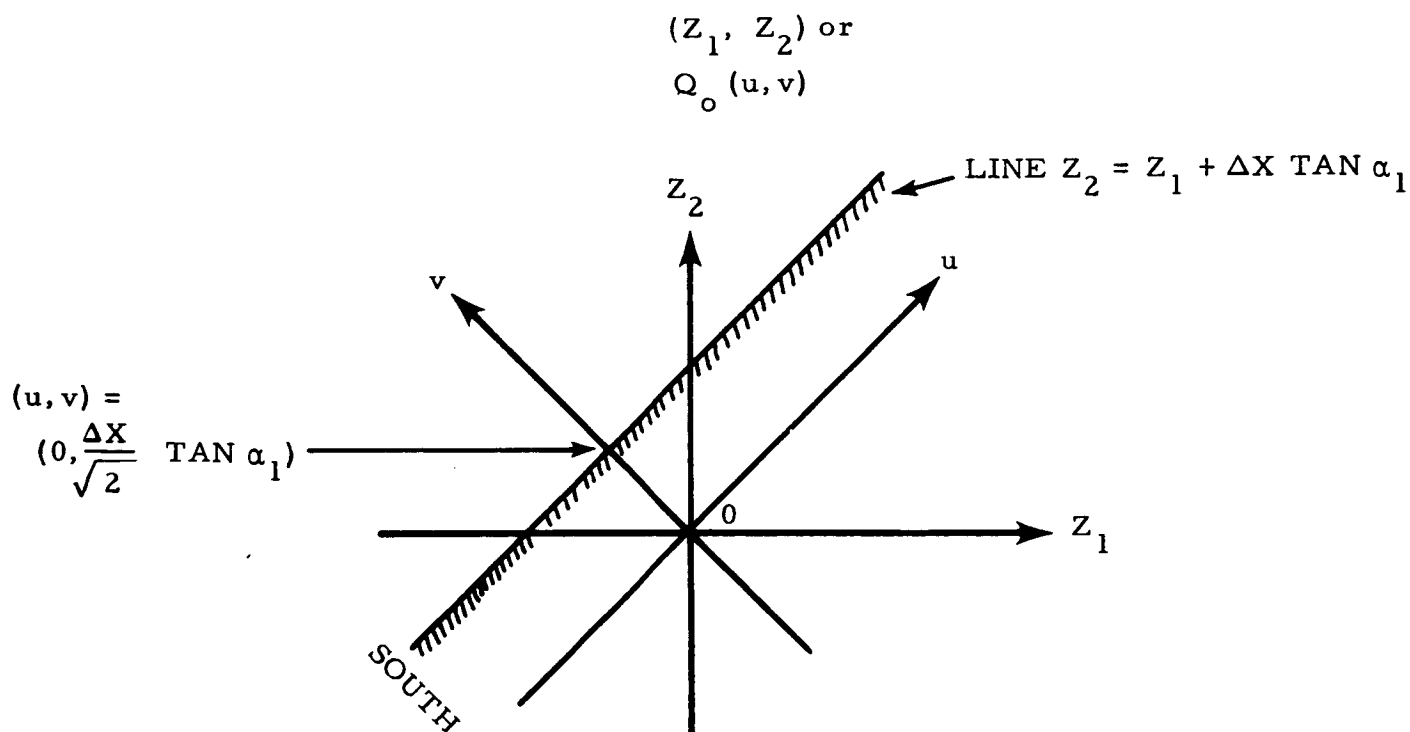


Figure C-1. The Coordinate Systems (z_1, z_2) and (u, v)

The change of variables associated with this rotation is given by

$$z_1 = \frac{u}{\sqrt{2}} - \frac{v}{\sqrt{2}} \quad (\text{C-1})$$

$$z_2 = \frac{u}{\sqrt{2}} + \frac{v}{\sqrt{2}} \quad (\text{C-2})$$

for which the Jacobian is unity.

One has

$$z_1^2 - 2\tau z_1 z_2 + z_2^2 = u^2(1 - \tau) + v^2(1 + \tau) \quad (C-3)$$

so that Equation (III-18) becomes

$$\underline{F}(\alpha_1) = \frac{1}{2\pi\sigma^2 \sqrt{1-\tau^2}} \int_{-\infty}^{+\infty} e^{-\frac{u^2}{2\sigma^2(1+\tau)}} du \int_{-\infty}^{\frac{\Delta x}{\sqrt{2}} \tan \alpha_1} e^{-\frac{v^2}{2\sigma^2(1-\tau)}} dv \quad (C-4)$$

The first integral can be evaluated readily (Peirce and Foster, 1957). One finds

$$\underline{F}(\alpha_1) = \frac{1}{\sqrt{2\pi} \sigma \sqrt{1-\tau}} \int_{-\infty}^{\frac{\Delta x}{\sqrt{2}} \tan \alpha_1} e^{-\frac{v^2}{2\sigma^2(1-\tau)}} dv \quad (C-5)$$

One recognizes this immediately, except for a simple change of variable, as the Gaussian distribution for $\tan \alpha_1$. Hence, if one defines

$$t_1 = \tan \alpha_1$$

and $\int_{t_1}^{t_1 + \Delta t_1} P(t_1) dt_1 = \text{probability that } t_1 \leq \tan \alpha_1 \leq t_1 + \Delta t_1$

one finds
$$P(t_1) = \frac{1}{\sqrt{2\pi}\sigma_t} e^{-t_1^2/2\sigma_t^2}$$

with
$$\sigma_t = \frac{\sigma \sqrt{2(1-\tau)}}{\Delta x}$$

B. REFERENCE CITED

Peirce, B. O. and R.M. Foster, 1957: Short Table of Integrals, 4th Ed., Blaisdell Publ. Co., N.Y., n.492.

APPENDIX D

TREND PLANE REMOVAL

APPENDIX D

TREND PLANE REMOVAL

Let z be the elevation relative to a horizontal plane, the x - y plane. At any point (x_j, y_i) the elevation is z_{ij} . Data are available for MN points, i. e., $i = 1, 2, \dots, N$ and $j = 1, 2, \dots, M$. It is desired to determine the plane that gives the best approximation in the sense of least squares where a , b and c are constants to be defined.

$$z = a x + b y + c \quad (D-1)$$

That is, it is desired to define the constants a , b and c which minimize the expression

$$I = \sum_{j=1}^M \sum_{i=1}^N \left[z_{ij} - a x_j - b y_i - c \right]^2 \quad (D-2)$$

Holding x_j , y_i , z_{ij} , b , and c constant and taking the derivative of I with respect to a , yields

$$\frac{\partial I}{\partial a} = -2 \sum_{j=1}^M \sum_{i=1}^N \left[z_{ij} - a x_j - b y_i - c \right] x_j \quad (D-3)$$

Setting Equation D-3 = 0 to minimize I , cancelling constant terms and regrouping produces

$$a \sum_{j=1}^M \sum_{i=1}^N x_j^2 + b \sum_{j=1}^M \sum_{i=1}^N x_j y_i + c \sum_{j=1}^M \sum_{i=1}^N x_j = \sum_{j=1}^M \sum_{i=1}^N x_j z_{ij} \quad (D-4)$$

Similarly, the partial derivative with respect to b results in

$$a \sum_{j=1}^M \sum_{i=1}^N x_j y_i + b \sum_{j=1}^M \sum_{i=1}^N y_i^2 + c \sum_{j=1}^M \sum_{i=1}^N y_i = \sum_{j=1}^M \sum_{i=1}^N y_i z_{ij} \quad (D-5)$$

and with respect to c

$$a \sum_{j=1}^M \sum_{i=1}^N x_j + b \sum_{j=1}^M \sum_{i=1}^N y_i + \sum_{j=1}^M \sum_{i=1}^N c = \sum_{j=1}^M \sum_{i=1}^N z_{ij} \quad (D-6)$$

Equations D-4, D-5 and D-6 now constitute a set of three linear equations in the three unknowns a , b and c .

Solution of the simultaneous equations is simplified considerably by making the geometric center of the data matrix the origin of the coordinate system. When this is done,

$$\sum_{j=1}^M \sum_{i=1}^N x_j \text{ and } \sum_{j=1}^M \sum_{i=1}^N y_i$$

vanish and Equation D-6 reduces to

$$\sum_{j=1}^M \sum_{i=1}^N c = \sum_{j=1}^M \sum_{i=1}^N z_{ij} \quad (D-7)$$

Since c is independent of i and j , the left-hand term is simply $MN c$ and

$$c = \frac{1}{MN} \sum_{j=1}^M \sum_{i=1}^N z_{ij} \quad (D-8)$$

That is, c is the average elevation.

Furthermore, with the origin at the geometric center of the data,

$$\sum_{j=1}^M \sum_{i=1}^N x_j y_i$$

also vanishes.

Equations D-5 and D-6 reduce to

$$a \sum_{j=1}^M \sum_{i=1}^N x_j^2 = \sum_{j=1}^M \sum_{i=1}^N x_j z_{ij} \quad (D-9)$$

$$b \sum_{j=1}^M \sum_{i=1}^N y_i^2 = \sum_{j=1}^M \sum_{i=1}^N y_i z_{ij} \quad (D-10)$$

That is,

$$a = \frac{\sum_{j=1}^M \sum_{i=1}^N x_j z_{ij}}{\sum_{j=1}^M \sum_{i=1}^N x_j^2} = \frac{\sum_{j=1}^M \sum_{i=1}^N x_j z_{ij}}{N \sum_{i=1}^N x_j^2} \quad (D-11)$$

$$b = \frac{\sum_{j=1}^M \sum_{i=1}^N y_i z_{ij}}{\sum_{j=1}^M \sum_{i=1}^N y_i^2} = \frac{\sum_{j=1}^M \sum_{i=1}^N y_i z_{ij}}{M \sum_{i=1}^N y_i^2} \quad (D-12)$$

Note that if $M = N$,

$$\sum_{j=1}^M x_j^2 = \sum_{i=1}^N y_i^2$$

Now that the trend plane has been defined, subtracting it from the data matrix must be done. Thus

$$z'_{ij} = z_{ij} - (ax_j + by_i + c) \quad (D-13)$$

where z'_{ij} is the resultant data point. Essentially, the foregoing is the analysis utilized in the computer programs to remove any large-scale effects of trend planes in the data.

APPENDIX E

PEARSON'S METHOD OF CURVE FITTING
(Kendall, 1947; Elderton, 1927)

APPENDIX E

PEARSON'S METHOD OF CURVE FITTING
(Kendall, 1947; Elderton, 1927)

1. Determine the numerical values of the first four moments of the observed distribution.
2. Calculate the numerical values of β_1 , β_2 , κ and, hence, determine the type to which the distribution belongs.
3. Equate the observed moments to the moments of the appropriate distribution expressed in terms of its parameters.
4. Solve the resulting equations for those parameters whereupon the distribution is determined.

The moments μ_n are defined

$$\mu_n = \frac{1}{M} \sum_{i=1}^M (x_i - \bar{x})^n$$

where \bar{x} is the mean value. From the first four moments, β_1 and β_2 are calculated and are defined

$$\beta_1 = \frac{\mu_3^2}{\mu_2^3}$$

and

$$\beta_2 = \frac{\mu_4}{\mu_2^2}$$

Then, the type determining κ is

$$\kappa = \frac{\beta_1 (\beta_2 + 3)^2}{4(2\beta_2 - 3\beta_1 - 6) (4\beta_2 - 3\beta_1)}$$

Type I is indicated when $\kappa < 0$ and Type IV when $0 < \kappa < 1$.

Elderton (1927), has established already the formulas required by step 3. For Type I curves the formulas are

$$r = \frac{6(\beta_2 - \beta_1 - 1)}{6 + 3\beta_1 - 2\beta_2}$$

$$a_1 + a_2 = \frac{1}{2} \sqrt{\mu_2} \sqrt{\beta_1 (r+2)^2 + 16(r+1)}$$

$$m_{1,2} = \frac{1}{2} \left[r - 2 \pm r(r+2) \sqrt{\frac{\beta_1}{\beta_1 (r+2)^2 + 16(r+1)}} \right]$$

where m_2 is the positive root when μ_3 is positive and

$$y_o = \frac{N}{a_1 + a_2} \cdot \frac{m_1^{m_1} m_2^{m_2}}{(m_1 + m_2)^{m_1 + m_2}} \cdot \frac{\Gamma(m_1 + m_2 + 2)}{\Gamma(m_1 + 1) \Gamma(m_2 + 1)}$$

where N is the total frequency (in this problem, 841) and $\Gamma(x)$ is the standard gamma function. The origin is at the mode where

$$\text{Mode} = \bar{x} - \frac{1}{2} \cdot \frac{\mu_3}{\mu_2} \cdot \frac{r+2}{r-2}$$

For Type IV the formulas are

$$r = \frac{6(\beta_2 - \beta_1 - 1)}{2\beta_2 - 3\beta_1 - 6}$$

$$m = \frac{1}{2} (r + 2)$$

$$v = \frac{r(r-2) \sqrt{\beta_1}}{\sqrt{16(r-1) - \beta_1(r-2)^2}}$$

$$a = \sqrt{\frac{\mu_2}{16}} \sqrt{16 (r - 1) - \beta_1 (r - 2)^2}$$

$$y_o = \frac{N}{a F(r, v)}$$

Evaluation of $F(r, v)$ requires statistical tables, but if r is large

$$y_o \approx \frac{N}{a} \cdot \sqrt{\frac{r}{2\pi}} \cdot \frac{e\left(\frac{\cos^2 \phi}{3r} - \frac{1}{12r} - \phi v\right)}{(\cos \phi)^{r+1}}$$

where $\phi = \tan^{-1} \frac{r}{v}$. The origin of the curve is $\frac{va}{r}$ after the mean.

APPENDIX F

FINITE, EQUISPACED DATA

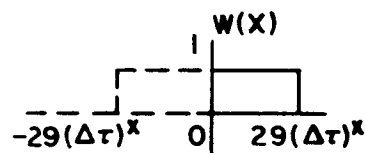
APPENDIX F

FINITE, EQUISPACED DATA

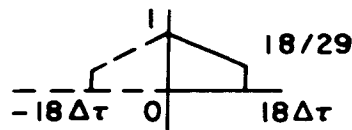
Let $P(f)$ be the power spectrum of interest and $P'(f)$ be the calculated power spectrum. This corresponds to a true autocorrelation function $C(\tau)$ and a calculated autocorrelation function $C'(n\Delta\tau)$. Thus,

$$C'(n\Delta\tau) = C(\tau) \cdot w(\tau) \cdot \sum_{\Delta\tau}^{\text{III}}$$

where $w(\tau)$ is the autocorrelation window. (In the data itself, the window is "boxcar" function, i. e.,



but the autocorrelation window is



because as lag increases, fewer pairs are available in the finite sample for the calculation of the autocorrelation function). The symbol for an infinite series of Dirac delta functions of unit amplitude with spacing $\Delta\tau$ is $\sum_{\Delta\tau}^{\text{III}}$.

From this follows

$$P'(f) = P(f) * W(f) * \sum_{1/\Delta\tau}^{\text{III}}$$

where $W(f)$ is the transform of $w(\tau)$, i. e.,

$$W(f) = 2(18 \Delta\tau) \frac{18}{29} \frac{\sin \left[\frac{2(18 \Delta\tau) \pi f}{2(18 \Delta\tau) \pi f} \right]}{\left[\frac{2(18 \Delta\tau) \pi f}{2(18 \Delta\tau) \pi f} \right]} + (18 \Delta\tau) \frac{11}{29} \frac{\sin \left[\frac{(18 \Delta\tau) \pi f}{(18 \Delta\tau) \pi f} \right]}{\left[\frac{(18 \Delta\tau) \pi f}{(18 \Delta\tau) \pi f} \right]}$$

The function $W(f) * \sum_{\Delta\tau} \frac{1}{\Delta\tau}$ is presented in Figure F-1. $P'(f)$ for each of the four areas is given in Figures F-2 through F-5.

The window $w(\tau)$ is the result of the finite width ($18 \Delta\tau$) of the autocorrelation function. It, in turn, is the result of the finite width of the data matrix ($29 \Delta\tau$) available.

The comb function $\sum_{\Delta\tau} \frac{1}{\Delta\tau}$ is the result of the equispaced sampling of the data; i. e., the data is not continuous. Its detrimental effect is aliasing or folding back energy at frequencies above the Nyquist frequency into the lower frequencies. Consequently, Figures F-2 through F-5 probably do not represent good estimates of the power spectra since appreciable energy at frequencies above the Nyquist frequency is believed present. Aliasing causes the power spectrum curve to repeat itself beyond the folding frequency; hence, continuation beyond this point is of no value.

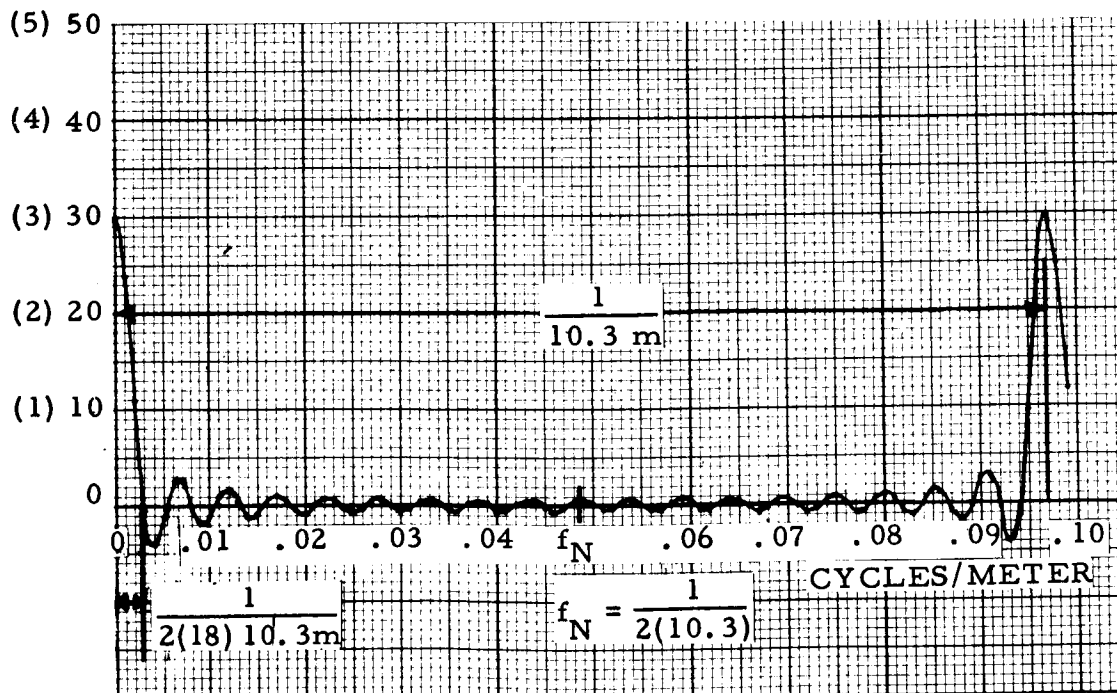


Figure F-1. Power Spectra of Window Containing Sampling and Aliasing Effects

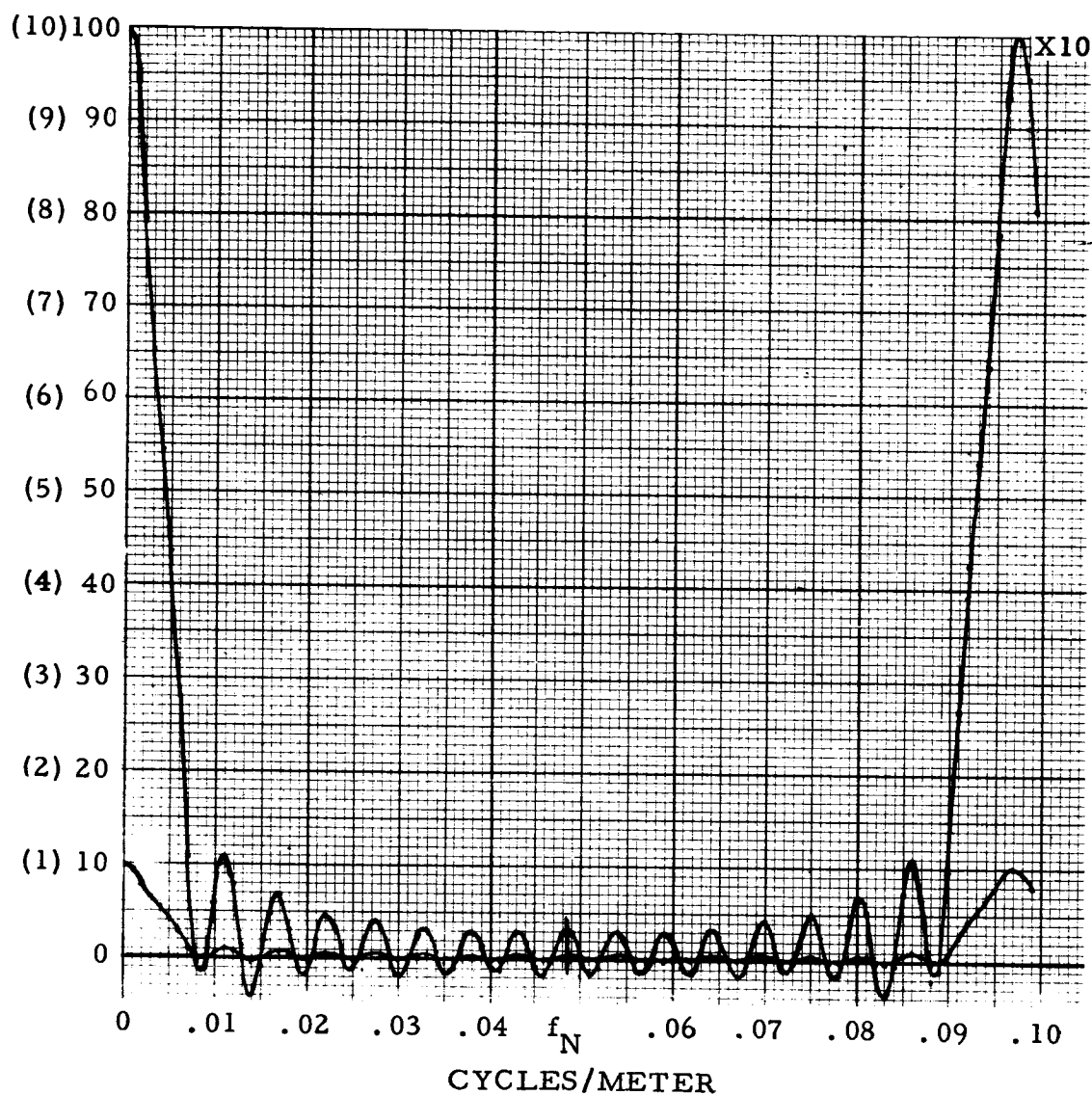


Figure F-2. Power Spectra Prior to Removal of Sampling and Aliasing Effects (Area D)

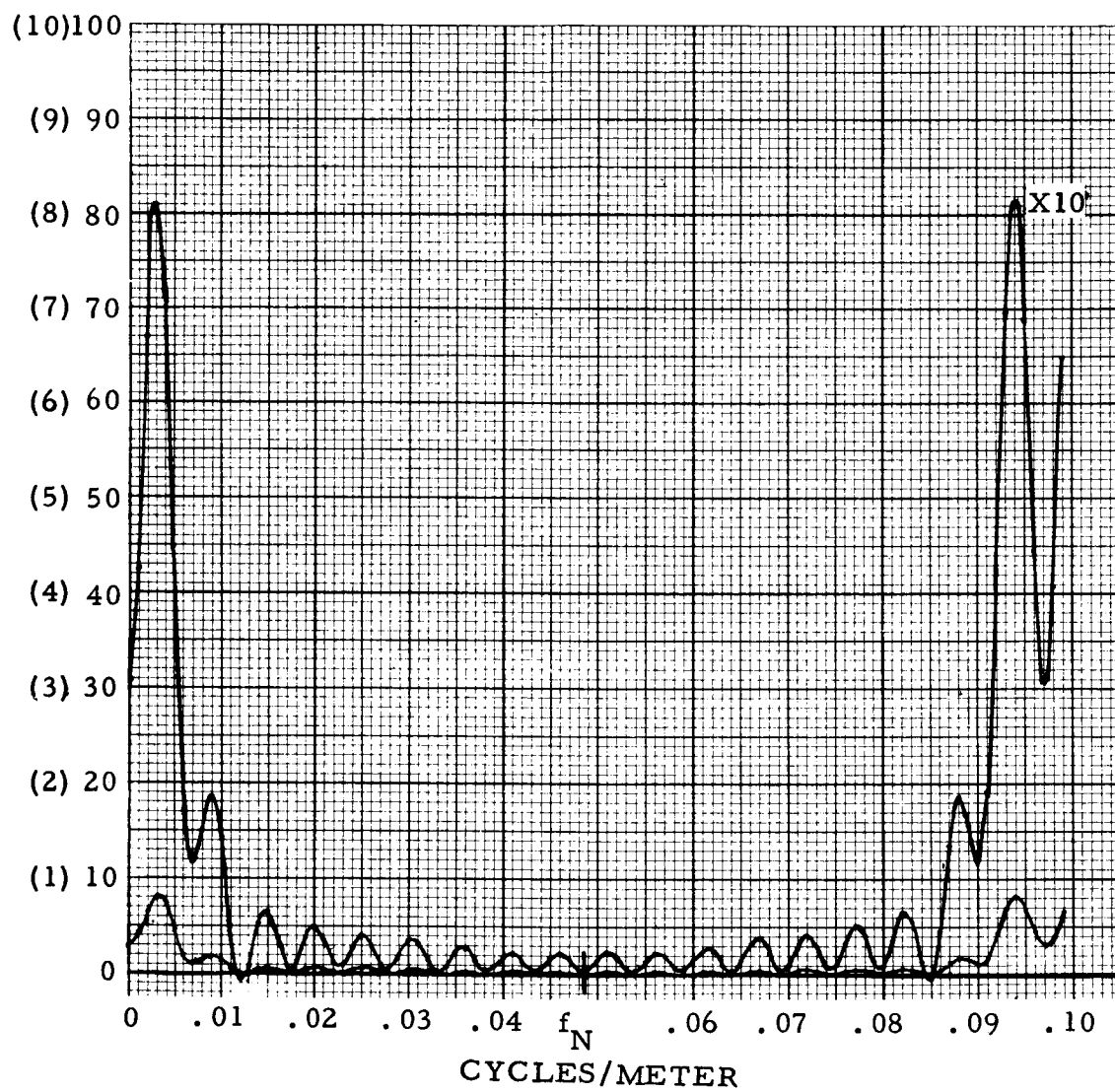


Figure F-3. Power Spectra Prior to Removal of Sampling and Aliasing Effects (Area B)

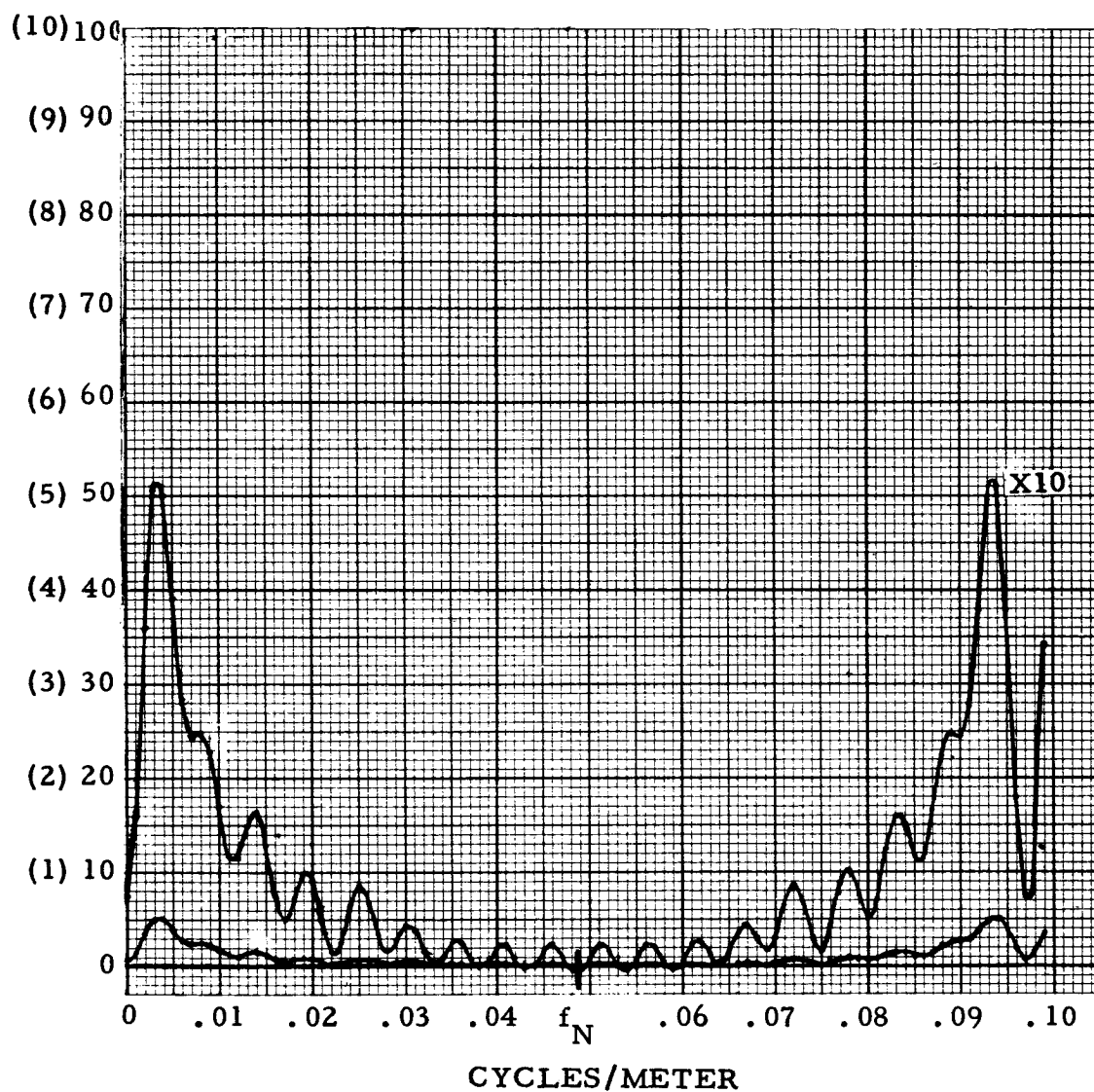


Figure F-4. Power Spectra Prior to Removal of Sampling and Aliasing Effects (Area A)

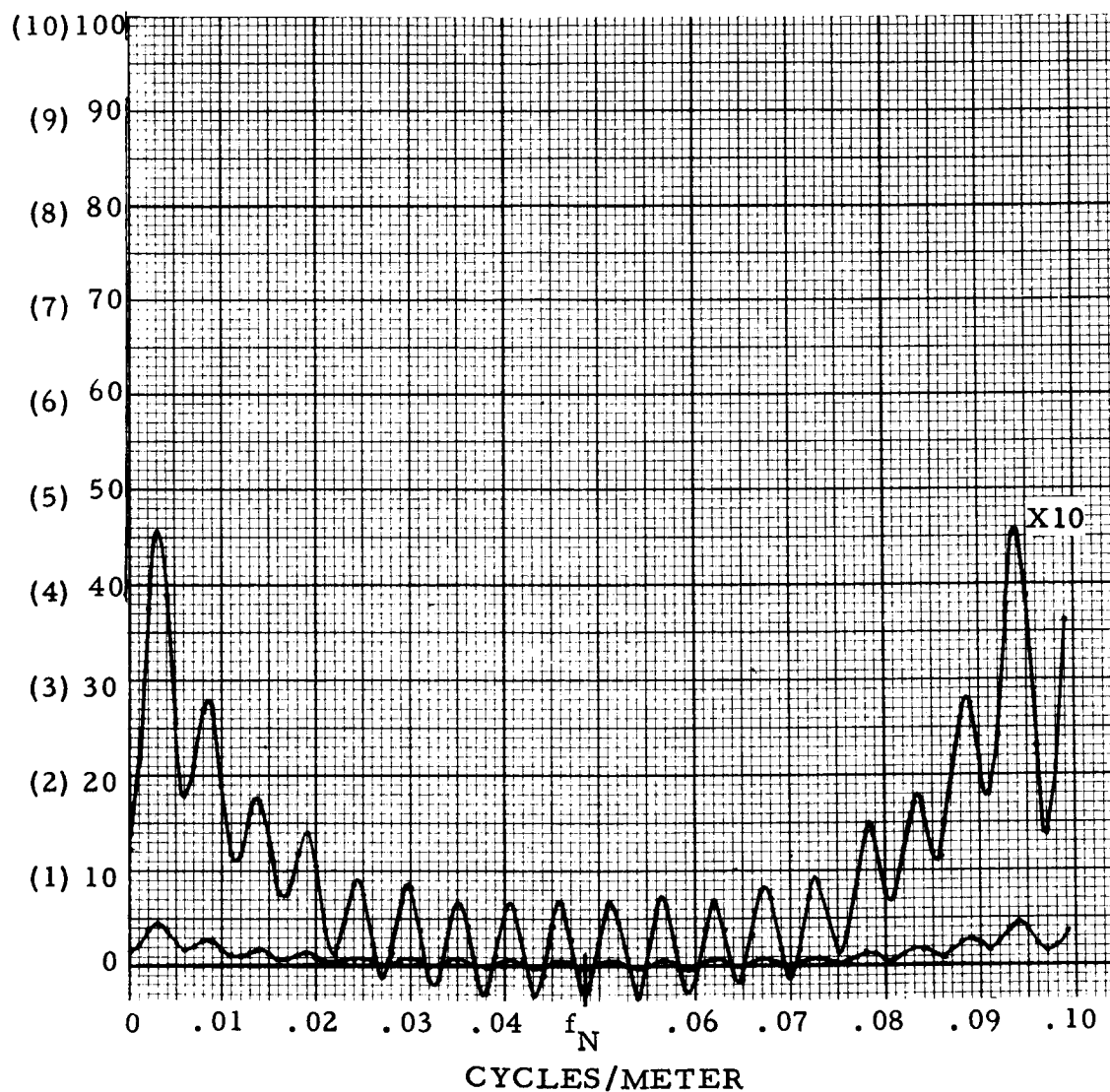
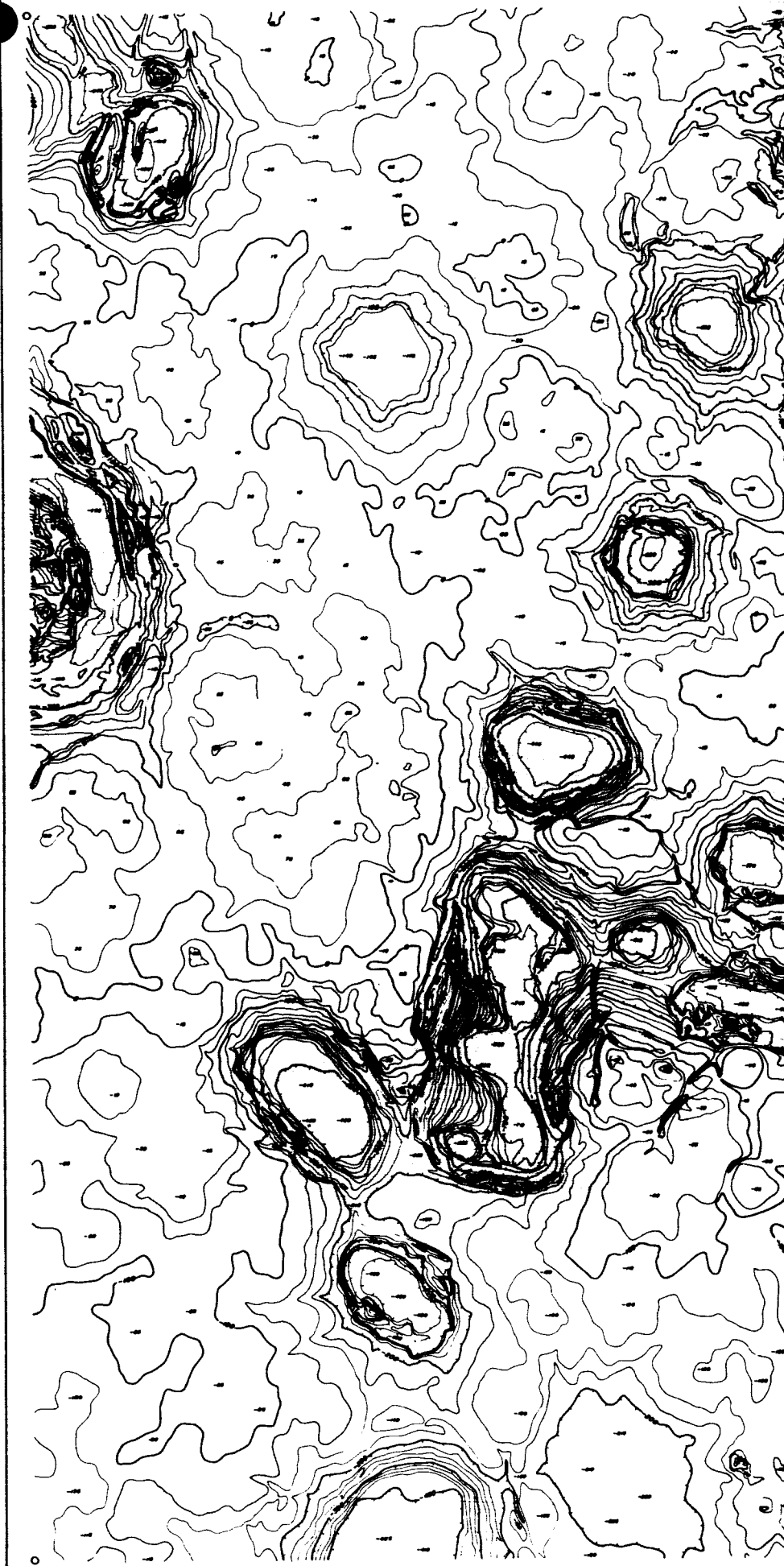


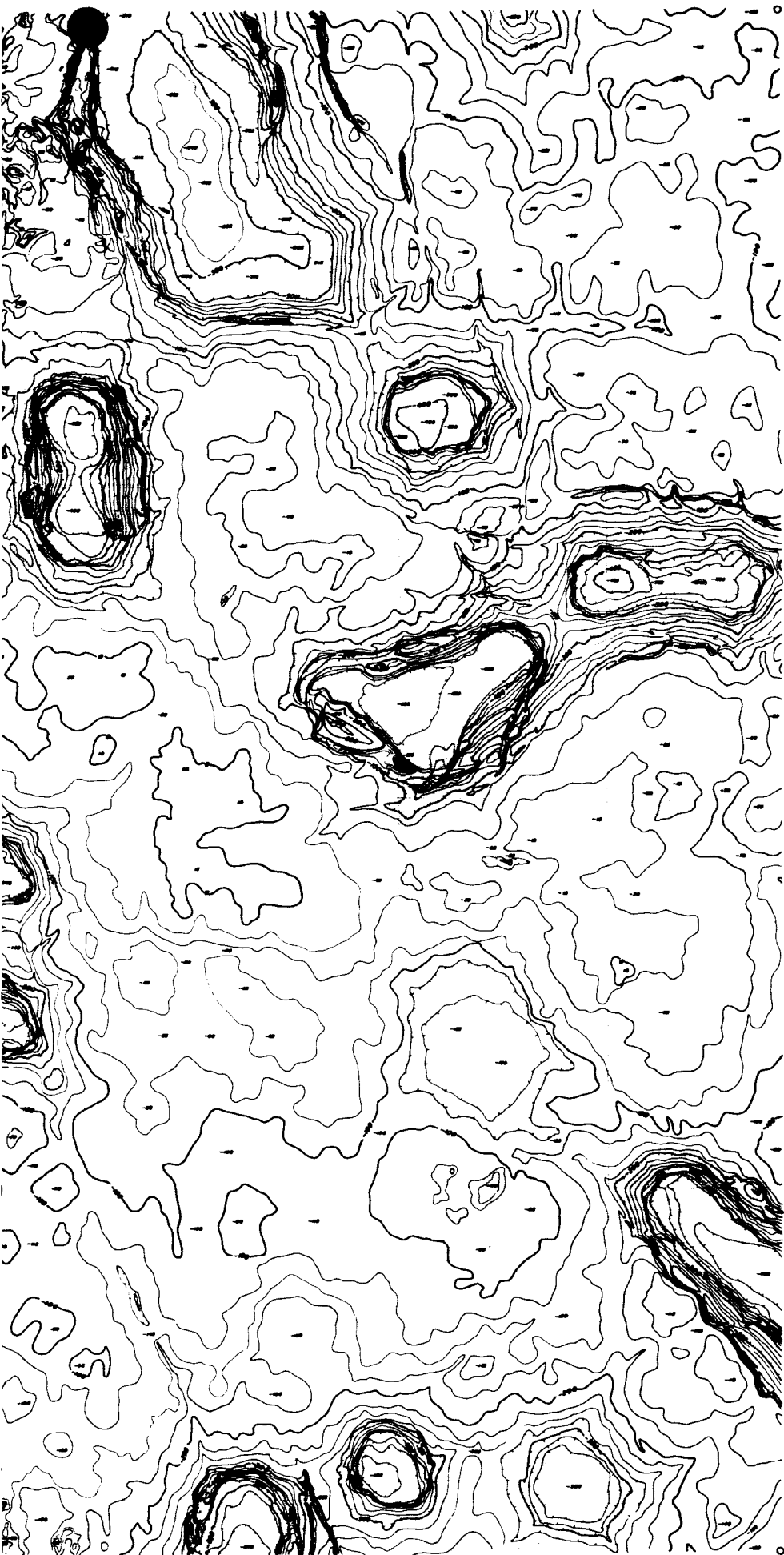
Figure F-5. Power Spectra Prior to Removal of Sampling and Aliasing Effects (Area C)

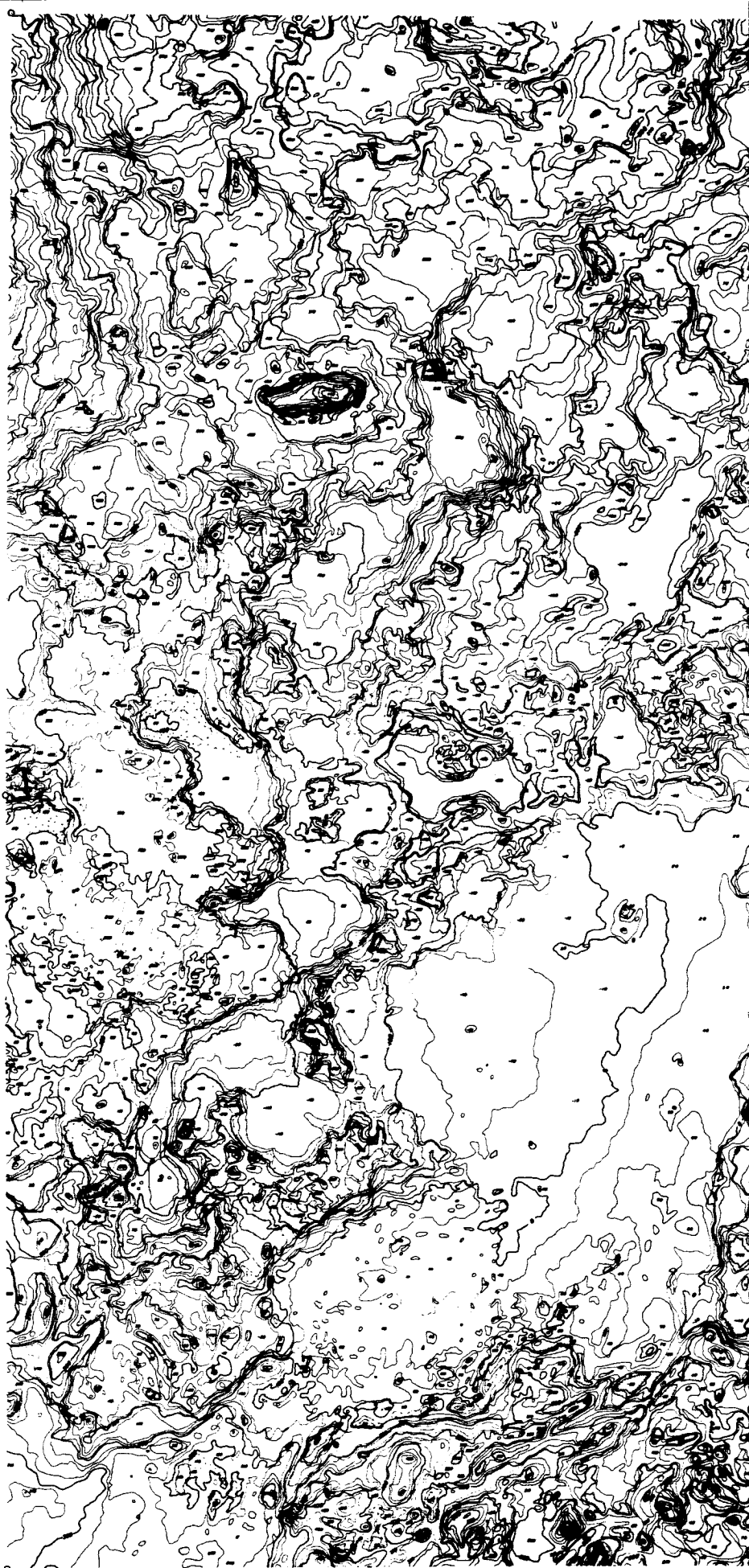


TOPOGRAPHY COMPILED BY PHOTOGRAMMETRIC SERVICE (REDACTED) - ELEVATION DATA FROM 1:62,500

NORTH AMERICAN
SPACE AND DEFENSE
DOWN
PISGAH
SCALE 1" = 1 MI

A ①





TOPOGRAPHY COMPILED BY PHOTOGRAPHIC FROM AIRCRAFT - USED SERVICE ENGINEER'S REPORT - SALT LAKE CITY, UTAH - 1-25-1964

BT

NORTH AME
SPACE AND INFO
DOWN
PISGAH

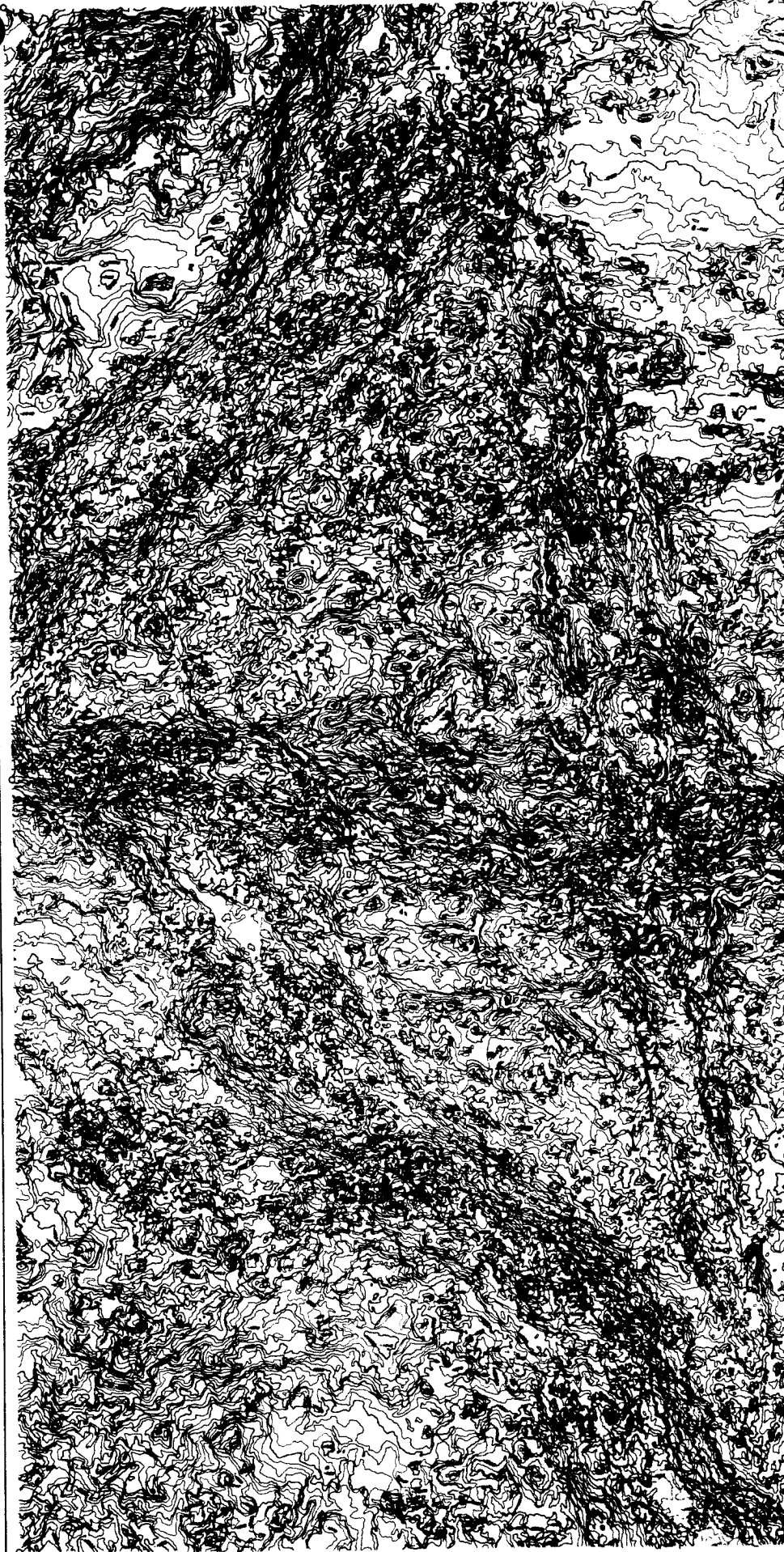
SCALE 1" = 30'



B (2)



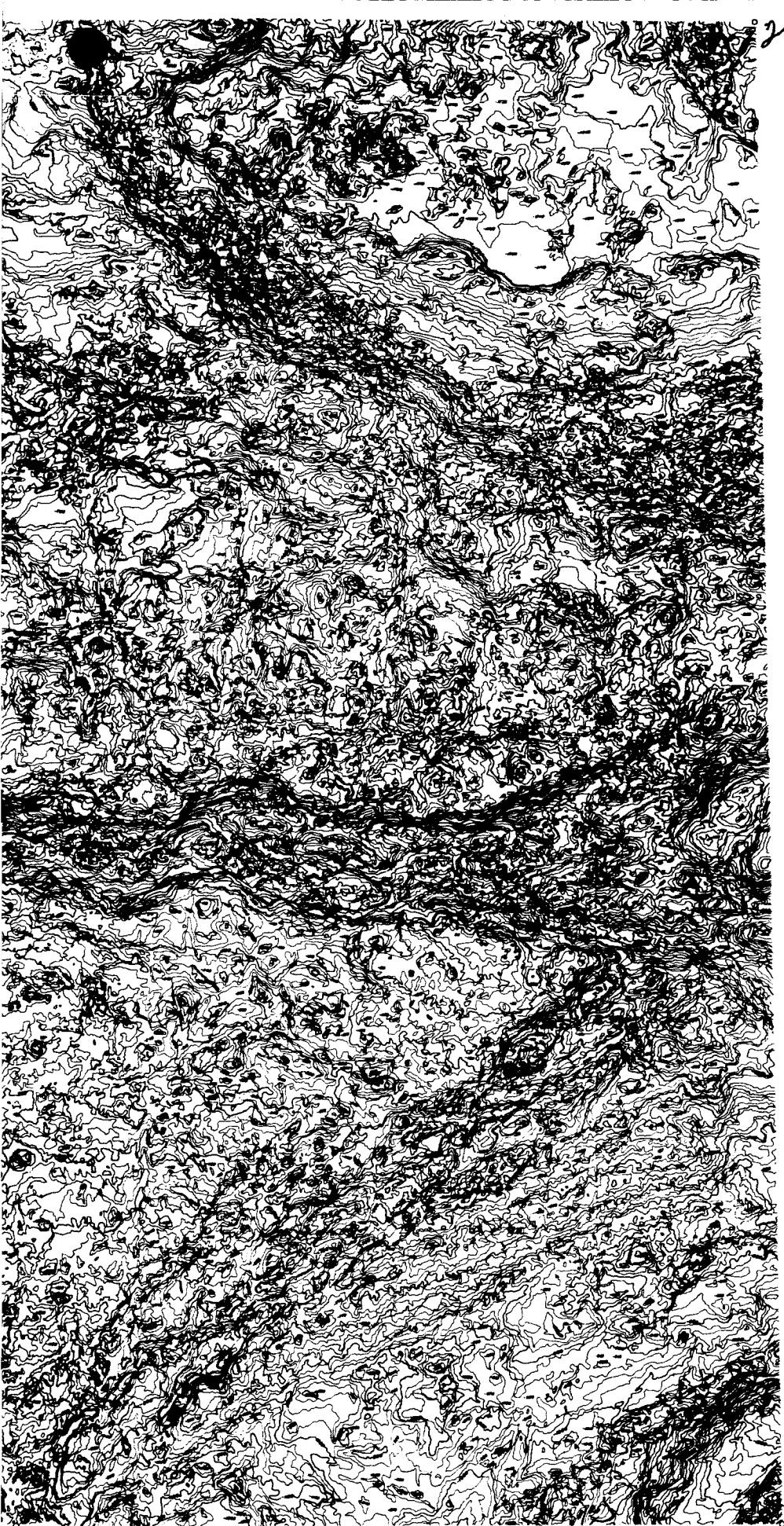
CO



TOPOGRAPHY COMPILED BY PHOTOGRAMMETRIC METHODS - AERO SERVICE CORPORATION (WESTERN) - SALT LAKE CITY, UTAH - 1-48 - 1951

0 1

NORTH AMERICAN
SPACE AND INFORMATION
CORPORATION
PISGAH
SCALE 1" = 50'



AN AVIATION, INC.
ION SYSTEMS DIVISION
CALIFORNIA

RATER AREA

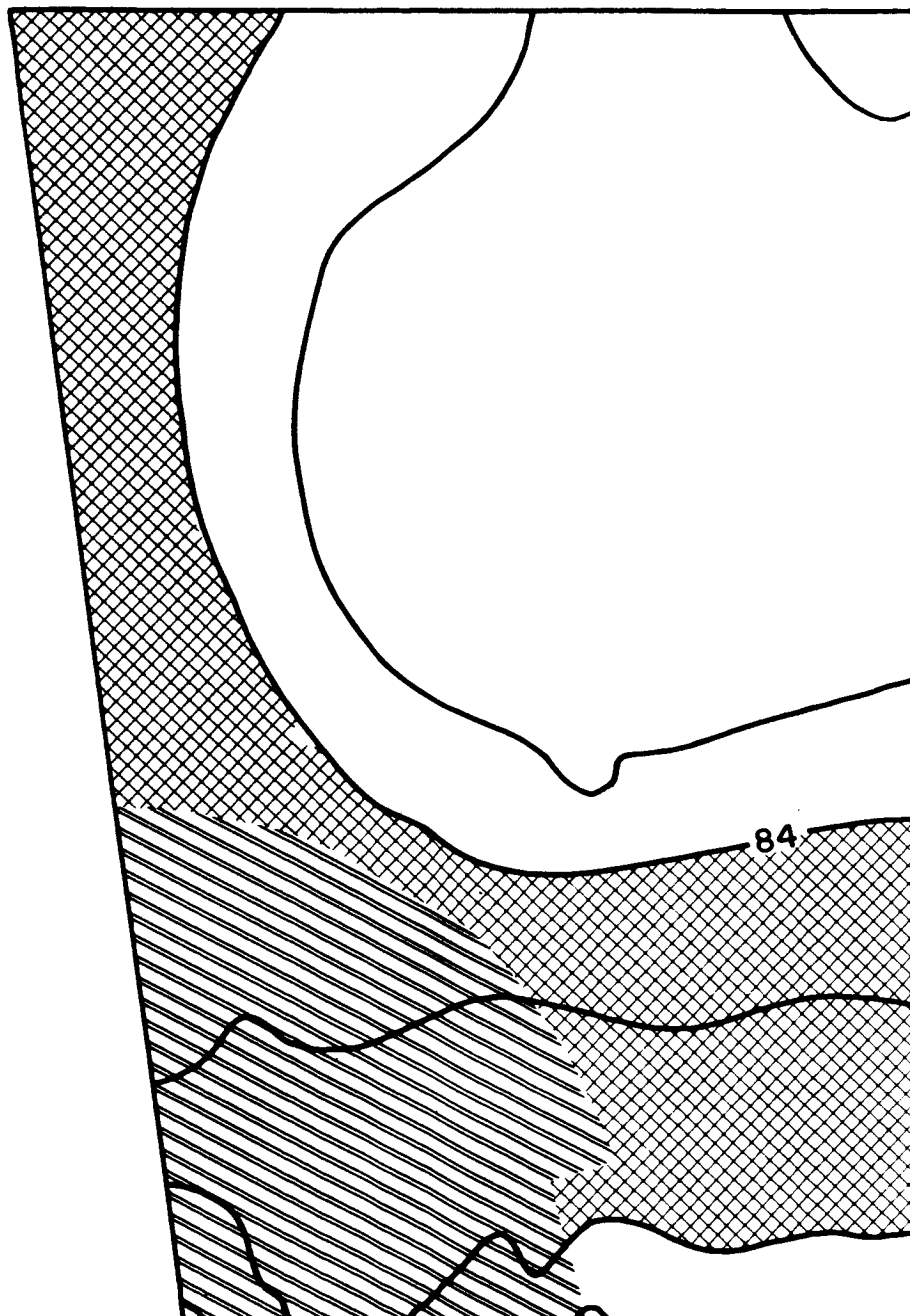
CONTOUR INTERVAL 25 CM

PLATE III AREA-D

2

RECONTOURED AT 0.42 CM
PREPARED BY THE U. S. GEOLOGICAL SURVEY
WITH THE NATIONAL AERONAUTICS AND SPACE ADMINISTRATION

PLATE V
1 of 6

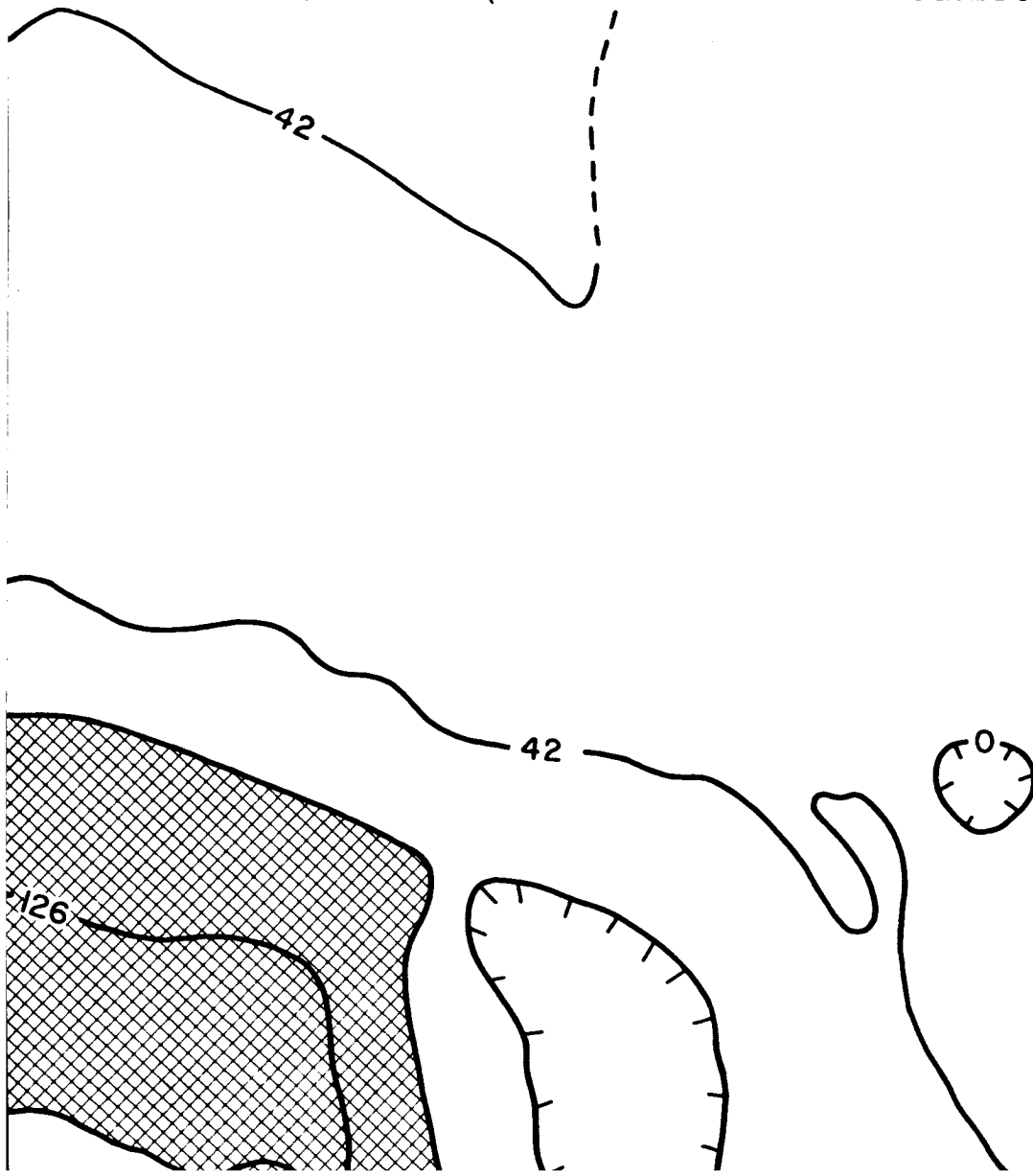


FROM A MAP
SURVEY IN COOPERATION
SPACE ADMINISTRATION

2 of 6

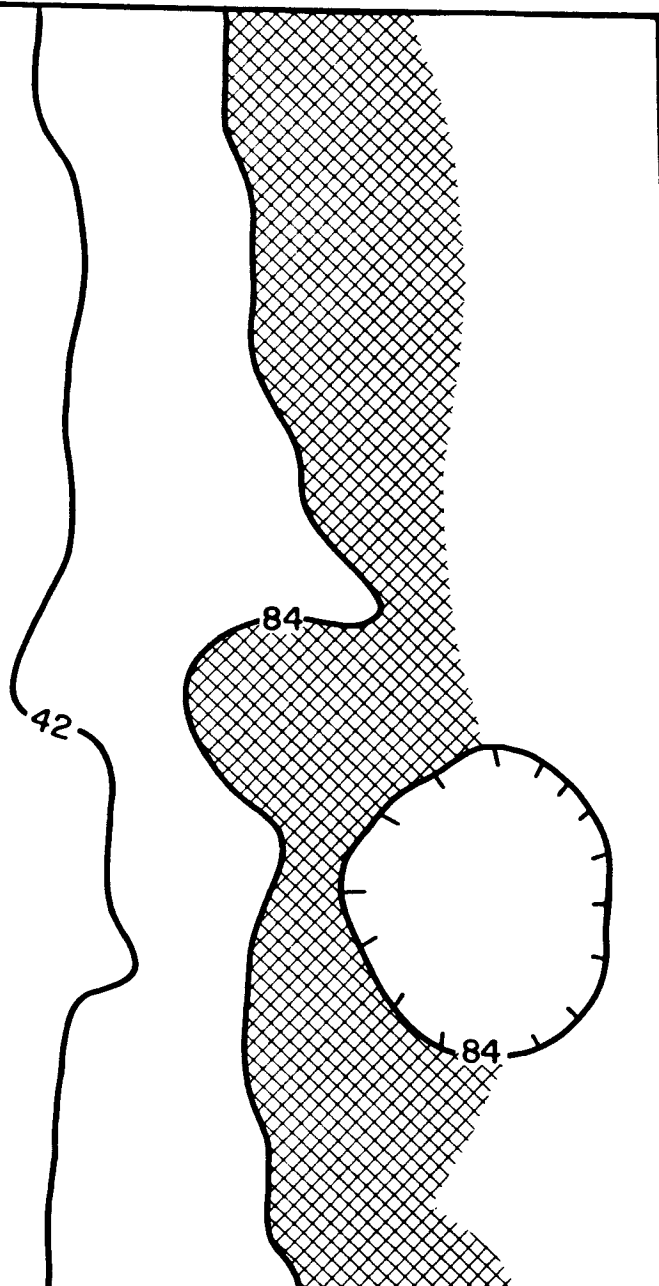
MOON'

- LUNAR MAP (SMALL AREA IN MARE COGNITUM)



TOPOGRAPHIC MAP
OF A SMALL AREA OF THE
S SURFACE IN MARE COGNITUM

3 of 6



4066

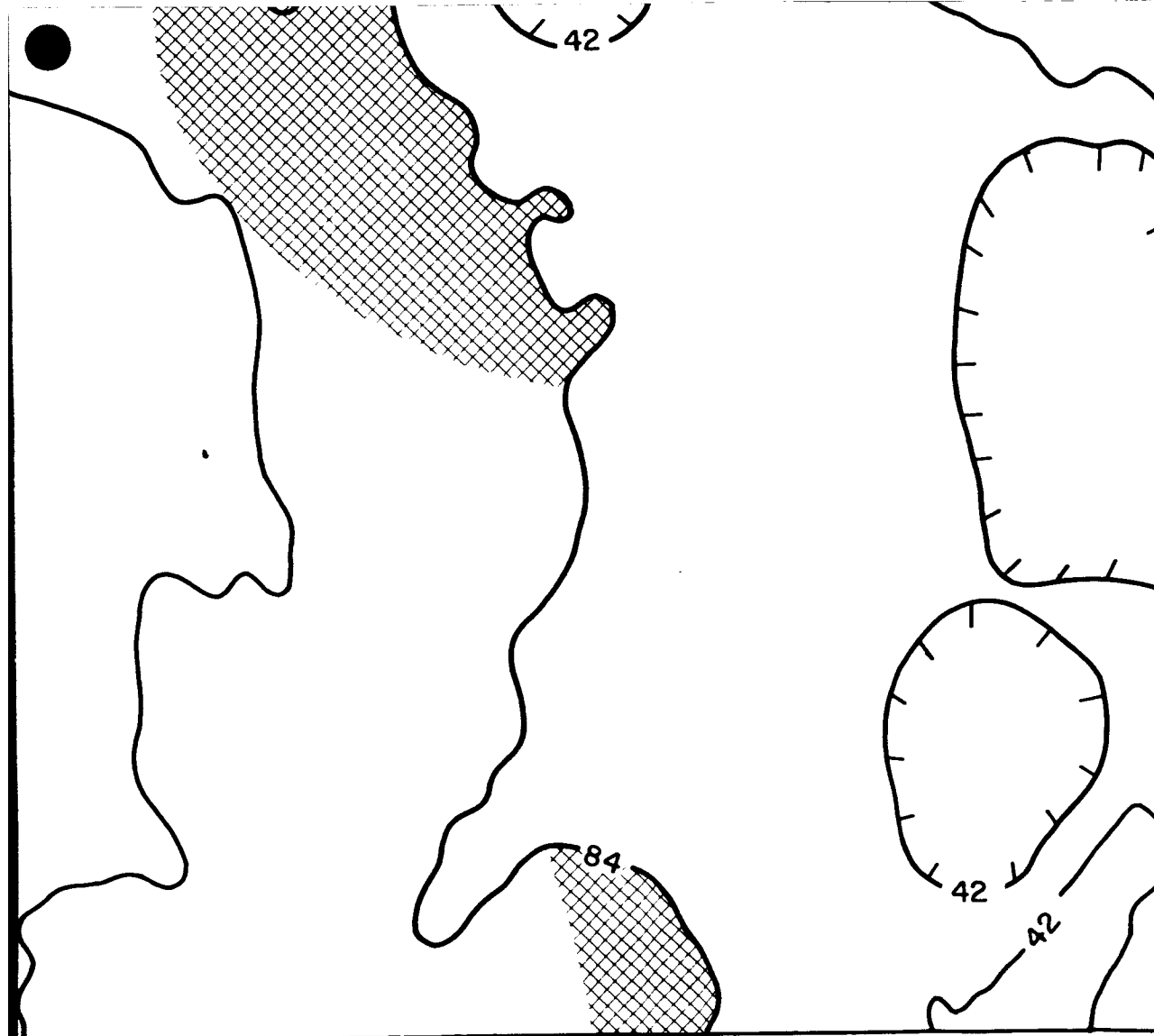
210

168

84

z

1 0



CONTOUR INTERVAL 10 CENTIMETERS

SCALE 1:80

1 2 3 4 5 6 7 8 9 10 METERS

50/6

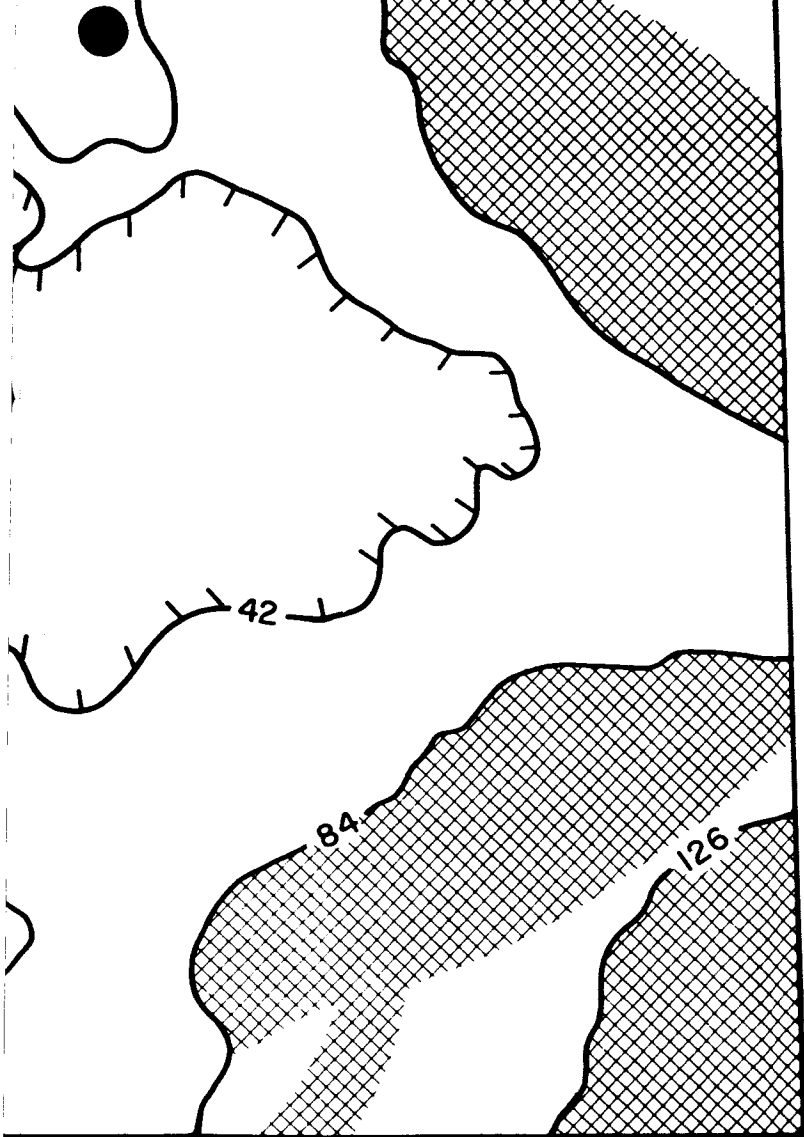


PLATE V

TIPPING AREAS



UNCERTAIN AREAS



APPROXIMATE LOCATION

• 41° West Longitude 10° 35' South Latitude

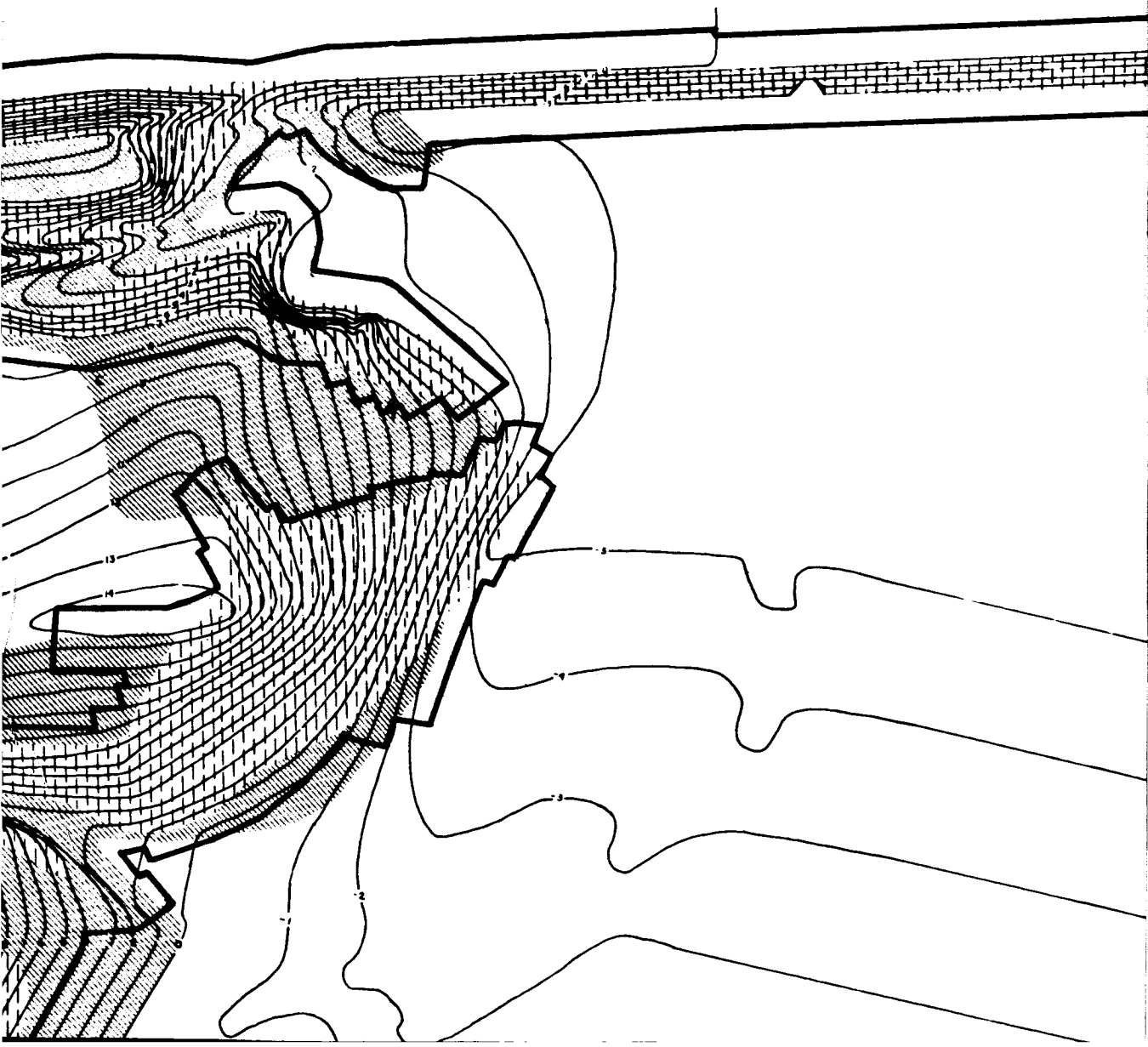
{ Areas designated with
respect to possible
positions of LEM landing
gear circle center }

60/6

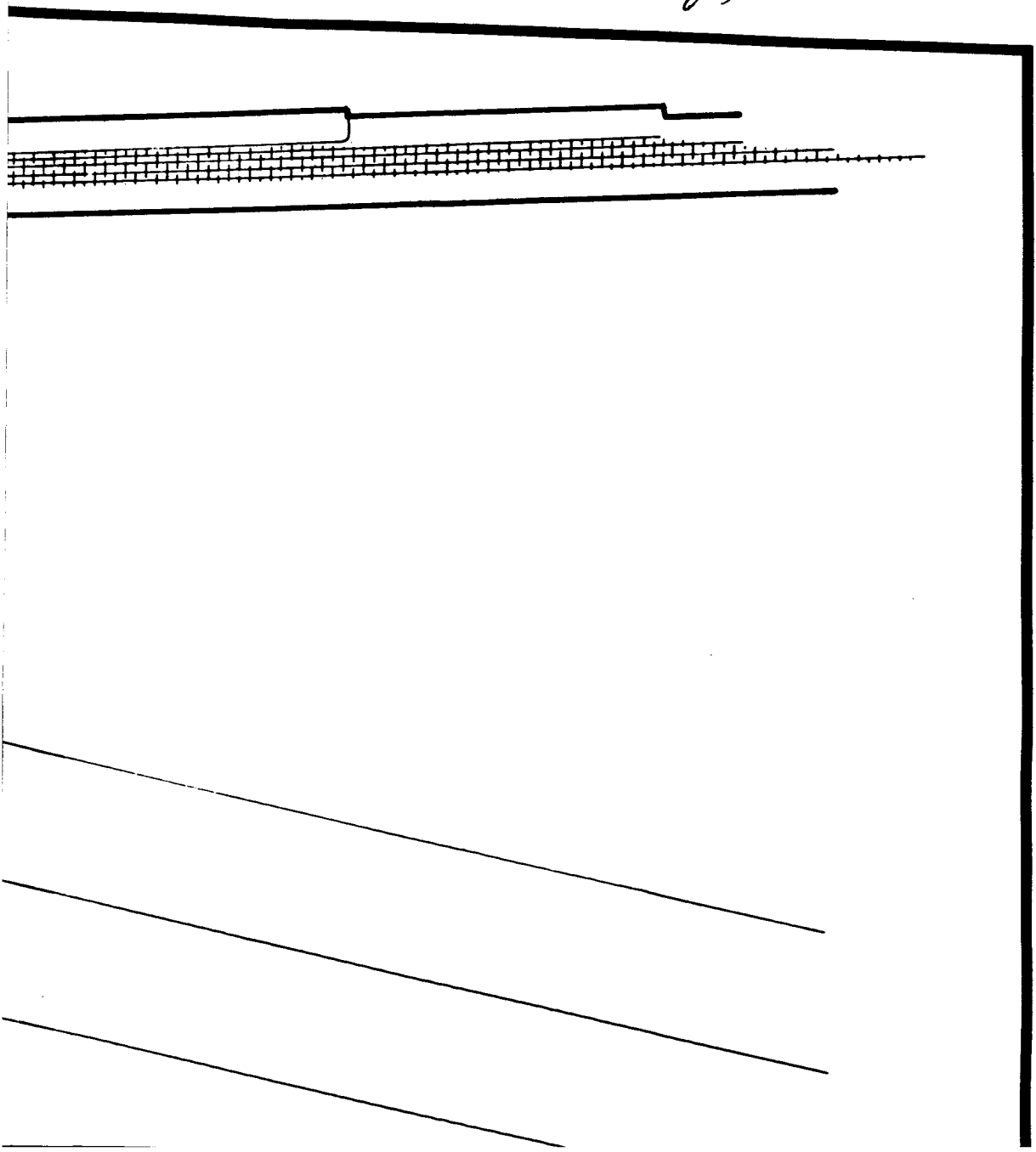
PLATE
VI

1069

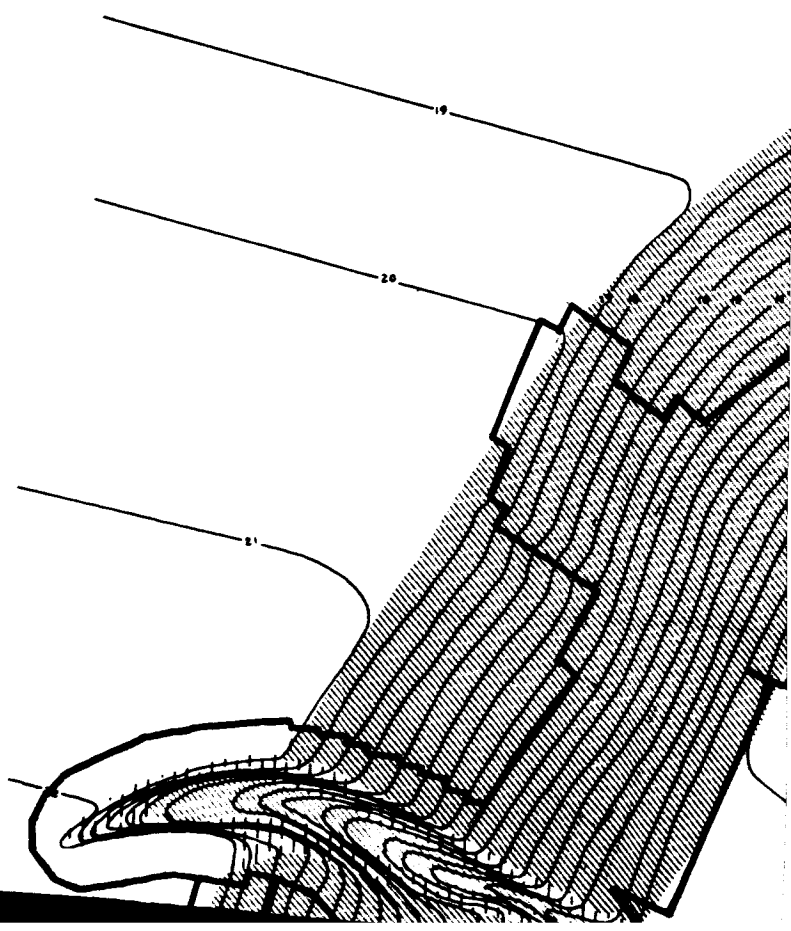
2069



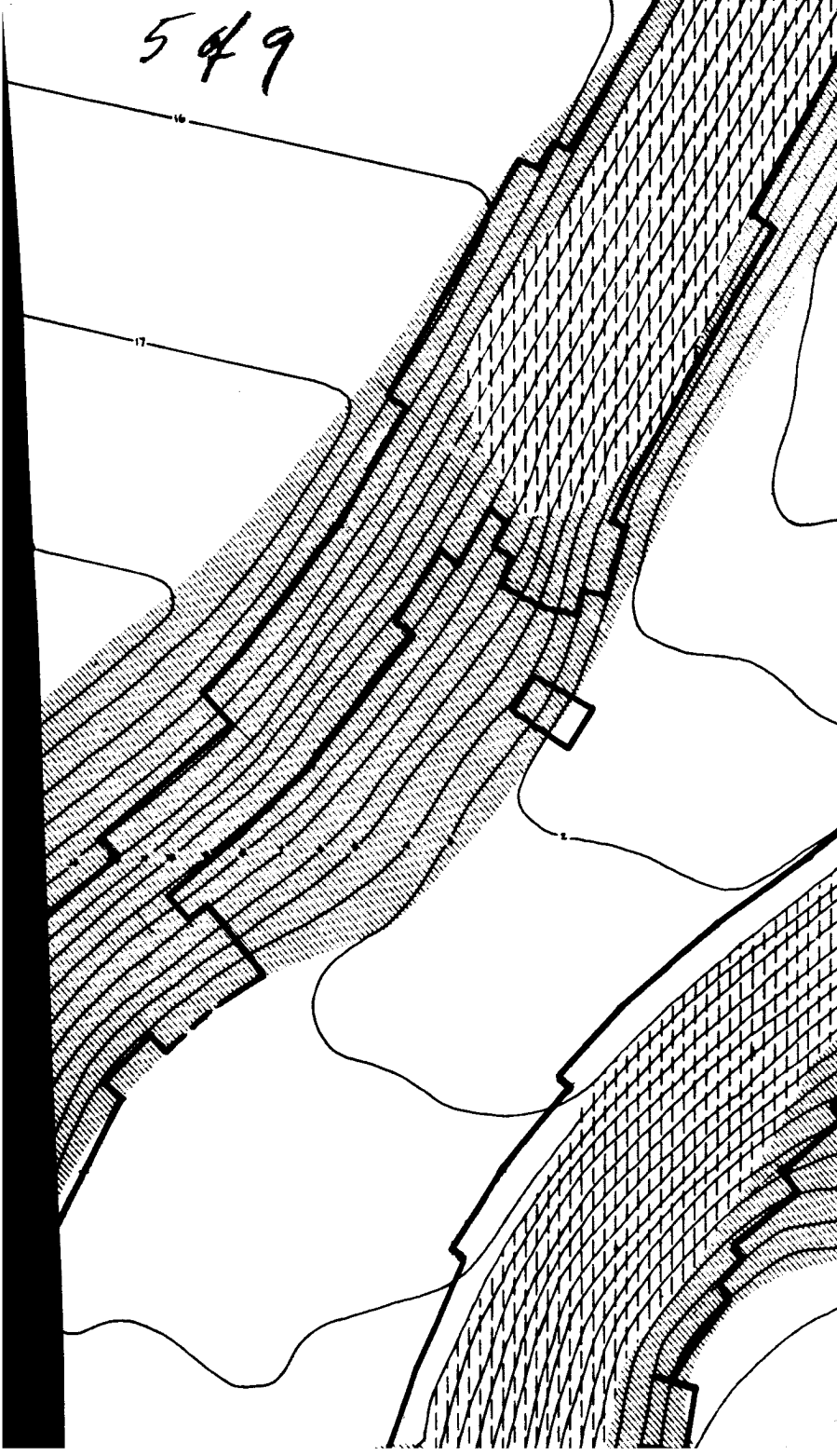
3089



4049



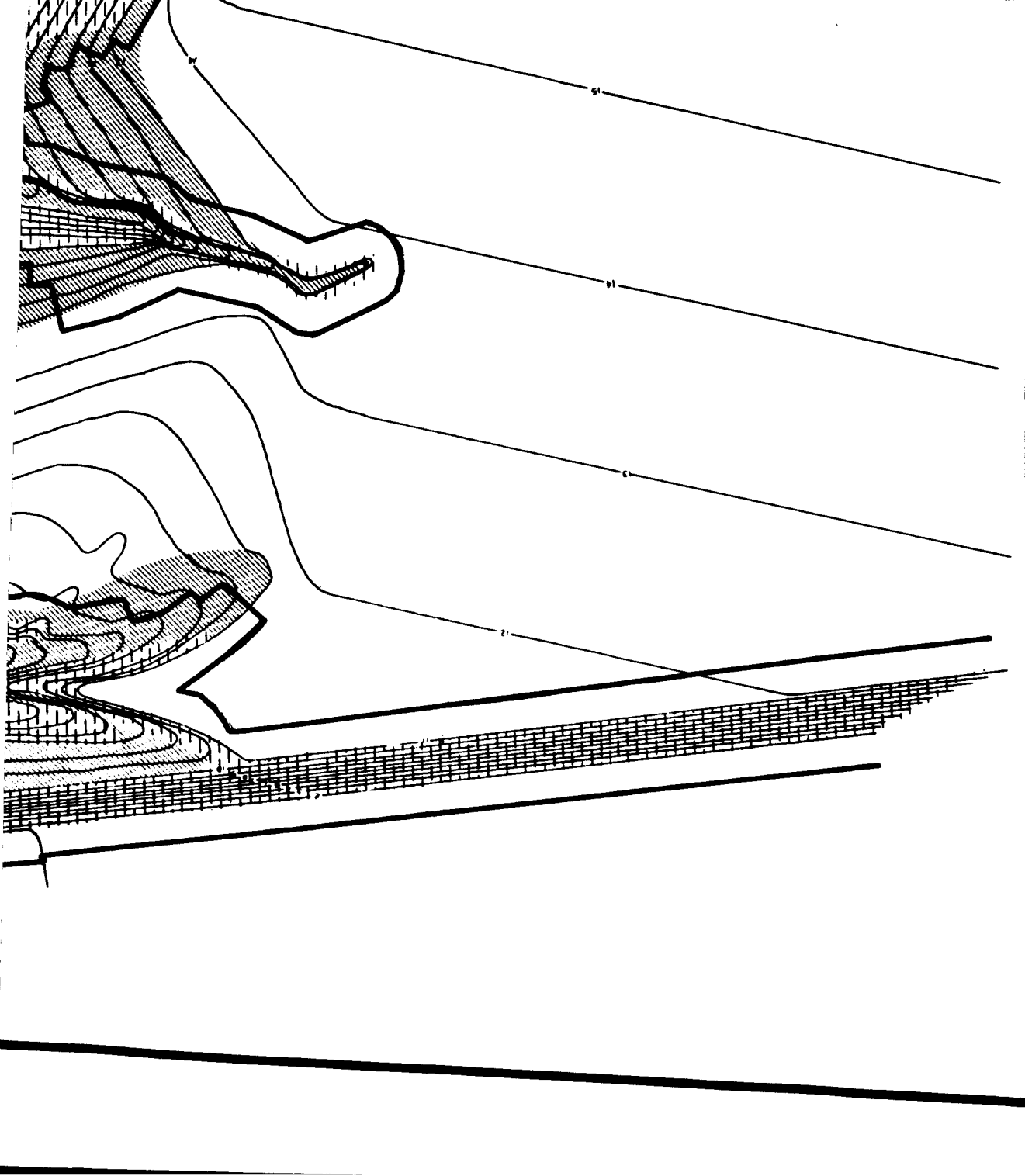
549

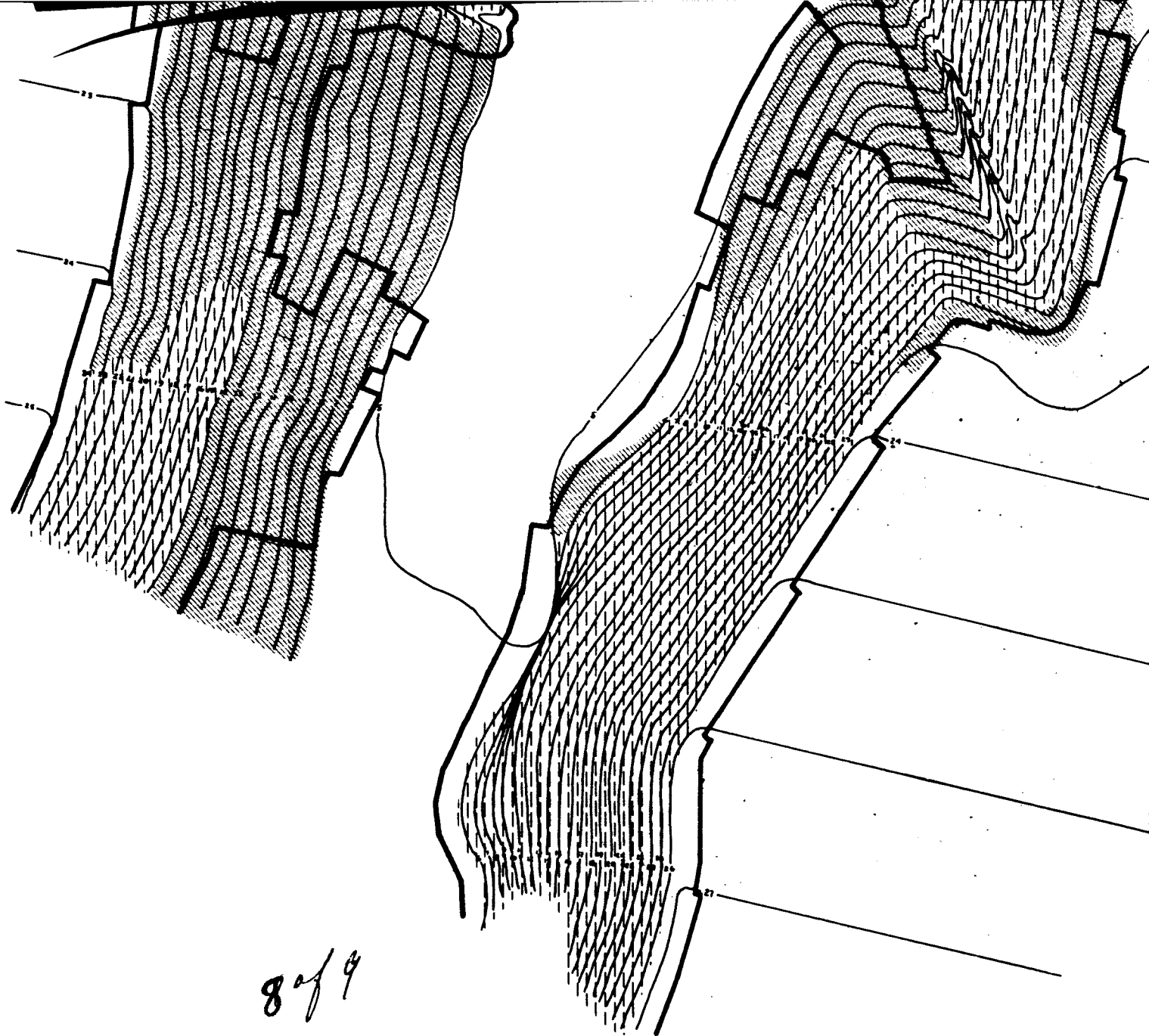


6009

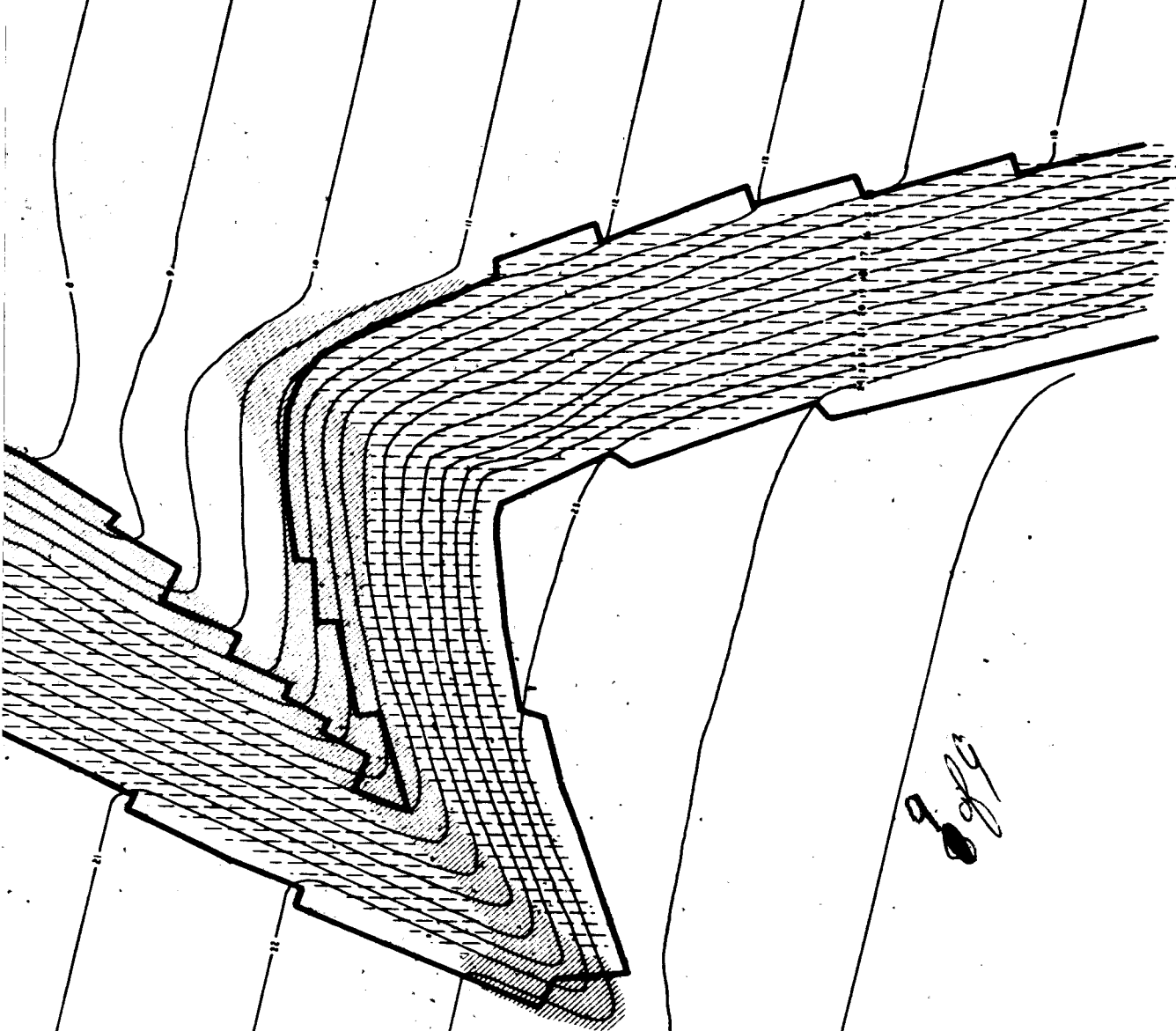


7089





8 of 9




9884

PLATE VI

SLOPE DISTRIBUTION MAP

CLASS I: SLOPES $< 6^\circ$ 

CLASS II: SLOPES $6-12^\circ$ 

CLASS III: SLOPES $> 12^\circ$ 

UNSAFE LANDING AREAS 

TOPOGRAPHIC MAP OF A PORTION OF THE
NEENACH RANCH

SCALE 1:1330

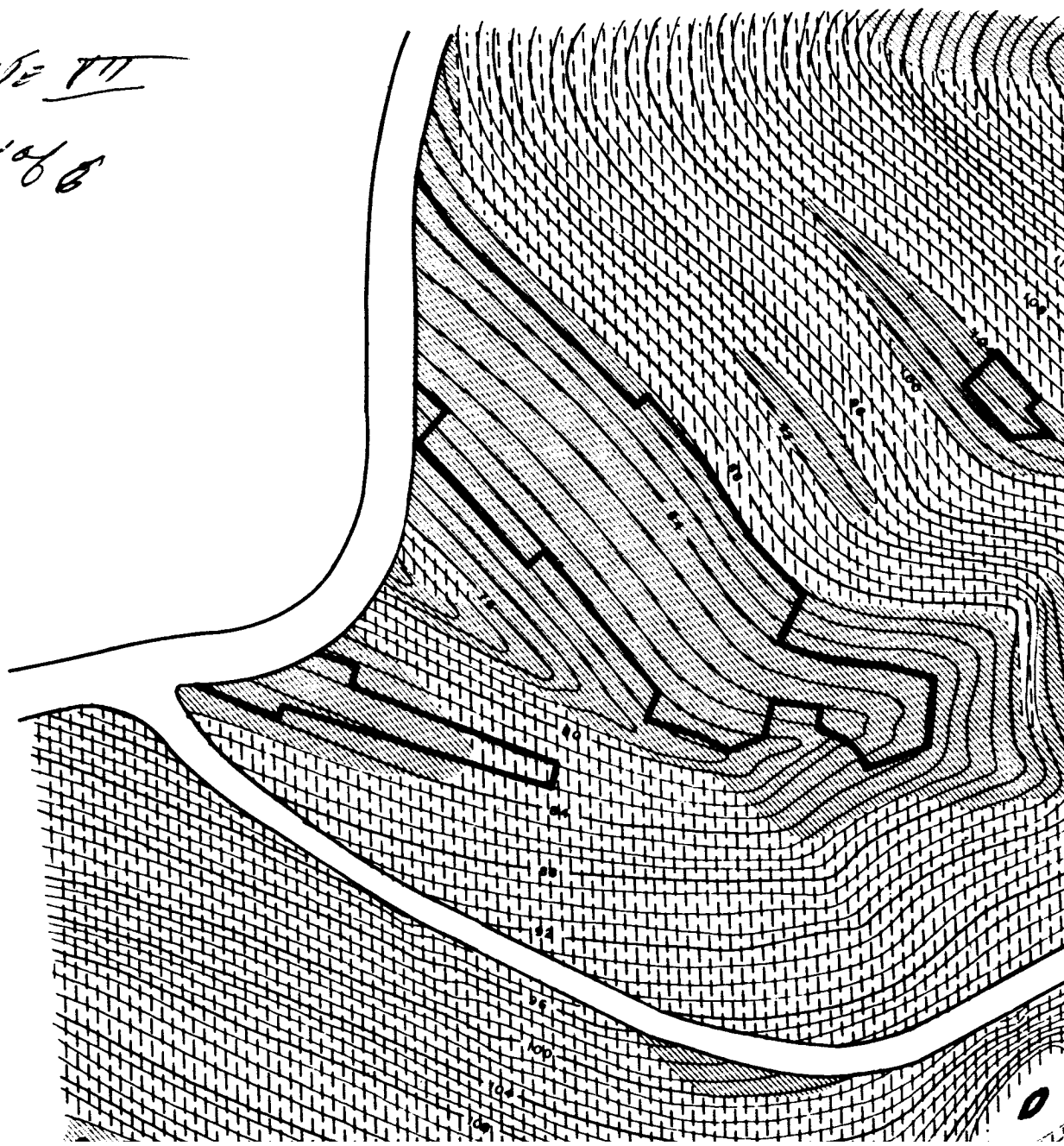
(1" = 80')

CONTOUR INTERVAL = 0.625 m.
(2.74 feet)

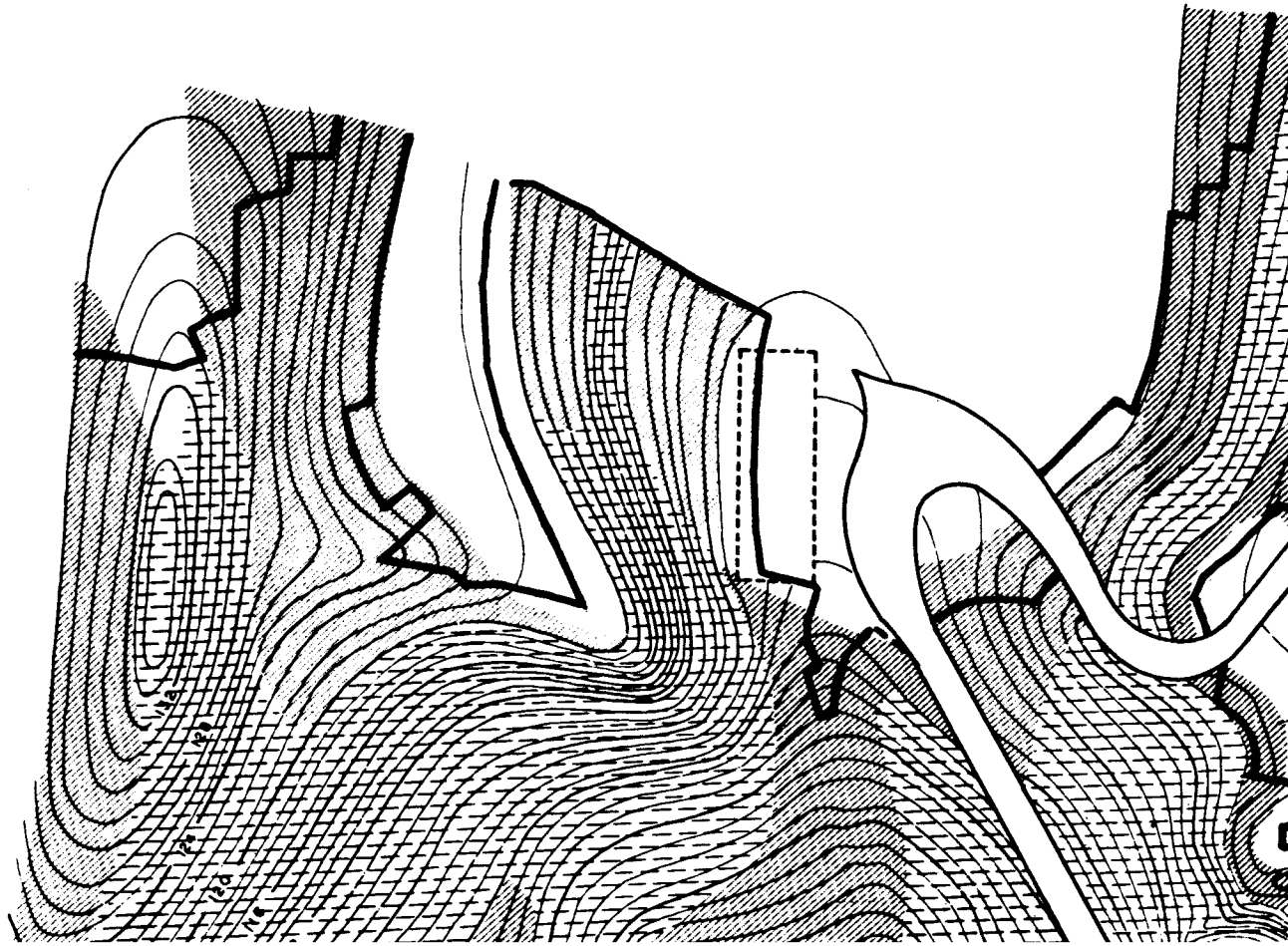
10/10

PLATE VII

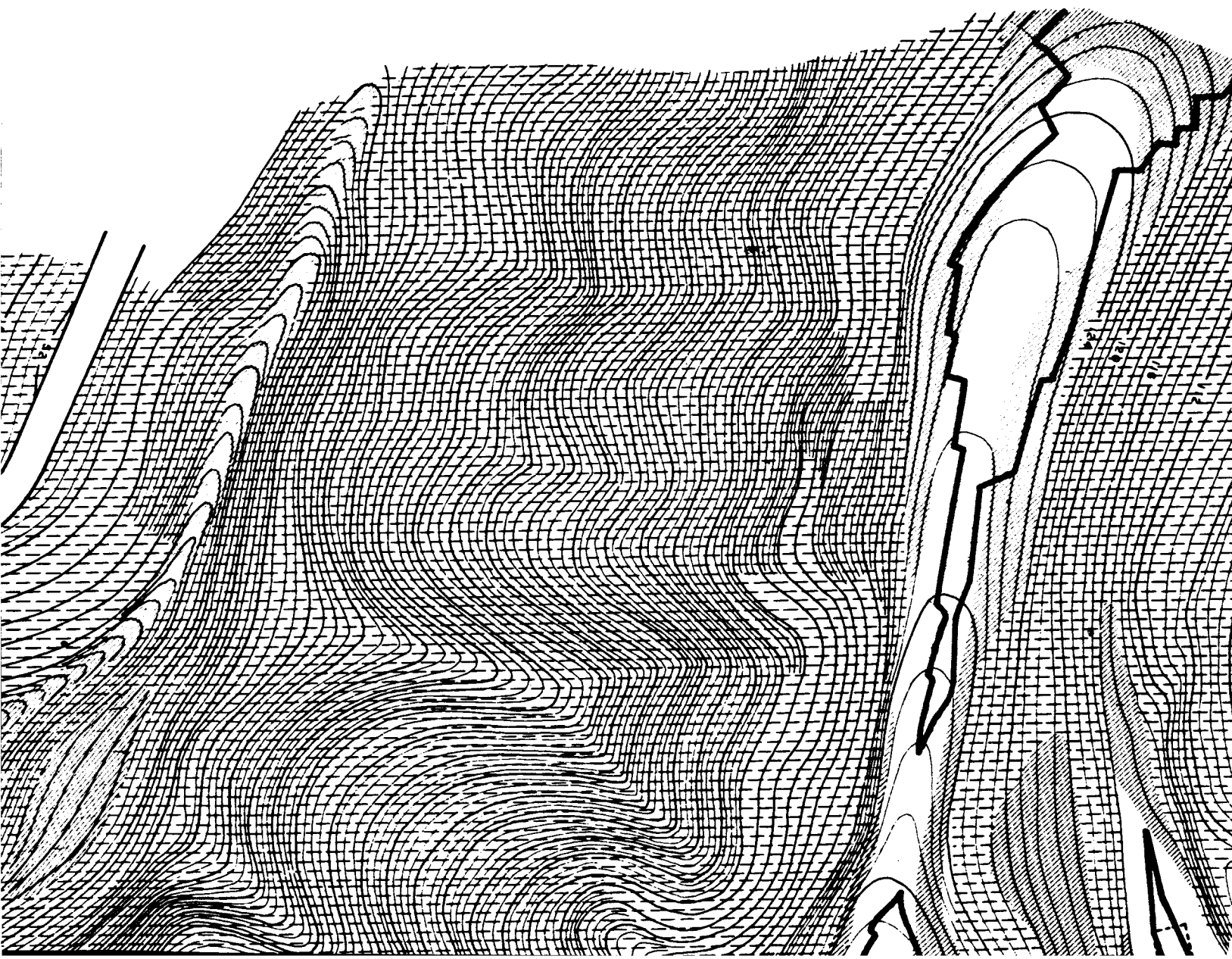
1068



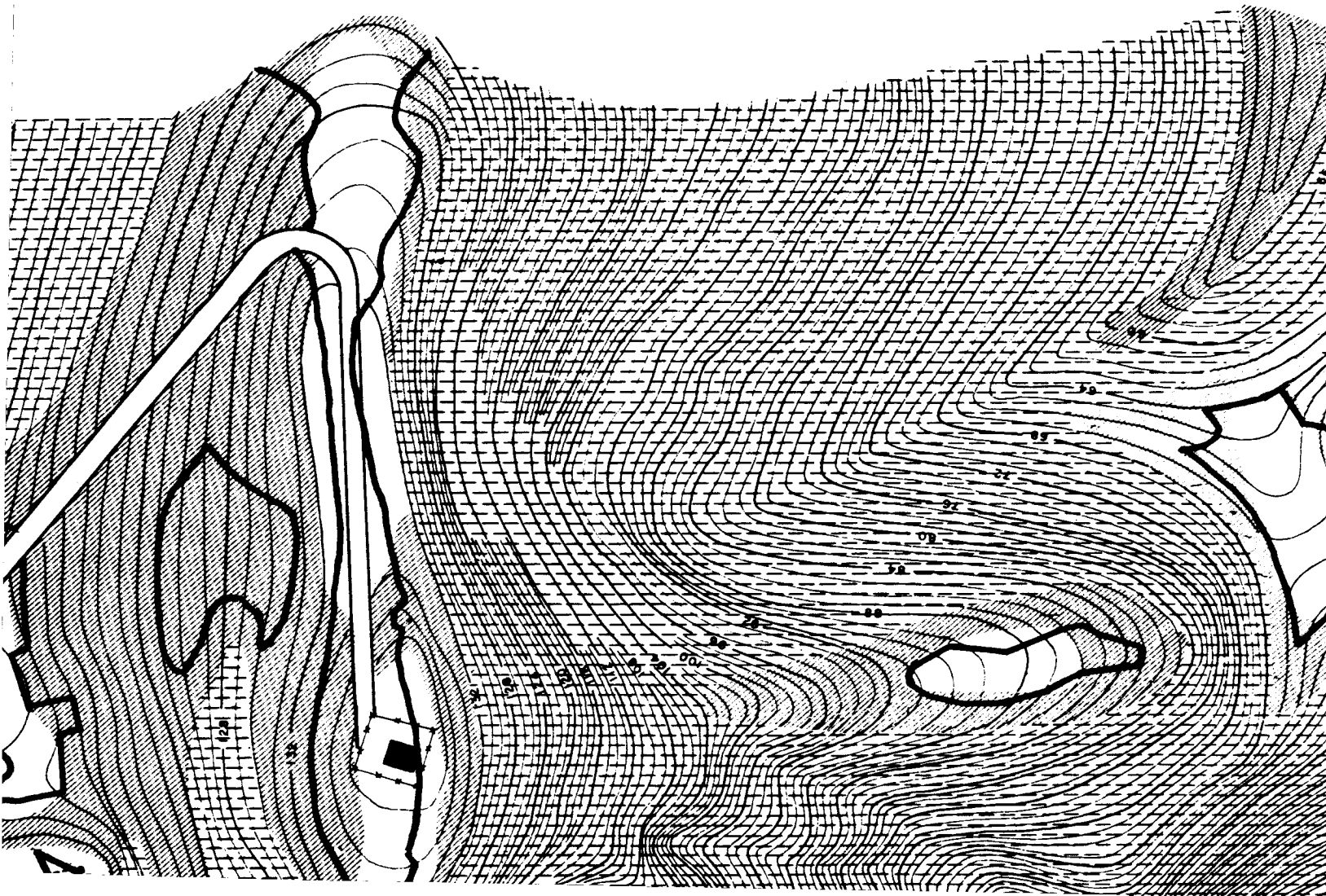
2 of 6



8076



4066



5
Topo

TOPOGRAPHIC MAP
OF
COVINA KNOLLS AREA
L.A. COUNTY, CALIFORNIA

CONTOUR INTERVAL 2.5 FT.



SCALE 1: 1330

CLASS I: SLOPES $< 6^\circ$
 CLASS II: SLOPES $6-12^\circ$
 CLASS III: SLOPES $> 12^\circ$
 SAFE LANDING AREAS

SLOPE DISTRIBUTION MAP

PLATE VII

692

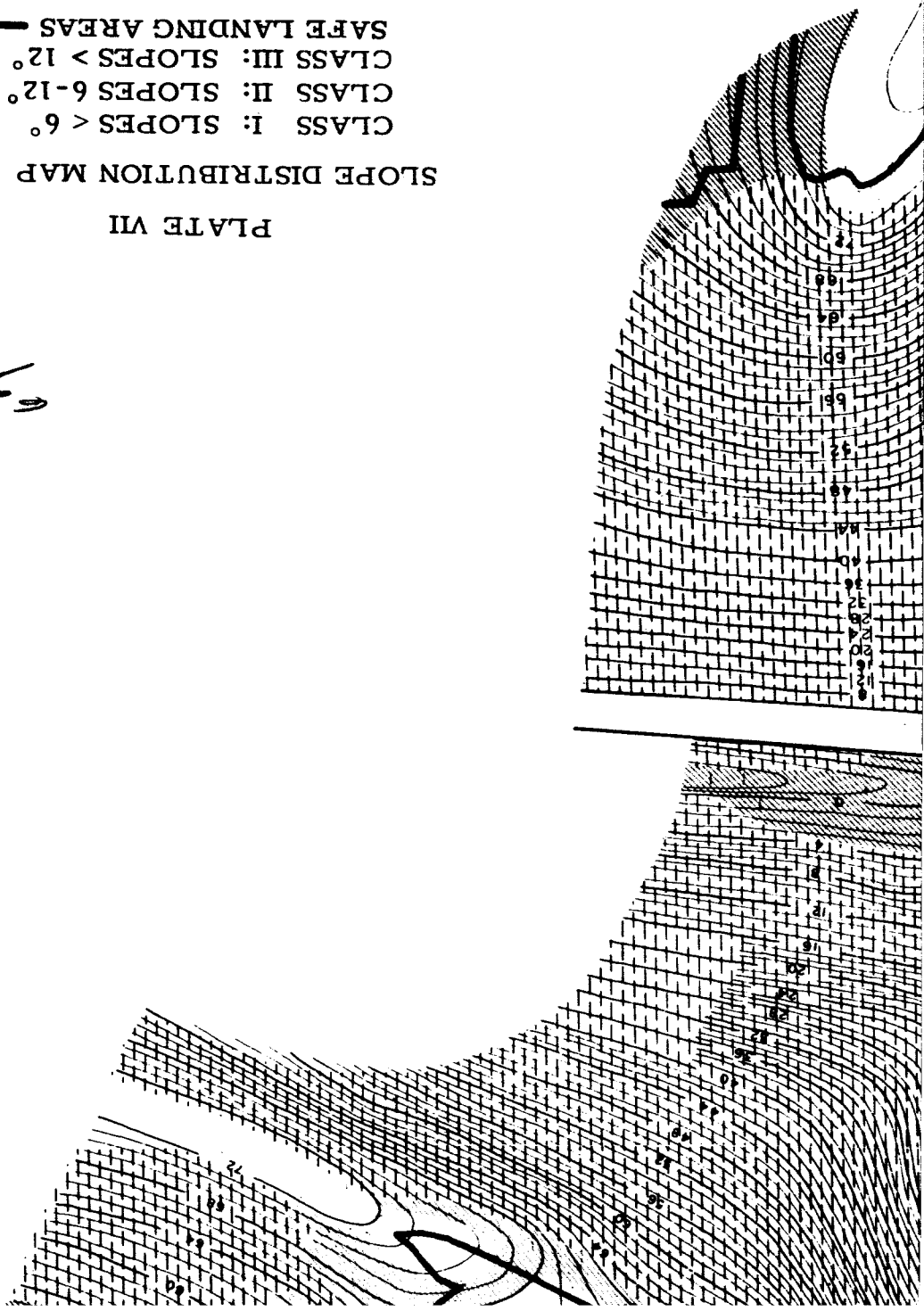
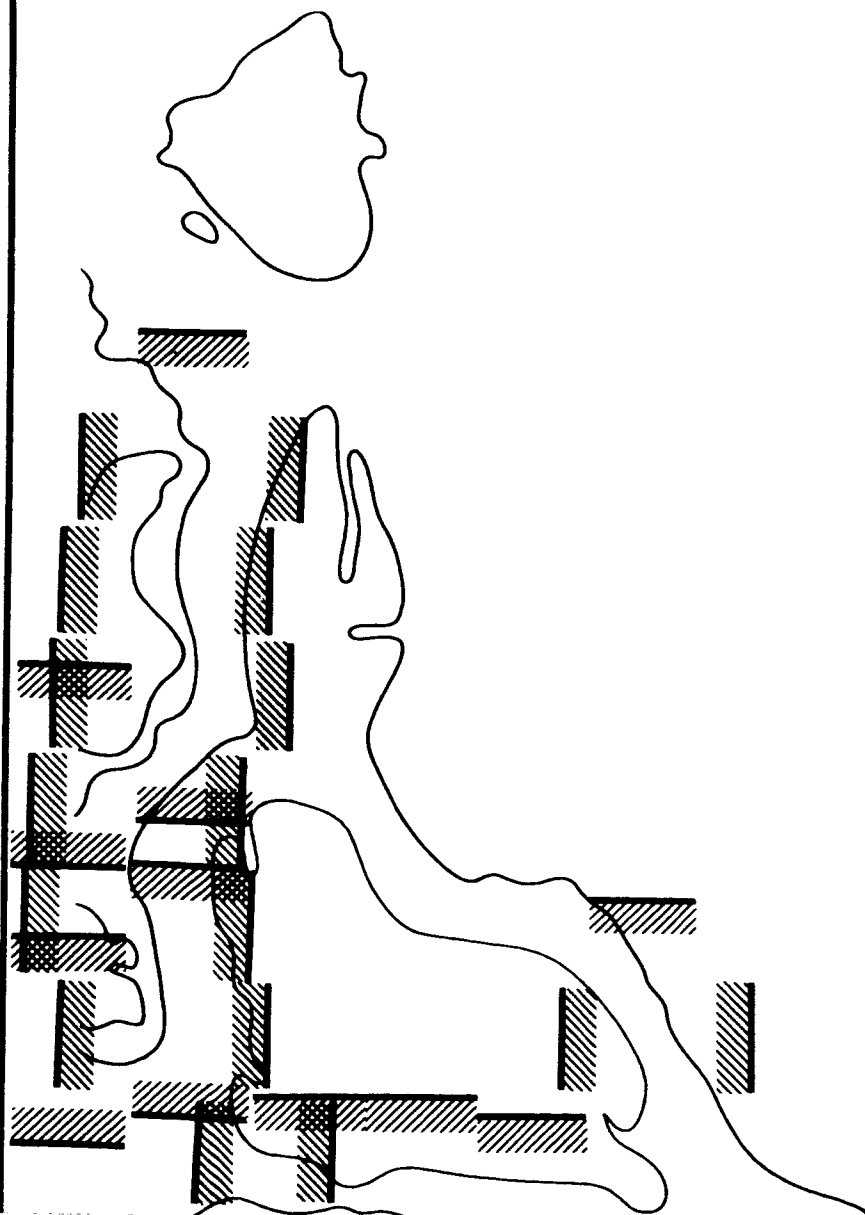
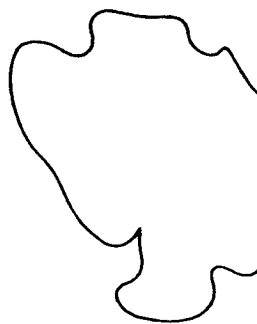


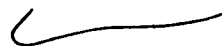
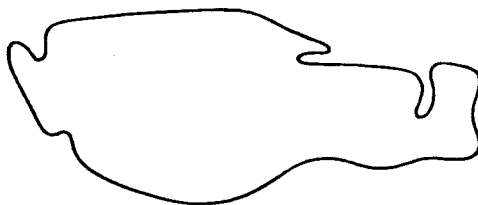
Plate IX

1086



2066





3 of 6





4 of 6

PISGAH CRATER AREA



SCALE 1:540

PLATE IX - PIS

RECONTOURED

SCANNED BY CI
SAFE AREAS

UNSAFE SLOPE
BY HORIZONTAL

UNSAFE SLOPE
BY VERTICAL S

5 of 6



GAH LAVA FLOW (AREA C)

@ ≈ 0.83 m

RCULAR 8m TEMPLET

ZONES DETERMINED
L SWEEPS



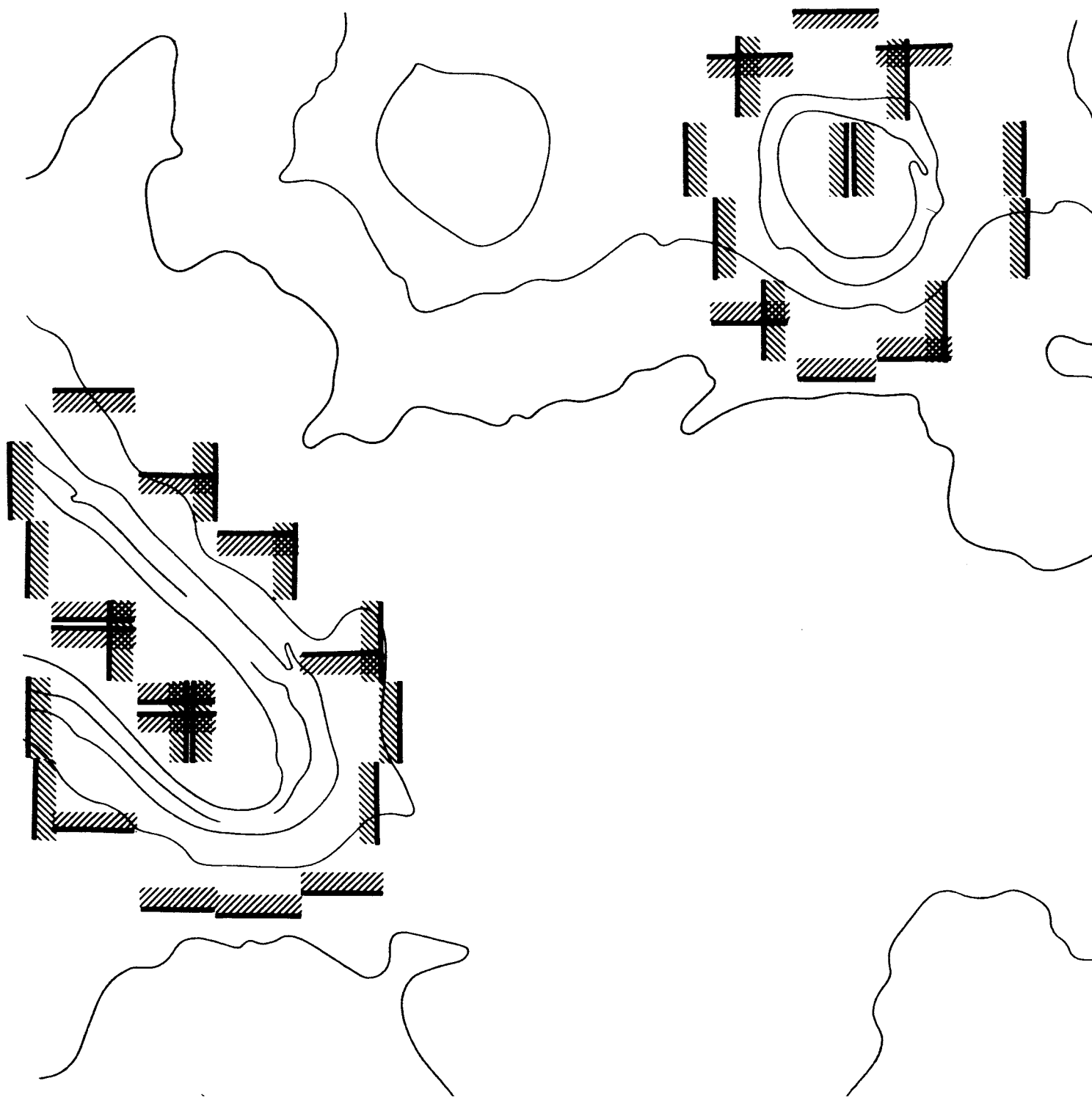
1.5%

ZONES DETERMINED
WEEPS

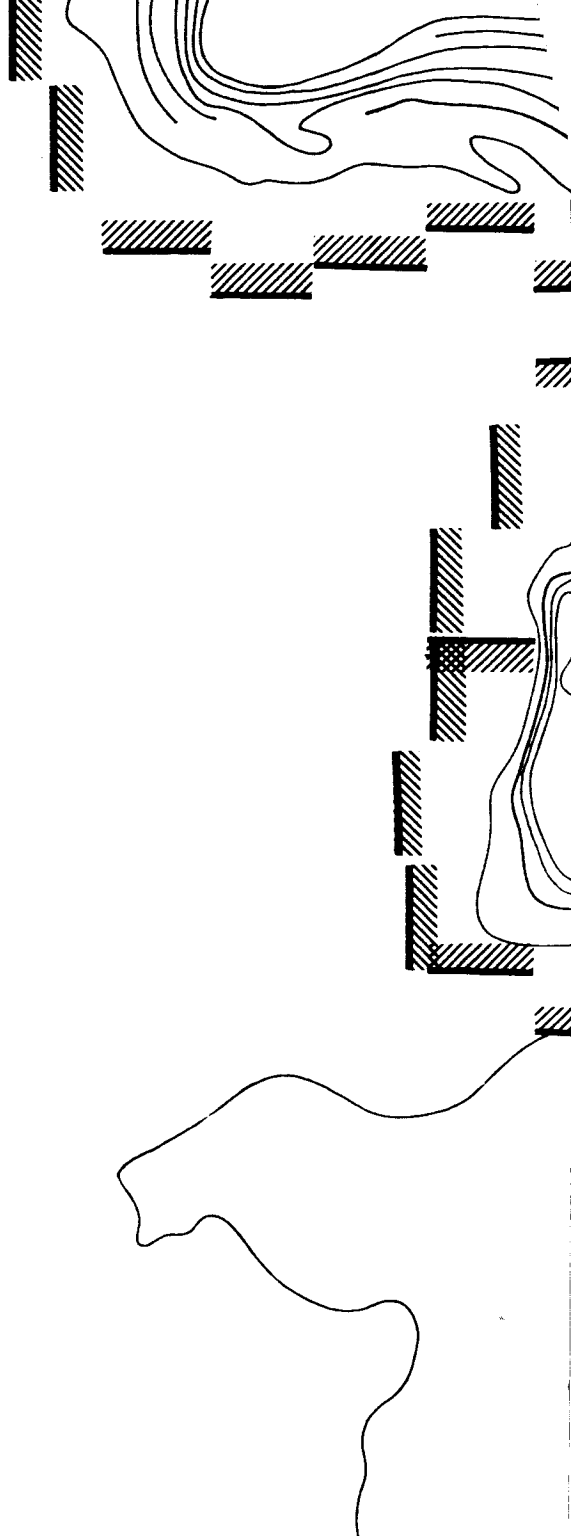
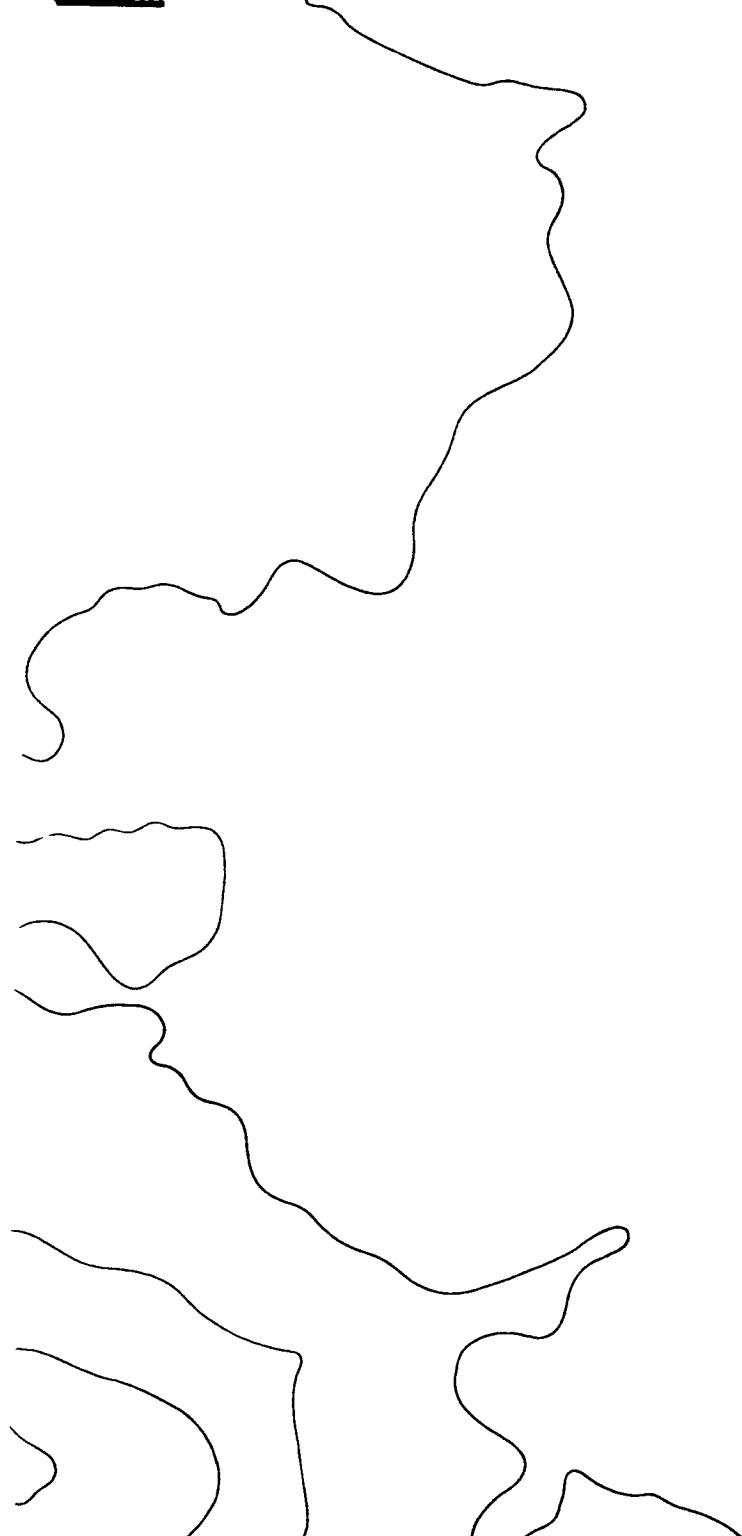


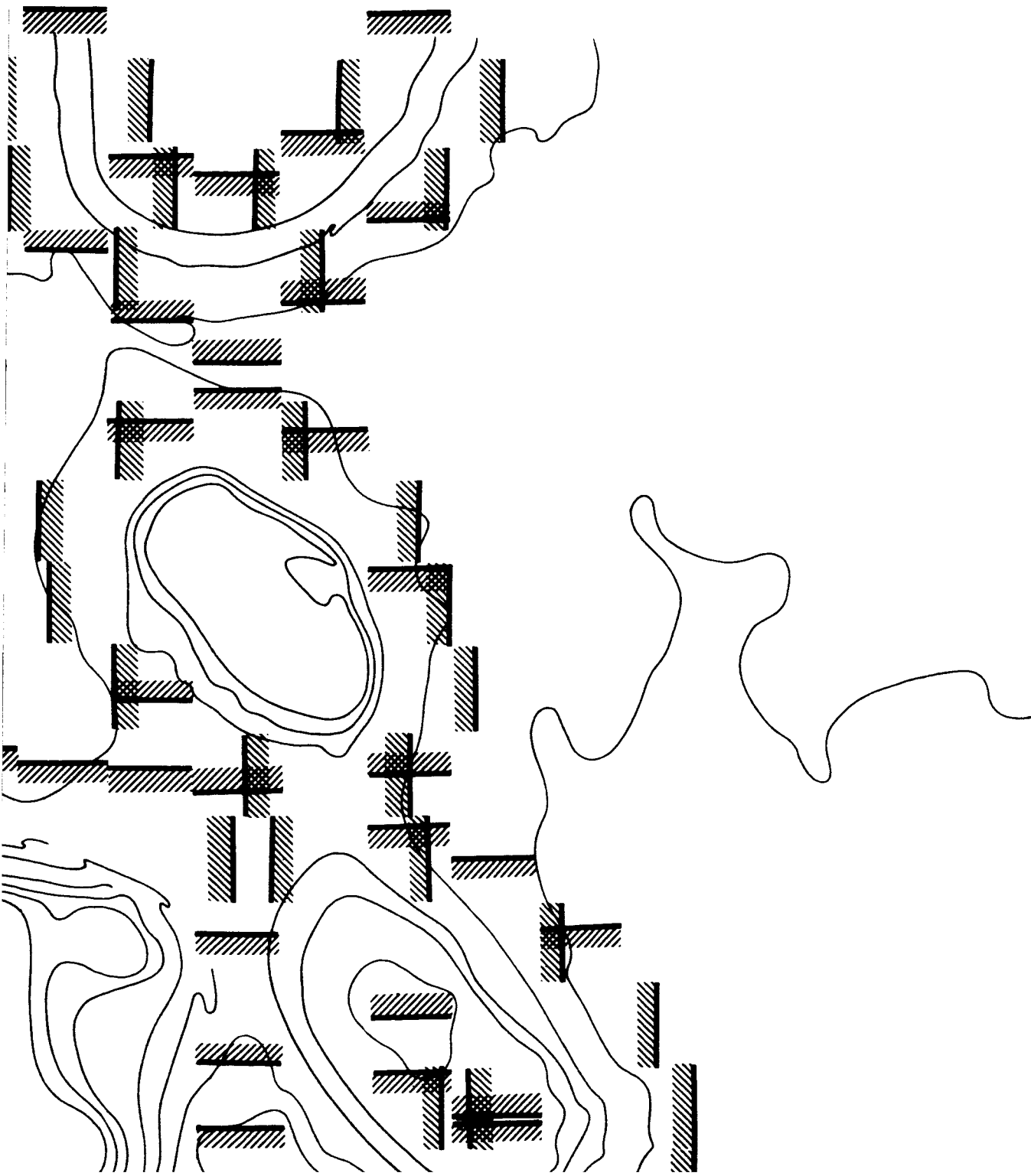
2.3%

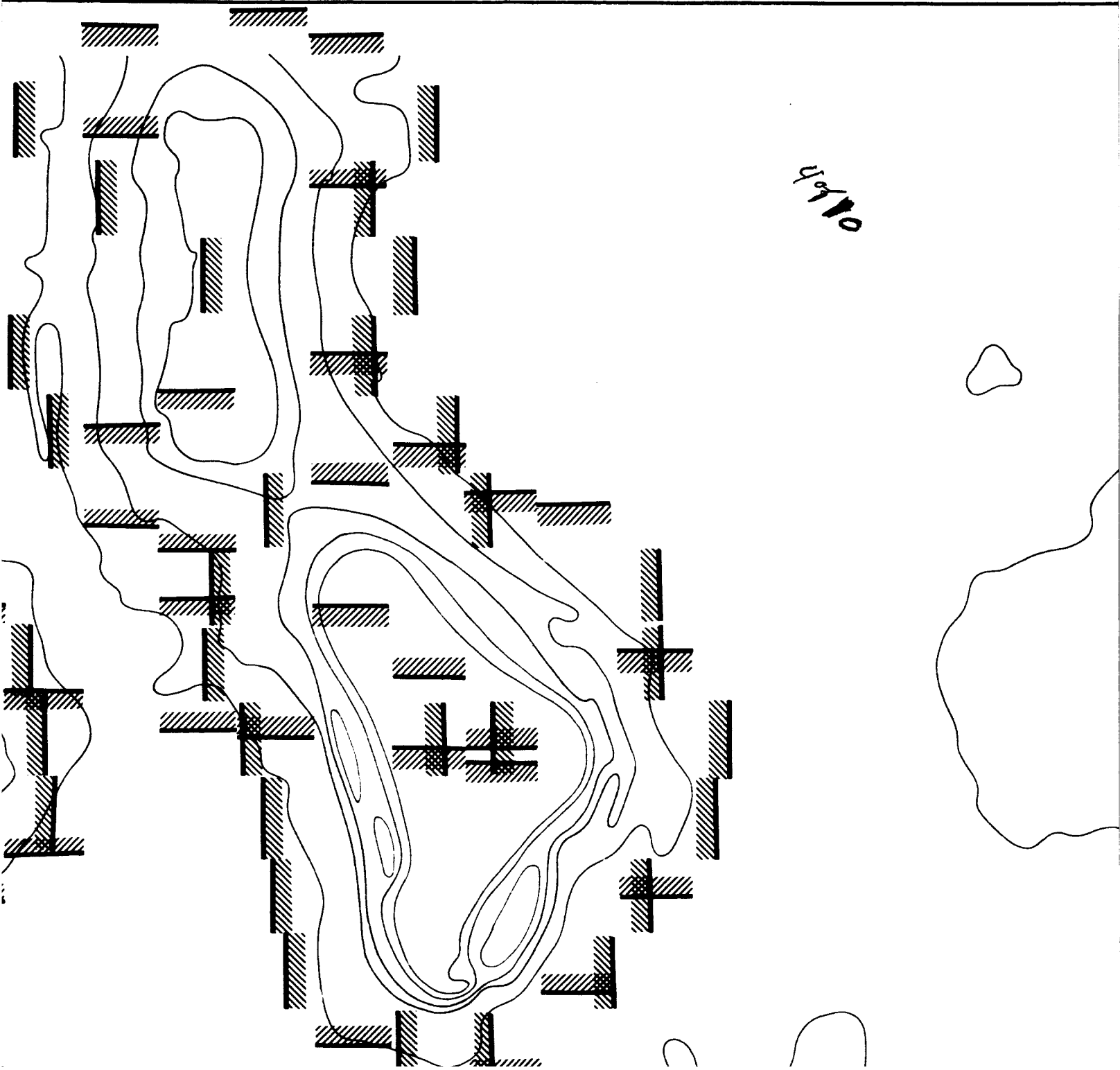
6 of 6



208

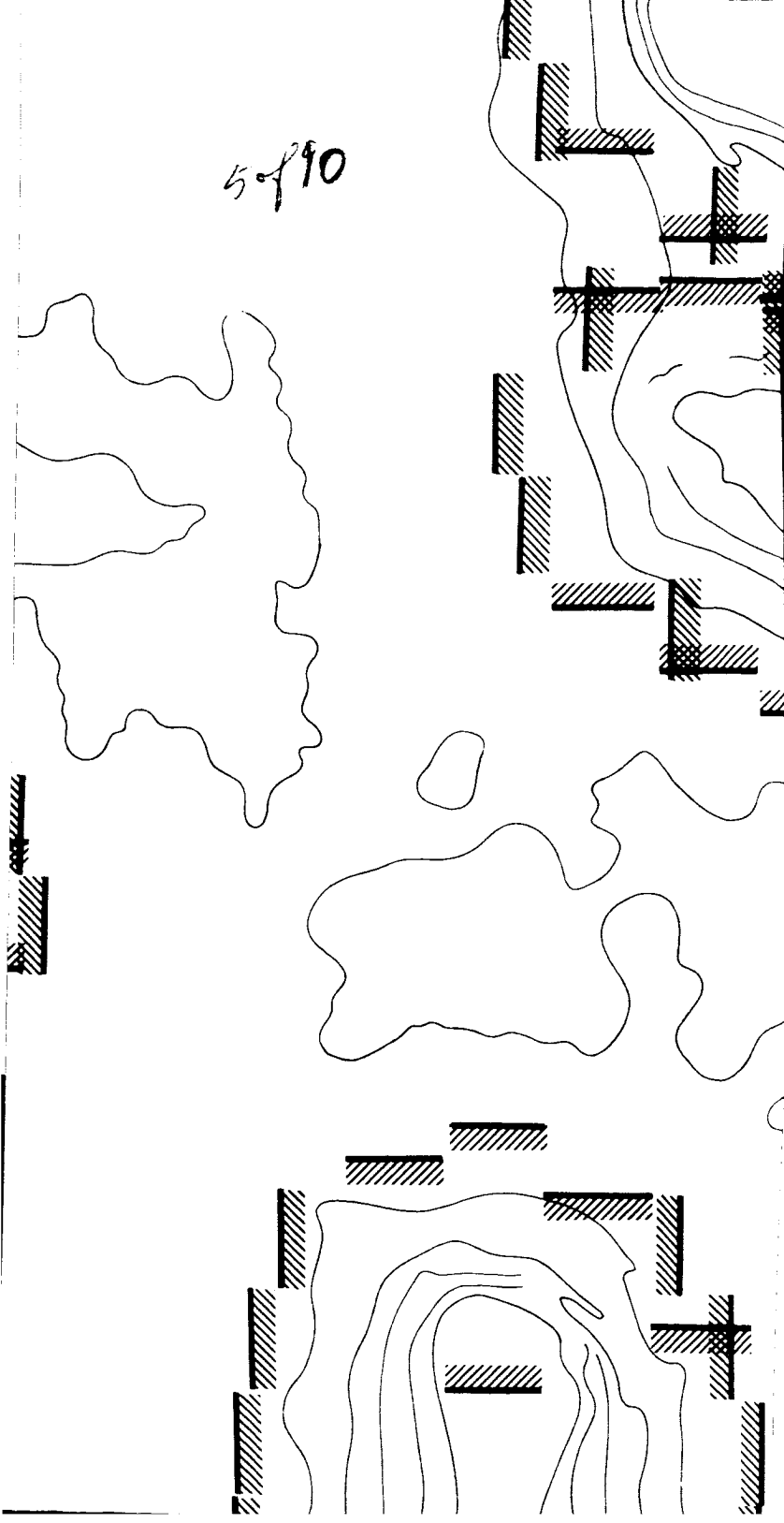




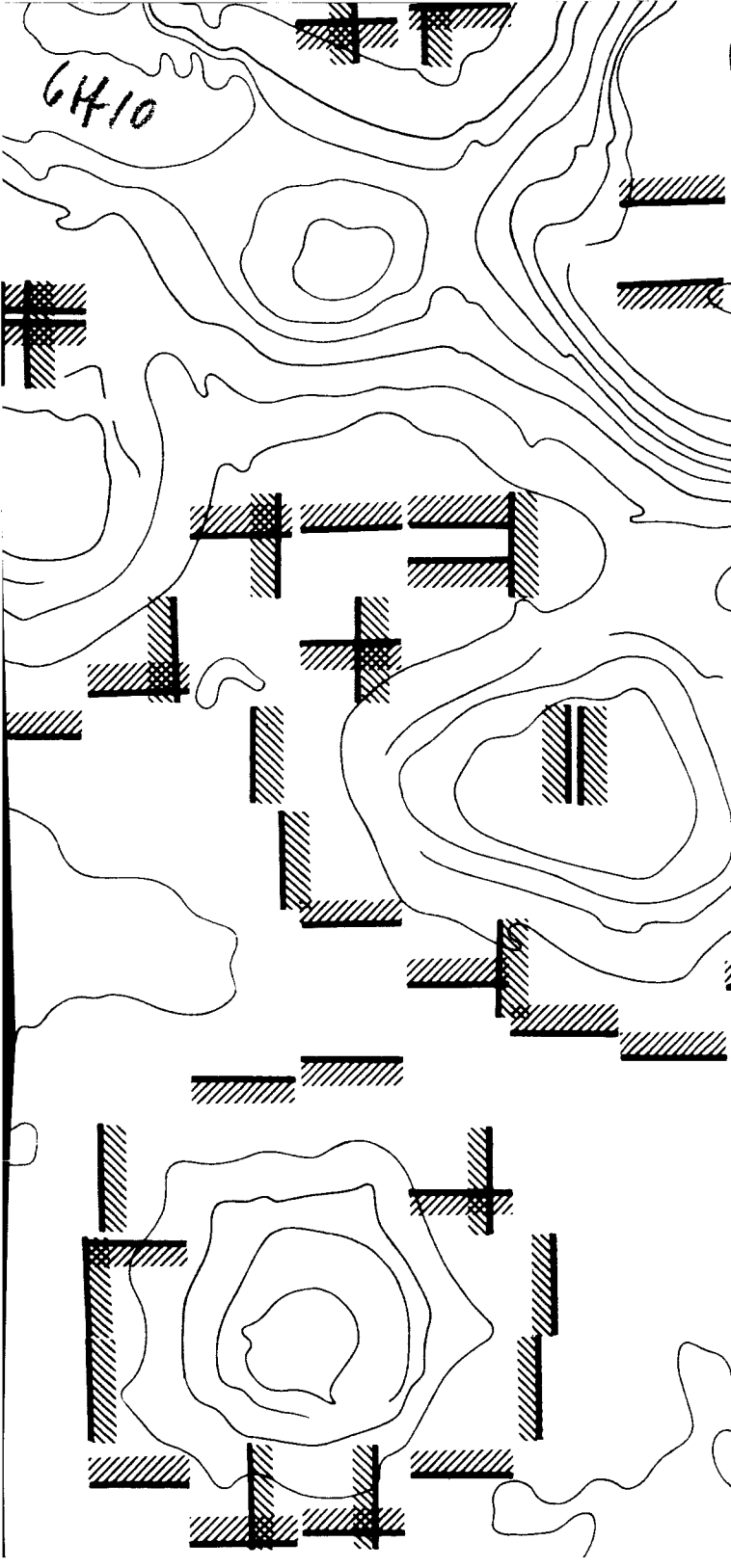


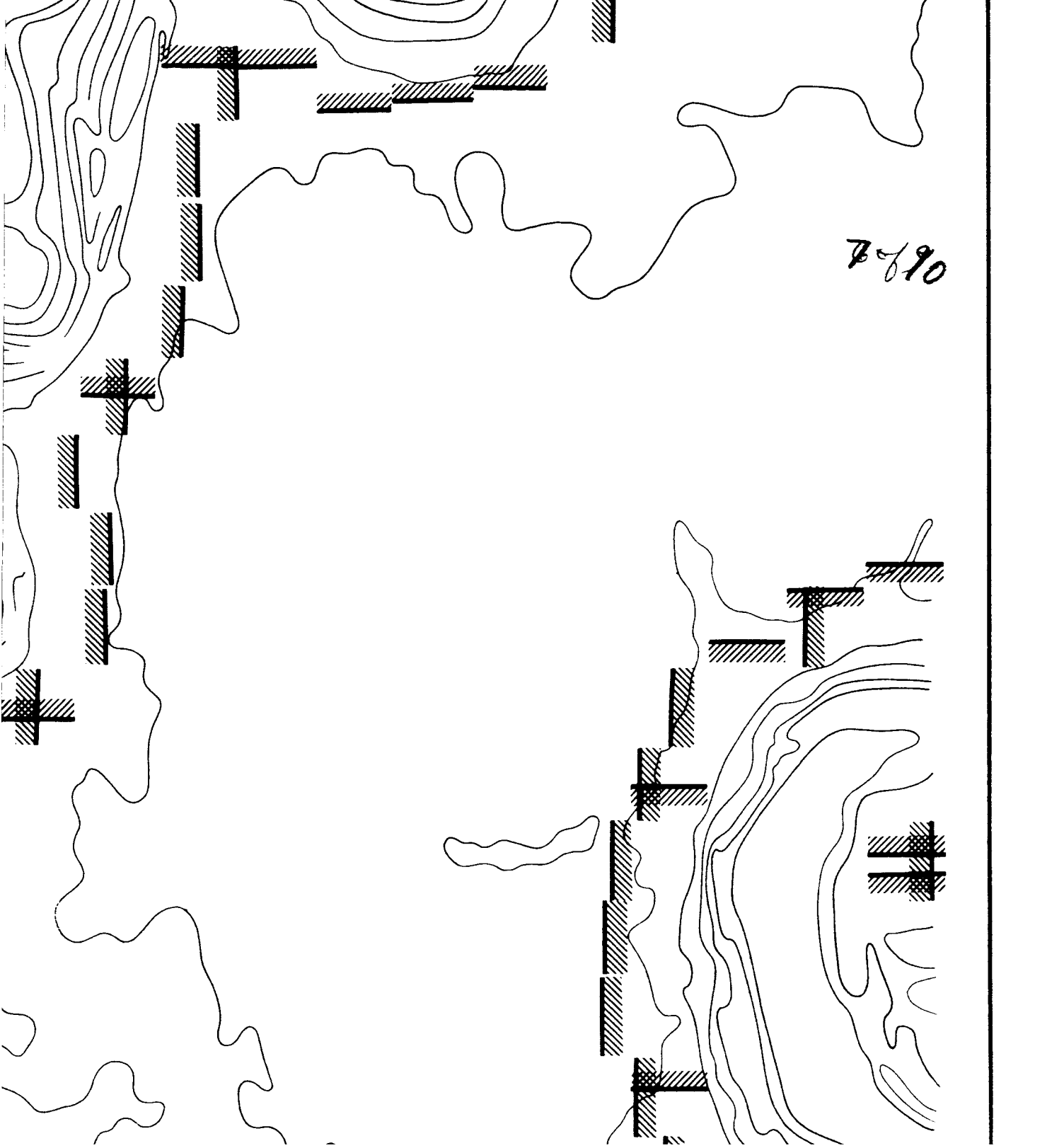
49/10

5-f90

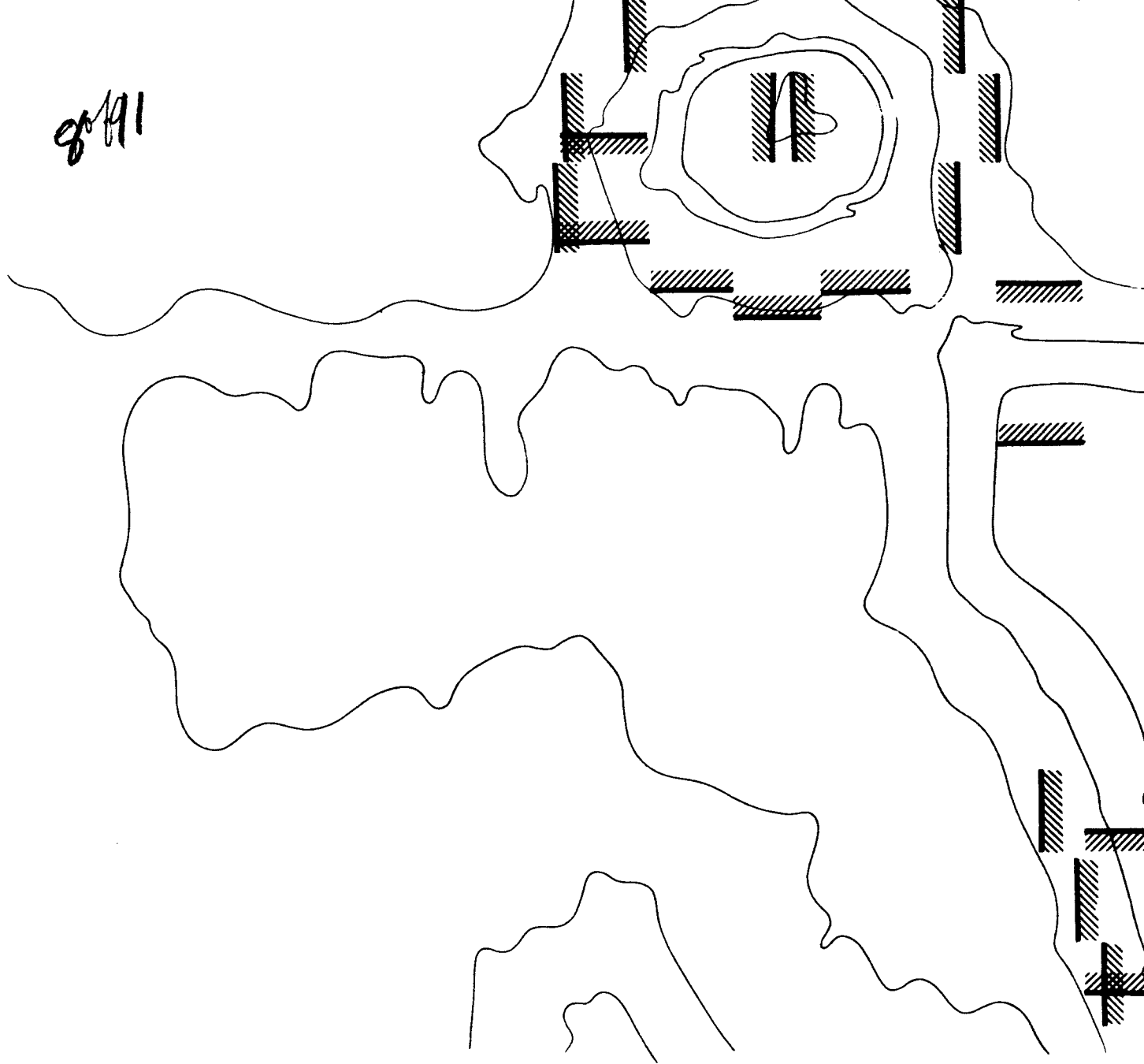


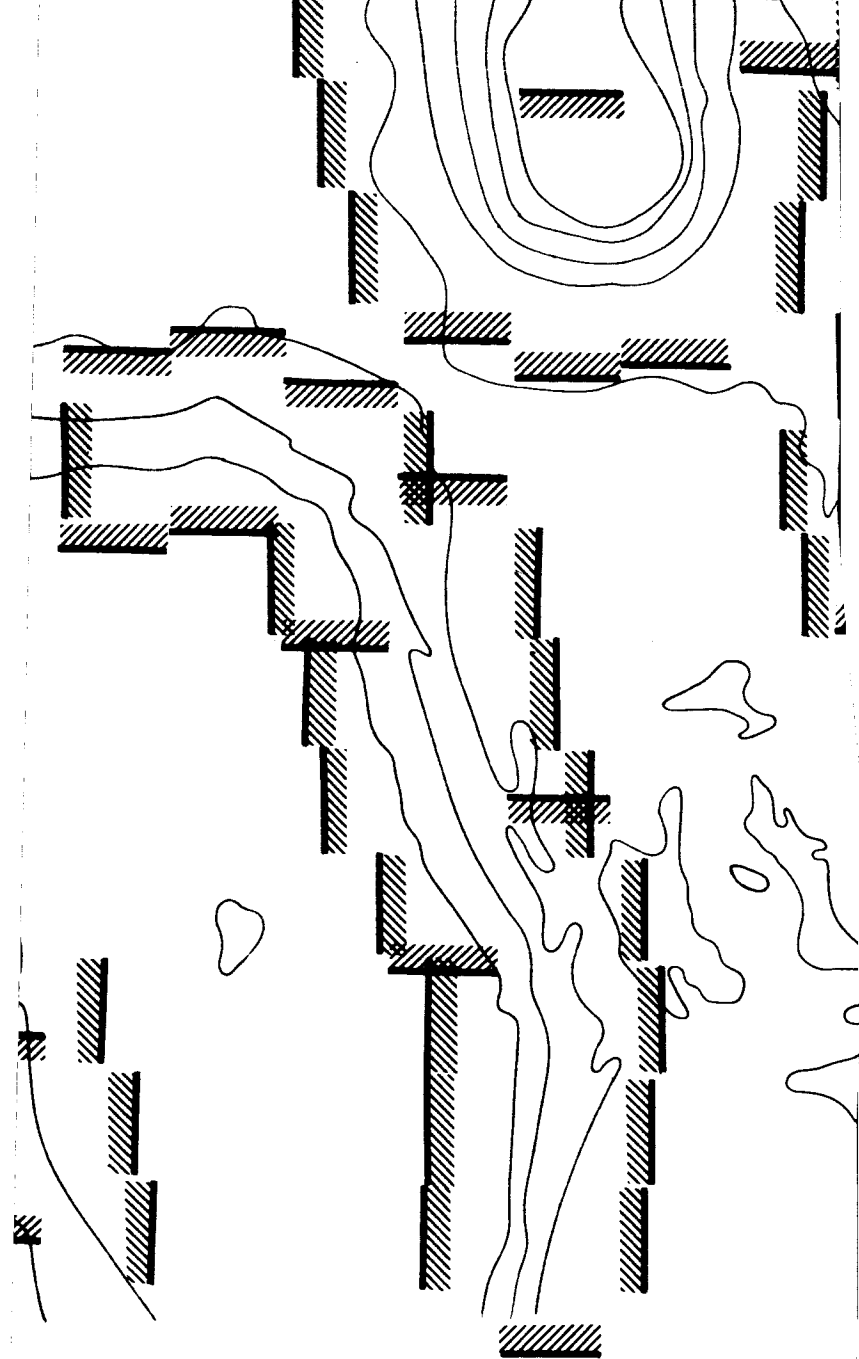
6410



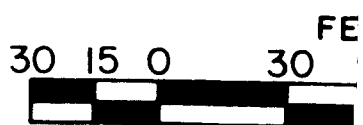


8/19/1



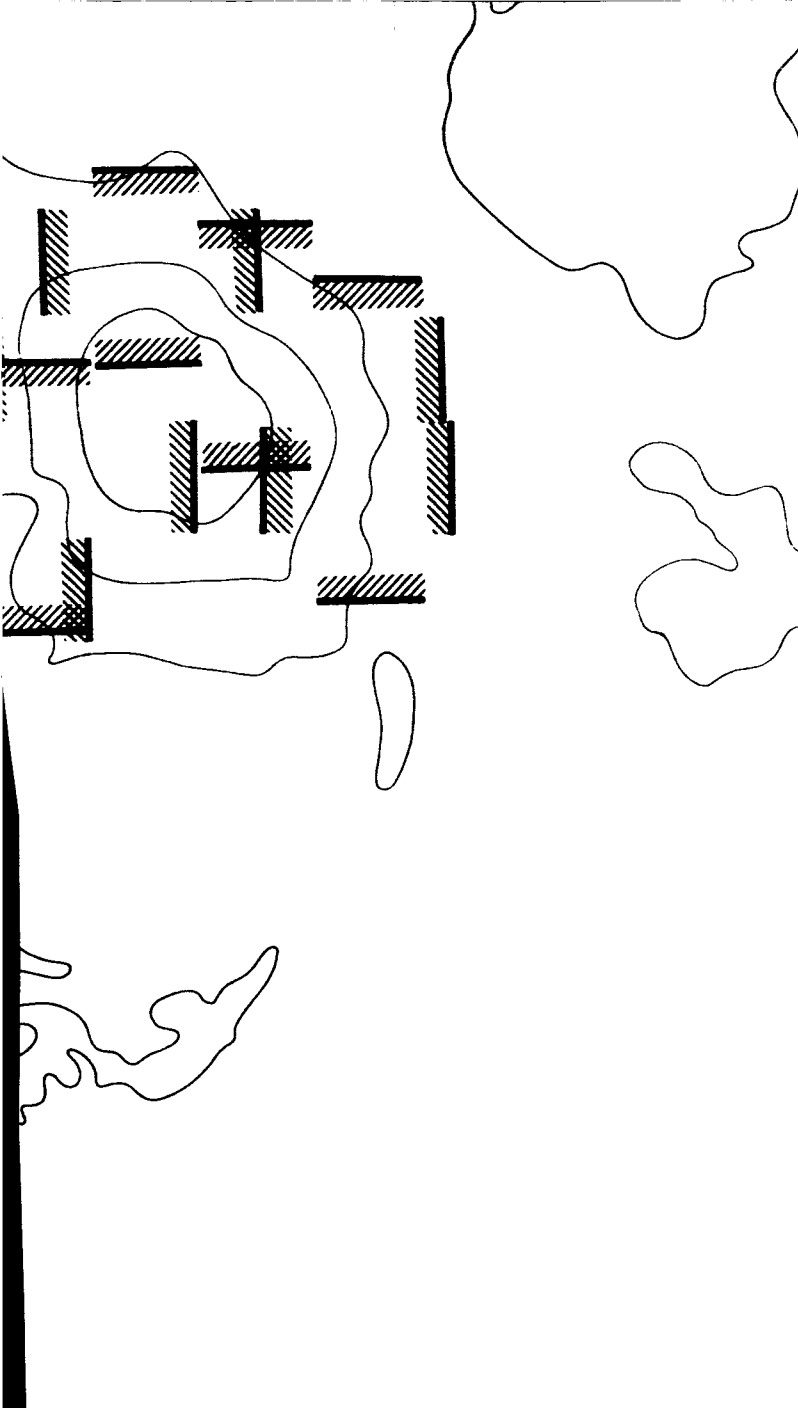


PISGAH CRA



SCALE

9 of 11



WATER AREA

ET

60

90

120

1:540

10/91

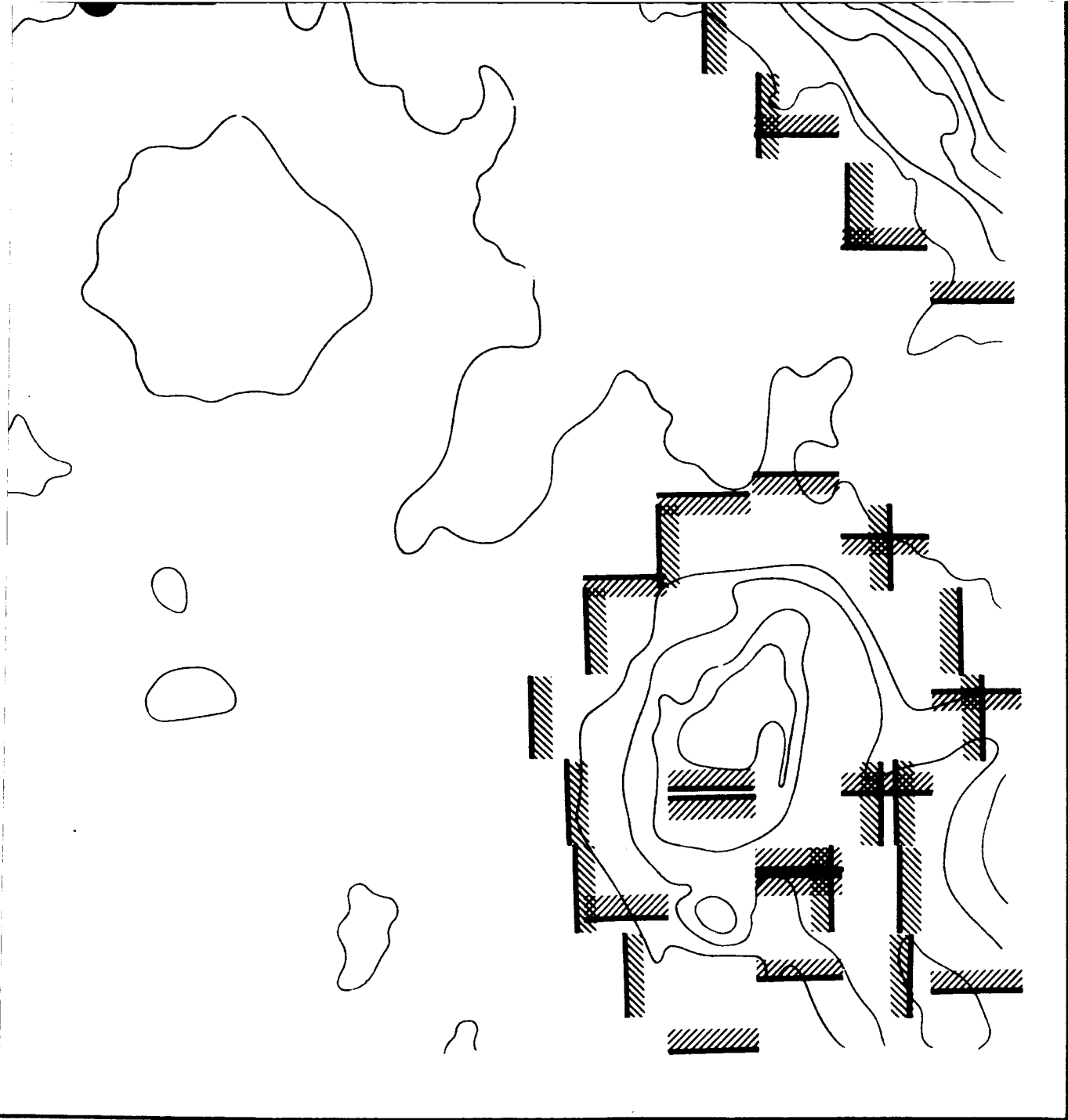
PLATE V

RECONF

SCANNED
SAFE AR

UNSAFE
BY HORI

UNSAFE
BY VERT



III - PISGAH LAVA FLOW (AREA A)

MEASURED $\frac{1}{4}$ 0.83 m

BY CIRCULAR 8m TEMPLET
EAS

11 of 91

SLOPE ZONES DETERMINED
HORIZONTAL SWEEPS



SLOPE ZONES DETERMINED
CIRCULAR SWEEPS

